



HAL
open science

Hydro-glaciological behaviour of the Arve catchment in the French Alps: climate variability and consequences on water resources availability

Alessandra Viani

► **To cite this version:**

Alessandra Viani. Hydro-glaciological behaviour of the Arve catchment in the French Alps: climate variability and consequences on water resources availability. *Climatology*. Université Grenoble Alpes; Università degli studi (Brescia, Italie), 2019. English. NNT: 2019GREAU015 . tel-02289646

HAL Id: tel-02289646

<https://theses.hal.science/tel-02289646>

Submitted on 17 Sep 2019

HAL is a multi-disciplinary open access archive for the deposit and dissemination of scientific research documents, whether they are published or not. The documents may come from teaching and research institutions in France or abroad, or from public or private research centers.

L'archive ouverte pluridisciplinaire **HAL**, est destinée au dépôt et à la diffusion de documents scientifiques de niveau recherche, publiés ou non, émanant des établissements d'enseignement et de recherche français ou étrangers, des laboratoires publics ou privés.



UNIVERSITÀ
DEGLI STUDI
DI BRESCIA

Communauté
UNIVERSITÉ Grenoble Alpes

THÈSE

Pour obtenir le grade de

**DOCTEUR DE LA COMMUNAUTE UNIVERSITE
GRENOBLE ALPES**

**préparée dans le cadre d'une cotutelle entre la
Communauté Université Grenoble Alpes et
L'Università degli Studi di Brescia**

Spécialité : **Océan, Atmosphère, Hydrologie (CEOAH)**

Arrêté ministériel : le 6 janvier 2005 – 25 mai 2016

Présentée par

Alessandra VIANI

Thèse dirigée par **Thomas Condom, Roberto RANZI et
Baldassare BACCHI**

préparée au sein de l'**Institut des Géosciences de
l'Environnement** dans l'Ecole Doctorale **Terre, Univers,
Environnement**

et du **Département de Génie Civil** de l'**Università degli Studi di
Brescia**

Fonctionnement hydro- glaciologique du bassin versant de l'Arve dans les Alpes françaises : variabilité climatique et disponibilité de la ressource en eau

Thèse soutenue publiquement le **14 Mai 2019**,
devant le jury composé de :

M Simon GASCOIN

Charge de recherche CNRS, CESBIO, Toulouse, France, Examineur

M Daniele BOCCHIOLA

Professeur, Politecnico di Milano, Milano, Italie, Examineur

Mme Giovanna GROSSI

Professeur associé, Università degli Studi di Brescia, Brescia, Italie, Examinatrice

M Massimo TOMIOTTI

Professeur, Università degli Studi di Brescia, Brescia, Italie, Examineur

M Thomas CONDOM

Charge de recherche IRD, IGE, Grenoble, France, Directeur

M Roberto RANZI

Professeur, Università degli Studi di Brescia, Brescia, Italie, Directeur



“Il segreto della riuscita è continuamente ricominciare”

Acknowledgements

Tout d'abord, merci Thomas. Ce travail n'aurait jamais eu lieu sans toi. Merci pour ton aide et soutien constant. Merci pour avoir été toujours disponible. Merci pour ton intérêt, ton dynamisme, ta curiosité, tes incitations permanentes et merci d'avoir cru en moi. Grâce à nos discussions scientifiques j'ai pu apprendre et améliorer mes connaissances dans le monde de l'hydrologie. J'emmènerai toujours avec moi la phrase "No problem, just solutions".

Merci à tous les autres experts qui ont contribué à la production de mon travail, notamment en me donnant des suggestions et des informations utiles. Merci à Antoine, Christian, Isabelle, Jean Emmanuel et Delphine. Je vous remercie pour votre réactivité, votre aide et votre considération. Je tiens à remercier Chales. Merci pour ta disponibilité et tes conseils.

Un pensiero inoltre non può che andare al Prof. Bacchi. Il primo ad avermi presentato il mondo della ricerca e datomi la possibilità di farne parte. Un ringraziamento anche al Prof. Ranzi per aver accettato il ruolo di supervisor a lavori avviati.

Grazie ai miei colleghi d'ufficio che hanno reso questo percorso molto più piacevole. Un ringraziamento speciale va ad Eleni. Grazie per avermi ascoltata, e grazie per i tuoi preziosi consigli. Non sei stata semplicemente una collega, ma un'amica.

Merci à tous mes amis "sherpa". Merci à JeanCa, Hans, Diego et George. Merci pour les discussions scientifiques, le temps libre passé ensemble, le soutien, les déjeuners, les soirées. Je me souviendrai agréablement des discours pendant les repas. Et merci de m'avoir fait rire. Sans vous ma vie à Grenoble ne serait pas la même. Je remercie également Gregoire. Merci pour les échanges d'idées utiles, les bons plans et les soirées passées ensemble.

Un enorme grazie va alla mia famiglia. Grazie ai miei genitori, ai miei zii, ai miei nonni ed al mio ragazzo. Grazie per avermi supportato, sopportato, incoraggiato, dato la carica in ogni momento durante questo percorso. Grazie per esserci sempre.

To conclude, thank to me. Thanks to me for having no day off and never quitting.

Ale

Summary

Glacier recession and the anticipation of spring snow melt driven by a warming climate could lead to changes in the hydrological cycle affecting not only the headwater catchments but also the areas downstream. In order to correctly predict the magnitude of future possible changes and to consider appropriate strategies of water management, a good understanding of the interaction between glaciers, climate and hydrology is needed. The aim of this study is to assess the effect of climate variability on the hydro-glaciological behaviour and its consequence on water availability in the Arve River catchment (French Alps) since 1960. It covers 1958 km² and is composed by five nested catchments (Arveyron d'Argentière, Arveyron de la Mer de Glace, Arve at Pont des Favrands, Arve at Sallanches and Arve at Bout du Monde), all influenced by glacier and snow melt but characterized by various percentages of glacier cover ranging from 5 to 53%. This research is based on a long dataset of in situ or remote sensing glaciological, meteorological, hydrological and snow cover area data.

Trend analyses are performed on the hydrological and meteorological data at all the considered sites.. To make easier the assessment of the evolution of the past and future discharge, the discharge seasonal cycle of each catchment is fitted using the asymmetric peak model, composed by a mathematical function made up of two half-gaussian curves. In addition, changes in the discharge are related to observed changes in the meteorological variables and the glaciers' evolution. Results point out a contrasting behaviour among the catchments characterized by different glacier covers, showing an increasing trend on the discharge values in highly glacierized catchments (with a glacier cover >30%) and a decrease in the low glacierized ones. The sensitivity of the seasonal cycle to the future climate is evaluated. In the mid-21st century the annual runoff would be reduced by 16% for Arveyron d'Argentière and 31% for Arveyron de la Mer de Glace. Over the summer season, a detailed quantification of each term of the hydrological balance equation, as well as their uncertainties, on the Argentière and Mer de Glace-Leschaux drainage basins allows to underline the importance of considering the groundwater transfers to represent and predict the hydro-glaciological behaviour of a considered catchment. Two different distributed temperature index melt models coupled with a linear reservoir discharge model are used to simulate the hydro-glaciological processes and subglacial discharge on the Arveron d'Argentière catchment over the 1960–2009 period. The calibration is carried out against discharge only and with a multi-criteria approach considering the discharge, the snow cover area and the glacier-wide annual mass balance values at daily time step. The suitability of the models in reproducing the subglacial hydrology is tested against the subglacial runoff measured in a gallery located in the observatory built under the glacier considered. Results demonstrate the suitability of the use of a classical degree day model in simulating the hydro-glaciological behaviour and the subglacial water production of a highly glacierized catchment. A KGE of

0.85 is obtained between the observed and simulate discharge values over the 1960–2004 period. The use of a multi-criteria approach seems to reduce the simulation uncertainties.

KEYWORDS: Glacierized catchment; Discharge seasonal cycle; Glacier mass balance; Water resource availability; Hydro-glaciological modelling; Subglacial discharge; Alps.

Résumé

La réduction du volume des glaciers et la fusion printanière plus précoce de la neige causée par le réchauffement climatique provoquent des variations du cycle hydrologique à la fois pour les têtes de bassin versant, mais aussi pour les zones situées plus à l'aval. Afin de prédire correctement l'amplitude des changements possibles futurs et d'envisager une gestion adaptée, une bonne connaissance de l'interaction entre les glaciers, le climat et les écoulements hydriques est nécessaire. L'objectif de cette étude est d'évaluer l'effet de la variabilité climatique sur le fonctionnement hydro-glaciologique et ses conséquences sur la disponibilité de l'eau du bassin versant de l'Arve (Alpes françaises) depuis 1960. Ce bassin s'étend sur une surface de 1958 km² et est composé de cinq bassins versants emboîtés (Arveyron d'Argentière, Arveyron de la Mer de Glace, Arve au Pont des Favrans, à Sallanches et au Bout du Monde), tous influencés par la fusion glaciaire et nivale mais dans différentes proportions étant donnée la large gamme d'extension de couverture glaciaire de 5 à 53%. Ce travail est basé sur des longs jeux de données glaciologiques, météorologiques, hydrologiques et de couverture de neige qui sont issus soit de mesures ponctuelles dans l'espace soit de données obtenues par télédétection.

L'analyse des tendances a été réalisée sur des données hydrologiques et météorologiques des cinq bassins versants emboîtés. Pour faciliter l'évaluation de l'évolution présent et future du débit, le cycle saisonnier du débit est ajusté en utilisant le modèle à pic asymétrique, composé par une fonction mathématique constitué de deux courbes demi-gaussiennes. En outre, les changements observés des débits ont été reliés aux variables météorologiques ainsi qu'à l'évolution de la couverture glaciaire. Les résultats indiquent un comportement contrasté entre les bassins versants selon les taux d'englacements, avec une tendance croissante des valeurs de débit dans les bassins versants fortement englacés (couverture de glacier >30%) et décroissante pour les moins englacés. La sensibilité du cycle hydrologique au changement climatique futur a été évaluée. Pour le milieu du 21^{ème} siècle, on prévoit que le volume annuel écoulé serait réduit de 16% pour l'Arveyron d'Argentière et de 31% pour l'Arveyron de la Mer de Glace. Pour la période estivale, la quantification détaillée de chaque terme de l'équation du bilan hydrologique, ainsi que leurs incertitudes, sur les bassins versants de l'Arveyron d'Argentière et de l'Arveyron de la Mer de Glace a permis de souligner l'importance des transferts d'eau souterraine pour représenter et prédire le comportement hydro-glaciologique d'un bassin versant donné. Deux modèles d'écoulement distribués de type degré-jour couplés à un modèle de routage hydrologique à réservoir linéaire ont été utilisés pour simuler les processus hydro-glaciologique et le débit sous sous-glaciaire sur le bassin versant de l'Arveyron d'Argentière sur la période 1960–2009. La calibration est effectuée à pas de temps journalier à la fois sur les débits mais aussi sur l'évolution de la couverture neigeuse et des bilans de masse annuels. L'aptitude des modèles dans la reproduction de l'hydrologie sous-glaciaire est testée par rap-

port au débit sous-glaciaire mesuré dans une galerie située dans l'observatoire construit sous le glacier considéré. Les résultats démontrent la bonne aptitude du modèle classique degré-jour pour simuler le comportement hydro-glaciologique et la production d'eau sous-glaciaire d'un bassin versant fortement glaciaire. Pour la période 1960–2004, nous avons obtenu pour le critère de 'Kling Gupta Efficiency' une valeur de 0.85 entre le débit simulé et observé. La calibration multicritère semble réduire les incertitudes des simulations.

MOTS CLÉS: Bassin versant englacé; Cycle saisonnier du débit; Bilan de masse glaciaire; Ressources en eau; Modélisation hydro-glaciologique; Débit sous-glaciaire; Alpes.

Riassunto

La riduzione del volume glaciale e l'anticipato scioglimento nivale primaverile causati dal riscaldamento globale provocano una rapida variazione del ciclo idrologico non solo nelle immediate vicinanze dei bacini glaciali ma anche nelle regioni più a valle. Al fine di prevedere correttamente l'entità dei futuri possibili cambiamenti e di individuare appropriate strategie di gestione della risorsa idrica, è necessaria una buona conoscenza dell'interazione tra ghiacciai, clima e idrologia. L'obiettivo di questo studio consiste nel valutare l'effetto della variabilità climatica sul comportamento idro-glaciologico e sulle conseguenze relative alla disponibilità della risorsa idrica all'interno del bacino del fiume Arve (Alpi francesi) a partire dal 1960. Quest'ultimo si estende su una superficie di 1958 km² ed è costituito da cinque sottobacini (Arveyron d'Argentière, Arveyron de la Mer de Glace, Arve a Pont des Favrandes, Arve a Sallanches and Arve a Bout du Monde), tutti influenzati dalla fusione nivale e glaciale ma caratterizzati da una diversa estensione della copertura glaciale che va dal 53 al 5% (dato del 2003). Questo studio si basa su una lunga serie di dati glaciologici, meteorologici, idrologici e di copertura nivale ottenuti sia attraverso misure dirette (in-situ) che mediante telerilevamento.

Per ogni bacino considerato sono state eseguite analisi dei trend su dati idrologici e meteorologici ed inoltre il ciclo stagionale del deflusso è stato approssimato mediante l'ausilio del modello a picco asimmetrico, costituito da una funzione matematica composta da due curve semi-gaussiane. I cambiamenti osservati nel regime dei deflussi sono stati messi in relazione con le variabili meteorologiche e con le variazioni della copertura glaciale. I risultati ottenuti mettono in evidenza un comportamento contrastante tra i bacini caratterizzati da una diversa estensione della copertura glaciale, mostrando un aumento del volume di deflusso all'interno dei bacini altamente glaciali (con una copertura glaciale >30%) ed una diminuzione in quelli con una copertura inferiore. È stata inoltre valutata la sensibilità del ciclo idrologico alle possibili variazioni climatiche future. Per la metà del XXI secolo è stata prevista una diminuzione del volume di deflusso prodotto pari al 16% nel bacino dell'Arveyron d'Argentière ed al 31% in quello dell'Arveyron de la Mer de Glace. La quantificazione dettagliata di ogni termine dell'equazione del bilancio idrologico, nonché delle loro incertezze, sui bacini che drenano i ghiacciai dell'Argentière e della Mer de Glace-Leschaux ha permesso di sottolineare l'importanza di considerare i flussi d'acqua sotterranei per rappresentare e prevedere il comportamento idro-glaciologico di un determinato bacino. Due modelli distribuiti ad indice di temperatura insieme ad un modello di trasformazione afflussi-deflussi a serbatoio lineare sono stati utilizzati per riprodurre i processi idro-glaciologici ed il deflusso sotto-glaciale nel bacino dell'Arveyron d'Argentière sul periodo 1960–2009. La loro calibrazione è stata fatta a scala giornaliera, adottando sia una modalità mono-obiettivo che un algoritmo multi-obiettivo. La capacità dei modelli nel riprodurre l'idrologia sotto-glaciale è stata valutata comparando i valori del deflusso

sotto-glaciale simulati con quelli misurati in una galleria situata nell'osservatorio costruito sotto il ghiacciaio considerato. I risultati mostrano l'attitudine del modello base ad indice di temperatura nel simulare correttamente il comportamento idro-glaciologico ed il deflusso sotto-glaciale prodotto da un bacino. Un valore di KGE pari a 0.85 è stato ottenuto sui valori giornalieri di deflusso sul periodo 1960–2004. L'ausilio di un approccio multi-obiettivo sembra ridurre l'incertezza sui valori simulati.

PAROLE CHIAVE: Bacini glaciali; Ciclo stagionale del deflusso, Bilancio di massa glaciale; Disponibilità della risorsa idrica; Modellazione idro-glaciologica; Deflusso sotto-glaciale; Alpi.

Contents

Acknowledgements	iii
Summary	v
Résumé	vii
Riassunto	ix
Introduction	1
1 Reasons of the research	1
2 Main objectives	3
3 Content of the report	4
Chapter I	
Study area and data	5
I.1 Characteristics of the study domain	7
I.1.1 Geographical location and morphology	7
I.1.2 Geology	9
I.1.3 Land cover	9
I.1.4 Glaciers	10
I.1.5 Hydropower	14
I.1.5.1 Description of the Waterpower Development	15
I.1.5.2 Impact on the catchment hydrology	18
I.1.6 Climate setting and weather patterns	18
I.1.6.1 Climatology	18
I.1.6.2 Weather patterns	19
I.1.6.3 Hydrological regimes	20
I.2 Observation networks and instruments	22
I.2.1 Meteorological data	22
I.2.1.1 Punctual data	24
I.2.1.2 Reanalysis	25
I.2.1.3 Future climate projections	26
I.2.1.4 Precipitation phases	26
I.2.2 Hydrological data	27
I.2.2.1 Surface hydrology	27

I.2.2.2	Subglacial hydrology	28
I.2.3	Snow data	30
I.2.3.1	In-situ data: punctual snow depth observations	30
I.2.3.2	MODIS data	30
I.2.4	Glaciological data	31
I.2.4.1	Mass balance	31
I.2.4.2	Glacier surface area	32
I.2.4.3	Glacier equilibrium-line altitude	32
I.2.5	DEMs and land cover maps	33
Chapter II		
Characterization of the current and future glacier influence on the discharge		
seasonal cycle of five nested catchments in the French Alps		35
	Summary of the research paper	37
	Abstract	39
II.1	Introduction	39
II.2	Study site	41
II.3	Dataset	43
II.3.1	Meteorological data	43
II.3.2	Hydrological data	44
II.3.3	Glaciological data	45
II.3.4	DEMs	46
II.4	Methods	46
II.4.1	Filtering of the discharge data	47
II.4.2	Asymmetric peak model (APM)	47
II.4.2.1	Fitting process	47
II.4.2.2	Calibration and optimization procedures	49
II.4.2.3	Performance	49
II.4.3	Trend analysis	50
II.4.4	Estimation of the glacier volume changes	51
II.4.5	Principal Component Analysis (PCA) on highly glacierized catchments	52
II.4.5.1	Variables influencing the discharge seasonal cycle	52
II.4.5.2	Sensitivity of the discharge seasonal cycle to future climate	
	changes	53
II.5	Results	54
II.5.1	Hydrological regime of the five nested catchments	54
II.5.2	Asymmetric peak model	54
II.5.3	Trend analysis	55

II.5.3.1	1983–2004 period	55
II.5.3.2	1960–2004 period	59
II.5.4	Result of the Principal Component Analysis	60
II.5.4.1	Variables influencing the discharge seasonal cycle	60
II.5.4.2	Sensitivity of the model to glacio-meteorological changes	63
II.6	Discussion	65
II.7	Conclusion	68
Appendix		71
A.1	Extended Extreme Studentized Deviate (ESD)	71
A.2	Mann-Kendall test	71
A.3	Test statistic Z	72
A.4	The Theil-Sen slope	72
Acknowledgments		74
Chapter III		
Glacier-wide summer surface mass-balance calculation: hydrological balance applied to the Argentière and Mer de Glace drainage basins (Mont Blanc)		
	Summary of the research paper	75
	Abstract	77
III.1	Introduction	79
III.2	Study site	80
III.3	Data	84
III.3.1	DEM, glacier surfaces, land cover and geology	84
III.3.2	Meteorological data	84
III.3.3	Glaciological data	85
III.3.4	Snow cover	85
III.3.5	Hydrological data	86
III.4	Methods	86
III.4.1	Hydrological method	86
III.4.2	Glaciological method	89
III.4.3	SAFRAN precipitation adjustment	90
III.4.4	Uncertainty in the simulated and 'observed' glacier-wide summer surface mass balances	91
III.5	Results	92
III.5.1	Glacier-wide summer surface mass balance from in situ glaciological measurements	92
III.5.2	Glacier-wide summer surface mass balance from hydrological data	93
III.6	Discussion	96

III.7 Conclusion	98
Acknowledgments	100
Chapter IV	
Multi-criteria calibration of distributed temperature index models in a highly glacierized alpine catchment under climate variability	101
Summary of the research paper	103
Abstract	105
IV.1 Introduction	105
IV.2 Study site	108
IV.3 Data	108
IV.3.1 Meteorological data	108
IV.3.2 Hydrological data	110
IV.3.3 Glaciological data	110
IV.3.4 Snow cover area data	111
IV.3.5 Grid data	111
IV.4 Methods and model' setup	111
IV.4.1 Model description	111
IV.4.1.1 Melt model	111
IV.4.1.2 Discharge routing	112
IV.4.2 Model forcing and data preprocessing	113
IV.4.3 Sensitivity analysis	114
IV.4.4 Fixing the not-sensitive parameters	116
IV.4.5 Models calibration, validation and evaluation metrics	116
IV.4.6 Temporal stability of the models' parameters	118
IV.4.7 Simulations uncertainties	118
IV.5 Results and discussion	119
IV.5.1 Single vs. multi calibration approach	119
IV.5.2 Performance of the models calibrated with a multi-criteria approach	120
IV.5.2.1 Total discharge, glacier runoff contribution and subglacial hydrology	121
IV.5.2.2 Glacier-wide surface mass balances and snow line altitude	124
IV.5.2.3 Snow Cover Area	127
IV.5.3 Temporal stability of the models	128
IV.6 Conclusion	131
Further developments	133

Conclusion and perspectives	135
1 Conclusion	135
2 Outlook for further research	137
Bibliography	139
Personal Bibliography	163
Curriculum Vitae	165
Dichiarazione di conformità	167

Introduction

1 Reasons of the research

This work of thesis consists in the evaluation of the effect of the climate variability on the hydro-glaciological behaviour and its consequence on water availability in the Arve River catchment (French Alps).

But why are we concerned about the Alps? And why the attention is focused on a highly glacierized catchment?

The Alps are the largest mountain system in Europe, stretching along an arc of about 1200 km (190000 km²). Their importance has been declared officially on March 6th, 1995, when the Convention on the Protection of the Alps, signed by the European Union as well as the Alpine states, came into force, contributing to reinforce the recognition of special qualities and specific characteristics of this environment. As the 'water towers' of the Europe, the Alps are crucial for the water accumulation and supply for large part of the continent (Viviroli and Weingartner, 2004; Viviroli et al., 2007). Their snow fields and glaciers provide indispensable water resources for municipal and industrial water uses, irrigation and hydropower production (e.g. Barnett et al., 2005; Viviroli et al., 2011). They provide 40% of European Union consumption (EEA, 2009; Isoard et al., 2009). In addition, most of the largest rivers of the Central Europe, such as Rhine, Po, Rhône, originate in the alpine region. The EU White Paper on Adaptation (European Commission, 2009) recognized the Alps as among the most sensitive areas to climate change in Europe (Beniston et al., 2018). They appear the most severely and rapidly impacted ecosystem (Beniston, 2003; Loarie et al., 2009; Maragno et al., 2009; Bocchiola and Diolaiuti, 2010; Confortola et al., 2013; Gobiet et al., 2014). As evidence, from the late 19th century until the end of the 20th century, a marked temperature increase of around +2°C, leading to a melting of glaciers, a shift on the snowmelt season and a change in discharge regime of the rivers has been documented (Auer et al., 2006; Vaughan et al., 2013). It is thus essential to assess in details the impacts of a changing climate on these regions and to understand how they respond to, are affected by, and may adapt to these changes.

Glaciers are identified as sensitive indicators of climate variability at different scale (Oerlemans, 1986; Chen and Ohmura, 1990; Oerlemans and Fortuin, 1992; Haeberli, 2005; Vaughan et al., 2013); they affect the catchment hydrology even for low percentages of glacier coverage and constitute an important water reservoir in the form of snow and ice (Jansson et al., 2003).

In glacier-fed catchments, after a transient phase of increasing runoff, the retreat of the ice coverage is expected to be accompanied by a decrease in the discharge (Jansson et al., 2003; Gleick and Palaniappan, 2010; Baraer et al., 2012; Huss and Hock, 2018). When the glacier surface becomes too small, the increasing melt rates do not compensate the glacier shrinkage and the total amount of water provided by the glacier decreases, as well as the streamflow assuming no variations in precipitation (Huss et al., 2008). These changes in hydrological regime affect the availability of the water resource and influence the production of the hydropower energy (Immerzeel et al., 2010; Kaser et al., 2010; Huss, 2011; Schaeffi et al., 2019). They pose new challenges for the management of the water resources, since the management regimes based on historic climate and hydrological variability will likely be inadequate within the next decades. For these reasons, understanding the sensitivity of the hydrological regime, melt water runoff and glaciers' evolution to the climate variability is a key issue.

Assessments of the glacier retreat and resulting hydrological consequences have been carried out at global scale (Bliss et al., 2014; Radić and Hock, 2014; Huss and Hock, 2018). Given that long-time series in high complex terrain are rarely available, few studies have paid attention in providing evidence for the sensitivity of high-alpine runoff to the climate variability (*e.g.* Birsan et al., 2005; Pellicciotti et al., 2007, 2010; Bard et al., 2015). In the French region, Giuntoli et al., 2012 performed a trend analysis on streamflow data at both locally and regional scales, not focusing on the glacierized areas, whereas Renard, 2006, Lang et al., 2006 and Renard et al., 2008 detected the trends at national and regional scales. According to the authors' knowledge, no study has been focused on the discharge changes at catchment scale in the French high-alpine regions. In addition, assessments of how the glacier mass changes affect the streamflow and the different percentage of glacier cover can influence the water production of areas submitted to the same regional climate are required. Several studies have been carried out on the French alpine glaciers (*e.g.* Rabatel et al., 2013; Berthier et al., 2014; Six and Vincent, 2014; Rabatel et al., 2016; Réveillet et al., 2017, 2018; Vincent et al., 2018a) but without focusing on the interaction between hydrology and glaciology. The assessment of the hydro-glaciological behaviour of a high-mountain area is conditioned by the scarcity of the available data and by the difficulty to have a representative estimation of precipitation due to their high spatial variability and the bias that can affect the gauged precipitation due to under catch of snow and rain, as well as gauge icing (Sevruk, 1983, 1987; Schaeffi et al., 2005; Sieck et al., 2007; Grossi et al., 2017).

In addition, the impact of the climate change on the groundwater component is rarely considered even though the assessment of the subterranean fluxes dynamic is required to forecast the evolution of water resources and related hazards under a changing climate (Vincent et al., 2018). Also the evaluation of effects of the climate variability on the subglacial hydrology is required. These gaps in knowledge have to be addressed.

In this context, a detailed study on the investigation of all the available hydrological, glaciological, meteorological and snow dataset to improve the understating on their interaction and

on the groundwater fluxes is needed.

2 Main objectives

This study is focused on the valley of the Arve River, located in the western Alps in the region of Haute-Savoie. The Arve catchment covers 1958 km² with an elevation ranging from 380 to 4800 m a.s.l. and is bounded by two mountain ranges: the Chablais Alps to the north and the Graian Alps to the south. It is composed by five nested catchments, *i.e.* Arveyron d'Argentière (32 km²), Arveyron de la Mer de Glace (79 km²), Arve at Pont des Favrandes (202 km²), Arve at Sallanches (588 km²) and Arve at Bout du Monde (1958 km²), all influenced by glacier and snow melt but characterized by a various percentages of glacier cover ranging from 53 to 5% (in 2003). Here, the anthropogenic influence is not negligible; the streamflow is affected by water withdraws for electricity production. The water diverted is provided by the ice/snow melt and is collected by headrace tunnels built under the glaciers. Since the hydropower industries are strongly dependent on the availability of water resources of this area, the ability in simulating the catchment water production and the subglacial discharge is an important task. The results of these study could be useful for the hydro-electricity producers, such as the company of Emosson (Electricité d'Emosson S.A.), EDF (Electricité de France) and the CNR (Compagnie Nationale du Rhône), the stakeholders in charge of the planning and managing of the water resources (the BERGER, "Biologie des Ecosystèmes et Ressource en eau: anticiper l'impact des Glaciers En Recul", project supported by the Auvergne-Rhône-Alpes Region) and who deals with the ecosystem issue. Furthermore, knowledge on the evolution of the glacier contribution allows to make medium and long-term forecasts on hydrology at local and regional level. The research has been done at different spatial resolution considering the overall valley, at catchment and glacier scales. It was made possible by the extensive meteorological, glaciological and hydrological available dataset. The main objectives of this work are:

1. To characterize the current and future glacier's influence on the discharge seasonal cycle of the five nested catchments located in the Arve River valley;
2. To demonstrate the importance of considering the groundwater fluxes to calculate future runoff;
3. To identify the best suitable simple model allowing the simulation of the hydro-glaciological processes and the subglacial discharge in the Arveyron d'Argentière catchment.

The limitation due to the issue on precipitation are considered and their spatial distribution is adjusted using winter accumulation values on the glaciers.

3 Content of the report

In addition to this introductory part this thesis consists of four chapters.

Chapter 1 provided the main characteristic of study area and the dataset used. Furthermore, definitions and basic aspect of climatology, hydrology and glaciology accompanied by literally reviews are also given to facilitate the comprehension.

The main body is composed by the three subsequent chapters, each of which is based on an article: one under review in the *Journal of Hydrology* (Chapter 2), one published in the *Journal of Glaciology* (Chapter 3) and one in preparation for *Water Resources Research* (Chapter 4). Each article is introduced by a short summary in which the elements of novelty and the main results are highlighted. In addition, at the end of the Chapter 4 further developments are presented. More in detail, Chapter 2 addresses the first objective by performing a trend analysis on the hydrological and meteorological series over the 1983–2004 period and only including the discharge dataset over 1960–2004, depending on data availability; by identifying the causes of the observed changes in streamflow; and by evaluating the sensitivity of the discharge seasonal cycle to future climate change for the 2030–2040 and 2050–2060 periods. The discharge seasonal cycle of each catchment is fitted using a mathematical function, that makes the assessment of its temporal and spatial evolution easier. Chapter 3 tackles the second objective. The method proposed here consists in the estimation of the glacier-wide summer surface mass balance of Argentière and Mer de Glace-Leschaux glaciers, using the hydrological method. To this end, the quantification of each term of the hydrological balance equation as well as their uncertainties on the considered glacier drainage basins during the summer season is carried out over the 1996–2004 period. The performance of this computation is evaluated by the comparison with data obtained using a glaciological method. Chapter 4 addresses the third objective. Two different distributed temperature index melt models, *i.e.* the classical and the one with the inclusion of the potential clear-sky direct solar radiation, coupled with a linear reservoir discharge model are used to simulate the hydro-glaciological behavior of the Argentière catchment. Their performance in simulating discharge, glacier-wide surface mass balance, snow cover area and snow line altitude at glacier scale and their ability in reproducing the subglacial runoff are evaluated. The calibration is carried out using a single and multi-variables approach. In addition, the short and long-terms temporal stabilities of the models' parameters are assessed over the 2000–2003 and 1960–2009 periods, respectively.

Finally, the overall conclusion of this work and an outlook for the future research are given.

Among the different chapters, the structure of this thesis implies some repetition and the use of different mass balance units, *i.e.* m w.e. a⁻¹ or m w.e. yr⁻¹ (both in compliance with [Cogley et al., 2011](#)) according to the styles of the considered journals.

Chapter I

Study area and data

I.1 Characteristics of the study domain

I.1.1 Geographical location and morphology

This work focused on the valley of the Arve River, located in the western Alps in the region of Haute-Savoie (France), between $45^{\circ}45'$ and $46^{\circ}15'$ north latitude and between $6^{\circ}5'$ and $7^{\circ}5'$ east longitude (Fig. I.1a). The Arve is an alpine river with a glacial regime. Rising in the Col de Balme (Graian Alps) at 2191 m a.s.l., it drains the northwestern side of the Mont Blanc massif before flowing into the Rhône River in the west of Geneva (Switzerland).

The Arve catchment covers 1958 km², stretching from the Mont Blanc massif to the Geneva lake, bordering Switzerland to the northeast and Italy to the southeast. It is bounded by two mountains ranges: the Chablais Alps to the North and the Graian Alps to the South (Fig. I.1a). The catchment is characterized by a high degree of topographic heterogeneity, with steep slopes at high altitudes and at the contact between hill slopes and the valley, and gentle slopes on the large glacierized areas and at the low elevations. This heterogeneity affects the spatial distribution and temporal evolution of snow and ice covers. The elevation of the overall catchment ranges from 380 to 4800 m a.s.l., with 8.5% of the surface area above 2500 m a.s.l.. Its mean slope is 21%. It is highly glacierized with glaciers localized on the eastern side, on the Mont Blanc border. Furthermore, this area is densely urbanized (urban centers of Chamonix, Sallanches, Cluses, Bonneville, La Roche sur Foron, Annemasse/Geneva), industrialized and a sought-after tourist destination (especially in its upper part).

In the overall drainage basin, 5 nested catchments can be identified, *i.e.* Arveyron d'Argentière, Arveyron de la Mer de Glace, Arve at Pont des Favrands, Arve at Sallanches and Arve at Bout du Monde (Fig. I.1b). They differ in terms of surface area, elevation range, glacier and land covers (Table I.1). Their surface area ranged from 32.2 km² (Arveyron d'Argentière) to 1958 km² (Arve at Bout du Monde), their elevation at the outlet from 380 to 1363 m a.s.l. and their glacier cover from 5% (Arve at Bout du Monde) to 53% (Arveyron de la Mer de Glace), in 2003. On the base of the shape and the integral of their hypsometric curves (Fig. I.2a), they can be divided in three groups, characterized by different stages of the Davisian geomorphic cycle (Strahler, 1952). The two high glacierized basins, the Arveyron d'Argentière and Arveyron de la Mer de Glace, are in an "inequilibrium stage" (youth) with integrals equal to 0.70 and 0.65 respectively. Arve at Pont des Favrands and at Sallanches are in an "equilibrium stage" (maturity or old age), characterized by a smoothly S-shaped curves with integrals values of 0.58 to 0.41, respectively. Arve at Bout du Monde has a strongly concave curve with a very low integral (0.29).

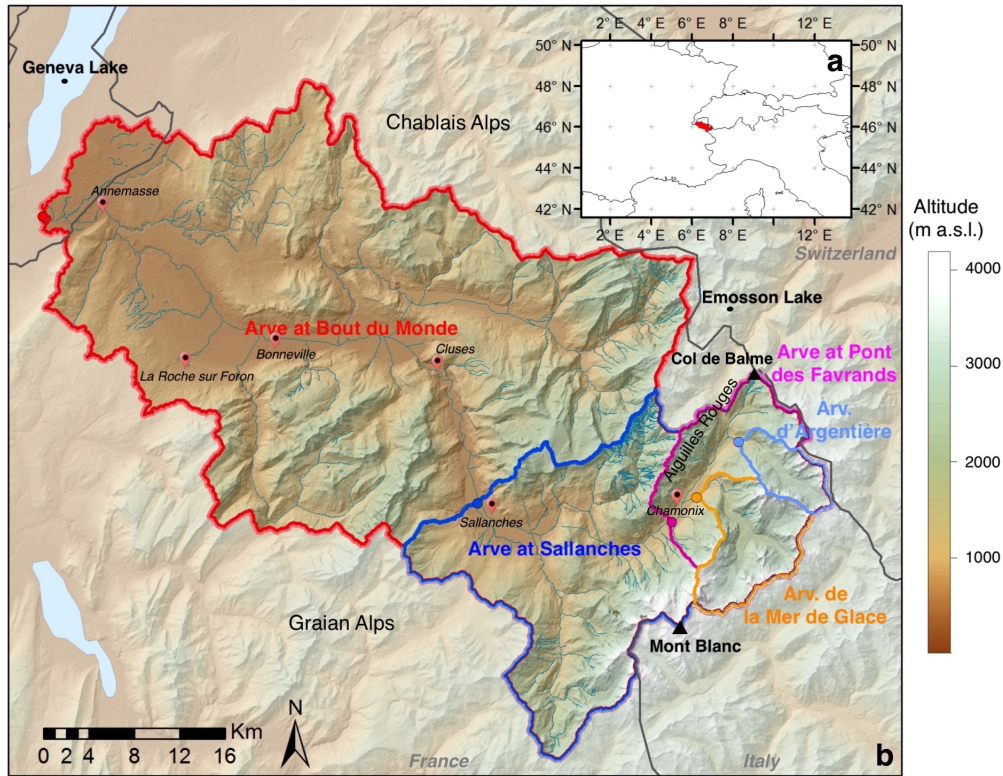


Figure I.1: a) Location of the study area. b) Topography of the five nested catchments in the valley of the Arve River: Arveyron d'Argentière (light blue), Arveyron de la Mer de Glace (orange), Arve at Pont des Favrandes (pink), Arve at Sallanches (blue) and Arve at Bout du Monde (red). The colored points indicate the location of the hydrological gauging station of each catchment considered. The topography is provided by ASTER satellite images, with 25 m of spatial resolution.

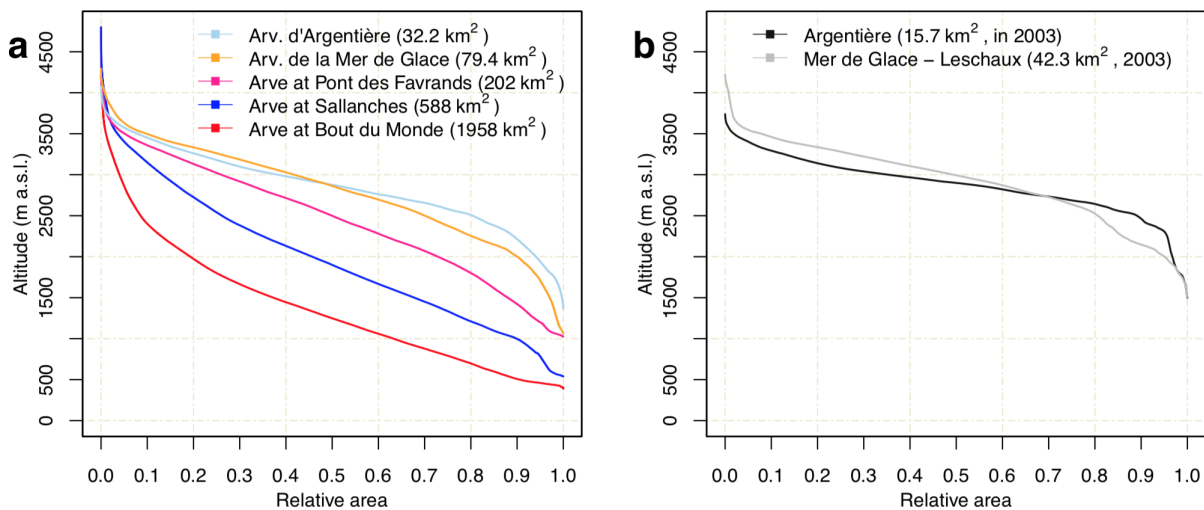


Figure I.2: Hypsometric curves of (a) the five nested catchments and (b) the two main considered glaciers in 2003.

Table I.1: Main characteristics and land cover (CLC 00, [Bossard et al., 2000](#)) of the five considered catchments. The glacier cover is obtained using Landsat and ASTER satellite images ([Gardent et al., 2014](#); [Rabatel et al., 2016](#)).

	Arveyron d'Argentière	Arveyron de la Mer de Glace	Arve at Pont des Favrands	Arve at Sallanches	Arve at Bout du Monde
Surface area (km ²)	32.2	79.4	202	588	1958
Median altitude (m a.s.l.)	2880	2865	2498	1900	1330
Elevation range (m a.s.l.)	1363–4079	1060–4295	1020–4295	535–4800	380–4800
Glacier cover in 2003 (%)	48.8	53.3	34.2	17.3	5.3
Mean slope (degree)	29	29	28	25	21
Land Cover					
Glacier cover in 2003 (%)	48.8	53.3	34.2	17.3	5.3
Forest in 2000 in km ² (in %)	0.7 (2.2)	3.0 (3.7)	26.0 (12.8)	154.4 (26.3)	695.9 (35.5)
Sparsely vegetated areas in km ² (in %)	0.6 (2.0)	3.5 (4.4)	14.6 (7.3)	39.6 (6.7)	80.9 (4.6)
Natural grassland in km ² (in %)	0.0	0.0	6.6 (3.3)	52.2 (8.9)	210.3 (10.7)
Moors and heathland in km ² (in %)	2.2 (6.8)	3.5 (4.4)	19.1 (9.5)	51.9 (8.8)	81.7 (4.1)
Urban fabrics in 2000 in, km ² (in %)	0.0	0.04 (0.1)	5.8 (2.9)	35.4 (6.0)	159.2 (8.1)
Bare rocks in 2000 in km ² (in %)	14.3 (44.4)	24.5 (30.9)	61.8 (30.6)	125.0 (21.3)	243.3(12.4)
Agricultural areas in 2000 in km ² (in %)	0.0	0.0	0.2 (0.1)	31.9 (5.4)	309.3 (15.8)
Water bodies in km ² (in %)	0.0	0.0	0.0	0.0	0.4 (0.2)

I.1.2 Geology

According to 1:500 000 geological map (GK500-Geol) provided by the Swiss federal authorities (<https://opendata.swiss/fr/dataset/geologische-karte-der-schweiz-1-500000>), the Mont Blanc and Aiguilles Rouges massifs are mainly composed of granites and gneiss, which pushed through the older rocks some 300 million years ago (Fig. [I.3](#)). The areas along the Arve River consist of alluvial soils and scree, of high percolation. The lower parts of the Arve catchment characterized by shallow slopes underlines an important presence of moraines.

The southern part of the upper Arve catchment is characterized by a network of subvertical shear zones in a N-S and NE-SW direction that isolates large boudins of weakly strained to unstrained granite (Fig. [I.3](#), [Rossi and Rolland, 2014](#)). Their formation is associated with the crystallization of epidote, chlorite, and white micas, under high pressure and temperature conditions, *i.e.* of 300–500 MPa and 400–450°C respectively ([Rolland et al., 2003](#), [Rossi et al., 2005](#)). The abundance of open fractures disturbs the permeability of the ground, leading it greater than that of undisturbed crystalline rocks.

I.1.3 Land cover

The Corine Land Cover map produced in 2000 ([Bossard et al., 2000](#); Fig. [I.4](#)) shows that 35.5% of the entire area of the Arve catchment is covered by forests, which are mainly localized

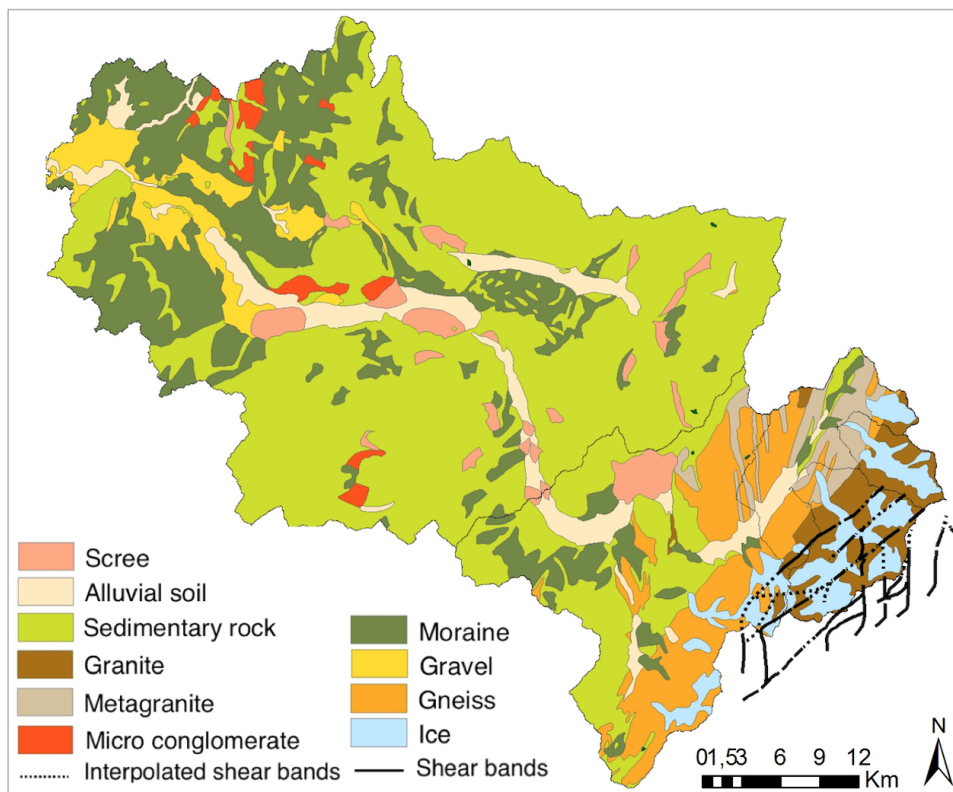


Figure I.3: Land cover map of the study area in 2000 (Corine Land Cover 2000, [Bossard et al., 2000](#)).

at low elevations (Table [I.1](#)). Bare rocks occupy the area close to the glaciers; they represent more than 30% of the surface area of the highly glacierized catchments, *i.e.* Arveyron d'Argentière, Arveyron de la Mer de Glace and Arve at Pont des Favrandes. Furthermore, they are also present along the Aiguilles Rouges ridges and the Chablais Alps, on the Swiss-French border. Agricultural lands and urban fabrics are concentrated in the lower part of the Arve valley. Sparsely vegetated areas and natural grassland range from 2% (Arveyron d'Argentière) to 15.6% (Arve at Sallanches).

The glacier extents provided by the CLC map are only indicative. We have adopted a more accurate estimation of glacier outlines, provided by [Gardent et al., 2014](#) and [Rabatel et al., 2016](#) (Section [I.2.4.2](#)).

I.1.4 Glaciers

The alpine chain is characterized by the presence of 3927 glaciers currently with a surface area of 2092 km², among which 105 km² are localized in the Arve catchment (values taken from the Randolph Glacier Inventory (RGI) version 6.0, released July 28, 2017; <https://www.glims.org/RGI/>). The retreat of these glacier is evident since the final phase of the Little Ice Age ([Vincent et al., 2005](#)).

The Arve drainage basin contains 64 glaciers, 51 with an extension smaller than 1 km²,

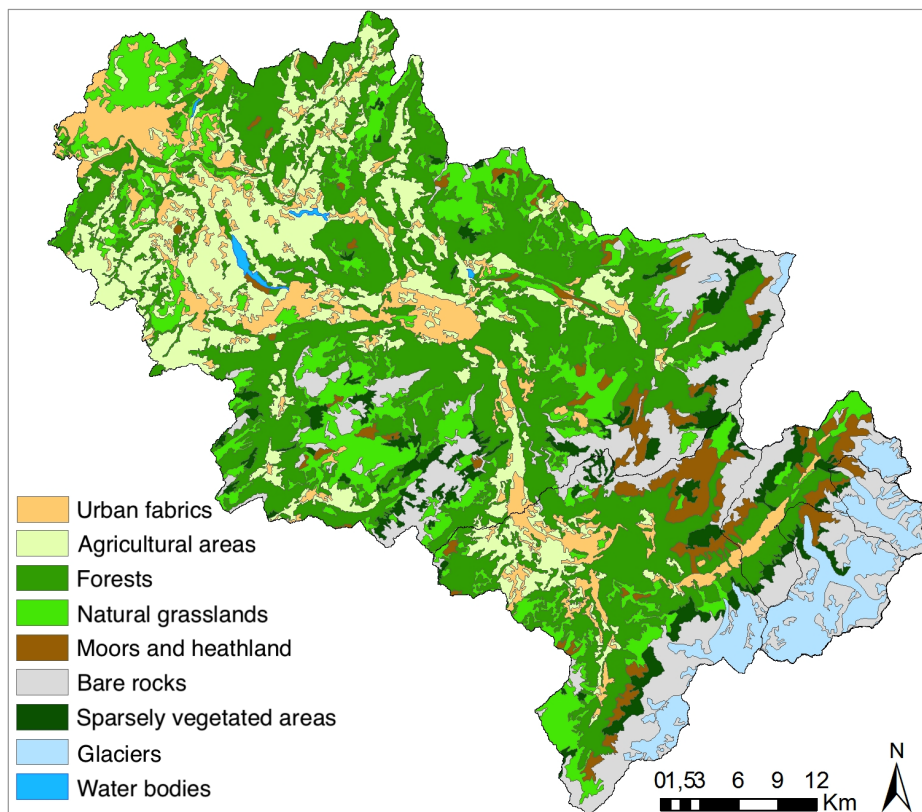


Figure I.4: Land cover map of the study area in 2000 (Corine Land Cover 2000, [Bossard et al., 2000](#)).

covering 5.3% of its entire surface area in 2003 ([Gardent et al., 2014](#)) (Fig. [I.5a](#)). The largest glaciers, localized in the upper eastern side of the overall catchment, are: Glacier du Tour (8.2 km² in 2003), Glacier d'Argentière (11.4 km² in 2003), and Glacier de la Mer de Glace-Leschaux (31.6 km² in 2003). Their major tributaries are Glacier des Améthystes (1.3 km² in 2003) and Glacier du Tour Noir (1.2 km² in 2003) for Argentière and Glacier de Talèfre (7.7 km² in 2003) for Mer de Glace-Leschaux. The extents of glacier covers given above in the brackets are obtained using Landsat and ASTER satellite images ([Rabatel et al., 2016](#); See Section [I.2.4.2](#)). Two of these largest glaciers belong to the GLACIOCLIM (Les GLACIers, un Observatoire du CLIMat) observatory (<https://glacioclim.osug.fr>, [Six and Vincent, 2014](#)), *i.e.* Glacier d'Argentière (Fig. [I.5b](#), Table [I.2](#)) and Glacier de la Mer de Glace-Leschaux (Fig. [I.5c](#), Table [I.2](#)), monitored since 1976 and 1979 respectively. On these glaciers the measured parameters concern glaciology, meteorology, hydrology and glacier thermal monitoring. Point measurements of the winter and annual mass balances are performed. The former ones are determined with stakes inserted in the boreholes down to the previous summer surface whereas the latter ones from wood stakes inserted in the ice. Furthermore, the thickness and the length fluctuations and the surface velocities of the glacier are measured using the DGPS (Differential Global Positioning System). To complete the permanent measurements, some temporary field campaigns to document a specific aspect of an environmental process are carried out, such as

the characterization of the turbulent flow using the Eddy-covariance method, surface albedo measures using a spectro-radiometer, bedrock mapping with a RADAR and surface topography using a terrestrial LIDAR.

The Argentière and Mer de Glace-Leschaux are valley glaciers, held in by the side of the mountains with a thin, convex tongue. The hypsometric curves of the glaciers and their tributaries are shown in Fig. I.2b. Their annual mass balance is consistently negative since 1987, except for 1995 (glaciological year 1994/95). In addition their cumulative mass balances reveal that the loss of ice has been more pronounced since 2001 (Vincent et al., 2009; Vincent et al., 2014).

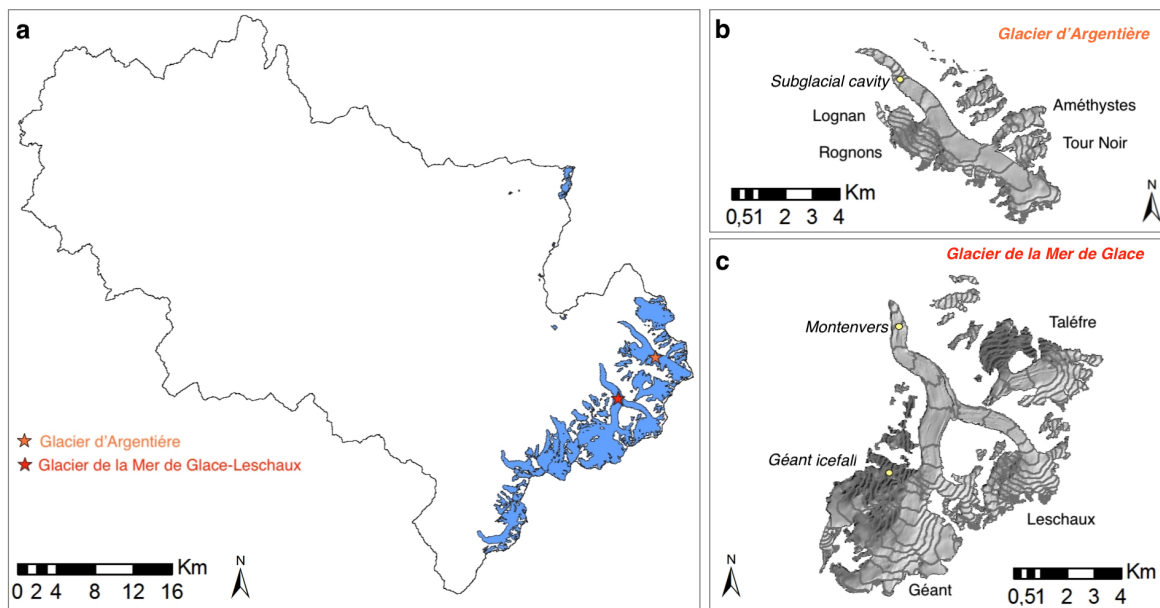


Figure I.5: (a) Glacier cover of the Arve catchment in 2003, obtained using Landsat and ASTER satellite images (Rabatel et al., 2016). The main glaciers considered in this work are indicated by a star; (b) Argentière and (c) Mer de Glace-Leschaux glaciers with all their tributaries in 2003.

Argentière

Glacier d'Argentière ($45^{\circ}55'$ N, $6^{\circ}57'$ E; 11.4 km^2 in 2003) extends from an altitude of 3738 m a.s.l. at the upper part to 1455 m a.s.l. at the snout in 2003. The length of the main glacier is ~ 10 km. It faces north, except for a large part of the accumulation area (south-orientated tributaries). Its ELA ranges between 2430 and 2914 m a.s.l. over the 1984–2014 period, with a mean values of 2772 m a.s.l. (Rabatel et al., 2013).

The first topographic measurements were performed on its ablation area in the beginning of the 20th century (Six and Vincent, 2014). Surface annual mass balances were monitored in the ablation area between 1975 and 1993, from 20–30 ablation stakes. Furthermore since 1993, systematic winter and summer mass-balance measurements have been carried out on the entire surface of this glacier (Vincent, 2002). 39 sites have been selected at various elevations representative of the whole surface, distributed over both ablation (30 sites) and accumulation

Table I.2: Main characteristics of the Argentière and Mer de Glace-Leschaux glaciers and their tributaries. The surface areas, elevations and Equilibrium-Line Altitudes (ELA) are obtained using satellite images (Rabatel et al., 2013). The number of measurement sites in the ablation and accumulation areas are also listed (Six and Vincent, 2014).

	Argentière	Mer de Glace-Leschaux
Main glacier tributaries	Améthystes, Tour Noir	Talèfre
Glacier surface area in 2003 in km ² (in % of the glacier drainage basin area)	15.7 (48.8)	42.3 (53.3)
Elevation range in 2003 (m a.s.l.)	1455–3738	1465–4221
Aspect	North-South	North-South
No. of stakes (accumulation area)	9	7
No. of stakes (ablation area)	30	31
Mean ELA main glacier (1984–2014) (m a.s.l.)	2772	2890

areas (9 sites).

A subglacial observatory has been set up at 2173 m a.s.l. to monitor the sliding movement continuously since 1997 (Fig. I.5b, Moreau, 1995). The sliding velocity is measured from a cavity that opens behind a bedrock bump using a 'cavitometer' designed by Vivian, 1975. It consists of a bicycle wheel with a circumference of 1.55 m attached to a 1.30 m long articulated arm that is fixed to the rock (Fig. I.6a). A 100 Ω potentiometer with 500 turns is used to measure the rotational movement of the wheel. Each turn of the potentiometer corresponds to 3.1 mm. The displacement is recorded on a paper attached on a rotating drum (Fig. I.6b). On the printed graph it is possible to count the number of turns and extract the daily velocities from the slope of the curve drawn. The accuracy of the measured daily sliding velocity has been assessed to be better than ± 1 cm d⁻¹ (Vincent and Moreau, 2016). A second potentiometer is set up on the articulation point of the arm. It is designed to measure vertical displacement on the cavity roof. In this way, the sudden downward acceleration related to the passage of the wheel on a rock inserted in basal ice can be detected. This happens very rarely and such records have been removed from data. The mean gliding speed measured over the 2000–2013 period is equal to 30 cm d⁻¹. In addition, since 2000 in this observatory the subglacial runoff is monitored in a gallery at 2060 m a.s.l.. It is measured during each summer season using an Endress Hauser sensor, with an accuracy of ± 0.1 m³s⁻¹ and a frequency of 15 min (Vincent and Moreau, 2016). Above a value of 13 m³s⁻¹, the water is diverted into another conduit, and the real runoff is not measured. The subglacial discharge is collected in a headrace tunnel directed to the Emosson lake for electricity production (Section I.1.5.1).

Mer de Glace-Leschaux

Mer de Glace-Leschaux (45°55' N, 6°57' E; 31.6 km²) is the largest glacier in all of France

and the third in the Alps, after Gorner (65km²) and Aletsch (80 km²) glaciers, both located in Switzerland. The glacier extends from an altitude of 4221 m a.s.l. to 3738 m a.s.l. in 2003. The width of the main glacier ranges from 700 to 1950 m. The mean ice thickness is 200 m, but may exceed the 400m. The length of this glacier is \sim 7 km. It faces north and is free of rock debris except for the tongue. The ELA of the main glacier ranges between 2537 and 3133 m a.s.l. over the 1984–2014 period, with a mean values of 2890 m a.s.l. (Rabatel et al., 2013).

The first topographic measurements were performed on the ablation area of Mer de Glace by Joseph Vallot at the end of the 19th century (Vallot, 1905). Since 1993, systematic point measurements of winter and summer mass balances of Mer de Glace-Leschaux and its main tributaries have been carried out at 38 sites, distributed over accumulation (7 sites) and ablation (31 sites) areas. In addition, annual surface mass balances were measured at 10–30 stakes in the ablation area between 1979 and 1993. However, these measurements were only collected systematically at the end of the ablation period from 1990 to 1993 (Vincent et al., 2009).

The ice flows rapidly: maximum surface velocities of 900 m yr⁻¹ were measured by Reynaud, 1973 and 700 m yr⁻¹ by Berthier and Vincent, 2012 at the Géant icefall, between 2700 and 2400 m a.s.l., using remote sensing measurements. Below Montenvers, at \sim 1900 m a.s.l., the gliding speed is estimated to be 30 m yr⁻¹ (Fig. I.5c).

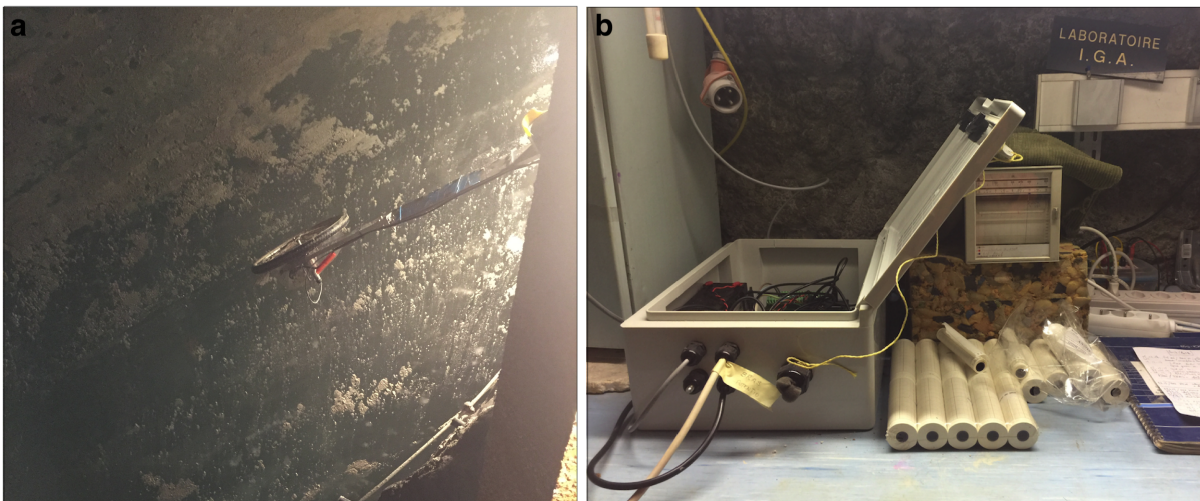


Figure I.6: (a) Cavitometer in the subglacial observatory seen from below; (b) Device to record/print the glacier displacement.

I.1.5 Hydropower

In the Arve catchment the anthropogenic influence is not negligible, since the streamflow is affected by various water withdraws for electricity production.

I.1.5.1 Description of the Waterpower Development

A first headrace tunnel (Collector South) drains the water coming from an area of 42.2 km² located in left bank of the Upper Arve river passing under the Argentière and Tour glaciers (Fig. I.7). This collector of 5.7 m² of section starts at 2060 m a.s.l. in the region of the Argentière, under Lognan glacier (Fig. I.5b). It is designed for a discharge of 12 m²s⁻¹ and is 8.55 km long. The water is routed to the Emosson lake, an artificial reservoir located in Switzerland managed by the hydroelectric power company Electricité d'Emosson S.A.. The Emosson lake is composed by a double-curved arch, with a crest 554 m long at 1931.50 m a.s.l. and a design flood water level of 180 m. It has a reservoir volume of 225 million m³ and collects also the waters coming from the French valley of the Eau-Noire, through the Collector West, and the Swiss ones of Val Ferret and Trient, through the Collector East (Fig. I.7). The Collector West drains an area of 12.70 km² and is 7.95 km long; the East ones has a contributing area of 115.25 km², it is 18.29 m long and is designed for a maximum discharge of 22.8 m²s⁻¹. The Collector North and the secondary Collector East drawn in the Fig. I.7 have not been built because of economic reasons. 50% of the Emosson lake volume comes from the Collector East and around 33% from the Collector South.

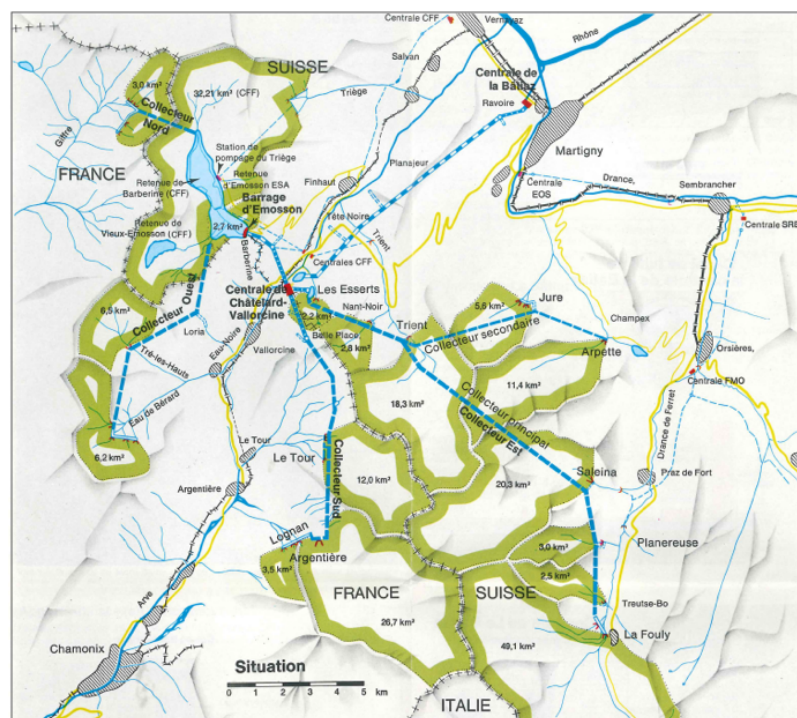


Figure I.7: Scheme of water withdrawals in the Upper Arve catchment, that are routed to the Emosson lake (Mottier, 1970).

The water produced by the French valleys is routed to the lake by gravity, while that of Swiss valleys by pumps (Fig. I.8). The power of the water storage in the Emosson lake is exploited by four hydroelectric power plants, two belonging to the Emosson S.A. Company, *i.e.* Centrale

de Châtelard-Vallorcine and Centrale de La Bâtiaz, and two to the Swiss Federal Railways (Compagnie des Chemins de Fer Fédérale, CFF), *i.e.* Centrale du Châtelard and Centrale de la Vernayaz (Fig. I.7). Then, the water is released in the Rhône river, close to Martigny (Switzerland). A mean gross head of 1400 m with two headraces is used to produce energy: the upper at Emosson-Châtelard-Vallorcine and the lower at Châtelard-La Bâtiaz. The overall production of the upper and lower headraces is 870 GWh, of which 250 GWh are produced in summer and 620 GWh in winter (Mottier, 1970). The Châtelard-Vallorcine power station is equipped with three ternary hydroelectric units with a vertical axis (Fig. I.8). The first (G1) consists of a three-phase alternator coupled with a Pelton turbine (5 injectors) with a capacity of 64000 kW and a Francis turbine with a capacity of 50000 kW. Both the second (G2) and the third (G3) units are composed by a three-phase alternator with a Pelton turbine and a three-stage storage pump with a capacity of 38200 kW. The Francis turbine and the pumps are fueled by a divider at low pressure while the Pelton turbines by one at high pressure. It has an installed capacity of 270 MW, for a maximum of 430GWh produced. La Bâtiaz power station is composed by two units with a vertical axis, each one with a three-phase alternator coupled with a Pelton turbine (5 injectors).

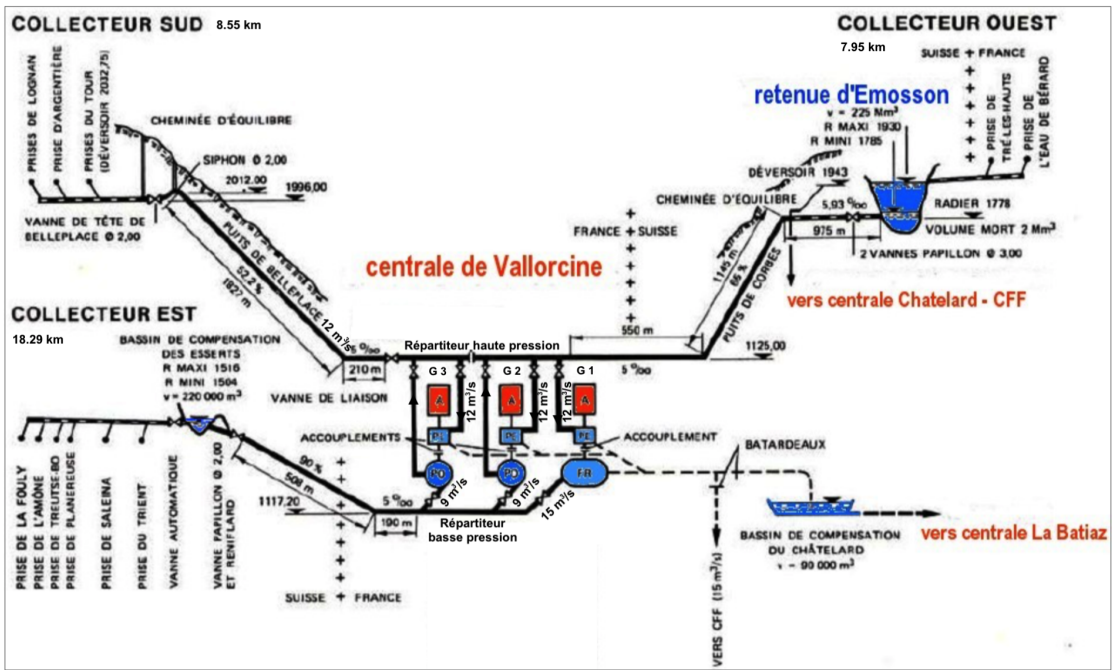


Figure I.8: Hydraulic scheme of the Emosson adductions and the Châtelard-Vallorcine hydroelectric power plant units (G1, G2 and G3).

A brief history of the Emosson Waterpower Development:

The Emosson Waterpower Development is the result of an agreement on transfer of water between France and Switzerland. At the beginning of the 1950s, studies carried out on the unexploited hydroelectric potentials in Switzerland have focalized the attention on the

Barberine-Emosson region, in the hinterland of Martigny (Switzerland). The project which foresaw the exploitation of the water resources on this area faced two problems: to provide the supply of the lake and to negotiate with the CFF who operate on the Barberine dam since 1920. EDF (Électricité de France) entered in the capital of Emosson Société Anonyme and an agreement provided for the use of 75 millions of m³ of water drained by a catchment in France in the Savoyard-Valais plant was signed with the CFF. The hydroelectric power company Electricité d'Emosson S.A was founded on 9 July 1954. In 1956 this partner company was 50% owned by EDF, 25% by Motor-Columbus S.A. and 25% by Aare and Tessin S.A. (ATEL). This company was established to develop and exploit the hydraulic force coming from the reservoir of the Emosson lake, supplied by the water of several valleys of the Valais and French Alps. On 23 August 1963 the French State and the Swiss Confederation reached two agreements concerning the use of the Emosson Waterpower Development and the rectification of the French borders. A third agreement was signed on 11 July 1967, fixing the reciprocal exchange of the territory: for safety reasons and in order that the plant is inspected according to the Swiss law once in service, France has ceded to Switzerland part of its national territory. In return, part of the Helvetic swiss territory is given to France. The Emosson Waterpower Development was built between 1969 and 1973 and the Emosson lake has been operating since July 1975. Following the agreement concluded in 2009, EDF took a 25% stake of the capital of the Alpiq Holding S.A. energy company which manages the Emosson group. To finance the increase of its stake in the capital of the Swiss company, EDF has brought to Alpiq Holding S.A. its right to energy from 50% stake in the Emosson dam, valued at 480 million euros in 2009.

Under the Mer de Glace-Leschaux glacier at 1560 m a.s.l., there is another collector that supplies the subterranean hydroelectric plant (Centrale des Bois, 1075 m a.s.l.) managed by EDF (Fig. I.9). The water coming from the melting ice of the Mer de Glace-Leschaux glacier is turbined (up to 15 m³s⁻¹) and then returns to the river upstream the Arveyron de la Mer de Glace hydrological gauging station. With an installed capacity of 42 MW, this power plant generates 115 million kWh of renewable energy, equivalent to the residential consumption of 50 000 habitants. The greatest part of the energy production is done during the melt season, from May to October (EDF, 2012). During winter, since the low temperatures does not allow to generate a sufficient energy production, the maintenance of the installation is performed.

When this hydroelectric plant started in 1973, the water intake took place 200 m under the ice, at 1490 m a.s.l.. In spring 2009, the water intake was out in the open and has been covered by a mass of glacial rock and sediment following a number of storms. To ensure the electricity production without having an impact on the landscape, EDF decided to move the intake upstream in the glacier under 100 m of ice. In 2008/2009, a temporary solution was found by digging a channel 150 m upstream of the old collector that allows to collect the subglacial runoff produced by the glacier and to ensure the functioning of the power plant over

the 2009–2011 period. A new uptake was built at 1560 m a.s.l. between the 2009 and 2011. It has been operating since April 2011 and is connected to the water intake by a permanent tunnel about 1 km.



Figure I.9: Scheme of the Waterpower Development under the Mer de Glace-Leschaux glacier. Figure based on an image taken from [EDF, 2016](#).

I.1.5.2 Impact on the catchment hydrology

The water withdrawals below the Argentière glacier strongly affect the hydrology of its drainage basin: the ratio between the volume of these extractions and the natural discharge reveals that during the melt season they represent $\sim 78\%$ of the water production of the Arveyron d'Argentière catchment, on average over the 1983–2004 period. Therefore, the discharge values registered by the gauging station located at the outlet of the Arveyron d'Argentière underestimate its real water production. Going downstream, the impact of the presence of the collector South became less marked. The water extractions represent $\sim 24\%$, 12% and 6% of the total water production (natural discharge) of the Pont des Favrandes, Arve at Sallanches and Arve at Bout du Monde catchments, respectively, on average over the 1983–2004 period.

On the contrary, since the outflow of the Les Bois hydroelectric power plant is located upstream of the Arveyron de la Mer de Glace hydrological gauging station, the direct anthropogenic influence on the discharge values measured at the outlet of this catchment can be considered negligible.

I.1.6 Climate setting and weather patterns

I.1.6.1 Climatology

The Arve catchment has a mountain climate, influenced by the height and location of the valley. The temperature is characterized by a marked annual cycle, with maxima in summer

and minima in winter (Fig. I.10a). Furthermore, it exhibits a diurnal cycle whose amplitude varies over time and altitude. Monthly temperature is characterized by a marked interannual variability, with a standard deviation ranging from 2.9 to 4.3°C. The annual mean temperature over the 1983–2009 period is equal to 7.3°C at Chamonix (1042 m a.s.l.), 10.8°C at Sallanches-La Charlotte (541m a.s.l.) and 11°C at Geneve-Cointrin (410 m a.s.l.). The mean altitude reached by the 0°C isotherm is at \sim 3600 m a.s.l. in summer and \sim 2100 m a.s.l. in winter, over the 1959–2012 period. The amount of total precipitation at monthly time scale is relatively stable all-year round, with a small reduction during springtime (Fig. I.10b). The highest precipitation amount falls in June at Chamonix (1042 m a.s.l.) and Sallanches-La Charlotte (541 m a.s.l.) while in October at Geneve-Cointrin (410 m a.s.l.). This difference is due to the orographic effects and the presence of summer rainstorms in the high mountains areas in comparison with the regions at lower elevations. The increase of precipitation with the altitude is also visible at monthly scale. The mean annual precipitation amount over the 1983–2009 period is equal to 1275 mm at Chamonix, 1146 mm at Sallanches-La Charlotte and 938 mm at Geneve-Cointrin.

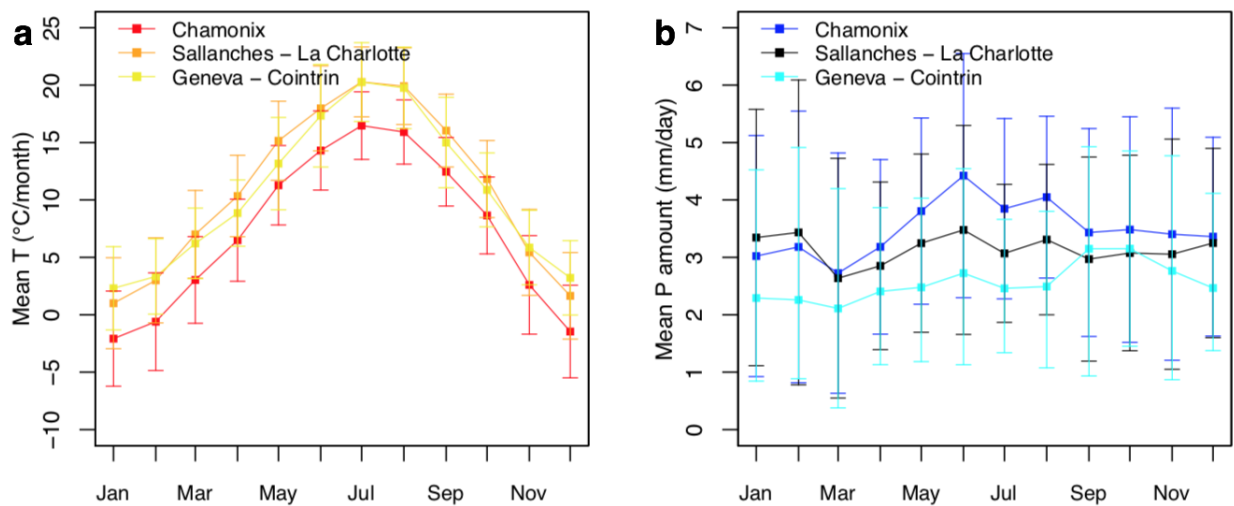


Figure I.10: Mean monthly (a) temperature and (b) precipitation amount over the 1983–2009 period registered by the meteorological stations at Chamonix (1042 m a.s.l.), Sallanches-La Charlotte (541m a.s.l.), and Geneve-Cointrin (410 m a.s.l.), in the Arve catchment (Fig. I.13, Section I.2.1).

I.1.6.2 Weather patterns

Precipitation are produced by the condensation of the atmospheric water vapor that falls under gravity. In mountainous areas, one of the main source of precipitation increase is the atmospheric uplift by hills and mountains (Barry, 2001). The spatial structure of the precipitation cannot indeed be dissociated from the influence of the large-scale atmospheric circulation (Littmann, 2000). The association between precipitation and pressure fields has been demonstrated by Bénévent, 1926. From this point of view, a classification based on a limited number of typical synoptic situations (or weather patterns, WP) is useful to link rainfall events with its

generating processes (Garavaglia et al., 2010). This approach has been used in several domains, such as the forecast of the avalanches (Obled and Good, 1980), temperature and precipitation interpolations (Jabot, 2013; Gottardi, 2009), downscaling the Global Climate Model (Courault and Monestiez, 1999) and more recently for the study of the extreme events of precipitation and flood (Paquet et al., 2006). A WP classification over France and surrounding areas has been established at EDF by Joël Gailhard. The WP were defined on the basis of the analogue method, used in a context of the quantitative precipitation forecasting (Duband, 1970; Djerboua, 2001; Obled et al., 2002). The similarity comes from the fact that in order to establish a classification of the rainy days in space, the definitions of the metric to measure the distance between synoptic situations and the centroids of the rainy classes are needed. The dataset used to define a daily synoptic situation in the EDF classification are the following (Guilbaud, 1997; Bontron, 2004): (i) geopotential height fields at 700 and 1000 hPa pressure levels, at 0 h and 24 h, defined on 110 grid points; (ii) analysis centered on south-eastern France; (iii) Twelves-Wobus score (Teweles and Wobus, 1954) as measure of proximity between synoptic situations. The eight WP obtained (Fig. I.11) are defined using a “bottom-up” approach, *i.e.* from the shape of the rain field to the synoptic situations described by geopotential fields (See details in Garavaglia et al., 2010). These patterns give an idea of the rainy synoptic situation over France. They were named in relation with the atmospheric circulation they generate: WP1 is referred to as Atlantic Wave, WP2 as Steady Oceanic, WP3 as South West-Circulation, WP4 as South Circulation, WP5 as North East, WP6 as East Return, WP7 as Central Depression, and WP8 as Anticyclonic. WP1 and WP7 are the rainiest patterns over our study area.

I.1.6.3 Hydrological regimes

The discharge of the five nested basins in the Arve catchment is characterized by a marked seasonal variation, in accordance with the temperature regime that induce high snow/ice melting, with high flow in summer and low flow in wintertime (Fig. I.12). Discharge volumes are clearly higher for the larger basins, with the highest runoff produced by the Arve at Bout du Monde, with a maximum annual value of about $133 \text{ m}^3\text{s}^{-1}$, on average over the 1983–2004 period. The lowest runoff is observed for Arveyron d’Argentière which is the smallest catchment compared to the others, with a maximum annual value of about $9 \text{ m}^3\text{s}^{-1}$, on average over the 1983–2004 period. The maximum discharge values given above are based on the real water production of the catchments, without being affected by the anthropogenic influence (Sections I.1.5.2 and I.2.2.1). During wintertime the discharge produced by the two highly glacierized catchments, *i.e.* Arveyron d’Argentière and Arveyron de la Mer de Glace, is basically zero as all the precipitation occurs in solid form due to the low temperatures. An almost constant winter streamflow induced by the rainfall and groundwater recession can be observed for the larger catchments, *i.e.* Arve at Sallanches and at Bout du Monde. The discharge seasonal

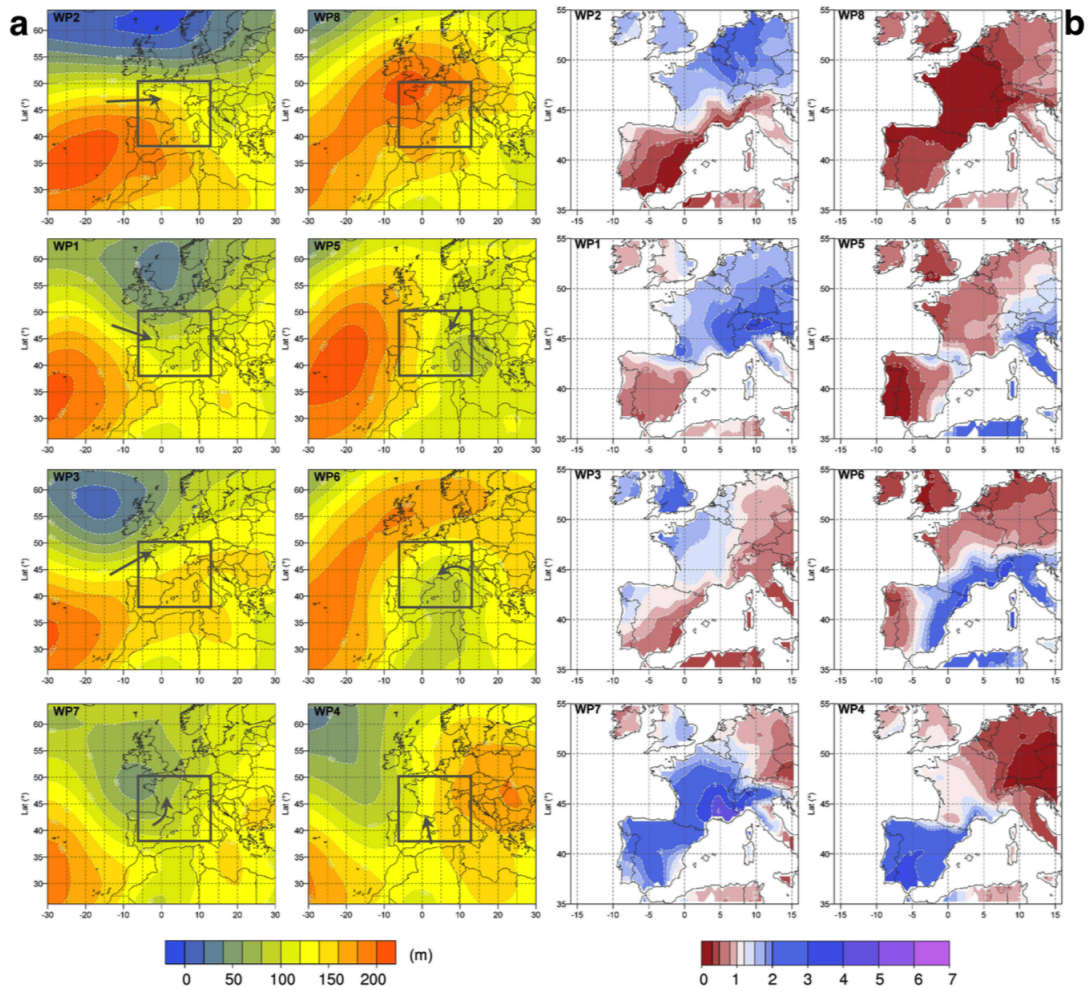


Figure I.11: (a) Average geopotential height at 1000 hPa of the eight WP and (b) the ratio of the mean WP to global mean precipitation. The arrows indicate the atmospheric flow of low layers (Source [Garavaglia et al., 2010](#)).

cycle is characterized by a marked interannual variability, which is generally small in winter and large over the melt season at Arveyron d'Argentière, Arveyron de la Mer de Glace and Arve at Pont des Favrands and at Sallanches, whereas at Arve at Bout du Monde it does not show a clear temporal pattern. It is interesting to note that the considered catchments are characterized by different hydrological regimes: nivo-glacial in the highly glacierized ones, with high flow rates in summer and low flow rates in wintertime when snowfalls accumulate on the ground, pluvio-nivo-glacial at Arve at Sallanches and pluvio-nival at Arve at Bout du Monde, characterized by a decrease in runoff during late summer related to the limited glacial cover. Furthermore, with the decrease in percentage of the glacier cover within the nested catchments, the discharge peak occurs earlier, *i.e.* at the end of July in the highly glacierized catchments, so advanced in the melt season, at mid-June for Arve at Sallanches and at the beginning of June for Arve at Bout du Monde, because of very limited glacier cover (5%).

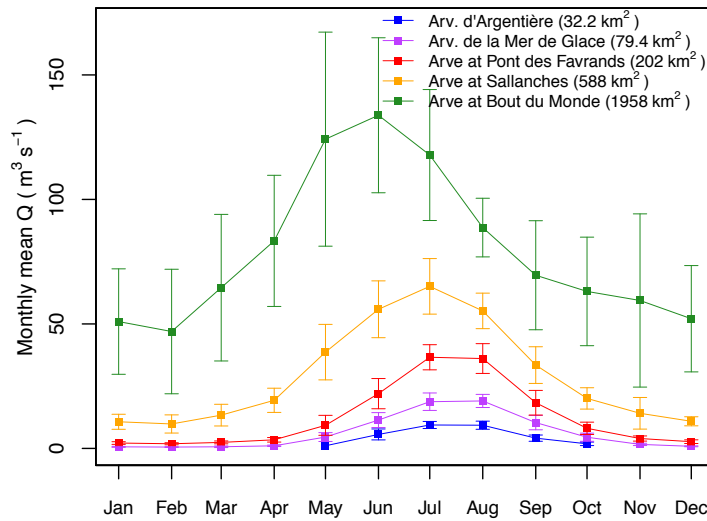


Figure I.12: Mean monthly discharge produced by the five nested catchments, without anthropogenic influences, considered over the 1983–2004 period. The bars represent the standard error.

I.2 Observation networks and instruments

I.2.1 Meteorological data

In this work two type of meteorological data are used: punctual observations and reanalysis. The punctual data are registered by 10 stations: 3 belonging to the Météo-France (MF) network, 1 to MétéoSwiss (MS) and 6 are part of an additional network that is temporarily installed in the Arve catchment during summer time. These considered datasets contain no missing data. The precipitation and temperature dataset provided by MF and MS network span over a long term period, while those of the additional network just on a short one (Table I.3). Trend analysis (Chapter II) have been done using the longer series, while the shorter ones are used to estimate the environmental lapse rate in the Arveyron d'Argentière catchment (Chapter IV). A summary of the coordinate and the elevation of the stations used are listed in Table I.3 and their locations are represented in Fig. I.13. Concerning the reanalyses, SAFRAN dataset are used (Chapters II, III and IV). To estimate the future evolution, the rates of change for the meteorological variables are obtained from ADAMONT v1.0 (Chapter II).

Table I.3: Characteristics of the meteorological stations used.

	Elevation (m a.s.l.)	Lat	Lon	Variable measured	Time-period
Chamonix (MF)	1042	45.92950	6.87750	T; P	1983–2009; 1934–2018
Glacier d'Argentière (MF)	2416	45.96806	6.97528	T; P; SR	2010–2019
Sallanches - La charlotte (MF)	541	45.93200	6.65100	T; P	1870–2018
Geneva - Cointrin (MS)	410	46.25000	6.13333	T; P	1981–2018
Albert 1er (S)	2709	45.99739	6.98753	T; P	2014–2018
Couvercle (S)	2691	45.91058	6.96691	T; P	2014–2018
Fond d'Argentière (S)	2830	45.94088	7.01771	T; P	2014–2018
Plan Aiguille (S)	2250	45.90327	6.88592	T; P	2014–2018
Requin (S)	2584	45.88407	6.92774	T; P	2014–2018
Station Argentière (S)	2434	45.96779	6.97611	T; P	2014–2018

MF: Météo-France network; A: additional network; MS: MeteoSwiss network; P: Precipitation; T: Temperature; SR: Solar radiation

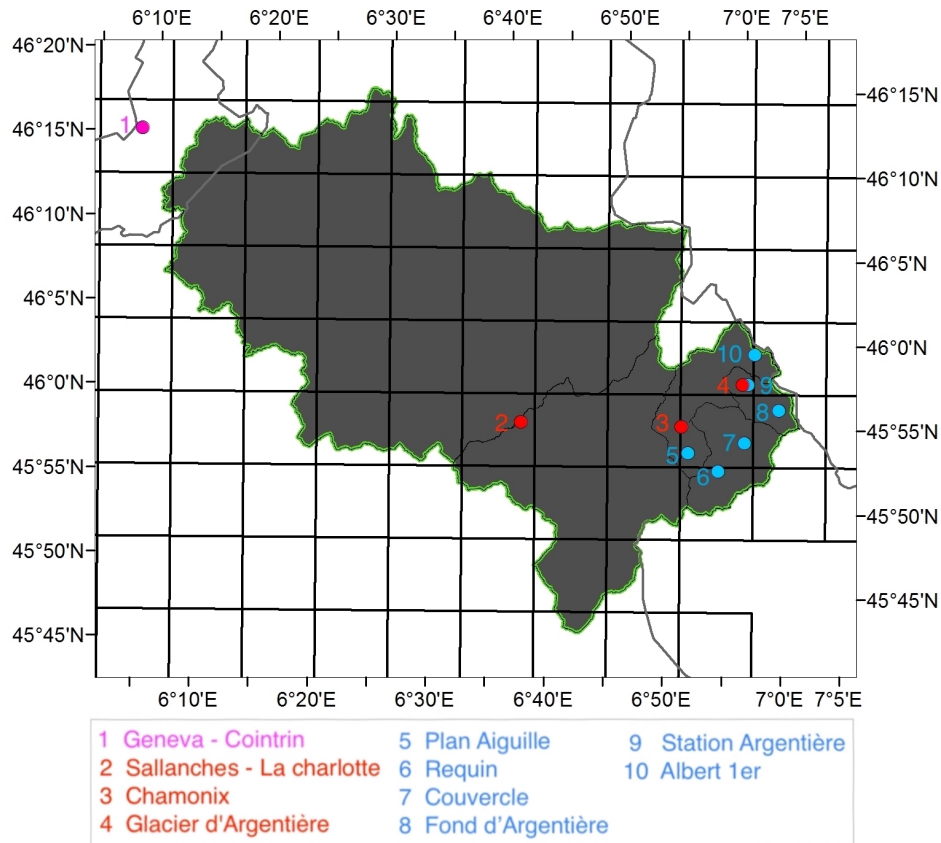


Figure I.13: The grid represent the size of the mesh (8 km resolution) of the SAFRAN-France and ADAMONT dataset. The red dots correspond to the meteorological stations belonging to the Météo-France network, the blue to those of the additional network and the purple to those of MétéoSwiss.

I.2.1.1 Punctual data

I.2.1.1.1 Météo-France network

The automatic weather station (AWS) located at Chamonix (1042 m a.s.l.) and the manual weather station (MWS) at Sallanches-La Charlotte (541 m a.s.l.) belong to the MF network (Chapters II and IV). The meteorological data are provided by the AWS at hourly time step whereas the MWS transmits the daily precipitation amount and the values of the daily minimum and maximum temperature to the MF central database. Both stations are equipped with heated tipping bucket rain gages that measure rain, snow, and other frozen precipitation. In addition, the values of the shortwave radiation in clear-sky days are used (Chapter IV). Since 2010, they are registered by the automatic weather station located on the moraine of Glacier d'Argentière (2416 m a.s.l.) (Fig. I.14a), that is equipped with a radiometer measuring the four components of the radiation balance (short and long wave incident and reflected) (Fig. I.14b).

I.2.1.1.2 Additional network

As part of the Arve-SM3A (Syndicat Mixte d'Aménagement de l'Arve et de ses Affluents) project consisting in the improvement of the knowledge related to the floods of the Arve River, since 2014 a temporary network of 10 meteorological stations is installed in the upper Arve catchment over each summer period, from mid-June to mid-October (Fig. I.14c). The objective of these additional stations is to allow the study of the meteorological variability at small scale in the upper Arve catchment. They are installed on both the Mont Blanc and Aiguilles Rouges massifs. Each meteorological station consists of a tipping bucket rain gage (Fig. I.14e) and a Multi-Plate Radiation Shield containing the HOBO Pendant Temperature/Event Data Logger (Fig. I.14d), to measure the intensity of the liquid precipitation and temperature, respectively, with a time step of 15 minutes. The data are stored locally in each station, and are regularly downloaded.

In this thesis, only the data provided by the 6 stations localized on the Mont Blanc massif (Table I.3, Fig. I.13) are used (Chapter IV).

I.2.1.1.3 MétéoSwiss network

The precipitation and air temperature data provided by the station located at Geneva-Cointrin (410 m a.s.l.) belonging to the MS network are used in the Chapter II. This automatic monitoring station is equipped with a heated tipping bucket rain gage that measures the total precipitation (solid and liquid phases) and transmits the weather and climate data every ten minutes to the MeteoSwiss central database. Here various quality checks are performed. The data are available since 1981.

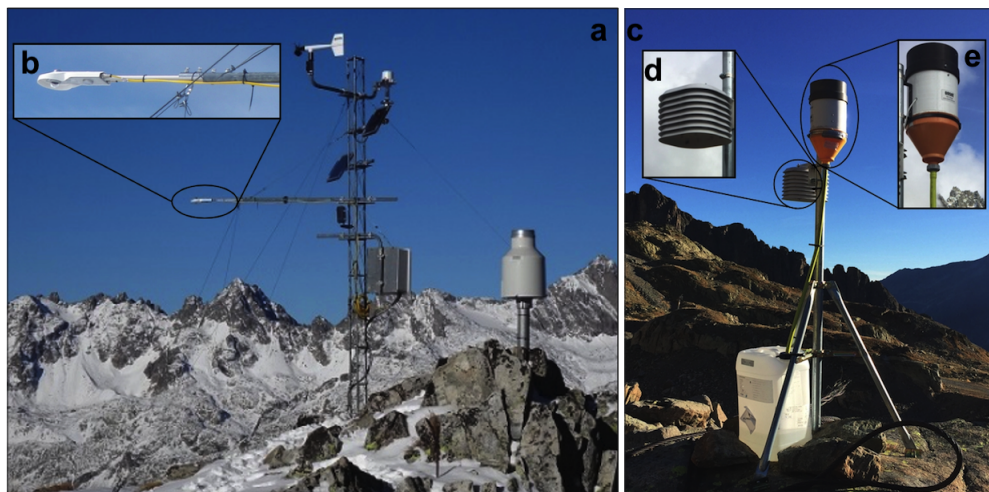


Figure I.14: (a) Automatic weather station on the Argentière Glacier (2416 m a.s.l.); (b) The radiometer installed; (c) Meteorological station belonging to the additional network; (d) Gill Multi-Plate Radiation Shield containing the HOBO Pendant Temperature/Event Data Logger sensor; (e) Tipping bucket rain gauge.

I.2.1.2 Reanalysis

I.2.1.2.1 SAFRAN

SAFRAN (Système d'Analyse Fournissant des Renseignements Adaptés à la Nivologie, [Durand et al., 1999, 2009](#)) is a mesoscale atmospheric analysis system for near-surface atmospheric variables (temperature, precipitation rate and phase, incoming shortwave and longwave radiations, wind speed and relative humidity). It produces an analysis at the hourly time step combining in situ and remotely sensed observations with prior estimation provided by the results of the ARPEGE (Action Recherche Petite Echelle Grande Echelle) French meteorological model ([Courtier et al., 1991](#)) or from the ECMWF (European Centre for Medium-range Weather Forecasts) analyses through appropriate downscaling operators ([Hagemann et al., 2005](#)). These datasets are available over the period 1958–2012.

The SAFRAN reanalysis is available under two different formats: SAFRAN-France (Chapter [II](#)) and SAFRAN-Bands-of-Altitude (Chapters [III](#) and [IV](#)). SAFRAN-France is available on a grid of 8km of resolution (distributed configuration, Fig. [I.13](#)) while SAFRAN-Bands-of-Altitude under a semi-distributed configuration. The SAFRAN-Bands-of-Altitude output are provided on 300-m elevation steps from 1200 to 3600 m a.s.l. for 23 areas of the French Alps, known as “massifs” (Fig. [I.15](#)). Each different massif have been defined for their climatological homogeneity ([Durand et al., 1993](#)). The spatial scale of the performed analyses determines the dataset that should be used, *i.e.* SAFRAN-France at regional scale and SAFRAN-Bands-of-Altitude at local one.

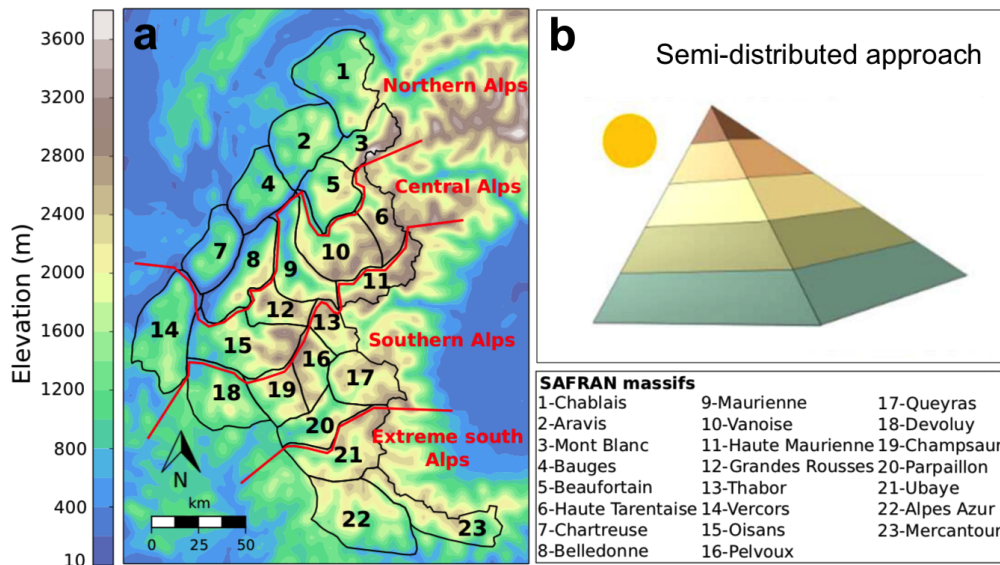


Figure I.15: (a) Contours of the SAFRAN-Bands-of-Altitude massifs (black) and limits of climatological regions (red) (Vionnet et al., 2016); (b) Schematic representation of the semi-distributed approach used by the SAFRAN-Bands-of-Altitude to account for mountain spatial heterogeneity (Revue et al., 2018).

I.2.1.3 Future climate projections

I.2.1.3.1 ADAMONT V1.0

ADAMONT v1.0 is a method of downscaling and bias adjustment of GCM+RCM (Global Climate Model - Regional Climate Model) projections in the French Alps based on a quantile mapping adjustment. The period covered ranges from 1950 to 2100 and the data are available with a horizontal resolution of 8 km. ADAMONT uses SAFRAN-Band-of-Altitude (Section I.2.1.2.1) as observational dataset (Fig. I.13). For details see Chapter II, Section II.3.1. In the current study, three GCMs/RCMs combinations (*i.e.* CNRM-CM5/ALADIN53 (r1i1p1 ensemble), MPI-ESM-LR/REMO2009 (r1i1p1 ensemble), EC-EARTH/RCA4 (r12i1p1 ensemble)) forced by RCP 2.6 are used. This dataset is used to estimate the rates of change of the meteorological variables over the periods 2030–2040 and 2050–2060 (Chapter II).

I.2.1.4 Precipitation phases

The separation of the precipitation phases (solid or liquid) is important in modelling the mass balance of the glacier, snow-cover dynamics and to determine whether water is available for runoff and infiltration, or is stored as snow. A misclassification of the aggregational state of precipitation might have a strong impact on the performance of the used model, since the hydrological processes of transformation of the precipitation into surface flow are different in case of snowfall or rainfall.

Thickness and the temperature of the atmospheric layers are the main factors influencing the precipitation phases (Gray and Prowse, 1993). In addition, even type of clouds, movement of the air masses and humidity may play an important role (Kienzle, 2008). Since in mountainous regions the snow and rain portions observed at the climate station cannot be transferred to location far from the measurement point because of the spatial variability of the precipitation due to the topographic effect, the air temperature is generally used for the partition of the precipitation phases (Braun, 1985). Nowadays, four approaches based on air temperature have been developed for discriminating precipitation phase: (i) a static threshold method (used in HBV model, *e.g.* Bergstrom, 1995); (ii) a linear transition of the portion of rain and snow (Pipes and Quick, 1977); (iii) a S-shaped curve describing the snow/rain transition (Kienzle, 2008); (iv) an approach in which the snow portion is function of the daily maximum and minimum temperature values (Leavesley et al., 1983). A review on the current tools for predicting precipitation phases could be found in Harpold et al., 2017. The estimations of the constant threshold and the interval of temperature are not easy: they require numerous observation and most of the time the weather stations don't specify which is the phase of the precipitation (Dingman, 2002). If no observed climate data are available in the considered area, values estimated in other studies focusing on the same region of interest should be used as initial default values (Kienzle, 2008). Several studies have been carried out to develop a relation between temperature and snow portion. In the Alps generally the used temperature range for the separation of the precipitation phases is $[-1^{\circ}\text{C} - +3^{\circ}\text{C}]$ (Boehm, 1975; Braun, 1985; Rohrer, 1989; L'hôte et al., 2005).

In this work, a constant threshold value is used to separate the precipitation phases to carry out the trend analysis (Chapter II), whereas the scheme used in the hydro-glaciological modeling consists in a gradual change of the proportion of rain and snow based on a linear transition over two degrees $[+1^{\circ}\text{C} - +3^{\circ}\text{C}]$ (Chapter IV).

I.2.2 Hydrological data

I.2.2.1 Surface hydrology

Five hydrological stations are used in this thesis (Table I.4). All the stations are equipped with a limnimentric scale and sensors such as radar or ultrasonic sensors. In the Argentière drainage basin, only the 43% of the data are available over the study period since the sensors are removed during winter. Because of the water withdrawals below the Argentière and Tour glaciers (Section I.1.5.1), the total discharge produced by four of the five considered nested catchments, *i.e.* Arveyron d'Argentière, Arve at Pont des Favrandes, at Sallanches and at Bout du Monde, are obtained by adding the data measured at the extraction point to the stream discharge values registered by the gauging station located at the outlet of each considered

catchment. The amount of the water withdrawals is provided by the company Electricité d’Emosson S.A. at daily time step. Since it is difficult to estimate the transfer time of the water between the collector and the hydrological gauging stations, the discharge reconstruction is done assuming that the water collected by the headrace tunnel on a day reaches the outlet of the nested catchments on the same day. This is a strong hypothesis which constitutes a source of an additional uncertainty of the discharge values.

On the contrary, the discharge values provided by the gauging station of the Arveyron de la Mer de Glace represent the real production of the catchment, because at this point the direct anthropogenic influence can be neglected (Section [1.1.5.1](#)).

Table I.4: Characteristics of the hydrological stations used.

	Altitude (m a.s.l.)	Lat	Long	Time period	Missing data (%)
Arveyron d’Argentière	1363	45.97678	6.94071	1955–2004	57.0
Arveyron de la Mer de Glace	1060	45.93462	6.88973	1950–2014	9.3
Arve at Pont des Favrandes	1020	45.91599	6.86042	1983–2010	7.2
Arve at Sallanches	535	45.93819	6.64014	1980–2015	28.4
Arve at Bout du Monde	380	46.18034	6.15947	1904–2013	0.0

EDF= Électricité de France

I.2.2.2 Subglacial hydrology

Glaciers are divided into three categories, depending on their thermal structure: cold, warm (or temperate) and polythermal ([Paterson, 1994a](#)). The bed of cold glaciers is generally below its pressure-melting point, implying no liquid water at the bed, except for thin layer up to 10–15 m thick that might warm to the melting point seasonally ([Cogley et al., 2011](#)). They tend to move slowly via internal deformation as a frozen glacier bed inhibits the rapid-flow mechanisms of sediment deformation and basal sliding ([Kleman and Glasser, 2007](#)). Cold glaciers exist in Antarctica and at high altitudes at lower latitudes. In the Alps, they are observed at altitudes above 3900 m a.s.l., *i.e.* Punta Gnifetti (4550 m a.s.l., Mont Rosa). Furthermore, a temperature profile from a cold glacier contains information on past climate conditions ([community Members et al., 2004](#); [Baccolo et al., 2018](#)). The bed of a warm glacier is at its pressure-melting point, except for a surface layer which may experience seasonal freezing. The presence of meltwater at the base of a glacier encourages basal sliding and rapid ice velocities. A polythermal glacier is an intermediate type; usually the highest accumulation areas are cold, whereas the surface and the base are at melting temperature. These glaciers typically move via basal sliding or subglacial deformation under warm-based ice, but only by internal ice deformation in the colder parts. Polythermal glaciers occur in different climates and at different geographic locations.

In warm and polythermal glaciers, the meltwater reaches the ice-bed interface through basal melting from geothermal heating and by ice melting under pressure from the weight of the ice mass above. The liquid water, generated from melting snow or direct input from rainfall is routed downwards by supraglacial and englacial systems (Fountain and Walder, 1998). The latter are structures in the ice produced by tension, such as crevasses (open fractures) and moulins (nearly vertical shafts), that allows the water to penetrate into the ice and reach the glacier bed (Fig. I.16). Subglacial water flows from zones of high pressure to zones of low pressure, in contrast with surface water that simply follows the surface slope (See details on Subglacial Water Flow in Lefeuvre, 2016). Several studies have shown that the basal water system affects the glacier's basal sliding motion (Bindschadler, 1983): increased water pressures reduce the frictional drag and increase the sliding rate (Moreau, 1995). The water pressure varies greatly in daily cycles and over seasons (*e.g.* Bartholomaus et al., 2008). Its variation also depends on the subglacial drainage system that can be of two different types: an efficient channelized type and an inefficient distributed type. The efficient system involves semi-circular channels incised in the ice (the R othlisberger channels, R othlisberger, 1972), Hooke channels that are in the ice, low and broad (Hooke et al., 1990) and Nye channels, that are incised in bedrock (Nye, 1976). This system is characterized by fast drainage. On the other hand, the inefficient distributed system water flows within a thin water film (Shoemaker, 1986) or sheet (Weertman, 1972) or through a linked cavity system (Walder, 1986; Fountain and Walder, 1998). As water is not evacuated efficiently, subglacial water is stored in this system and water pressure increases to near-overburden pressure (Schoof et al., 2014). Basal velocity can be estimated with different methods: from the difference between the measured surface velocities and the internal deformation obtained from inclinometers (*e.g.* Hooke et al., 1992), models (*e.g.* Hubbard et al., 1998) and direct observations in boreholes (*e.g.* Blake et al., 1994; Amundson et al., 2006; Ryser et al., 2014). Furthermore, direct measurements in the subglacial cavities are allowed by the tunnels excavated for hydroelectric projects (Moreau, 1995; Jansson et al., 1996; Lefeuvre et al., 2015)

In this work, the values of subglacial daily runoff produced by the Argenti ere glacier have been used in the Chapter IV to demonstrate the ability of the calibrated hydro-glaciological model to reproduce the interannual variability of the subglacial water production. Since 2000, the runoff is monitored in a gallery at 2060 m a.s.l. built in the subglacial observatory set up to monitor the glacier sliding movement (Section I.1.4).

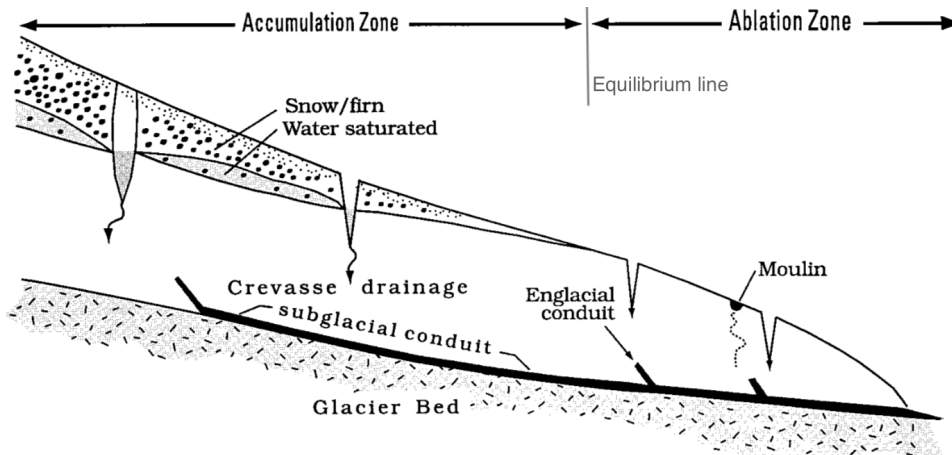


Figure I.16: Longitudinal cross section of a temperate alpine glacier showing the hydro-logical components (Figure based on the Figure 1 of [Fountain and Walder, 1998](#)).

I.2.3 Snow data

I.2.3.1 In-situ data: punctual snow depth observations

Punctual snow depth data are provided by four stations belonging to the MF observation network located in the upper Arve catchment at different elevations (Table [I.5](#)). At each station the temporal evolution of the snow depth is observed at daily time step through an ultrasonic snow depth sensor SR50A from Campbell Scientific. The instrumental error of these sensors (about 1 cm) is low compared to the spatial variability of snow depth in the meadow. Before being used, these data are corrected, checked and validated by MF. These data are used to estimate the amount of winter snow contribution to the summer discharge (Chapter [III](#)).

Table I.5: Location and characteristics of the punctual snow depth stations.

	Altitude (m a.s.l.)	Lat	Long	Time period	Missing data (%)
Chamonix (MF)	1025	45.91	6.86	1990–2018	11.7
Le Tour Nivo (MF)	1470	46.00	6.94	1990–2018	68.4
Lognan (MF)	1970	45.96	6.94	1995–2018	60.0
Aiguilles Rouges Nivos (MF)	2365	45.98	6.89	1990–2018	23.3

MF= Météo-France

I.2.3.2 MODIS data

The “Snow Cover Daily Tile” and “Fractional Snow Cover” of the Terra (MOD10A1) Moderate Resolution Imaging Spectroradiometer (MODIS) ([Riggs et al., 2009](#)) satellite sensors are adopted to identify the range of altitude characterized by the presence of snow at the beginning

of the summer (Chapter III). They are available since 2000, at daily time scale with a horizontal resolution of 500m.

The ‘‘Snow Cover Daily Tile’’ field from Aqua (MYD10A1) and Terra (MOD10A1) MODIS snow products version 5 are used to generate a daily gap-filled time series of the extent of the snow cover area with a horizontal resolution of 500 m since 2000 (Gascoin et al., 2015). These data are used to calibrate and validate the considered hydro-glaciological model (Chapter IV). The used gap-filled algorithm derived from (Parajka and Blöschl, 2008b) and (Gafurov and Bárdossy, 2009) consists in the sequence of the following four steps (see details in Gascoin et al., 2015):

1. Aqua/Terra combination: the value from MYD10A1 is taken for each pixel if no-data was found in MOD10A1;
2. Spatial deduction: a no-data pixel is re-classified as snow/no-snow if at least five of the eight adjacent pixels are classified as snow/no-snow;
3. Temporal deduction: a no-data pixel is re-classified as snow/no-snow if the same pixel is classified as snow/no-snow in both the previous and the following grids. These grids are selected within a sliding temporal window whose size is incremented up to 9 days accordingly to the position of the no-data value.
4. Classification tree: the class of the no-data pixels is predicted on the base of their geographic/topography characteristics, *i.e.* elevation, aspect, easting and northing.

I.2.4 Glaciological data

I.2.4.1 Mass balance

The punctual measurements of the winter surface mass balances of Argentière, Mer de Glace-Leschaux glaciers and their tributaries are available (Chapters III and IV). Since 1995, these measurements are done at the end of the accumulation season (end of April/beginning of May) by the GLACIOCLIM observatory (Six and Vincent, 2014). In the accumulation area, a PICO (Polar Ice Coring Office) ice drill is used to take out snow cores to get the layering and density of the snow in order to determine the water height equivalence. This technique makes it easy to measure the winter snow remaining at the end of summer by reading the stakes and prevents any possible misinterpretation of snow layering. In the ablation zone, winter mass balances were also measured by drilling cores. The uncertainties of these direct measurements have been assessed at ± 0.21 m w.e. yr^{-1} in the accumulation zone and ± 0.14 or ± 0.27 m w.e. yr^{-1} in ablation one depending on the surface concerned, *i.e.* ice or firn respectively (Thibert et al., 2008). As already said, the network of the in-situ surface mass-balance measurements

is composed of 39 sites on Argentière and 38 on Mer de Glace-Leschaux, distributed over both accumulation and ablation areas.

The glacier-wide annual surface mass balances of Argentière (Vincent et al., 2009) and Mer de Glace-Leschaux (Vincent et al., 2014) glaciers are used as explanatory variable of the discharge changes (Chapter II), to quantify the glacier-wide summer glaciological surface mass balances (Chapters III) and to carried out the calibration and validation of the used hydro-glaciological model (Chapter IV). Available from 1979 to nowadays, they are calculated using the multivariate statistical model proposed by Lliboutry, 1974 adjusted by the geodetic method (Vincent et al., 2017). The model assumes that the mass balance can be decomposed into two independent spatial and temporal variation terms. It allows to extract a temporal signal of the mass balance for each glacier. The obtained values using the models (glaciological method) have been corrected to match volumetric mass balances from geodetic measurements. The uncertainty in the glacier-wide annual surface mass balances of the Argentière glacier is estimated as ± 0.40 m w.e. yr^{-1} (Berthier et al., 2014).

I.2.4.2 Glacier surface area

Glaciers outlines on 1967, 1985, 2003 and 2012 are used to consider the evolution of the glacier surface area (Chapters II, III and IV). They are obtained using topographic maps (scale 1:25000) published by the French National Geographic Institute (IGN, Institut Géographique National, France), IGN 50-cm pixel orthophotographs, Landsat (Landsat 5 TM, Landsat 7 ETM + images) and ASTER GDEM V2 (27-m resolution, vertical accuracy of about 10 m; Tachikawa et al., 2011) satellite images (Gardent et al., 2014). Glacier outlines from topographic maps and orthophotographs have been manually delineated while those from Landsat and ASTER satellite images are obtained performing an automatic delineation followed by a manual adjustment. The uncertainties of the glacier outlines in the presence of clean ice/debris-covered ice are equal to 2–3.5 m for glaciers derived from orthophotos, 6–10.5 m for glaciers derived from topographic maps and 42–62 m for glaciers derived from satellite images (Gardent et al., 2014). They considered the errors associated with (i) the pixel size of the image; (ii) the visual identification and manual delineation of the glacier outline; (iii) the possible residual snow cover and (iiii) the process of geometric correction and georeferencing of the images.

I.2.4.3 Glacier equilibrium-line altitude

The equilibrium-lines altitude (ELA) of Argentière, Mer de Glace-Leschaux glaciers and their main tributaries are used in the Chapters III and IV. The ELA of a glacier separates the accumulation zone (where the annual mass balance is >0) from the ablation zone (where the annual mass balance is <0), *i.e.* is the point at which accumulation equals melting (Fig. I.16, Armstrong et al., 1973). Its position is determined by the climatological environment and the

net budget for each individual year (Kuhn, 1989). The ELA can be computed from direct field measurements of mass balance and snow accumulation using a network of ablation stakes and snow pits on the glacier considered (Young, 1981). Such approach allows to estimate the ELA at glacier scale but it still has limitations resulting from the scarce number of available in situ data due to the cost, in terms of money, manpower, and time and the difficulties in accessing measurement points. Alternatively, the ELA can be estimated using remote-sensing in areas where field observations are lacking or on regional scales (Østrem, 1975). For mid-latitude mountain glaciers, Lliboutry, 1965, Braithwaite, 1984 and Rabatel et al., 2005 have demonstrated that end-of-summer snow line altitude (SLA) is a good indicator of the ELA. This make the reconstruction of the ELA simpler, because the snow line is generally easy to identify using aerial photographs and satellite images (Lachapelle, 1962; Meier, 1980)

In this work, the temporal evolution of the ELA is reconstructed using the end-of-summer SLA computed from satellite images acquired by Landsat 4TM, 5TM, 7 ETM+, SPOT 1–5, and ASTER, with spatial resolutions ranging from 2.5 to 30 m (Rabatel et al., 2013). The snow line is delineated using multispectral images combining green, near-infrared, and short-wave infrared bands (Rabatel et al., 2012). To avoid to generate equilibrium-line position dependent on local conditions, the delineation of the snow line is computed on the central part of the glaciers to avoid border effects on the glacier banks. The total uncertainty of the SLAs, as the root of the quadratic sum of the independent errors, ranged from ± 15 to ± 170 m, depending on the year and glacier concerned (See details in Rabatel et al., 2013). These data are available since 1984.

I.2.5 DEMs and land cover maps

The RGE ALTI DEM provided by the IGN with a horizontal resolution of 5m is used to extract topographic information. In the Chapter III three additional DEMs are considered to estimate the rate of glacier volume changes. The first one, dated to 1979 for the Mont Blanc massif, is a photogrammetric DEM with a horizontal resolution of 25 m provided by IGE (Berthier et al., 2006). The two others DEMs, with 20 m resolution, are derived from SPOT5 2.5 m stereo-pairs acquired on 8 August 2003 and 15 October 2011 (Rabatel et al., 2016).

The land cover is investigated using the CORINE Land Cover (CLC) map produced in 2000, 2006 and 2012 generated with an automatic classification for the whole of Europe (EEA, 2007, <https://land.copernicus.eu/pan-european/corine-land-cover>). The CLC inventory consists of land cover divided in 44 classes. CLC uses a Minimum Mapping Unit of 25 ha for areal phenomena and a minimum width of 100 m for linear phenomena. The maps are obtained from satellite data, such as Landsat-7 ETM single date for the CLC2000, SPOT-4/5 and IRS P6 LISS III dual date for the CLC2006 and IRS P6 LISS III and RapidEye dual date for the CLC2012.

Chapter II

Characterization of the current and future glacier influence on the discharge seasonal cycle of five nested catchments in the French Alps

This chapter in its current form is under review in the Journal of Hydrology (HYDROL29345): **Viani, A.**^{1,2}, Condom, T.¹, Rabatel, A.¹, Panthou, G.¹, Sicart, J.E.¹, Gouttevin, I.³ and Ranzi, R.². Characterization of the current and future glacier influence on the discharge seasonal cycle of five nested catchments in the French Alps. *Under review in Journal of Hydrology.*

¹ University of Grenoble Alpes, CNRS, IRD, Institut des Géosciences de l'Environnement (IGE) - UMR 5001, Grenoble, France; ² Department of Civil Engineering, Architecture, Land, Environment and Mathematics (DICATAM), University of Brescia, Brescia, Italy; ³ Météo-France - CNRS, CNRM UMR 3589, Centre d'Études de la Neige (CEN), Grenoble, France

Summary of the research paper

Paper 1

Viani, A., Condom, T., Rabatel, A., Panthou, G., Sicart, J.E., Gouttevin, I. and Ranzi, R. **Characterization of the current and future glacier influence on the discharge seasonal cycle of five nested catchments in the French Alps.** *Under review in Journal of Hydrology - (HYDROL29345). Submitted the 18th September, 2018.*

In this paper, the past changes and the future evolution of the discharge seasonal cycle of five nested catchments along the Arve River (*i.e.* Arveyron d'Argentière, Arveyron de la Mer de Glace, Arve at Pont des Favrandes, Arve at Sallanches and Arve at Bout du Monde) are presented. These catchments are influenced by glacier and snow melt but are characterized by a various percentages of glacier cover ranging from 5% to 53%. Trend analysis are performed on the hydrological and meteorological series over the 1983–2004 period and only including the discharge dataset over 1960–2004, depending on data availability. Changes in the discharge are related to observed changes in the meteorological variables and the glaciers behaviors. In addition, a principal component analysis is carried out to evaluate the sensitivity of the seasonal cycle to the future climate for the 2030–2040 and 2050–2060 periods. This work is original in several aspects. Firstly, it focuses on a highly glacierized area. Secondly, a combined analysis of the discharge volume production and changes in glacier volume is performed in order to evaluate the contribution of the glaciers to the streamflow. Lastly, a mathematical function composed of two half-gaussian curves (the asymmetric peak model, APM) is used to describe the discharge seasonal cycle. To focus on the discharge changes driven by glacier and snow melt processes, the APM is performed on a filtered discharge dataset so as to remove the isolated rainfall-induced peaks.

This research can be used to complete the results of previous studies and helps improve our understanding of the temporal and spatial evolution of the discharge seasonal cycle in high-alpine glacierized catchments.

This study has led to the following results and conclusions:

- The temperature increase plays an important role in the discharge changes, resulting in an increase in the snow/rain limit, an early snowmelt season and a reduction in the seasonal snow cover.
- Over the 1983–2004 period, the precipitation does not show a clear temporal variation at all the considered stations.
- The APM is well suited to reproduce the seasonal cycle of the catchment with a nivo-

glacial regime. The percentage of glacier cover required for high performances of the APM must be greater than 30%.

- The trend analysis on the discharge values points out a contrasting behavior among the catchments characterized by different glacier covers, showing an increase in highly glacierized catchments and a decrease in the low glacierized ones, over both 1960–2004 and 1983–2004 periods. The observed discharge reduction may be influenced by the changes in land use and in the evapotranspiration losses, but further investigations are needed to quantify the proportion due to each processes.
- Moving from 1960–2004 to 1983–2004 periods the magnitude of the increasing trend on the discharge registered at Arveyron d’Argentière and Arveyron de la Mer de Glace (highly glacierized catchments) became less pronounced. These changes underline the relationship between the discharge of highly glacierized areas and glaciers changes.
- Mer de Glace glacier could have already passed or would be currently passing the phase of enhanced contribution to the total discharge; meaning that the increase in melt rate does not compensate the reduction in glacier surface area.
- Glaciers do not seem to strongly affect the regime of the catchments with glacier cover less than 20%. However, we must be careful to draw a conclusion because at this scale the anthropogenic impacts may mask the influence of the glaciers.
- The PCA help to shows that temperature can be considered as the main driving force of the evolution of the discharge seasonal cycle in high-mountain catchments.
- Under future climate condition, in the mid-21st century, the peak of the discharge seasonal cycle of the highly glacierized is projected to decrease and to occur later compared with the 1983–2004 period. The discharge values tend to increase in early summer because of an earlier snowmelt due to a marked temperature increase, and to decrease in the late summer, because of the decrease in glacier melt contributions.

Abstract

This study assesses the evolution of the seasonal discharge cycle of five nested catchments located along the Arve River (French Alps) characterized by various percentages of glacial cover (from 5 to 53%) and hydrological regimes. The seasonal cycle of each catchment is fitted using a mathematical function (the asymmetric peak model, APM) characterized by four main parameters. Trend analyses are performed on the discharge values, the APM parameters and on the hydrological and meteorological series, at both annual and seasonal scales. Changes in the discharge are related to the observed changes in the meteorological variables and in the evolution of the glaciers. Two time periods are considered: a short one (1983–2004) for which all of the hydrological and meteorological data are available, and a longer one (1960–2004) that only includes the hydrological dataset. The APM gives better performances for catchments with a glacier cover higher than 30%. The discharge produced by highly glacierized catchments exhibits an increase at both annual and seasonal scales. Conversely, that of the low glacierized catchments shows a negative trend probably related to changes in land use. Although the air temperature showed a marked increase in terms of the mean, maximum and minimum values at all of the sites, the precipitation trends are mostly not statistically significant. Going from the longer time period (1960–2004) to the shorter one (1983–2004), the magnitude of the discharge trend observed in highly glacierized catchments becomes less marked, highlighting the influence of glacier changes. Last, the sensitivity of the hydrological cycle to future climate change for the 2030–2040 and 2050–2060 periods is analyzed. In the mid-21st century, the peak of the discharge seasonal cycle is projected to decrease. In addition, discharge values are expected to increase in early summer, due to an earlier snowmelt, and to decrease in late summer, because of the decrease in glacier melt contribution.

KEYWORDS: Trend analysis; Discharge seasonal cycle; Hydrological regime; Glacierized catchment; Ice volume change.

II.1 Introduction

Historical changes in atmospheric and hydrological variables must be detected and characterized in order to predict their potential future changes (Zhang et al., 2001). This is especially valid for high mountain catchments characterized by glaciers identified as sensitive indicators of climate variability at different scales (Oerlemans and Fortuin, 1992; Haeberli, 2005; Vaughan et al., 2013).

Alpine glaciers have shown a general loss in mass over the last decades with an increasing

trend since the early 2000s (e.g., Vincent et al., 2004; Huss et al., 2010; Rabatel et al., 2016; Vincent et al., 2017; Beniston et al., 2018). Glaciers affect the catchment hydrology even for low percentages of glacier coverage and constitute an important water reservoir in the form of snow and ice (Jansson et al., 2003). In temperate regions, the precipitation is stored on the glaciers during the winter season and is released by summer melt, producing a marked seasonality in the discharge. This leads to significant differences in the hydrological behavior of glacierized basins compared to non-glacierized ones (Chen and Ohmura, 1990). Higher glacier melts increase the annual runoff; however, this increase is limited in time. When the glacier surface becomes too small, the increasing melt rates do not compensate the glacier shrinkage and the total amount of water provided by the glacier decreases, as well as the streamflow assuming no change in precipitation (Huss et al., 2008). The peak of water discharge is frequently called 'peak water' (e.g., Huss and Hock, 2018). Therefore, it is useful to analyze the hydrological records in order to determine if there are changes that can be used as indicators of climate variations (Zhang et al., 2001). Given that long-time series in highly glacierized catchments are rarely available, very few studies have paid attention to providing evidence for changes in high-alpine runoff (e.g., Birsan et al., 2005; Pellicciotti et al., 2007, 2010; Weber et al., 2010; Bard et al., 2015). In the French region, Giuntoli et al., 2012 performed a trend analysis on streamflow data at both local and regional scales, but with no focus on glacierized catchments. Furthermore, based on runoff series arising from a set of French rivers, Lang et al., 2006,

Renard, 2006 and Renard et al., 2008 detected the trends at national and regional scales. Due to the numerous socio-environmental services provided by high mountain snow fields and glaciers, such as water resources for municipal and industrial supplies, irrigation and hydropower production (e.g., Barnett et al., 2005; Viviroli et al., 2007, 2011), changes in hydrological regimes pose new challenges for water resources management (Gabbi et al., 2012). For this reason, several studies have recently addressed the evaluation of the effects of climate change on discharge projections in alpine catchments (e.g., Horton et al., 2006; Schaeffli et al., 2007; Farinotti et al., 2012). It is assessed that glacier shrinkage will continue throughout the 21st century in response to climate warming causing an increase in runoff in early summer and a decrease in late summer (Huss and Hock, 2018).

Within this context, the purpose of this study is to assess the past changes and to estimate the future evolution of the discharge seasonal cycle of five nested catchments along the Arve River (French Alps), influenced by glacier and snow melt but characterized by a various percentages of glacier cover ranging from 5 to 53%. To this end, our aims are to: (1) perform a trend analysis on the observed discharges of each catchment over a shorter common period (1983–2004) and a longer one (1964–2004) depending on data availability; (2) investigate the meteorological causes of the observed changes in streamflow; (3) identify the meteorological and glaciological variables that can be used to reproduce the evolution of the discharge seasonal cycle driven by the glacier and snow melt contributions; and (4) evaluate the sensitivity of

the discharge seasonal cycle in highly glacierized catchments to future climate change for the 2030–2040 and 2050–2060 periods. To estimate the future evolution, the rates of change for the meteorological variables are obtained from ADAMONT v1.0 which provides downscaling of the Global Climate Model-Regional Climate Model (GCM+RCM) projections in the French Alps based on quantile mapping adjustments (Verfaillie et al., 2017). The analysis described here is original in several aspects. Firstly, it focuses on a highly glacierized area. Secondly, a combined analysis of the discharge volume production and changes in glacier volume is performed in order to evaluate the contribution of the glaciers to the streamflow. Lastly, a mathematical function composed of two half-gaussian curves, hereafter called the asymmetric peak model (APM), is used to describe the discharge seasonal cycle. This research can be used to complete the results of previous studies by performing a trend analysis on the meteorological and hydrological data collected in glacierized catchments.

The paper is organized as follows. Sections 2 and 3 describe the study sites and the dataset. The methods developed and used to investigate the seasonal cycle of the streamflow are presented in Section 4. The results are presented in Section 5 and discussed in Section 6. The conclusions and perspectives are given in Section 7.

II.2 Study site

This study focuses on five nested catchments, *i.e.* Arveyron d’Argentière, Arveyron de la Mer de Glace, Arve at Pont des Favrand, Arve at Sallanches and Arve at Bout du Monde, located in the Arve River valley in the region of Haute-Savoie (Figs. II.1a and b). The Arve drains the northwestern side of the Mont Blanc massif before flowing into the Rhone River in the west of Geneva (Switzerland). The nested catchments considered here differ in terms of surface area, elevation range as well as glacier and land covers (Table II.1). Their surface area ranged from 32.2 km² (Arveyron d’Argentière) to 1958 km² (Arve at Bout du Monde), their elevation at the outlet from 380 to 1363 m a.s.l. and in 2003 their glacier cover from 5% (Arve at Bout du Monde) to 53% (Arveyron de la Mer de Glace). In 2000, the extent of the forested and natural areas ranged from 11% (Arveyron d’Argentière) to 58% (Arve at Bout du Monde) (Bossard et al., 2000). Agricultural lands are concentrated in the lower part of the Arve catchment.

The entire Arve drainage basin contains 64 glaciers (Gardent et al., 2014) among which 51 have an extension smaller than 1 km² (Fig. II.1b) (Rabatel et al., 2016). The largest glaciers are: Tour (8.2 km² in 2003) (Fig. II.1c), Argentière (11.4 km² in 2003) with its main tributaries Glacier des Améthystes (1.3 km² in 2003) and Glacier du Tour Noir (1.2 km² in 2003) (Fig. II.1d), Mer de Glace-Leschaux (31.6 km² in 2003) and its main tributary Talèfre (31.6 km² and 7.7 km² in 2003, respectively) (Fig. II.1e). Among these glaciers, two belong

to the GLACIOCLIM observatory: Glacier d’Argentière, monitored since 1976, and Glacier de la Mer de Glace-Leschaux, since 1979 (Table II.2). In average, their equilibrium-line altitude (ELA) has been close to 2800 m a.s.l. over the past 30 years (Rabatel et al., 2013). In the present study, due to data availability, attention is primarily focused on Glacier d’Argentière and Glacier de la Mer de Glace-Leschaux as well as on all of their tributaries. Hereafter, Arveyron d’Argentière, Arveyron de la Mer de Glace and Arve at Pont des Favrands will be referred to as highly glacierized catchments while Arve at Sallanches and at Bout du Monde as low glacierized ones.

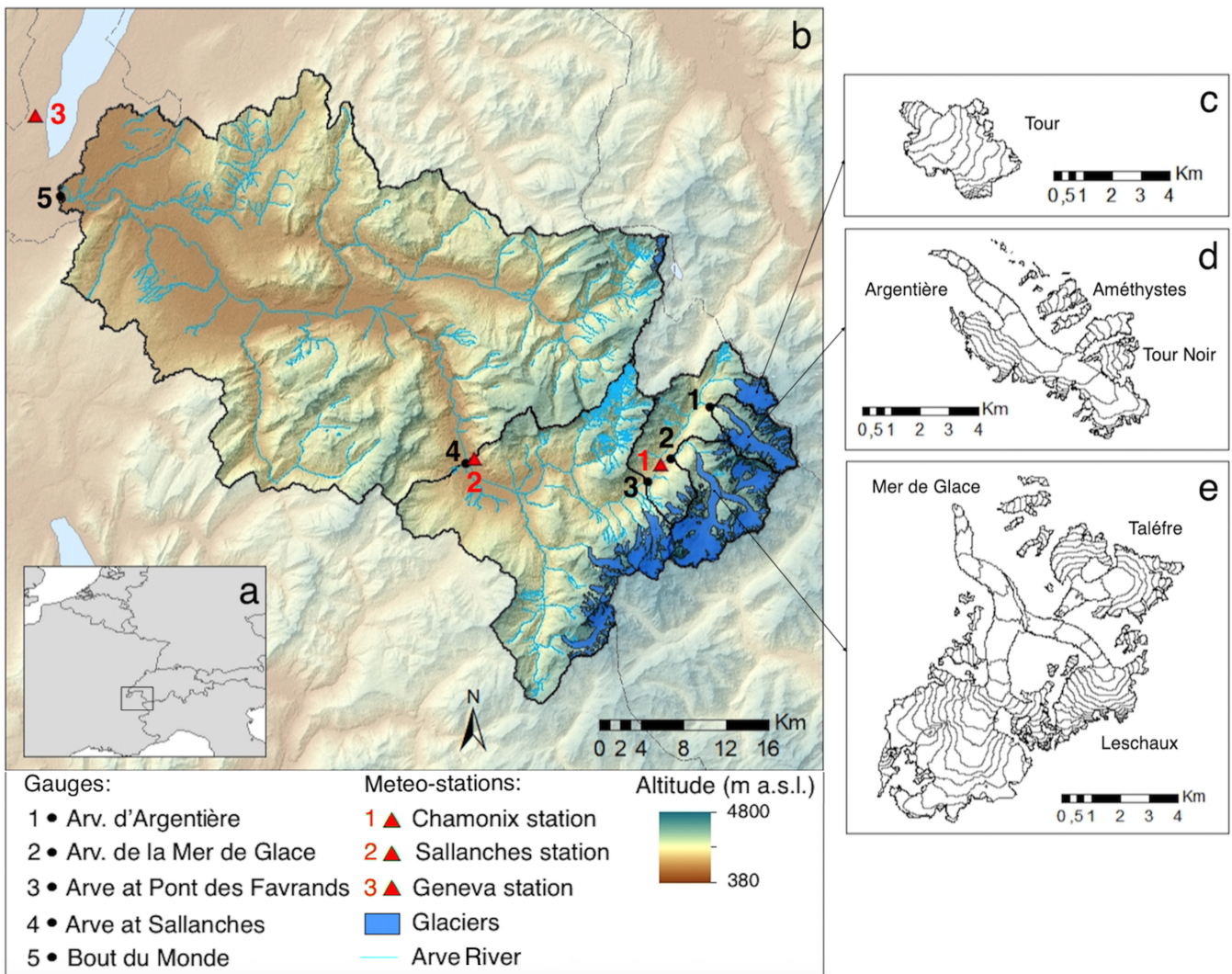


Figure II.1: (a) Location of the study area. (b) Topography of the five nested catchments in the Arve River valley. The black points and red triangles respectively indicate the location of the hydrological gauging stations of the catchments considered here and the meteorological stations. The 63 glaciers located in these catchments in 2003 are shown in blue. The black narrows highlight the location of the largest glaciers presented with all of their tributaries in 2003 (Gardent et al., 2014; Rabatel et al., 2016), such as c) Glacier du Tour d) Glacier d’Argentière and e) Glacier de la Mer de Glace-Leschaux.

Table II.1: Main characteristics and land uses of the five considered catchments. The glacier cover is obtained using Landsat and ASTER satellite images (Rabatel et al., 2016) while the land cover is taken from Corine Land Cover (CLC) 2000 (Bossard et al., 2000). The elevation of the catchments reported below may differ slightly from the true one due to the DEM resolution.

	Arveyron d'Argentière	Arveyron de la Mer de Glace	Arve at Pont des Favrans	Arve at Sallanches	Arve at Bout du Monde
Surface area (km ²)	32.2	79.4	202	588	1958
Median altitude (m a.s.l.)	2880	2865	2498	1900	1330
Elevation range (m a.s.l.)	1363–4079	1060–4295	1020–4295	535–4800	380–4800
Glacier cover in 2003 (%)	48.8	53.3	34.2	17.3	5.3
Forest in 2000 in km ² (in %)	0.7 (2.2)	3.0 (3.7)	26.0 (12.8)	154.4 (26.3)	695.9 (35.5)
Natural areas in 2000 in km ² (in %)	2.8 (8.8)	7.0 (8.8)	40.4 (20.0)	144.6 (24.6)	449.0 (22.9)
Urban fabric in 2000 in km ² (in %)	0.0	0.04 (0.1)	5.8 (2.9)	35.4 (6.0)	159.2 (8.1)
Bare rocks in 2000 in km ² (in %)	14.3 (44.4)	24.5 (30.9)	61.8 (30.6)	125.0 (21.3)	243.3(12.4)
Agricultural areas in 2000 in km ² (in %)	0.0	0.0	0.2 (0.1)	31.9 (5.4)	309.3 (15.8)

Table II.2: Characteristics of the two considered glaciers presented in the upper part of the Arve catchment. Their surface areas, elevations and equilibrium-line altitude (ELA) are obtained using satellite images (Rabatel et al., 2013, 2016).

	Argentière	Mer de Glace-Leschaux
Main glacier tributaries	Améthystes, Tour Noir	Talèfre
Glacier surface area in 2003 in km ²	15.7	42.3
Elevation range in 2003 (m a.s.l.)	1455–3738	1465–4221
Aspect	North-South	North-South
Mean ELA main glacier (1984–2014) (m a.s.l.)	2772	2890

II.3 Dataset

II.3.1 Meteorological data

Meteorological data are collected by three weather stations: two automatics (AWS) located at Chamonix (1042 m a.s.l.) and Geneva-Cointrin (410 m a.s.l.), and one manual (MWS) at Sallanches-La Charlotte (541 m a.s.l.) (Fig. II.1b). Air temperature and precipitation data are available at hourly time steps for the AWS whereas for the MWS daily values of minimum and maximum temperature and daily precipitation amount are available. These stations are selected based on their locations and the length of the available time series. Their datasets

contain no missing data. The AWS in Geneva is associated with the Arve at Bout du Monde catchment, the one in Sallanches-La Charlotte with the Arve at Sallanches and the one in Chamonix with the three highly glacierized catchments. It should be noted that long-term meteorological records at high altitudes close to glaciers do not exist. For each meteorological station the period of data availability is listed in Table II.3.

ADAMONT v1.0 is a method used to downscale and adjust biases in regional climate projections. It has been applied to EURO-CORDEX GCM-RCM (Global Climate Model-Regional Climate Model) couples to provide ensemble projections in the French Alps based on various future radiative forcing scenarios (Representative Concentration Pathways, RCPs) (Verfaillie et al., 2017). The approach used for ADAMONT consists of adjusting the quantiles of the simulated historical distributions to the quantiles of the SAFRAN meteorological reanalysis (Durand et al., 1993, 1999, 2009) which is considered as an observational dataset. Then, similar corrections are applied to the projections. This method allows to obtain continuous projections of hourly near-surface atmospheric variables, such as temperature, rainfall and snowfall. The period covered ranges from 1950 to 2100. 14 historical simulations and 31 future projections, 3 obtained using RCP 2.6, 14 using RCP 4.5 and 14 using RCP 8.5, are available (<https://opensource.umr-cnrm.fr/projects/adamont>). In the current study, we used projections from three GCMs/RCMs combinations (*i.e.* CNRM-CM5/ALADIN53 (r1i1p1 ensemble), MPI-ESM-LR/REMO2009 (r1i1p1 ensemble), EC-EARTH/RCA4 (r12i1p1 ensemble)) forced by RCP 2.6. Our attention is focused on RCP 2.6 because it is the closest scenario to the target of the 2015 Paris climate agreement.

Meteorological data from SAFRAN and AWS are compared over the same time period and the results show a high correlation. This justifies the use of ADAMONT to estimate the rate of future change of the observed variables. Furthermore, ADAMONT is the most recent and accurate method to have alpine regional climate projections.

II.3.2 Hydrological data

The hydrological data used in this study are provided by Electricité de France (EDF). Due to water withdrawals below the Argentière and Tour glaciers managed by Electricité d’Emosson S.A. and directed toward Emosson Lake (Switzerland) for electricity production, reconstructed discharge datasets are used for four of the five considered catchments, *i.e.* Arveyron d’Argentière, Arve at Pont des Favrand, at Sallanches and at Bout du Monde (Fig. II.2). The discharge reconstruction has been done at daily time scale by adding the data measured at the extraction points to the discharge values registered at the gauging stations located at the outlet of each considered catchment (Fig. II.1b). For Arveyron de la Mer de Glace the discharge values are provided by the gauging station because here the direct anthropogenic influence can be neglected. The time period of the discharge data availability differs for each station (Table II.3)

but the series share a common period: 1983–2004. In the Argentière drainage basin, the available data are mainly concentrated from May to October as the sensors are removed during winter. The discharge data are assumed to be affected by a 10% standard uncertainty (Viani et al., 2018).

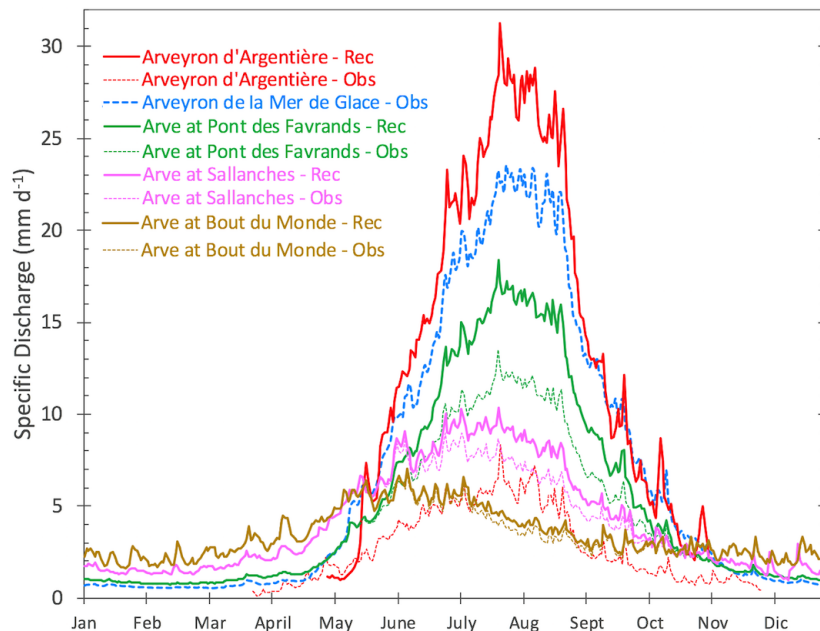


Figure II.2: Mean daily reconstituted specific discharge of the five nested catchments considered over the 1983–2004 period. The dashed lines indicate the discharge values observed (“Obs”) at the gauging stations while the solid ones the reconstructed (“Rec”) discharges. The lines in bold (dashed and solid) indicate the dataset used in this study.

II.3.3 Glaciological data

The glacier-wide annual surface mass balances of Argentière and Mer de Glace-Leschaux, quantified by GLACIOCLIM (Vincent et al., 2009, 2014) are used. They represent the sum of surface accumulation and surface ablation of the entire glacier considered at annual time scale (Cogley, 2009). Available over the 1979–2017 period, these data are obtained using the linear model (Lliboutry, 1974; Vincent et al., 2017) combined with the geodetic method. The uncertainty in the glacier-wide annual surface mass balances is equal to ± 0.40 m w.e. yr^{-1} (Berthier et al., 2014).

Glacier outlines, obtained using topographic maps, LANDSAT and ASTER satellite images in 1967, 1985, 2003 and 2012 (Gardent et al., 2014; Rabatel et al., 2016), are used to calculate the changes in the glacier surface area, assuming an annual linear trend between the available dates. In addition, the ELA values obtained using satellite images (Rabatel et al., 2013) are considered for each glacier of the study catchments. Their uncertainty ranges from ± 15 to ± 170 m, depending on the year and glacier concerned (Rabatel et al., 2013).

Table II.3: Characteristics of the hydrological and meteorological stations.

Station	Time period	Time scale	Elevation (m a.s.l.)	Variable measured	Source
Arv. d'Argentière	1955–2004	daily	1363	Discharge	EDF
Arv. de la Mer de Glace	1950–2014	daily	1060	Discharge	EDF
Arve at Pont des Favrandes	1983–2010	daily	1020	Discharge	EDF
Arve at Sallanches	1980–2015	daily	535	Discharge	EDF
Arve at Bout du Monde	1904–2013	daily	380	Discharge	EDF
Chamonix	1983–2009	hourly	1042	Temperature	MF
Chamonix	1934–2015	daily	1042	Precipitation	MF
Sallanches-La Charlotte	1870–2017	2 meas./day; daily	541	Temperature; Precipitation	MF
Geneva-Cointrin	1981–2018	hourly; daily	410	Temperature; Precipitation	MeteoSwiss

EDF = Electricité de France; MF = Météo-France

II.3.4 DEMs

Three DEMs are used to estimate the rate of glacier volume changes. The first one is a photogrammetric DEM provided by the French National Geographic Institute (IGN, Institut Géographique National) with a horizontal resolution of 25 m, dated to 1979 for the Mont Blanc massif (Berthier et al., 2006). The two other DEMs, with 20 m resolution, are derived from SPOT5 2.5 m stereo-pairs acquired on 8 August 2003 and 15 October 2011. The accuracy of the SPOT5 DEM has been quantified using elevation profiles surveyed with DGPS measurements (see Rabatel et al., 2016 for full details).

II.4 Methods

Fig. II.3 shows the workflow of the analysis performed in this study. In a first step, the seasonal cycle of each catchment is fitted using a mathematical function (the asymmetric peak model (APM), Section II.4.2) characterized by four main parameters. The use of this model and thus the analysis of these parameters makes it easier to assess the current and future temporal and spatial evolution of the discharge seasonal cycle. In order to focus on the changes driven by glacier and snow melt processes, the APM is performed on a filtered discharge dataset (Section II.4.1) so as to remove the isolated rainfall-induced peaks. In a second step, the trend analysis is performed on temperature, precipitation, discharge data and on the parameters characterizing the function obtained using the APM (Section II.4.3). The glacier volume changes are calculated to evaluate and explain the trend observed on the discharge values (Section II.4.4). Finally, a principal component analysis (PCA) is carried out (i) to investigate the relationships

between the four main parameters of the fitted discharge seasonal cycle using the APM, the glaciological and meteorological variables (Section II.4.5.1); and (ii) to evaluate the evolution of the discharge seasonal cycle of the considered catchments under the climate change conditions (Section II.4.5.2).

II.4.1 Filtering of the discharge data

The daily discharge data are filtered as follows.

1. Extreme discharge values are detected using the Seasonal Hybrid Extreme Studentized Deviate (S-H-ESD) technique. This consists of applying a seasonal decomposition to filter the trend and the seasonal components of a time series with the STL (Seasonal and Trend decomposition using Loess) variant method, followed by the use of the extended Extreme Studentized Deviate (ESD) test (Hochenbaum et al., 2017). The extended ESD is a statistical test that uses the median and Median Absolute Deviation of the sample as metrics to accurately detect anomalies (Appendix A.1). This time-series decomposition is employed to avoid masking the detection of some 'true' anomalies, since the discharge data are not normally distributed.
2. The precipitation dataset is investigated to identify the extreme liquid precipitation events. Such events are defined as days with an amount of liquid precipitation above the quantile associated with a probability of occurrence of 95%.
3. The results obtained in the previous steps are combined. The extreme discharge values occurring on a day characterized by an extreme liquid precipitation event, or on the day after, are excluded from the original dataset, generating a filtered discharge time series.

II.4.2 Asymmetric peak model (APM)

II.4.2.1 Fitting process

The chosen function F (Fig. II.4), made up of two half-gaussian curves, is described by the following equations:

$$F(x_i) = \begin{cases} Q_B + (Y_p \exp(-\frac{(x_i - X_p)^2}{L_l^2})) & i < X_p \\ Q_B + (Y_p \exp(-\frac{(x_i - X_p)^2}{L_r^2})) & i \geq X_p \end{cases} \quad (\text{II.1})$$

where X_p , Y_p , L_l , L_r are the position of the peak from the beginning of the calendar year (in days), the height of the peak of the curve (in mm), the width (in days) of the curve to the left and right of the peak measured at peak mid-height, respectively (Fig. II.4). Q_B is

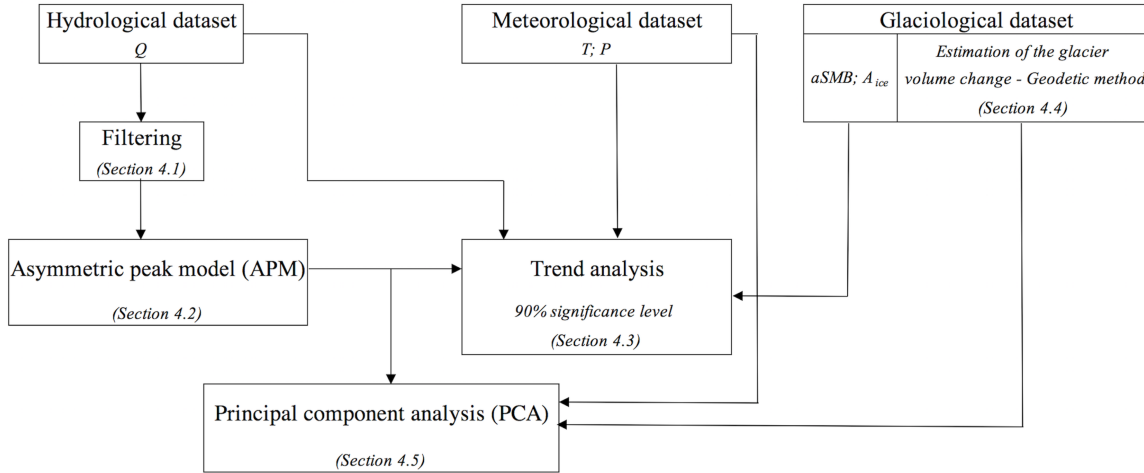


Figure II.3: Flowchart of the analysis performed in the presented work. Q = discharge; T = temperature; P = precipitation; $aSMB$ = glacier-wide annual surface mass balance; A_{ice} = glacier surface area.

the upward shift of the function F , taken as the mean of the discharge values in January and December of the year considered (in mm). The index i represents the current day number of the year considered. In the highly glacierized catchments the Q_B values are very close to zero.

Two other points of the function F are identified: Q_i and Q_f defined as the discharge values in mid-May and mid-October, respectively (Fig. II.4). These values allow to investigate changes in the discharge seasonal cycle during the snow melt season and at the end of the glacier melt period.

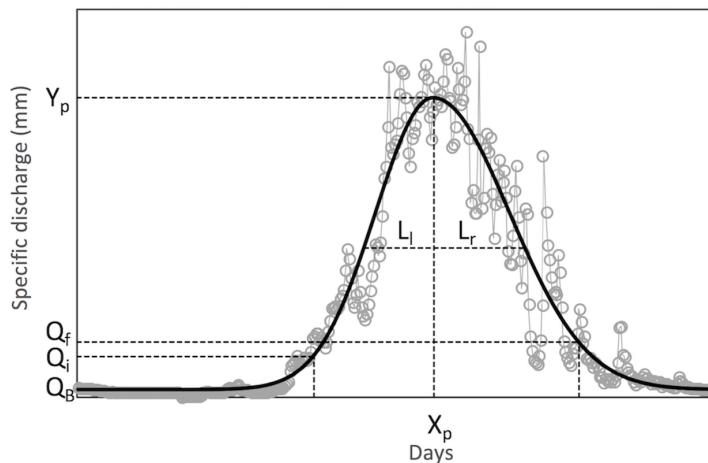


Figure II.4: Function F (solid black line) obtained by fitting the daily values of the measured streamflow (grey points) and its characteristic parameters: the position (X_p) and height (Y_p) of the peak, its width to the left (L_l) and right (L_r) of the peak, the discharge values in mid-May (Q_i) and mid-October (Q_f). Q_B represents the upward shift of the function F . This figure shows the result of the APM performed on the discharge values of the Arveyron de la Mer de Glace catchment in the year 1994.

II.4.2.2 Calibration and optimization procedures

To obtain the best fit of the function F to the annual seasonal cycle of the observed discharge, the optimization of its main four parameters, *i.e.* X_p , Y_p , L_l and L_r , is implemented to minimize the cost function (C) given by:

$$C(X_p, Y_p, L_l, L_r) = \alpha_1 \frac{\sqrt{\sum_{i=1}^N (Q_{Ob_i} - Q_{Sim_i})^2}}{\sqrt{\sum_{i=1}^N (Q_{Ob_i})^2}} + \alpha_2 \frac{|Q_{Oct,Ob} - Q_{Oct,Sim}|}{Q_{Oct,Ob}} + \alpha_3 \frac{|Q_{May,Ob} - Q_{May,Sim}|}{Q_{May,Ob}} + \alpha_4 \frac{|Q_{P,Ob} - Q_{P,Sim}|}{Q_{P,Ob}} + \alpha_5 \frac{|X_{P,Ob} - X_{P,Sim}|}{X_{P,Ob}} \quad (\text{II.2})$$

where i is the number of the days of the considered year, Q_{Ob_i} and Q_{Sim_i} are the observed and simulated discharge values at day i , $Q_{Oct,Ob}$ and $Q_{Oct,Sim}$ the mean of the observed and simulated discharge values over October, $Q_{May,Ob}$ and $Q_{May,Sim}$ the mean of the observed and simulated discharge values over May, $Q_{P,Ob}$ and $Q_{P,Sim}$ the observed and simulated discharge peak values and $X_{P,Ob}$ and $X_{P,Sim}$ the observed and simulated discharge peak positions. α_1 , α_2 , α_3 , α_4 and α_5 are the weights of the different terms of the Eqn. [II.2](#), equal to 1, 1, 1, 10 and 60, respectively. These values, which establish a satisfactory compromise among the individual parts of the cost function C (Eqn. [II.2](#)), have been identified by a sensitivity analysis. The same set of weights is adopted for all of the catchments considered.

The optimization procedure is performed for each catchment and for each year separately. The result consists of a set of parameters (X_p , Y_p , L_l , L_r) characterizing each year and each catchment. The cost function (Eqn. [II.2](#)) is minimized by testing various algorithms. The one that give the best result is based on the generalized simulated annealing function (GSA) which allows to process non-linear objective functions with a large number of local minima ([Xiang et al., 2012](#)). The GSA unifies the classical simulated annealing (CSA) proposed by [Kirkpatrick et al., 1983](#) and the fast simulated annealing (FSA) method proposed by [Szu and Hartley, 1987](#).

Y_p values are assumed to be affected by the same discharge measurement uncertainty, whereas for X_p , L_l and L_r the uncertainty is taken as the maximum variation of the respective parameters that characterized the curves obtained when performing the APM on the observed discharge values increased and decreased by 10%. Uncertainties are estimated to be equal to ± 2 days for X_p , ± 3 days for L_l and ± 4 days for L_r .

II.4.2.3 Performance

The ability of the APM to fit the annual discharge seasonal cycle is evaluated using the Pearson correlation coefficient (ρ) between the observed and simulated daily discharge values. The significance of ρ is determined by its conversion to a t-statistic with a 95% level of signif-

icance (Kendall and Stuart, 1961). The critical values of ρ depend on the degree of freedom of the considered time series, proportional to the autocorrelation values at lag 1 of the two considered samples (Bartlett, 1935; Trenberth, 1984; Bretherton et al., 1999). Furthermore, the representativeness of the APM results is also evaluated by comparing the simulated values of the annual 90th and 95th percentiles and the annual discharge volume with the respective observed values using the determination coefficient (R^2) and root-mean-square error (RMSE) as metrics. The performance of the APM is evaluated at annual time scale for each catchment separately.

II.4.3 Trend analysis

The nonparametric Mann-Kendall (MK) test (Mann, 1945; Kendall, 1975) is used to assess the significance of the trend analysis (Appendix A.2). The standardized test statistic Z (Motiee and McBean, 2009) is used to measure the significance of the trend at the 90% level of confidence (Appendix A.3). The MK requires data that are not serially correlated (Helsel and Hirsch, 1992) as the presence of a serial correlation alters the variance of the MK statistic, increasing the probability of detecting a significant trend whereas it may not even exist (Von Storch, 1995). Since the pre-whitening approach could also result in the removal of a portion of the trend, the trend-free pre-whitening (TFPW) technique proposed by Yue et al., 2002 is adopted. It consists of detrending the time series before the pre-whitening via the following steps: (i) estimating the slope b of a trend using the Theil-Sen approach (Sen, 1968; Theil, 1950) (Appendix A.4), (ii) if the slope b differs from zero, detrending the time series assuming a linear trend and compute the lag-1 serial correlation; (iii) removing the lag-1 serial correlation from the detrended time series (trend-free pre-whitening (TFPW) procedure); (iv) adding the monotonic trend back to the pre-whitened series; and (v) performing the MK trend test on the adjusted time series. This approach was used in several studies such as Abdul Aziz and Burn, 2006; Pellicciotti et al., 2010 and Danneberg, 2012. More precisely, the autocorrelation in the examined time series is checked using the empirical autocorrelation function (ACF) and then, in the presence of serial correlation, the TFPW approach is applied.

The trend analysis is performed on three variables: temperature, precipitation and discharge. For the temperature, we investigated the maximum (T_{\max}), minimum (T_{\min}) and mean values and the number of the positive degree days (PDD). The total (P_{tot}), liquid (P_{rain}) and solid (P_{snow}) precipitation amounts, the number of precipitation days (P_{days}), the number of days characterized by precipitation above the 90th percentile ($P_{\text{days } 90\%}$) and below the 10th ($P_{\text{days } 10\%}$) are analyzed. The precipitation phases (rain and snow) are separated according to the air temperature and a threshold value equal to 1°C is taken (L'hôte et al., 2005). With regards to the discharge, we considered its volume production (Q_{volume}) and the 10th (Q_{10}), 25th (Q_{25}), 50th (Q_{50}), 75th (Q_{75}) and 90th (Q_{90}) percentiles, as previously done by Lins and Slack,

[1999, Pellicciotti et al., 2010] and [Bard et al., 2015]. All of the variables described above are analyzed at both annual and seasonal scales. The following seasons are considered: spring (MAM), summer (JJA), autumn (SON) and winter (DJF). For the Arveyron d'Argentière catchment the first three quantiles are only evaluated in summer because of the incompleteness of the series in the other seasons and the trend analysis is not performed in winter because no data are available. The PDD have not been evaluated for the meteorological station at Sallanches-La Charlotte because hourly data are not available. Furthermore, for the discharge, six parameters characterizing the function obtained using the APM (Section II.4.2), *i.e.* X_p , Y_p , L_l , L_r , Q_i and Q_f (Fig. II.4), are considered. Their trend analysis is conducted at annual time scale and only for the catchments where the simulated discharge cycle using the APM represents more than the 80% of the variance of the observed data, at least over the 1983–2004 period, in order to ensure the representativeness of the results.

To perform the trend analysis, two different periods are selected: (i) a period of 22 years, from 1983 to 2004 for which all of the hydrological and meteorological series are available for all of the catchments; and (ii) a period of 45 years, from 1960 to 2004, only including the discharge dataset of Arveyron d'Argentière, Arveyron de la Mer de Glace and Arve at Bout du Monde. The slopes of the trends are estimated using the Theil-Sen method (Appendix A.4).

It is known that the length of the analyzed times series does affect the results of the trend analysis ([Birsan et al., 2005, Pellicciotti et al., 2010]). [Pekárová et al., 2003] concluded that the runoff time series may show a long-term periodic oscillation that influences the results if the trend analysis is not performed on a period that spans one single or multiple complete cycles. Following [Birsan et al., 2005], the evolution of the standardized annual discharge of each considered catchment is investigated to evaluate the representativeness of the trend analysis over a short-term period. The standardized annual discharge is obtained by dividing the annual discharge production by its mean value calculated over the considered period at each site.

To investigate the relationship between the trends in the hydrological variables of two highly glacierized catchments (Arveyron d'Argentière and Arveyron de la Mer de Glace) and the glacier contribution, glacier volume (Section II.4.4) and surface area change rates are calculated for Argentière, Mer de Glace-Leschaux and their tributaries.

II.4.4 Estimation of the glacier volume changes

The glacier volume change is calculated for the Argentière, Mer de Glace and their tributaries from the difference between the DEMs of the glacier surface (geodetic method). The estimation is performed over the 1979–2003 and 2003–2011 periods, based on the available DEMs. With regards to the extent of the glaciers, the first time period includes the mean glaciers surface over the 1985–2003 whereas the second the mean surface area over the 2003–2012. The difference between the two DEMs gives the total volume variation over the period

defined by the DEM dates. The mean annual rate of the glacier volume change is calculated by dividing the glacier volume variation by the product of the number of years in the period considered and the ice density, assumed to be constant and equal to 900 kg m^{-3} (Paterson, 1994a). This values of ice density has been used in many previous assessments of the geodetic mass balance of mountain glaciers (e.g., Bauder et al., 2007; Paul and Haeberli, 2008; Cogley, 2009), even though the use of a constant value does not consider the firn densification process over time. According to Huss, 2013, an ice density value of 850 kg m^{-3} is also applied. This change in the ice density value leads to a reduced annual rate of glacier volume change of 5%. The uncertainty in the mean glacier-wide mass balance, considering all of the different sources of error including the density value used to convert the differences in glacier surface elevation into mass changes, is estimated to be $\pm 0.12 \text{ m w.e. yr}^{-1}$ over the 1979–2012 period (Rabatel et al., 2016), *i.e.* $0.002 \text{ km}^3 \text{ yr}^{-1}$ and $0.004 \text{ km}^3 \text{ yr}^{-1}$ for Argentière and Mer de Glace-Leschaux, respectively.

II.4.5 Principal Component Analysis (PCA) on highly glacierized catchments

II.4.5.1 Variables influencing the discharge seasonal cycle

The PCA is carried out in order to find the main glaciological and meteorological variables (independent variables) through which the evolution of the main parameters of the function F , *i.e.* X_p , Y_p , L_l , L_r , (input variables) can be statistically explained and thus predicted. It was not possible to discern the relationship between the independent and input variables performing a multiple regression because of the high correlation of the independent variables (*i.e.* multicollinearity problem), thereby affecting the accuracy and the robustness of the prediction. This problem is addressed performing a PCA, that transforms a number of correlated variables, *i.e.* the independent variables, into a number of uncorrelated variables called principal components (PCs) (explanatory variables) through which the input variables can be explained. According to glaciological data availability, we focus only on the discharge seasonal cycle of Arveyron d'Argentière and Arveyron de la Mer de Glace catchments. The analysis is done over the 1983–2004 period, covered by all of the considered datasets (glaciological, hydrological and meteorological data).

We performed the following steps: (i) the set of input variables is divided into a calibration and validation dataset using a differential split-sample test (Klemes, 1986). Approximately 68% of the input data (*i.e.* 15 data points) is used to form the calibration dataset, whereas the other data points are used for the validation; (ii) the PCA is performed on the calibration group; (iii) the PC values associated with the validation dataset are estimated based on the PCA carried out on the calibration dataset; (iv) the multiple linear and polynomial regressions

are performed on the calibration dataset to establish the relationship between the explanatory variables and input ones. The number of PCs that explain more than the 80% of variability of the data are used; and (v) once the relationship resulting in the best regression is obtained, it is used to predict the input variable associated with the PC of the validation dataset.

This sequence of steps is performed by testing different combinations of the independent variables for each parameter considered, such as the glacier-wide annual surface mass balance and glacier surface area for the glaciological variables and temperature, liquid, solid and total precipitation values for the meteorological variables. Monthly and seasonal values of the meteorological variables are tested. The combinations of the independent variables able to explain the highest variance of the parameters of function F are selected. The performance of the prediction is evaluated using Pearson's coefficient (ρ).

II.4.5.2 Sensitivity of the discharge seasonal cycle to future climate changes

Once the multi-variables regression is defined, the evolution of the discharge seasonal cycle of each catchment under climate change conditions is evaluated. Projections of the atmospheric variables using RCP 2.6 are generated over the 2030–2040 and 2050–2060 periods. In order to do this, each variable considered in the multi-variable relationship is increased by its rate of change between historical (1983–2004) and future timespans (2030–2040 or 2050–2060), according to ADAMONT.

The future estimation of the glacier-wide annual surface mass balance ($aSMB_f$) for the two glaciers considered (*i.e.* Argentière and Mer de Glace-Leschaux) is obtained using Eqn. [II.3](#) according to [Ohmura et al., 1992](#) who showed that the main factors influencing the glacier-wide annual surface mass balance are summer temperature (T_{JJA}) and annual total precipitation at the ELA (P_{tot}).

$$aSMB_f = a + b T_{JJA} + c P_{tot} \quad (\text{II.3})$$

The P_{tot} values at the ELA are estimated increasing the observed values at Chamonix by a gradient equal to 3%/100 m for altitudes below 2550 m a.s.l. and to 2%/100 m above ([Viani et al., 2018](#)). The T_{JJA} values at the median altitude of the catchments considered are extrapolated from the measurements registered by the meteorological station at Chamonix, using a constant environmental lapse rate of 0.6°C/100 m. Parameters a , b and c , estimated separately for each glacier using a multiple linear regression, are listed in [Table II.4](#). To describe the evolution of the glaciers surface area, the future rate of change is assumed to be equal to that calculated over the 2003–2012 period, *i.e.* -0.11 km² yr⁻¹ and -0.18 km² yr⁻¹ for the Argentière and Mer de Glace-Leschaux glaciers, respectively.

Table II.4: Coefficients of Eq. 3, obtained using a multiple linear regression.

	Argentière	Mer de Glace-Leschaux
a	-1213.38	-500.51
b	-609.13	-914.19
c	1.68	1.61

II.5 Results

II.5.1 Hydrological regime of the five nested catchments

The mean seasonal cycle of the specific natural discharge of the five considered catchments over the 1983–2004 period shows that the most productive catchments are the highly glacierized ones (Fig. II.2). Arveyron de la Mer de Glace produces a lower outflow (2477 mm yr^{-1}) than Arveyron d’Argentière (2624 mm yr^{-1}) whereas both are subjected to the same regional climate and have a comparable glacial cover. This difference may be explained by the presence of aquifers and subterranean fluxes in the Arveyron de la Mer de Glace zone, which results in the underestimation of the real water production of this catchment (Viani et al., 2018). Furthermore, the study catchments are characterized by different hydrological regimes. The three highly glacierized show a nivo-glacial regime characterized by a marked seasonality: high flow rates in summer and low flow rates in wintertime when precipitation primarily occurs as snow. The Arve at Sallanches exhibits a pluvio-nivo-glacial regime, whereas Arve at Bout du Monde shows a pluvio-nival regime characterized by a decrease in runoff during late summer related to the very limited glacial cover. With the decrease in glacier cover within the nested catchments, the discharge peak occurs earlier, *i.e.* at the end of July in the highly glacierized catchments, mid-June for Arve at Sallanches and at the beginning of June for Arve at Bout du Monde (Fig. II.2).

II.5.2 Asymmetric peak model

The performance of the APM indicates that the observed seasonal cycle is well represented by this model for the three highly glacierized catchments over the periods considered at daily time step (Table II.5). In these cases, the model is able to reproduce on average at least 80% of the variance of the observed discharge data. With the decrease in glacier cover, the performance of the APM declines: only 65% and 27% of the variance in the daily discharges is explained for the Arve at Sallanches and Arve at Bout du Monde catchments, respectively. The simulated quantiles associated with the 90th and 95th percentiles show a good fit with the observed ones, except for Arve at Bout du Monde (Table II.5). The simulated annual discharge volumes are

characterized by a RMSE ranging from 5% (for Arveyron d'Argentière) to 13.5% (for Arveyron de la Mer de Glace) compared to the measured values. For the highly glacierized catchments, the APM is able to reproduce at least 80% of the variance of the observed annual volumes on average, while for the other catchments this value drops to approximately 70%. The best approximation of the discharge seasonal cycles using the APM is achieved for the catchments characterized by a nivo-glacial regime. Therefore, the trend analysis of the parameters of the function F describing the discharge seasonal cycle is only performed for the three highly glacierized catchments.

Table II.5: APM performance. The following metrics between the observed and the simulated discharge are listed for each catchment: the mean correlation coefficient ($\bar{\rho}$), the determination coefficient related to the 90th and 95th percentiles (R^2_{q90} and R^2_{q95}), the determination coefficient (R^2_{vol}) and the RMSE (%) values for the annual volume production over the period considered.

Catchments	Period	Daily time scale	Quantile		Volume	
		$\bar{\rho}$	R^2_{q90}	R^2_{q95}	RMSE(%)	R^2_{vol}
Arv. d'Argentière	1960–2004	0.900*	0.765	0.888	5.040	0.810
Arv. de la Mer de Glace	1960–2004	0.907*	0.826	0.896	5.910	0.890
Arve at Pont des Favrans	1983–2004	0.905*	0.767	0.829	6.210	0.790
Arve at Sallanches	1980–2004	0.807*	0.835	0.847	6.890	0.750
Arve at Bout du Monde	1960–2004	0.521*	0.639	0.553	13.500	0.690

*The correlation coefficients are statistically significant for each year

II.5.3 Trend analysis

The results of the trend analysis are presented in two sections: the first focuses on the time period common to all the catchments (1983–2004), while the second focuses on the longer one (1960–2004). The evolution of the standardized annual discharge for each catchment shows that the short period of analysis contains both low and high flow periods (not shown here). This means that the results presented for the shorter period are representative of the changes in discharge (Birsan et al., 2005).

II.5.3.1 1983–2004 period

II.5.3.1.1 Meteorological variables

A clear increase in air temperature at both annual and seasonal scales is observed (Table II.6). T_{mean} shows a statistically significant increase for all of the stations considered, mainly due to a significant increase in spring and summer. A statistically significant increase in winter is also registered, with the exception of Sallanches where the tendency is less marked. T_{max} exhibits a statistically significant warming trend at annual time scale with a strong increase during the spring and summer seasons (except for Chamonix). T_{min} shows a statistically significant increase at annual scale for the two lower stations, *i.e.* Sallanches-La Charlotte

and Geneva-Cointrin. A significant increase in T_{\min} is common to all of the stations during the summertime whereas there is no clear pattern in autumn and winter, probably due to the presence of cold air pool in the valley. A clear positive trend is shown by the PDD, at both annual and seasonal time scales, with a pronounced increase in spring and summer.

The precipitation does not show a clear temporal or spatial pattern (Table II.7). The trends for P_{tot} , P_{rain} and P_{snow} registered at Sallanches-La Charlotte are never statistically significant and those at Chamonix and Geneva-Cointrin are mostly not significant. A consistent decreasing trend in P_{snow} is observed for the three considered stations with a marked signal during the wintertime. The results show that more precipitation falls as rain. P_{days} generally tends to increase at all of the considered sites: significant positive trends are detected in summer and autumn at Chamonix and Geneva-Cointrin. At Chamonix, a marked increase in $P_{\text{days } 90\%}$ and a decrease in $P_{\text{days } 10\%}$ is observed.

Table II.6: Results of the trend analysis calculated on the mean (T_{mean}), minimum (T_{min}) and maximum (T_{max}) temperature values and on the number of the positive degree days (PDD), over the 1983–2004 period at both annual and seasonal time scales. \blacktriangle = Positive statistically significant trend; \circ = Not statistically significant trend. The color code indicates the location of the considered meteorological stations: blue for Chamonix (CH), green for Sallanches-La Charlotte (SA) and orange for Geneva-Cointrin (GE). The numbers indicate the trend slopes calculated with the Theil-Sen method. The slopes of the statistically significant trend are shown in bold. The slope units are given in brackets

	Annual			MAM			JJA			SON			DJF		
	CH	SA	GE	CH	SA	GE	CH	SA	GE	CH	SA	GE	CH	SA	GE
T_{mean} ($^{\circ}\text{C yr}^{-1}$)	\blacktriangle 0.064	\blacktriangle 0.070	\blacktriangle 0.085	\blacktriangle 0.123	\blacktriangle 0.097	\blacktriangle 0.120	\blacktriangle 0.054	\blacktriangle 0.090	\blacktriangle 0.103	\circ 0.016	\circ 0.004	\blacktriangle 0.066	\blacktriangle 0.100	\circ 0.068	\blacktriangle 0.099
T_{max} ($^{\circ}\text{C yr}^{-1}$)	\blacktriangle 0.063	\blacktriangle 0.082	\blacktriangle 0.098	\blacktriangle 0.157	\blacktriangle 0.143	\blacktriangle 0.130	\circ 0.017	\blacktriangle 0.082	\blacktriangle 0.101	\circ 0.021	\circ 0.008	\circ 0.047	\circ 0.090	\circ 0.070	\blacktriangle 0.107
T_{min} ($^{\circ}\text{C yr}^{-1}$)	\circ -0.005	\blacktriangle 0.036	\blacktriangle 0.071	\circ 0.017	\circ 0.034	\blacktriangle 0.088	\blacktriangle 0.082	\blacktriangle 0.104	\blacktriangle 0.096	\circ 0.003	\circ 0.0001	\circ 0.047	\circ -0.082	\circ -0.023	\circ 0.033
PDD ($^{\circ}\text{C yr}^{-1}$)	\blacktriangle 18.58	\blacktriangle 27.21	\blacktriangle 29.39	\blacktriangle 9.73	\blacktriangle 11.30	\blacktriangle 11.06	\blacktriangle 4.95	\blacktriangle 10.24	\blacktriangle 9.51	\circ 0.25	\circ 1.92	\blacktriangle 5.86	\blacktriangle 3.75	\circ 4.30	\blacktriangle 6.18

II.5.3.1.2 Hydrological variables

The trend analysis performed on the discharge variables over the common period 1983–2004 reveals a contrasting behavior between the catchments characterized by different glacier cover (Table II.8). At annual scale the Q_{volume} produced by the three highly glacierized catchments shows a slight increase, whereas the value produced by the low glacierized ones exhibits a negative trend, although not significant. Furthermore, a marked increasing trend in Q_{volume} is observed in spring for Arveyron d’Argentière and Arveyron de la Mer de Glace. During winter it exhibits a significant increase at Arveyron de la Mer de Glace and a significant decrease at Arve at Sallanches.

Over the spring and summer seasons, all of the quantiles of the highly glacierized catchments generally tend to increase: the lower ones (Q_{10} , Q_{25} , Q_{50}) exhibit a statistically significant

Table II.7: Results of the trend analysis calculated on the total (P_{tot}), liquid (P_{rain}) and solid (P_{snow}) precipitation amounts, the number of precipitation days (P_{days}), the number of days characterized by precipitation above the 90th percentile ($P_{\text{days } 90\%}$) and below the 10th ($P_{\text{days } 10\%}$) over the 1983–2004 period at both annual and seasonal time scales. \blacktriangle = Positive statistically significant trend; \blacktriangledown = Negative statistically significant trend; \circ = Not statistically significant trend; - = Absence of snowfall. The color code indicates the location of the considered meteorological stations: blue for Chamonix (CH), green for Sallanches-La Charlotte (SA) and orange for Geneva-Cointrin (GE). The numbers indicate the trend slopes calculated with the Theil-Sen method. The slopes of the statistically significant trend are shown in bold. The slope units are given in brackets.

	Annual			MAM			JJA			SON			DJF		
	CH	SA	GE	CH	SA	GE	CH	SA	GE	CH	SA	GE	CH	SA	GE
P_{tot} (mm yr ⁻¹)	\circ 6.70	\circ -2.86	\blacktriangle 8.19	\circ 0.02	\circ -2.62	\circ -2.90	\circ 5.00	\circ 1.50	\circ 5.96	\circ -0.61	\circ 0.03	\blacktriangle 7.08	\circ -0.01	\circ -0.01	\circ 0.02
P_{rain} (mm yr ⁻¹)	\blacktriangle 0.04	\circ -0.01	\blacktriangle 0.03	\circ 0.35	\circ -2.15	\circ -2.88	\circ 4.99	\circ 1.50	\circ 5.96	\circ -0.90	\circ -0.34	\blacktriangle 7.02	\blacktriangle 4.43	\circ 0.96	\circ 0.27
P_{snow} (mm yr ⁻¹)	\circ -6.02	\circ -1.35	\blacktriangledown -0.60	\circ -1.18	-	-	-	-	-	\circ -0.43	-	-	\blacktriangledown -5.35	\circ -1.22	\blacktriangledown -0.89
P_{days} (days yr ⁻¹)	\blacktriangle 2.30	\circ -0.13	\circ 1.08	\circ -0.16	\blacktriangledown -0.46	\circ -0.50	\blacktriangle 1.30	\circ 0.04	\blacktriangle 0.44	\blacktriangle 1.08	\circ 0.45	\blacktriangle 1.00	\circ -0.07	\circ 0.00	\circ -0.11
$P_{\text{days } 90\%}$ (days yr ⁻¹)	\blacktriangle 0.22	\circ 0.00	\blacktriangle 0.13	\circ 0.00	\circ 0.00	\circ 0.00	\blacktriangle 0.13	\circ 0.00	\blacktriangle 0.05	\blacktriangle 0.11	\circ 0.00	\blacktriangle 0.10	\circ 0.00	\circ 0.00	\circ 0.00
$P_{\text{days } 10\%}$ (days yr ⁻¹)	\blacktriangledown -0.50	\circ 0.00	\circ 0.00	\blacktriangledown -0.23	\circ -0.06	\circ 0.00	\circ -0.08	\circ 0.00	\circ 0.06	\blacktriangledown -0.13	\circ 0.00	\blacktriangle 0.10	\blacktriangledown -0.20	\circ 0.00	\circ 0.00

trend in summer, while the higher ones (Q_{50} , Q_{75} , Q_{90}) do so in spring. The Q_{50} , Q_{75} , Q_{90} values of the low glacierized catchments tend to decrease in a statistically significant way in summer. During winter, the discharge quantiles at Arveyron de la Mer de Glace show a statistically significant increase, whereas the lower ones at Arve at Sallanches tend to decrease in a statistically significant way.

The results of the trend analysis performed on the parameters characterizing the function obtained with the APM (Table II.9) show that L_l exhibits a statistically significant positive trend for all three highly glacierized catchments. A statistically significant increase is evident for Q_i (Fig. II.4) at Arveyron d'Argentière and Arveyron de la Mer de Glace. Both of these catchments show a statistically significant negative trend in Q_f (Fig. II.4). Y_p does not exhibit a trend at any of the sites. The trends of the parameters at Pont the Favrandes agree with those of the other two catchments considered but are not significant.

Table II.8: Results of the trend analysis calculated on the discharge volume production (Q_{volume}) and the 10th(Q_{10}), 25th(Q_{25}), 50th(Q_{50}), 75th(Q_{75}) and 90th (Q_{90}) percentiles over the 1983–2004 period at both annual and seasonal timescales for Arveyron d’Argentière (ARG, blue), Arveyron de la Mer de Glace (MdG, pink), Arve at Pont des Favrands (PF, light blue), at Sallanches (SA, red) and at Bout du Monde (BdM, gray). \blacktriangle = Positive statistically significant trend; \blacktriangledown = Negative statistically significant trend; \circ = Not statistically significant trend; - = Incompleteness of the series/no data available (see Section 4.3). The numbers indicate the trend slopes calculated with the Theil-Sen method. The slopes of the statistically significant trend are shown in bold. The slope units are given in brackets.

	Annual					MAM					JJA					SON					DJF				
	ARG	MdG	PF	SA	BdM	ARG	MdG	PF	SA	BdM	ARG	MdG	PF	SA	BdM	ARG	MdG	PF	SA	BdM	ARG	MdG	PF	SA	BdM
Q_{volume} (mm yr ⁻¹)	\circ 10.27	\circ 8.95	\circ 1.67	\circ -8.58	\circ -8.58	\blacktriangle 1.46	\blacktriangle 5.62	\circ 2.77	\circ 0.63	\circ -4.53	\circ 4.21	\circ 8.89	\circ 3.03	\blacktriangledown -5.16	\blacktriangledown -3.95	-	\circ -7.94	\circ -4.17	\circ -2.88	\circ -0.01	-	\blacktriangle 1.03	\circ 0.12	\blacktriangledown -0.68	\circ 1.36
Q_{10} (mm yr ⁻¹)	-	\circ 0.006	\circ -0.005	\blacktriangledown -0.020	\circ 0.003	-	\circ 0.005	\circ -0.006	\circ 0.007	\circ 0.011	\blacktriangle 0.262	\blacktriangle 0.191	\blacktriangle 0.125	\circ 0.004	\circ -0.010	-	\blacktriangle 0.013	\circ 0.009	\circ -0.022	\circ 0.001	-	\blacktriangle 0.001	\circ -0.006	\blacktriangledown -0.033	\circ 0.008
Q_{25} (mm yr ⁻¹)	-	\blacktriangle 0.001	\circ -0.003	\blacktriangledown -0.020	\circ 0.006	-	\circ 0.009	\circ 0.009	\circ -0.011	\circ -0.018	\blacktriangle 0.163	\circ 0.094	\circ 0.089	\circ 0.001	\circ -0.013	-	\circ 0.026	\circ 0.002	\circ -0.019	\circ 0.006	-	\blacktriangle 0.001	\circ -0.005	\blacktriangledown -0.027	\circ 0.006
Q_{50} (mm yr ⁻¹)	-	\blacktriangle 0.046	\circ -0.003	\circ -0.026	\circ -0.002	-	\blacktriangle 0.020	\circ -0.002	\circ -0.036	\circ 0.050	\blacktriangle 0.197	\circ 0.051	\circ 0.043	\circ -0.037	\blacktriangledown -0.050	-	\circ 0.008	\blacktriangledown -0.037	\blacktriangledown -0.049	\circ 0.008	-	\blacktriangle 0.011	\circ -0.001	\blacktriangledown -0.019	\circ 0.010
Q_{75} (mm yr ⁻¹)	\circ 0.044	\circ 0.012	\circ 0.023	\circ 0.020	\blacktriangledown -0.057	\blacktriangle 0.018	\blacktriangle 0.093	\circ 0.046	\circ 0.034	\circ -0.082	\circ 0.096	\circ 0.059	\circ 0.048	\blacktriangledown -0.103	\blacktriangledown -0.073	\circ -0.064	\circ -0.140	\circ -0.093	\circ -0.054	\circ -0.001	-	\blacktriangle 0.014	\circ 0.007	\circ -0.008	\circ 0.011
Q_{90} (mm yr ⁻¹)	\circ 0.133	\circ 0.023	\circ 0.044	\blacktriangledown -0.055	\blacktriangledown -0.084	\blacktriangle 0.091	\circ 0.159	\circ 0.051	\circ 0.040	\circ -0.088	\circ 0.048	\circ 0.019	\circ -0.019	\blacktriangledown -0.146	\blacktriangledown -0.072	\circ -0.131	\circ -0.102	\circ -0.070	\circ -0.048	\circ 0.001	-	\circ 0.013	\circ 0.003	\circ 0.005	\circ 0.018

Table II.9: Results of the trend analysis calculated on the parameters characterizing the function F , *i.e.* the position (X_p) and height (Y_p) of the peak, the width of the curve to the left (L_l) and right (L_r) of the peak, the beginning (Q_i) and end (Q_f) of the curve for Arveyron d'Argentière (ARG, blue), Arveyron de la Mer de Glace (MdG, pink) and Arve at Pont des Favrands (PF, light blue) catchments over the 1983–2004 period at annual timescale. \blacktriangle = Positive statistically significant trend; \blacktriangledown = Negative statistically significant trend; \circ = Not statistically significant trend. The numbers indicate the trend slopes calculated with the Theil-Sen method. The slopes of the statistically significant trend are shown in bold. The slope units are given in brackets.

	Annual		
	ARG	MdG	PF
X_p (day yr ⁻¹)	\blacktriangle 0.40	\circ 0.22	\circ 0.26
Y_p (mm yr ⁻¹)	\circ -0.1	\circ 0.01	\circ 0.01
L_l (day yr ⁻¹)	\blacktriangle 0.63	\blacktriangle 0.69	\blacktriangle 0.79
L_r (day yr ⁻¹)	\blacktriangledown -0.70	\circ -0.33	\circ -0.42
Q_i (mm yr ⁻¹)	\blacktriangle 0.06	\blacktriangle 0.13	\circ 0.07
Q_f (mm yr ⁻¹)	\blacktriangledown -0.12	\blacktriangledown -0.12	\circ -0.04

II.5.3.2 1960–2004 period

The trend analysis performed on the discharge data available over the 1960–2004 period shows distinct results with respect to the glacier cover of the catchments (Table II.10), as observed over the 1983–2004 period. Trends in the annual and summer Q_{volume} are statistically significant for Arveyron d'Argentière and Arveyron de la Mer de Glace, in contrast to those over the 1983–2004 period. The autumn Q_{volume} over 1960–2004 exhibits a reversed trend for all of the considered stations compared with the short time period: it changes from a negative to a positive trend that is statistically significant for Arveyron de la Mer de Glace.

The magnitude of the statistically significant trend of the spring Q_{volume} is decreased in the longer period compared to the shorter one for Arveyron d'Argentière (0.32 *vs* 1.46 mm yr⁻¹) and Arveyron de la Mer de Glace (2.18 *vs* 5.62 mm yr⁻¹). An increase in the Q_{volume} is observed at Arveyron de la Mer de Glace during winter, changing from a not statistically significant trend over the long period to a significant one over the shorter period. At annual scale, the Q_{75} and Q_{90} of the highly glacierized catchments exhibit an important change from a statistically significant (over the long period) to a not statistically significant trend. A reverse behavior is observed for Q_{75} and Q_{90} at Arve at Bout du Monde. Generally, in summer the quantiles show a stronger trend magnitude at Arveyron d'Argentière and Arveyron de la Mer de Glace than over the short period. The winter quantiles for Arveyron de la Mer de Glace exhibit a not

statistically significant trend, in contrast with those over the shorter period.

The analysis performed on the parameters of the function F shows that the trend magnitude of Y_p increases in the longer period for the two considered catchments (Table II.11). Q_f shows a reversed trend for both catchments, passing from a statistically significant increase over the long period to a statistically significant decrease over the short period of analysis. The increasing trends of L_r and Q_i are still statistically significant, as observed over the short period.

Table II.10: Results of the trend analysis calculated on the discharge volume production (Q_{volume}) and the 10th (Q_{10}), 25th (Q_{25}), 50th (Q_{50}), 75th (Q_{75}) and 90th (Q_{90}) percentiles over the 1960–2004 period at both annual and seasonal timescales for Arveyron d’Argentière (ARG, blue), Arveyron de la Mer de Glace (MdG, pink) and Bout du Monde (BdM, gray) catchments. \blacktriangle = Positive statistically significant trend; \blacktriangledown = Negative statistically significant trend; \circ = Not statistically significant trend; - = Incompleteness of the series/no data available (see Section 4.3). The numbers indicate the trend slopes calculated with the Theil-Sen method. The slopes of the statistically significant trend are shown in bold. The slope units are given in brackets.

	Annual			MAM			JJA			SON			DJF		
	CH	SA	GE	CH	SA	GE	CH	SA	GE	CH	SA	GE	CH	SA	GE
Q_{volume} (mm yr ⁻¹)	\blacktriangle 14.43	\blacktriangle 14.80	\circ -2.71	\blacktriangle 0.32	\blacktriangle 2.18	\circ -0.55	\blacktriangle 11.62	\blacktriangle 8.63	\blacktriangledown -2.38	-	\blacktriangle 2.82	\circ 0.45	-	\circ 0.18	\circ 0.71
Q_{10} (mm yr ⁻¹)	-	\circ 0.000	\circ 0.000	-	\circ -0.001	\circ 0.006	\blacktriangle 0.116	\blacktriangle 0.077	\blacktriangledown -0.016	-	\blacktriangle 0.006	\circ 0.001	-	\circ 0.000	\circ 0.001
Q_{25} (mm yr ⁻¹)	-	\circ 0.001	\circ -0.000	-	\circ 0.001	\circ -0.005	\blacktriangle 0.145	\blacktriangle 0.120	\blacktriangledown -0.021	-	\blacktriangle 0.016	\circ 0.000	-	\circ 0.000	\circ -0.001
Q_{50} (mm yr ⁻¹)	-	\blacktriangle 0.024	\circ -0.006	-	\blacktriangle 0.006	\circ -0.007	\blacktriangle 0.197	\blacktriangle 0.130	\blacktriangledown -0.026	-	\blacktriangle 0.036	\circ -0.002	-	\circ 0.001	\circ 0.005
Q_{75} (mm yr ⁻¹)	\blacktriangle 0.082	\blacktriangle 0.089	\circ -0.015	\blacktriangle 0.027	\blacktriangle 0.037	\circ -0.007	\blacktriangle 0.148	\blacktriangle 0.086	\blacktriangledown -0.029	\blacktriangle 0.055	\blacktriangle 0.059	\circ 0.005	-	\circ 0.002	\circ 0.008
Q_{90} (mm yr ⁻¹)	\blacktriangle 0.175	\blacktriangle 0.114	\circ -0.013	\blacktriangle 0.038	\blacktriangle 0.082	\circ -0.011	\circ 0.076	\circ 0.05	\circ -0.035	\circ 0.051	\circ 0.055	\circ 0.014	-	\circ 0.002	\circ 0.017

II.5.4 Result of the Principal Component Analysis

II.5.4.1 Variables influencing the discharge seasonal cycle

For Arveyron d’Argentière and Arveyron de la Mer de Glace catchments the same independent variables influencing each parameter (X_p , Y_p , L_l , L_r) are identified over the 1983–2004 period.

To explain Y_p , the first two PCs are extracted, accounting for approximately 92% of the variance of the input values for both catchments. The first PC explains 63.5% (70.7%) of the total variance for Arveyron d’Argentière (Arveyron de la Mer de Glace). It contains the highest positive loading on the mean temperature from 15 July to 15 August of the considered year at the median altitude of the considered catchment ($T_{15\text{JA}}$) and the highest negative on the glacier-wide annual surface mass balance (aSMB). The second PCs have the highest negative loading on the glacier surface area (A_{ice}). The evolution of the predicted Y_p values over the

Table II.11: Results of the trend analysis calculated on the parameters characterizing the function F , *i.e.* the position (X_p) and height (Y_p) of the peak, the width of the curve to the left (L_l) and right (L_r) of the peak, its beginning (Q_i) and end (Q_f) for Arveyron d'Argentière (ARG, blue) and Arveyron de la Mer de Glace catchments (MdG, pink) over the 1960–2004 period at annual timescale. \blacktriangle = Positive statistically significant trend; \blacktriangledown = Negative statistically significant trend; \circ = Not statistically significant trend. The numbers indicate the trend slopes calculated with the Theil-Sen method. The slopes of the statistically significant trend are shown in bold. The slope units are given in brackets.

	Annual	
	ARG	MdG
X_p (day yr ⁻¹)	\circ 0.09	\circ -0.01
Y_p (mm yr ⁻¹)	\blacktriangle 0.13	\blacktriangle 0.10
L_l (day yr ⁻¹)	\blacktriangle 0.16	\blacktriangle 0.34
L_r (day yr ⁻¹)	\circ -0.09	\circ 0.13
Q_i (mm yr ⁻¹)	\blacktriangle 0.02	\blacktriangle 0.06
Q_f (mm yr ⁻¹)	\blacktriangledown 0.03	\blacktriangledown 0.04

considered period is in good agreement with the observed ones, showing almost the same inter-annual variability for both catchments (Fig. II.5a and Fig. II.6a). The correlation between the predicted and the observed Y_p values is significant at the 99% confidence interval according to the Pearson's test ($R^2 = 0.76$ for Arveyron d'Argentière (Fig. II.5b) and $R^2 = 0.63$ for Arveyron de la Mer de Glace (Fig. II.6b)).

Regarding L_l , the two PCs are extracted. The first PCs explain 55.3% of the total variance in both catchments and have the negative loading on the mean temperature in May (T_{May}) and the amount of solid precipitation from November to May ($\text{Snow}_{\text{Nov-May}}$) at the medial altitude of the considered catchment. The observed and simulated values of L_l are almost the same inter-annual variability (Fig. II.5c and Fig. II.6c) and their correlations are significant at the 99% confidence. (the Pearson's test, $R^2 = 0.64$ for Arveyron d'Argentière (Fig. II.5d) and $R^2 = 0.70$ for Arveyron de la Mer de Glace (Fig. II.6d)).

X_p is predicted using the L_l values given the strong correlation detected between these two parameters, *i.e.* $\rho = 0.92$ for Arveyron d'Argentière (Fig. II.5f) and $\rho = 0.85$ for Arveyron de la Mer de Glace (Fig. II.6f). For both catchments, the estimated values of X_p show the same interannual variability as the observed ones.

L_r is explained with the two PCs. The first PC of Arveyron d'Argentière represents 64.3% of the total variance of the observed values whereas it only explains 52.8% of the variance

for Arveyron de la Mer de Glace. They are obtained as a linear combination of the aSMB and the September mean temperature values at the median altitude of the considered catchment (T_{Sept}). The simulated L_r values show a good fit with the observed ones (Fig. II.5g and Fig. II.6g) and represent 67% and 64% of the variance of the observed values for Arveyron d’Argentière (Fig. II.6h) and Arveyron de la Mer de Glace (Fig. II.5h), respectively.

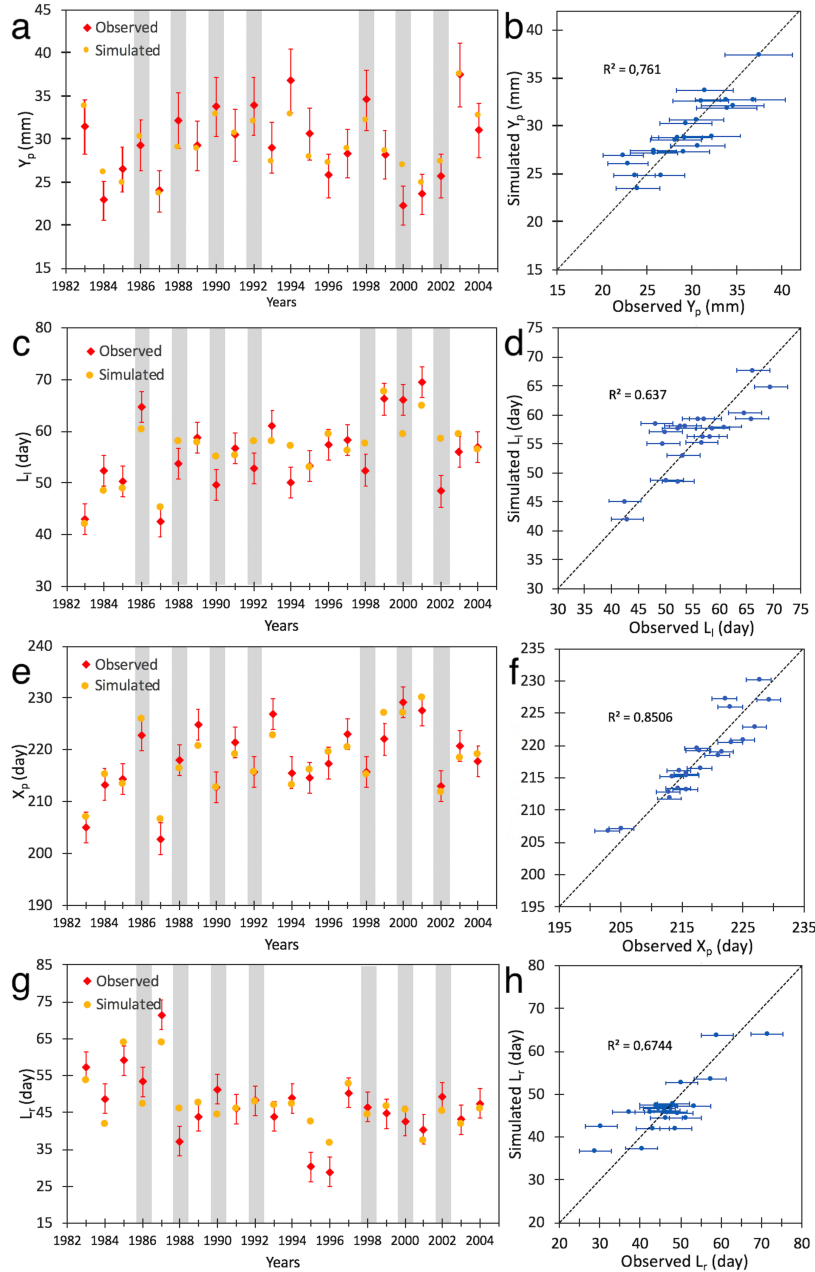


Figure II.5: Evolution of the simulated (red diamond) and observed (orange points) parameters of the function F , *i.e.* Y_p (a), L_l (c), X_p (e) and L_r (g), for the Arveyron d’Argentière catchment over the 1983–2004 period. Correlations between the observed and simulated Y_p (b), L_l (d), X_p (f) and L_r (h) values are also shown. The dashed lines presented in (b) (d) (f) and (h) represent the bisector. The bars represent the uncertainty of the observed values. The grey boxes presented in the graphs on the left column highlight the years used for the validation.

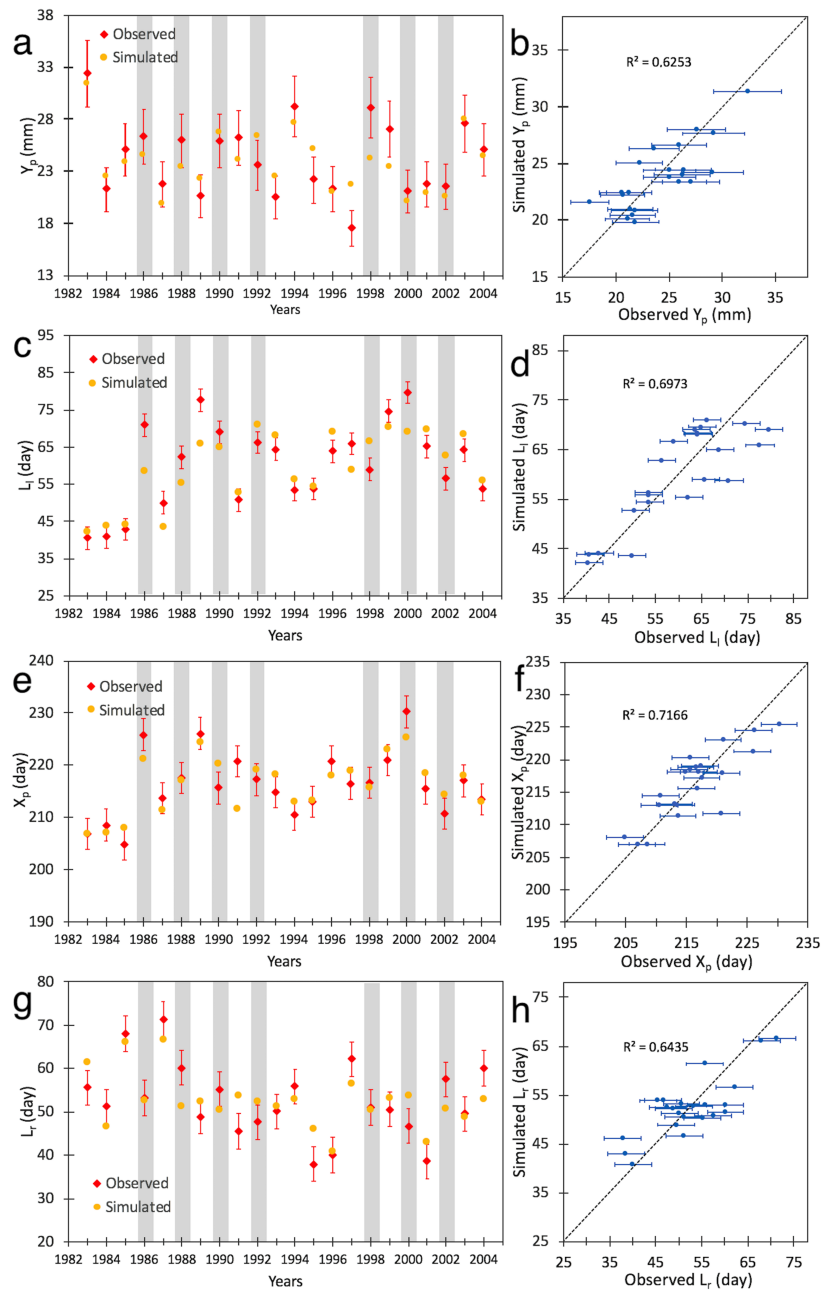


Figure II.6: Evolution of the simulated (red diamond) and observed (orange points) parameters of the function F , *i.e.* Y_p (a), L_l (c), X_p (e) and L_r (g), for the Arveyron de la Mer de Glace catchment over the 1983–2004 period. Correlations between the observed and simulated Y_p (b), L_l (d), X_p (f) and L_r (h) values are also shown. The dashed lines presented in (b) (d) (f) and (h) represent the bisector. The bars represent the uncertainty of the observed values. The grey boxes presented in the graphs on the left column highlight the years used for the validation.

II.5.4.2 Sensitivity of the model to glacio-meteorological changes

The three used combinations of GCMs/RCMs forced by RCP 2.6 predict a mean warming of 1.3°C and a slightly decrease in the annual total precipitation by the end of the 21st century.

With respect to the reference period 1983–2004, $T_{15\text{JA}}$, T_{May} and T_{Sept} are projected to

increase while $\text{Snow}_{\text{Nov-May}}$ to decrease by both the 2030–2040 and 2050–2060 periods (Table II.12). The A_{ice} of Argentière and Mer de Glace-Leschaux glaciers are projected to decrease by 25% and 16% between the reference state (1983–2004) and the 2030–2040 and by 38% and 25% for the 2050–2060 period, considering our hypothesis of a constant shrinkage rate (Section 4.5.2). According to the projected evolution of the glaciers surface area, the elevation of the glacier front would increase in average, depending on the GCM/RCM combination used, by 1240 m (1325 m) for Argentière and 865 m (1175 m) for Mer de Glace-Leschaux between the reference period and the 2030–2040 (2050–2060).

The sensitivity of the discharge seasonal cycle to the glacio-meteorological changes in the near future (2030–2040) and for the mid-21st century (2050–2060) are shown in Fig. II.7 for the Arveyron d’Argentière and Arveyron de la Mer de Glace catchments. In the Table II.13 we report the mean values and the range (in brackets) of the changes of the considered variables based on the projections used here. With respect to the initial state, the peak value (Y_p) of the seasonal discharge cycle is projected to decrease in average by 9% (14%) and 27% (36%) in the near future (the mid-21st century) for Arveyron d’Argentière and Arveyron de la Mer de Glace, respectively. For both catchments, the timing of the discharge peak is estimated to occur approximately 10 days later in the mid-21st century. When compared to the historical period, the spring discharge values (Q_{spring}) tend to increase both in the near future and mid-21st century. During autumn, the discharge (Q_{autumn}) is projected to decrease in average for both catchments. The annual runoff (Q_{annual}) would be reduced by 13% and 16% for Arveyron d’Argentière and 24% and 31% for Arveyron de la Mer de Glace in the near future and mid-21st century, respectively.

Table II.12: Mean values and range (in brackets) of the changes in the meteorological variables considered (mean temperature from 15 July to 15 August ($T_{15\text{JA}}$), mean temperature in May (T_{May}), mean temperature in September (T_{Sept}), amount of solid precipitation from November to May ($\text{Snow}_{\text{Nov-May}}$) for the 2030–2040 and 2050–2060 periods with respect to the reference state (1983–2004), based on the three used combinations of GCMs/RCMs forced by RCP 2.6.

Period	$T_{15\text{JA}}$	T_{May}	T_{Sept}	$\text{Snow}_{\text{Nov-May}}$
2030–2040	+0.03° yr ⁻¹ (+0.03 – +0.04°C yr ⁻¹)	+0.02°C yr ⁻¹ (+0.01 – +0.03°C yr ⁻¹)	+0.02°C yr ⁻¹ (+0.01 – +0.03°C yr ⁻¹)	-16% (-31 – -6)%
2050–2060	+0.02°C yr ⁻¹ (+0.02 – +0.03°C yr ⁻¹)	+0.01°C yr ⁻¹ (+0.01 – +0.02°C yr ⁻¹)	+0.03°C yr ⁻¹ (+0.02 – +0.04°C yr ⁻¹)	-20% (-37 – -5)%

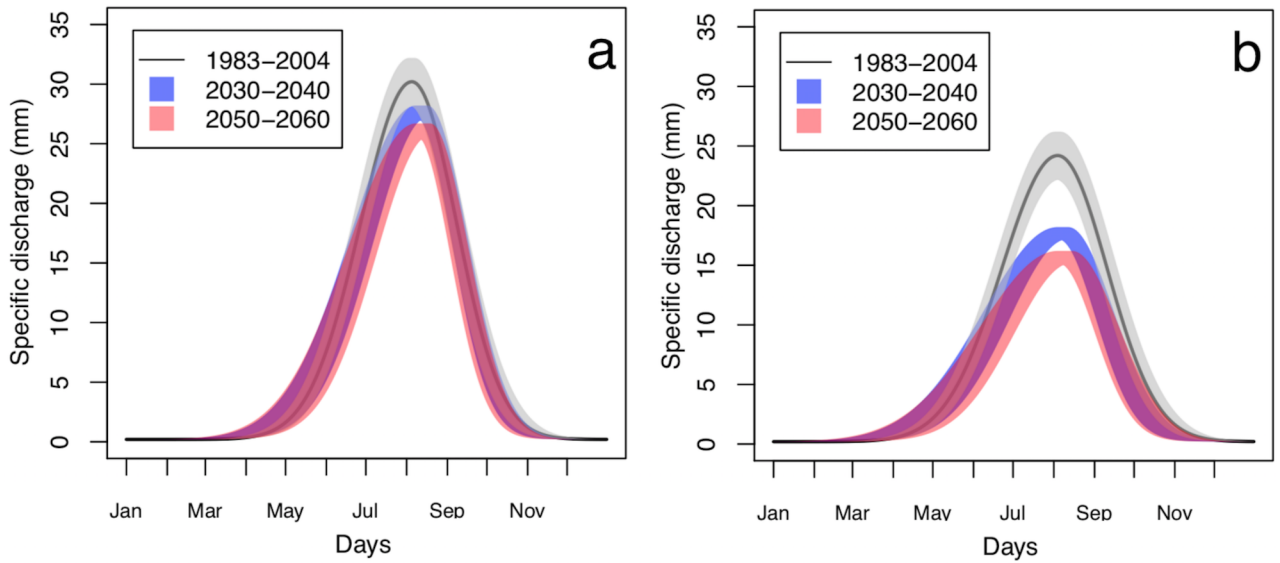


Figure II.7: Discharge seasonal cycle of (a) Arveyron d'Argentière and b) Arveyron de la Mer de Glace for the historic reference period (1983–2004, black line) and simulated for the near future (2030–2040, blue) and mid-21st century (2050–2060, red). The gray areas represent the uncertainty of the fitted seasonal cycle using the APM over the historical period.

Table II.13: The mean values and the range (in brackets) of the changes in the considered variables (discharge peak (Y_p), spring discharge (Q_{spring}), autumn discharge (Q_{autumn}) and annual discharge (Q_{annual})) based on the three combinations of GCMs/RCMs forced by RCP 2.6, for the near future (2030–2040) and mid-21st century (2050–2060) with respect to the reference state (1983–2004).

	Arveyron d'Argentière		Arveyron de la Mer de Glace	
	2030–2040	2050–2050	2030–2040	2050–2060
Y_p	-9% (-7 – -11%)	-14% (-12 – -16%)	-27% (-25 – -29%)	-36% (-33 – -38%)
Q_{spring}	+38% (-30 – +105%)	+35% (-42 – +113%)	+23% (-36 – +82%)	+14% (-51 – +79%)
Q_{autumn}	-15% (-53% – +23)	-26% (-64% – +12)	-42% (-70 – -15%)	-41% (-76 – -6%)
Q_{annual}	-13% (-2 – -23%)	-16% (-10 – -31%)	-24% (-8 – -40%)	-31% (-14 – -50%)

II.6 Discussion

The APM is better suited to reproduce the seasonal cycle of catchments with a nivo-glacial regime than with a nivo-pluvial one, characterized by the presence of high rain-induced peaks which worsens the model performance. The study of these five nested catchments has made it

possible to define the percentage of glacial cover that allows to obtain a good performance of the APM, which needs to be higher than 30%. The time series decomposition used to remove the peak discharge values generated by strong rainfall events may seem artificial, but is necessary to separate the ice and snow melt influence on the discharge.

The trend analysis performed on the discharge values exhibits contrasting behaviors among the catchments characterized by different glacier covers over both periods considered (1960–2004 and 1983–2004). The discharge produced by the three highly glacierized catchments shows an increase at both annual and seasonal scales, in contrast to the low glacierized ones, which exhibit a negative trend. Over the long period this increase is statistically significant and is mainly due to an increase in water production during the spring and summer. This suggests an increasing contribution of snow and glacier melt to the total discharge. Furthermore, since the 1960s, a hydrological regime shift is observed with a melting season that occurs earlier. The changes in land use observed in the lower part of the Arve catchment may play an important role on the observed discharge reduction. Over the last two decades, vegetated areas and complex cultivation patterns increased by 20% and 5%, respectively, for the Arve at Sallanches and by 15% and 16% for the Arve at Bout du Monde, respectively (<https://land.copernicus.eu/pan-european/corine-land-cover>). These changes could result in an increase in evapotranspiration losses, made stronger by the temperature increase, and in the amount of water pumped from the river and surrounding groundwater for irrigation purposes. Further investigations are needed to quantify the effects of these land use changes.

Generally, over the observed period the changes in the evolution of the streamflow seasonal cycle cannot be explained by only observing the precipitation trends. Indeed, precipitation did not show a clear increase or decrease and most of its seasonal trends are not statistically significant. Conversely, air temperature showed marked increasing trends in terms of the mean, maximum and minimum values over the spring, summer and winter seasons for all of the stations included in this work. These increases strongly affect the discharge seasonal cycle because of the impact of temperature on the precipitation phase and melt processes. Indeed, the results suggest that more precipitation falls as rain (statistically significant in winter) due to the higher temperature values and thus a higher altitude of the snow/rain limit. The reduction of the seasonal snow cover in the glacierized basins causes an exposition of glacier bare ice longer in time, which leads to higher melt due to the albedo effect (Pellicciotti et al., 2010).

The magnitude of the trend on the discharge registered at Arveyron d'Argentière and Arveyron de la Mer de Glace became less marked when moving from 1960–2004 to 1983–2004 period. Even the Y_p and Q_f values exhibit a change in their behavior. These changes indicate that the trends registered in highly glacierized catchments are not simply related to the interannual variation of temperature but are associated with glaciers changes. Since the 1980s, the annual surface mass balance of the Argentière and Mer de Glace-Leschaux glaciers is consistently negative, due to an ablation rise (Vincent et al., 2009, 2014) (Figs II.8c,f). The cumulative annual

surface mass balance reveals that the mass loss of both glaciers has been more pronounced since 2001; a similar trend has been observed for Swiss and Italian glaciers (Grossi et al., 2013; Carturan et al., 2016; Bauder, 2017). Furthermore, the analysis of the changes in ice volume shows a pronounced rate of reduction for both glaciers over the observed period (Figs II.8a,d). In the case of the Mer de Glace drainage basin, this glaciological change does not correspond to a continuous increase in the discharge production over the 1983–2013 period (Fig. II.8e). The results suggest that the Mer de Glace glacier could have already passed or would be currently passing the phase of enhanced contribution to the total discharge; meaning that the increase in melt rate does not compensate the reduction in glacier surface area. The annual discharge volume produced by the Argentière drainage basin seems to exhibit a relatively stable trend over the period 1983–2004 (Fig. II.8b); this would suggest that the glacier could have been close to equilibrium over this period (gaining mass in the 1970–80s and losing mass at a moderate rate in the 1990s). Anyway, no clear conclusion can be stated about the proximity/or not of the peak water for Argentière basin because the discharge data are only available up to 2004 (Fig. II.8b). In addition, because since 2003 the glacier-wide annual surface mass balance of Argentière is constantly negative and the rate of ice volume change became more pronounced (Fig. II.8a), getting access and analyzing the discharge data over the more recent years is necessary before giving a reliable conclusion. Last, glaciers do not seem to strongly affect the regime of the low glacierized catchments. However, at this scale the anthropogenic impacts may mask the influence of the glaciers.

The PCA shows that generally the highest load is associated with the temperature values. This confirms that temperature can be considered as the main driving force of the evolution of the discharge seasonal cycle in high-mountain catchments.

Under future climate conditions the peak of the discharge seasonal cycle of Arveyron de la Mer de Glace is projected to decrease more than that of Arveyron d'Argentière. This different behavior could be linked to the morphology of the two considered glaciers. Their hypsometric curves show that a greater part of the Mer de Glace-Leschaux glacier extends at low elevations in comparison with Argentière: the glacier surface area below 2300 m a.s.l. represents 14% and 3% of the total surface area of Mer de Glace-Leschaux and Argentière, respectively (Viani et al., 2018). Furthermore, this difference in the evolution of the discharge peak could be linked to the hypothesis adopted in the present study to describe the future glaciers surface area, considering a constant shrinkage rate that is higher for Mer de Glace-Leschaux glacier ($-0.18 \text{ km}^2 \text{ yr}^{-1}$) than for the Argentière ($-0.11 \text{ km}^2 \text{ yr}^{-1}$). In the mid-21st century the date of the discharge peak of both catchments tends to shift, occurring approximately ten days later in compared with the historical period. This change in the timing of the peak is greater than the uncertainty estimated with our approach, but additional studies need to be carried out for a more definitive statement. The discharge seasonal cycle of both considered glacierized catchments would shift, with a melting season occurring earlier due to the marked spring

temperature increase. On the contrary, the October discharge values tend to decrease, because of the decreasing of the glacier melt contributions. These results agree with those obtained by [Huss and Hock, 2018](#) on the alpine region. We are aware that the model used for the future discharge projections is very simple and does not consider all of the physical processes that occur in the reality. Despite this, it allows having an order of magnitude of what could happen in the future, without using complex models. These results could be useful for the stakeholders in charge of the planning and managing water resources and the hydro-electricity produces.

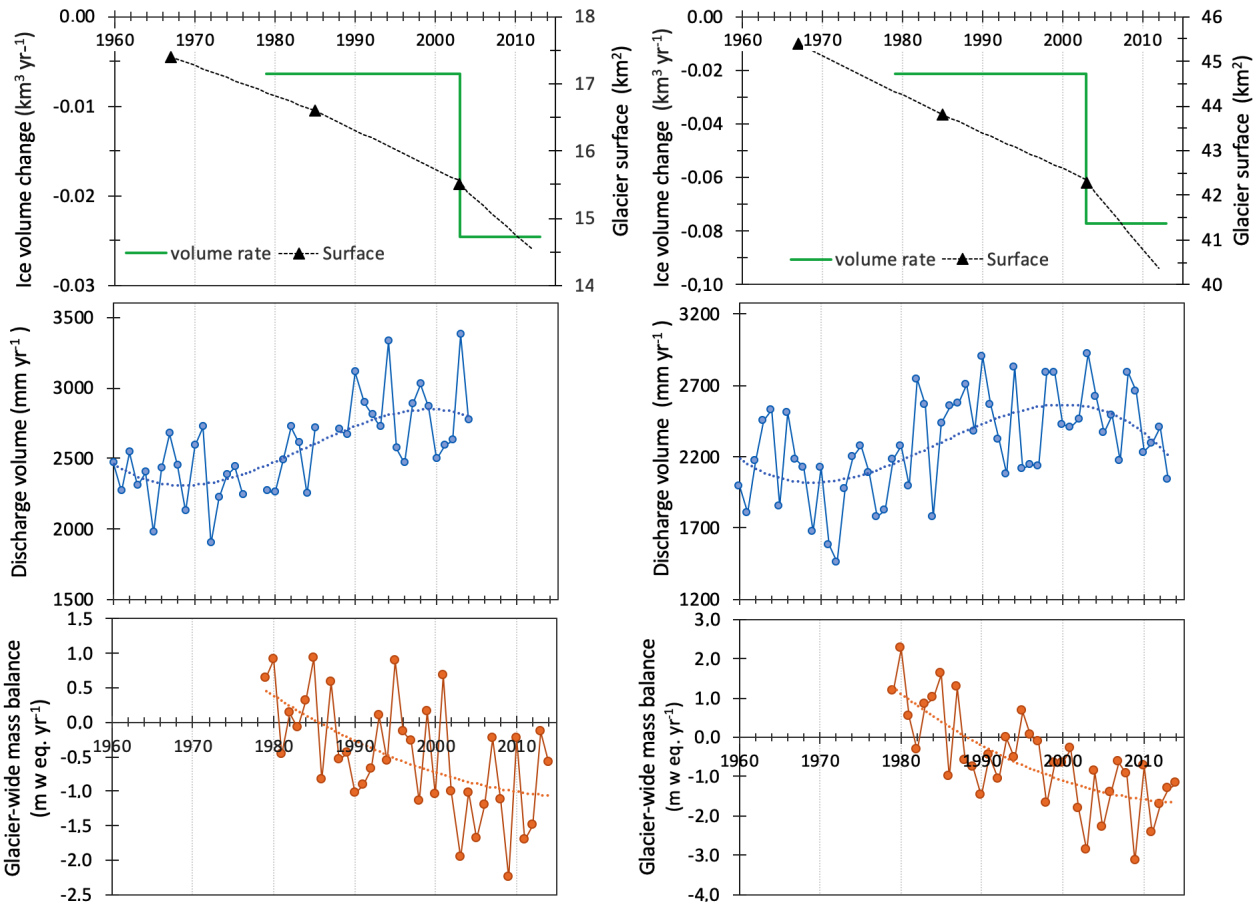


Figure II.8: Evolution over the 1960–2013 period of (a, d) the changes in the glacier volume (blue lines) and in the surface of the ice coverage (the triangles are obtained using Landsat and ASTER images while the dotted lines represent the annual linear change between the years considered); (b, e) the annual discharge production and (c, f) the glacier-wide surface annual mass balance of Argentière/Arveyron d'Argentière (left column) and Mer de Glace-Leschuax/Arveyron de la Mer de Glace (right column).

II.7 Conclusion

The objective of this study was to assess the past and future evolution of the discharge seasonal cycle of five nested catchments along the Arve River (French Alps) characterized by

different percentages of glacier cover (from 5 to 53%) and hydrological regimes. A trend analysis was performed on the discharge values and the parameters characterizing the mathematical function used to fit the seasonal cycle (the asymmetric peak model, APM). Changes in the discharge were related to observed changes in the meteorological variables and the glaciers behaviors. A principal component analysis (PCA) was carried out to evaluate the sensitivity of the seasonal cycle to the future climate projection. The main findings are as follows:

1. The APM is well suited to reproduce the seasonal cycle of the catchment with a nivoglacial regime. The percentage of glacier cover required for high performances of the APM must be greater than 30%. The APM can be used to describe variables characterized by a marked seasonality, in both temperate and tropical regions.
2. The trend analysis performed on the discharge values exhibits contrasting behavior among the highly glacierized catchments (with glacier cover varying from 34 to 53%, in 2003) and those characterized by a low percentage of glacier cover (ranging from 5 to 17%, in 2003) over both the 1960–2004 and 1983–2004 periods. In the highly glacierized catchments the discharge volume production shows an increase at both annual and seasonal scales whereas it exhibits a negative trend in the low glacierized ones. Although the air temperature shows marked increase in terms of the mean, maximum and minimum values, thereby playing an important role in the discharge changes, the precipitation trends are mostly not statistically significant. The increase in temperature results in an increase in the snow/rain limit, an early snowmelt season and a reduction in the seasonal snow cover. Changes in land use and in the evapotranspiration losses may influence the discharge reduction observed in the low glacierized catchments.
3. Passing from 1960–2004 to 1983–2004 the magnitude of the trend on the discharge registered at Arveyron d'Argentière and Arveyron de la Mer de Glace (highly glacierized catchments) became less marked. This behavior indicates that the trends of highly glacierized catchments are not simply related to the interannual variation of temperature but are associated also with glacier changes. There is a high probability that Mer de Glace glacier would be currently passing the phase of enhanced contribution to the total discharge, which means that the increase in melt rate does not compensate its surface reduction. Regarding Argentière glacier, given that the discharge data of its drainage basin are only available up to the year 2004, we cannot state on which phase the glacier is in. For that, discharge data over more recent years are definitely needed. Furthermore, glaciers do not seem to strongly affect the regime of the low glacierized catchments ($< 20\%$ of glacier cover). However, at this scale the anthropogenic impacts, *i.e.* water withdrawals, may mask the influence of the glaciers.

4. The PCA help to show that the seasonal temperature is the main driver of the evolution of the discharge seasonal cycle in high-mountain catchments.
5. Under future climate condition, in the mid-21st century, the peak of the discharge seasonal cycle of the Arveyron d'Argentière and Arveyron de la Mer de Glace catchments is projected to decrease and occurs approximately ten days later compared with the reference period (1983–2004). The discharge values tend to increase in early summer because of an earlier snowmelt due to a marked temperature increase, and to decrease in the late summer, because of the decrease in glacier melt contributions.

These results help improve our understanding of the temporal and spatial evolution of the discharge seasonal cycle in alpine glacierized catchments. They confirm that mountain basins are environments that are sensitive to climate variability given their vulnerability to temperature changes. Further research should be done to quantify the past and future evolution of the discharge components generated by snow and ice melts using a hydro-glaciological model, in order to better understand the potential changes in the discharge seasonal cycle and their implications for water management in the Arve catchment.

Appendix

A.1 Extended Extreme Studentized Deviate (ESD)

The generalized extreme studentized deviate (ESD) test is used to detect one or more outliers in a univariate dataset following an approximately normal distribution (Hochenbaum et al., 2017). It requires the definition of an upper limit (k) for the number of anomalies, that at most, can be set equal to 49.9% of the total number N of data points in the given time series. The null hypothesis states that there are no outliers in the dataset, while the alternative one is that there are at most k outliers. The extended ESD test statistic is calculated as follows:

$$R_j = \frac{\max_j |x_j - \hat{x}|}{MAD} \quad j=1,2, \dots, k \quad (\text{A-1})$$

where \hat{x} and MAD are the median and median absolute deviation of the given dataset, respectively.

R_j is then compared to a critical value λ_j (Eqn. A-2) corresponding to a level α of significance, to determine whether a value is anomalous.

$$\lambda_j = \frac{(N-j)t_{p,N-j-1}}{\sqrt{(N-j-1+t_{p,N-j-1}^2)(N-j-1)}} \quad (\text{A-2})$$

where $t_{\nu,p}$ is the upper critical values of the t distribution with ν degrees of freedom and p is equal to

$$p = 1 - \frac{\alpha}{2(N-j+1)} \quad (\text{A-3})$$

This process of comparison is performed k times, with the number of anomalies equal to the largest k such as that $R_j > \lambda_j$.

A.2 Mann-Kendall test

The Mann-Kendall trend test (Kendall, 1975; Mann, 1945) is based on the correlation between the ranks of a time series and their time order. It does not require normally distributed data or the presence of a linear trend. In this test, the null hypothesis H_0 , which assumes that there is no monotonic trend in the series, is tested against the alternative hypothesis H_1 , which assumes the presence of a trend. The M-K test statistic S is calculated using the formulas:

$$S = \sum_{k=1}^{n-1} \sum_{j=k+1}^n \text{sgn}(x_j - x_k) \quad (\text{A-4})$$

$$\text{sgn}(x_j - x_k) = \begin{cases} +1 & (x_j - x_k) > 0 \\ 0 & (x_j - x_k) = 0 \\ -1 & (x_j - x_k) < 0 \end{cases} \quad (\text{A-5})$$

where n is the length of the time series and x_j and x_k are the values of the observations in the j^{th} and k^{th} year. Under the assumption that the data considered are independent and identically distributed, the mean (E) and variance (Var) of the S statistic (Eqn. [A-4](#)) are given by

$$E(S) = 0 \quad (\text{A-6})$$

$$Var(S) = \frac{n(n-1)(2n+5) - \sum_{p=1}^q t_p(t_p-1)(2t_p+5)}{18} \quad (\text{A-7})$$

where q is the tied value and t_p the number of ties for the p^{th} value.

A.3 Test statistic Z

The significance of the trend can be evaluated by comparing the standardized variable Z (Eqn. [A-8](#)) with the standard normal variate Z_α at the desired significance level α .

$$Z = \begin{cases} \frac{(S-1)}{\sqrt{Var(S)}} & S > 0 \\ 0 & S = 0 \\ \frac{(S+1)}{\sqrt{Var(S)}} & S < 0 \end{cases} \quad (\text{A-8})$$

where S is defined in the Eq.A4. If $|Z|$ is greater than $Z_{\alpha/2}$ (two-tailed test), H_0 is invalid and the trend is considered as significant. A positive (negative) value of Z signifies an upward (downward) trend.

A.4 The Theil-Sen slope

The slope (change per unit of time) of a linear trend presented in a time series can be estimated by using a nonparametric procedure that is robust against outliers and distribution free, called Theil-Sen approach ([Sen, 1968](#); [Theil, 1950](#)). It involves estimating the slopes (b_i) of all lines passing through the pairs of sample points (x) as follows:

$$b_j = \left| \frac{(x_j - x_k)}{(j - k)} \right| \quad \forall k < j ; j = 1, 2, \dots, k \quad (\text{A-9})$$

If the sample is comprised of n values x , $N=n(n-1)/2$ values of b_i will be estimated. The slope b is defined as the median of these N values of b_i .

Acknowledgments

This study was conducted in the context of a research project to develop a flood forecasting system in the Arve catchment funded by the SM3A. It was also supported by the University of Brescia and the University Grenoble Alpes. The authors acknowledge the French glacier observatory GLACIOCLIM (<https://glacioclim.osug.fr>). We thank CNRM/CEN (Météo-France and CNRS) for providing the in situ meteorological data in France, SAFRAN reanalysis and ADAMONT data; Frederic Gottardi (EDF/DTG) for providing the hydrological data. Meteorological data at Geneva are provided by MeteoSwiss. We thank all those who collected data from field measurements on the glaciers as well as meteorological observations used for this study. Finally, we are very grateful to the anonymous reviewers whose comments and suggestions led to a great improvement of the quality of the manuscript.

Chapter III

Glacier-wide summer surface mass-balance calculation: hydrological balance applied to the Argentière and Mer de Glace drainage basins (Mont Blanc)

This chapter consists in the paper published in the Journal of Glaciology in 2018:

Viani, A.^{1,2}, Condom, T.¹, Vincent, C.³, Rabatel, A.³, Bacchi, B.², Sicart, J.E.¹, Revuelto, J.⁴, Six, D.³, Zin, I.¹, 2018. Glacier-wide summer surface mass-balance calculation: hydrological balance applied to the Argentière and Mer de Glace drainage basins (Mont Blanc). *Journal of Glaciology*. 64, 119–131. <https://doi.org/10.1017/jog.2018.7>

¹ University of Grenoble Alpes, CNRS, IRD, Institut des Géosciences de l'Environnement (IGE) - UMR 5001, Grenoble, France; ² Department of Civil Engineering, Architecture, Land, Environment and Mathematics (DICATAM), University of Brescia, Brescia, Italy; ³ University of Grenoble Alpes, CNRS, Institut des Géosciences de l'Environnement (IGE) - UMR 5001, Grenoble, France; ⁴ Météo-France - CNRS, CNRM UMR 3589, Centre d'Études de la Neige (CEN), Grenoble, France

Summary of the research paper

Paper 2

Viani, A., Condom, T., Vincent, C., Rabatel, A., Bacchi, B., Sicart, J.E., Revuelto, J., Six, D., Zin, I., 2018. **Glacier-wide summer surface mass-balance calculation: hydrological balance applied to the Argentière and Mer de Glace drainage basins (Mont Blanc)**. *Journal of Glaciology*. 64, 119–131. <https://doi.org/10.1017/jog.2018.7>

To provide future projections of runoff from specific glaciers, the used models are often calibrated/validated against glaciological and/or altimetric measurements of glacier mass balance. The prediction may be erroneous as they are not accounting for inter-basin transfer. The current study allows to evaluate the importance of considering the groundwater fluxes to represent and predict the hydro-glaciological behaviour of a catchment. The method proposed consists in the estimation of the glacier-wide summer surface mass balance of the Argentière and Mer de Glace-Leschaux glaciers using the hydrological method. A detailed quantification of each term of the hydrological balance equation, as well as their uncertainties, has been done on each glacier drainage basin during the summer season over the 1996–2004 period. The performance of the estimations is evaluated by comparing them with the glacier-wide summer surface mass balances based on the in situ glaciological observations. Because of the lack of long-term meteorological records at high altitudes close to glaciers, meteorological data are taken from the SAFRAN reanalysis. An adjustment of the precipitation data based on the winter field mass-balance measurements has been proposed. Therefore, in this study two precipitation datasets are considered: the original and the adjusted ones.

The results and conclusions of this study can be summarized as follows:

- Ice and snow melt from glacierized areas are the main components of the summer runoff. On average, the contributions of the glacier-wide summer surface mass balances to the discharge represent 58% for Arveyron d'Argentière and 54% for Arveyron de la Mer de Glace.
- The SAFRAN reanalysis yields an underestimation of winter precipitation above 2550 m a.s.l.. The multiplication factors used for the precipitation adjustment are 1.3 for Arveyron d'Argentière and 1.4 for Arveyron de la Mer de Glace.
- The glacier-wide summer surface mass balance obtained with the hydrological method has an uncertainty of ± 0.67 m w.e. yr^{-1} at Argentière and ± 0.66 m w.e. yr^{-1} at Mer de Glace-Leschaux. The greatest errors are introduced by precipitation and discharge measurements.

- Estimates of the hydrological glacier-wide summer surface mass balance for the Argentière glacier are in good agreement with the glaciological values ($R^2 > 0.81$), showing almost the same interannual variability. Their differences are comprised in their measurement uncertainties.
- A marked difference between the estimates of the hydrological glacier-wide summer surface mass balance and the glaciological values for the Mer de Glace-Leschaux glacier is detected. It cannot be explained by the measurement uncertainties only, but it could be attributed to the presence of subterranean fluxes in the Arveyron de la Mer de Glace catchment that prevents the transfer of the totality of the liquid water to its outlet. It can be hypothesized that in this catchment the groundwater term of the hydrological balance equation cannot be neglected and that the measured discharge underestimates the real water production of the catchment.
- The reconstruction of the glacier-wide summer surface mass balance based on hydrological data leads to a good estimation of the glacier behavior when groundwater fluxes are negligible or well known.
- The precipitation adjustment does not improve the computation of the glacier-wide summer surface mass balance based on the hydrological data. It allows for a better reproduction of the spatial distribution of the winter accumulation.
- We therefore caution in the use of calibrated/validated hydro-glaciological models against glaciological measurements of glacier mass balance to calculate future runoff when groundwater fluxes are not negligible, as they are not accounting for inter-basin transfer.

Abstract

We present the glacier-wide summer surface mass balances determined by a detailed hydrological balance (*sSMBhydro*) and the quantification of the uncertainties of the calculations on the Argentière and Mer de Glace-Leschaux drainage basins, located in the upper Arve watershed (French Alps), over the period 1996–2004. The spatial distribution of precipitation within the study area was adjusted using in situ winter mass-balance measurements. The *sSMBhydro* performance was assessed via a comparison with the summer surface mass balances based on in situ glaciological observations (*sSMBglacio*). Our results show that the *sSMBhydro* has an uncertainty of ± 0.67 m w.e. a^{-1} at Argentière and ± 0.66 m w.e. a^{-1} at Mer de Glace-Leschaux. Estimates of the Argentière *sSMBhydro* values are in good agreement with the *sSMBglacio* values. These time series show almost the same inter-annual variability. From the marked difference between the *sSMBhydro* and *sSMBglacio* values for the Mer de Glace-Leschaux glacier, we suspect a significant role of groundwater fluxes in the hydrological balance. This study underlines the importance of taking into account the groundwater transfers to represent and predict the hydro-glaciological behaviour of a catchment.

KEYWORDS: Glacier hydrology, glacier mass balance, mass-balance reconstruction, mountain glaciers

III.1 Introduction

The role of mountains in sustaining the social and economic wellbeing of millions of people is well known and unquestioned since snow fields and glaciers provide indispensable water resources for municipal and industrial water supplies, irrigation, hydropower production and other environmental services (e.g., [Viviroli and Weingartner, 2004](#); [Barnett et al., 2005](#); [Viviroli et al., 2007, 2011](#))

Glaciers are considered as one of the most reliable indicators of climate variations, having either an anthropogenic or natural origin ([Oerlemans, 1986](#); [Haeberli, 1995, 2005](#); [Johannesson, 1997](#)). Changes in melt rates impact runoff dynamics and mainly regulate summer stream flows ([Jansson et al., 2003](#); [Dahlke et al., 2012](#)). Therefore, in highly glacierized catchments, glacier melt provides an important contribution to the river discharge, particularly during the summer ([Verbunt et al., 2003](#); [Koboltschnig et al., 2008](#); [Jost et al., 2012](#)). The retreat of glaciers could lead to increased hazards, such as outbursts of glacier lakes, destabilization of slopes and floods. Furthermore, glaciers have been the biggest source of the observed sea-level rise since 1900 ([Vaughan et al., 2013](#)) and they will potentially contribute more strongly to sea-level rise within the 21st century than the ice sheets ([Church et al., 2013](#)). For this reason, it is

important to have a good understanding of the summer glacier surface mass-balance evolution in order to improve the knowledge of the interaction between glaciers, climate and hydrology. In addition, the assessment of meltwater runoff is crucial for both water supply and hydropower applications.

The determination of the glacier mass balances can be obtained using different methods, such as geodetic, glaciological and energy balance methods (Cogley et al., 2011). There are several studies on modelling of glacier surface mass balance, in the context of providing future projections of runoff from specific glaciers (Immerzeel et al., 2012) and all glaciers worldwide (Marzeion et al., 2012). These models are often calibrated/validated against glaciological and/or altimetric measurements of glacier mass balance. If such models are used to calculate future runoff, they may be erroneous, as they are not accounting for inter-basin transfer (*i.e.* subterranean fluxes).

The current study shows the importance of considering the groundwater fluxes. The method proposed is to estimate the glacier-wide summer surface mass balance using the hydrological method in two glacierized catchments. Our attention is focused on the Argentière and Mer de Glace-Leschaux glaciers, located in the upper part of the Arve watershed at Chamonix (French Alps). To this end, the glacier-wide summer surface mass balance is obtained using observed runoff data and the quantification of each term of the hydrological balance equation, as well as their uncertainties during the summer season (June, July, August, September, hereafter denoted as JJAS) over the period 1996–2004. Meteorological data are taken from the SAFRAN (Système d'Analyse Fournissant des Renseignements Adaptés à la Nivologie) (see Section 3.2) reanalysis due to the lack of in situ measurements. An adjusted precipitation dataset (adjusted SAFRAN) has been produced on the base of the SAFRAN reanalysis (original SAFRAN) taking into account the observed accumulation measurements at each glacier surface. The performance of the summer surface mass-balance estimations based on hydrological data (*sSMBhydro*) is evaluated by comparing them with the glacier-wide summer surface mass balances based on in situ glaciological observations (*sSMBglacio*), over the period 1996–2004.

This paper will first describe the study sites (Section 2) and the available data (Section 3). Then, we will focus on the methodology (Section 4). The estimation of the glacier-wide summer surface mass balances obtained with hydrological and glaciological methods (Section 5) and their comparison (Section 6) will be analysed in detail.

III.2 Study site

The Arve River is an alpine river with a glacial regime that flows mainly through France in the region of Haute-Savoie. Rising in the Graian Alps, close to the Swiss border, it receives water from many glaciers of the Mont Blanc massif before flowing into the Rhône River. The

Arve catchment covers a surface area of 2083 km². This study focuses on the upper Arve catchment at Chamonix (Fig. III.1a), located between the Mont Blanc and Aiguilles Rouges massifs. Its surface area is highly glacierized (35% of the total area, in 2003) with three main glaciers located in the eastern part: Glacier du Tour, Glacier d'Argentière and Glacier de la Mer de Glace-Leschaux, covering areas of 8.2, 11.4 and 31.6 km² in 2003, respectively (Gardent et al., 2014; Rabatel et al., 2016). Here, we focus on the glaciers that belong to the GLACIOCLIM (Les GLACIers, un Observatoire du CLIMat) observatory (<https://glacioclim.osug.fr>, Six and Vincent, 2014): Glacier d'Argentière, monitored since 1976, and Glacier de la Mer de Glace-Leschaux, monitored since 1979 (Fig. III.1b, Table III.1). All the tributaries of these glaciers are considered in the present study. The main tributaries are Glacier des Améthystes (1.3 km²) and Glacier du Tour Noir (1.2 km²) for Argentière and Glacier de Talèfre (7.7 km²) for Mer de Glace-Leschaux (Fig. III.1b). In 2003, the overall surface area of the Argentière glacier with its tributaries was 15.7 km², while that of Mer de Glace-Leschaux and its tributaries was 42.3 km². The hypsometric curves of the glaciers and their tributaries are shown in Fig. III.2.

In the upper Arve catchment, two main glacierized catchments can be identified: Arveyron d'Argentière (32.2 km²) and Arveyron de la Mer de Glace (79.4 km²) (Table III.2). The lowest point reached by the Arveyron de la Mer de Glace catchment is at 1060 m a.s.l. and the highest is at 4295 m a.s.l. (Fig. III.2a). The elevation range of the Arveyron d'Argentière catchment is between 1363 and 4079 m a.s.l. (Fig. III.2a). The largest part of the Arveyron d'Argentière catchment faces southwest (19.2%), while that of the Arveyron de la Mer de Glace faces northwest (17.9%). Nine percent of the area of both catchments faces southward. The extent of the forested and vegetated areas of the Arveyron de la Mer de Glace catchment is slightly higher (1.4%) than that of the Arveyron d'Argentière (Fig. III.1c, Table III.2). Upstream of the Arveyron d'Argentière gauging station (at 2060m a.s.l.), water from the Argentière main glacier is collected by a subterranean tunnel carved into the rock, managed by Electricité d'Emosson S.A. and directed toward Emosson lake (Switzerland) for electricity production (Fig. III.1a). Within the Arveyron de la Mer de Glace catchment, there is a subterranean hydroelectric power plant (centrale des Bois, 1075 m a.s.l.) managed by EDF (Electricité De France) using part of the water of the sub-glacial river of the Mer de Glace-Leschaux glacier (Fig. III.1a). The outflow of this hydroelectric plant is located upstream of the Arveyron de la Mer de Glace hydrological gauging station.

The major rock types present in the Mont Blanc and Aiguilles Rouges massifs, and thus also in the two glacierized catchments considered here, are granite and gneiss (Fig. III.1d). These crystalline rocks underwent several episodes of ductile and brittle tectonic deformation (Corbin and Oulianoff, 1930; Jamier, 1975). The results are fissure and fracture systems in a N-S and NE-SW direction that primarily stretch across the southern part of the upper Arve watershed (Fig. III.1d) (Dubois, 1992; Rossi and Rolland, 2014). It is also noticeable that there is a significant amount of alluvial soils and scree in the lowest part of the Arveyron de la Mer

de Glace catchment.

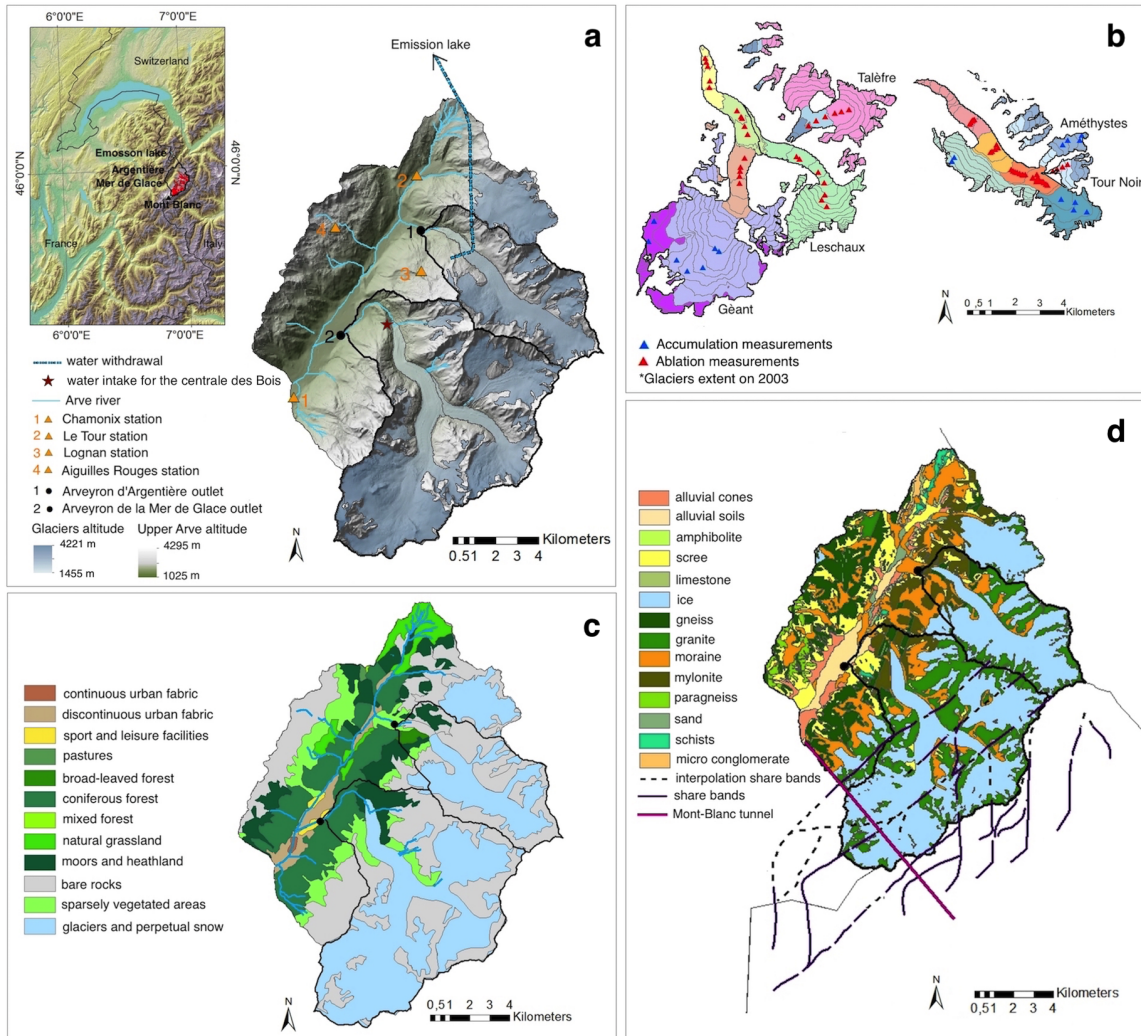


Figure III.1: (a) Location and altimetry of the upper Arve watershed, Arveyron d'Argentière and Arveyron de la Mer de Glace catchments and their respective glaciers (in 2003). The black points and orange triangles respectively indicate the location of the hydrological gauging stations of the two catchments considered and the network of the snow depth gauging stations. The star locates the water intake of the centrale des Bois hydroelectric plant. (b) Mer de Glace-Leschaux (left) and Argentière glaciers (right) with all their tributaries in 2003 (Gardent et al., 2014; Rabatel et al., 2016). The triangles represent the network of the in situ surface mass-balance measurements in both the accumulation (blue) and ablation (red) areas. The different coloured areas indicate the glacier divisions for the computation of the glacier-wide winter glaciological surface mass balance (see Section 4.2). (c) Land cover map of the study area (CLC 06 (Corine Land Cover 2006) (EEA (European Environment Agency), 2007)). (d) Geological map provided by BRGM (Bureau de Recherches Géologiques et Minières). The solid and dotted purple lines respectively represent the main shear zones and their interpolation (Rossi and Rolland, 2014). The pink line indicates the location of the Mont Blanc road tunnel. In figures (c) and (d), the glacier extents are indicative only.

Table III.1: Main characteristics of the two glaciers considered and their main tributaries. The surface areas, elevations and equilibrium-line altitude (ELA) were obtained using satellite images (Rabatel et al., 2013). The number of measurement sites in the ablation and accumulation areas are also listed (Six and Vincent, 2014).

	Argentière	Mer de Glace-Leschaux
Massif	Mont Blanc	Mont Blanc
Main glacier tributaries	Améthystes, Tour Noir	Talèfre
Glacier surface area in 2003 in km ² (in % of the glacier drainage basin area)	15.7 (48.8)	42.3 (53.3)
Glacier surface area in 2012 in km ² (in % of the glacier drainage basin area)	14.6 (45.2)	40.0 (50.4)
Min elevation in 2003 (in 2012) (m a.s.l.)	1455 (1627)	1465 (1538)
Max elevation in 2003 (in 2012) (m a.s.l.)	3738 (3738)	4221 (4221)
Aspect	North-South	North-South
No. of stakes (accumulation area)	9	7
No. of stakes (ablation area)	30	31
Mean ELA main glacier (1984–2014) (m a.s.l.)	2772	2772

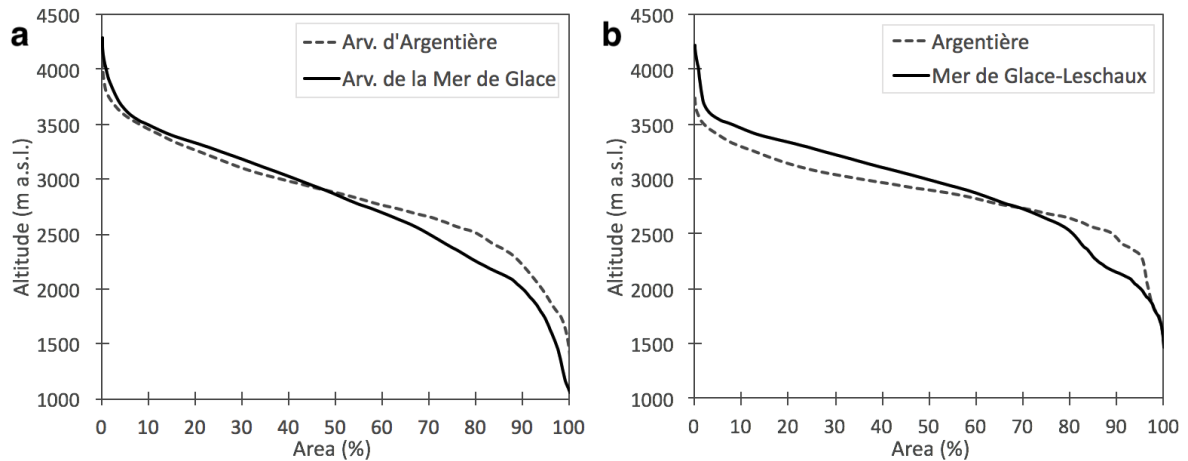


Figure III.2: (a) Hypsometric curves for the (a) Arveyron d'Argentière and Arveyron de la Mer de Glace catchments and (b) Argentière and Mer de Glace-Leschaux glaciers (with all of their tributaries) in 2003.

Table III.2: Main characteristics and land covers (CLC 06, (EEA, 2007) of the two glacierized catchments considered.

	Arv. d'Argentière	Arv. de la Mer de Glace
Surface area (km ²)	32.2	79.4
Min elevation (m a.s.l.)	1363	1060
Max elevation (m a.s.l.)	4079	4295
Median altitude (m a.s.l.)	2877	2063
Mean slope (degree)	30	30
Sport and leisure facilities in km ² (in %)	–	0.04 (0.10)
Broad-leaf forest in km ² (in %)	0.7 (2.2)	–
Coniferous forest in km ² (in %)	0.02 (0.07)	3.0 (3.7)
Moors and heathland in km ² (in %)	2.2 (6.7)	2.2 (6.7)
Bare rocks in km ² (in %)	14.6 (45.3)	24.7 (31.1)
Sparsely vegetated areas in km ² (in %)	0.6 (2.0)	3.5 (4.4)
Glaciers and perpetual snow in km ² (in %)	14.2 (43.8)	44.7 (56.3)

III.3 Data

III.3.1 DEM, glacier surfaces, land cover and geology

The RGE ALTI DEM provided by the French National Geographic Institute (IGN, Institut Géographique National, France) with a horizontal resolution of 5m is used to extract topographic information (elevation, slope and aspect) for the study area in 2012 and to calculate the potential solar radiation based on a hemispherical viewshed algorithm (Rich et al., 1994; Fu and Rich, 1999, 2002). In addition, glacier shapes obtained using Landsat and ASTER images in 2003 and 2012 (Gardent et al., 2014; Rabatel et al., 2016) are used to calculate changes in the glacier surface area, assuming an annual linear change between the two dates. The land cover is investigated using the 2006 Corine Land Cover map, generated with an automatic classification for the whole of Europe (EEA, 2007). Finally, the 1 : 50000 geological map provided by BRGM is used to investigate the lithology of the study area.

III.3.2 Meteorological data

Because of the lack of long-term meteorological records at high altitudes close to glaciers, atmospheric temperature and precipitation data are taken from the SAFRAN reanalysis, available at an hourly timescale over the 1958–2013 period at 300 m altitude steps from 1200 m to 3600 m a.s.l., at the scale of the Mont Blanc massif. SAFRAN (Durand et al., 1999, 2009) is a meteorological analysis system performing a spatialisation of the observed weather data available over the considered elevations and aspects of 23 different massifs within the French

Alps. SAFRAN provides near-surface atmospheric variables (temperature, precipitation rate and phase, incoming shortwave and longwave radiations, wind speed and relative humidity) combining in situ and remotely sensed observations with a prior estimation (called 'guess') provided by the results of the ARPEGE (Action Recherche Petite Echelle Grande Echelle) French meteorological model (Courtier et al., 1991) or from the ECMWF (European Centre for Medium-range Weather Forecasts) analyses through appropriate downscaling operators (Hagemann et al., 2005). The altitude parameters (air temperature, wind, humidity and cloudiness) are analysed by the Optimal Analysis (OI) method (Durand, 1985), a linear regression that uses a flexible statistical scheme, which allows an estimate of every analysed parameter with different possible adjacent data. In a first stage, air temperature, wind and humidity variables are interpolated horizontally using Bichard polynomials and vertically on analysis locations. Afterwards, the preliminary estimated variables are modified using observed values to fit daily meteorological conditions better (for further details see Durand et al., 1993).

In this study, only the Mont Blanc massif is considered since it covers the whole study area.

III.3.3 Glaciological data

Available point measurements of the summer ($psSMB$) and winter ($pwSMB$) surface mass balances over the accumulation and ablation areas of the Argentière and Mer de Glace-Leschaux glaciers and their main tributaries (Tour Noir, Améthystes and Taléfre glaciers) since 1995 are used (Six and Vincent, 2014) (Fig. III.1b). The $psSMB$ measurements, made at the end of September/beginning of October, are obtained from the difference between the point measurements of the annual and winter surface mass balances. The point winter surface mass balances are measured at the end of April/middle of May by drilling cores, based on snow layering (stratigraphy) and density, giving the amount of snow accumulated and its water equivalent. The point annual surface mass balances are determined from wood stakes inserted in the ice. The glacier-wide annual surface mass balances ($aSMB_{glacio}$) of the two considered glaciers quantified by GLACIOCLIM (Vincent et al., 2009, 2014) are also used. Available over the period 1979–2012, they are calculated using the linear model (Lliboutry, 1974; Vincent et al., 2017) adjusted by the geodetic method.

III.3.4 Snow cover

The MOD10A1 products (snow cover and fractional snow cover) with 500 m grid resolution, available from MODIS (MODerate resolution Imaging Spectroradiometer) satellite sensors since 2000, are used to investigate the extent of the snow cover (Hall et al., 2004). These data are based on a snow mapping algorithm that uses the Normalized Difference Snow Index (NDSI). The NDSI is a spectral band ratio that takes advantage of the spectral differences of snow in

short-wave infrared and visible MODIS spectral bands to distinguish snow from clouds and other nonsnow-covered conditions (Salomonson and Appel, 2004). Furthermore, point snow depth measurements provided by four stations (Fig. III.1a) located within the study area at different elevations (Chamonix at 1025 m a.s.l., Le Tour at 1470 m a.s.l., Lognan at 1970 m a.s.l. and Aiguilles Rouges Nivose at 2365 m a.s.l.), belonging to the Météo-France observation network, are used to estimate the amount of winter snow contributing to the summer discharge over the 1996–2004 period.

III.3.5 Hydrological data

The analyses presented in this study are carried out using the total discharge dataset for both Arveyron d’Argentière (available over the period 1955–2004) and Arveyron de la Mer de Glace (available over the period 1950–2014) catchments, available at daily time step and provided by EDF. Because of the water withdrawals below the Argentière glacier, the total discharge of the Arveyron d’Argentière was obtained by adding the data measured at the extraction point to the stream discharge values registered by the gauging station located at the outlet of the catchment. The discharge values of the Arveyron de la Mer de Glace catchment are provided by the gauging station at its outlet. In the Argentière drainage basin, the available data are mainly concentrated from the end of May–October as the sensors are removed during winter.

Finally, it should be noted that the common period covered by all of the datasets (except for the MODIS images) ranges from 1996 to 2004 over the summer season.

III.4 Methods

III.4.1 Hydrological method

The simulated glacier-wide summer surface mass balances are obtained by calculating the hydrological balance equation (Eqn. III.1) of each glacier drainage basin over the summer season (JJAS).

$$-sSMB_{hydro} = -Q_{in-situ JJAS} + P_{tot JJAS} - ETA_{JJAS} - S_{JJAS} + \Delta S_{JJAS} \quad (III.1)$$

$$\Delta S_{JJAS} = \Delta M_{snow JJAS} - \Delta G_{JJAS} \quad (III.2)$$

$$\Delta G_{JJAS} = 0 \quad (III.3)$$

where $sSMB_{hydro}$ is the simulated glacier-wide summer surface mass balance, $Q_{in-situ JJAS}$, $P_{tot JJAS}$, ETA_{JJAS} and S_{JJAS} are the runoff, the total amount of precipitation over the entire

catchment considered, the actual evapotranspiration of the overall catchment and the sublimation of the overall ice and snow surfaces of the catchment considered, respectively, over the JJAS period. ΔS_{JJAS} (Eqn III.2) represents the storage variation of the catchment during the summer, including the contribution given by the melting of snow ($\Delta M_{snow\ JJAS}$) accumulated during the wintertime (October–May) outside of the glacierized areas and the groundwater (ΔG_{JJAS}). The latter is assumed to be equal to zero (Eqn III.3). The glacier storage variation is included in the glacier-wide summer surface mass-balance term. All quantities are in $\text{m}^3\ \text{s}^{-1}$. A semi-distributed approach is used: each catchment has been divided into 10 elevation bands. We have added another band to the nine bands based on the SAFRAN division, in order to take the area of the catchments located above 3750 m a.s.l. into account (see the details of the elevation range of the bands in Table III.3).

Table III.3: Values of the central altitude of the bands and the Y multiplication factors used in Eqn III.6.

Band of altitude	1	2	3	4	5	6	7	8	9	10
Central altitude band (m a.s.l.)	1200	1500	1800	2100	2400	2700	3000	3300	3600	4025
Y [-]	0	0	0	0	0.220	0.415	0.610	0.805	1.000	0

The elevation ranges of each band are the following: Band 1 [1050–1350 m a.s.l.], Band 2 [1350–1650 m a.s.l.], Band 3 [1650–1950 m a.s.l.], Band 4 [1950–2250 m a.s.l.], Band 5 [2250–2550 m a.s.l.], Band 6 [2550–2850 m a.s.l.], Band 7 [2850–3150 m a.s.l.], Band 8 [3150–3450 m a.s.l.], Band 9 [3450–3750 m a.s.l.] and Band 10 [3750–4300 m a.s.l.].

The summer (JJAS) potential evapotranspiration (ETP) of glacierized catchments is obtained as the product of the reference evapotranspiration (ET_0) and the crop coefficient value (K_c), according to the FAO method (Allen et al., 1998). ET_0 is calculated using the formula proposed by Oudin et al., 2005, based on the mean daily air temperature and calculated extra-terrestrial radiation (Morton, 1983). Four reference K_c values (Allen et al., 1998), one for each summer month, are adopted for the different types of soil (Table III.4). The summer ETP ($\text{m}^3\ \text{a}^{-1}$) is then calculated as follows:

$$ETP_{JJAS} = \left(\sum_{b=1}^{10} \left(\sum_{m=6}^9 \left(\sum_{n=1}^N K_c(n, m) A(n, b) ET_0(m, b) \right)_n \right)_m \right)_b \quad (\text{III.4})$$

where the indexes b , m and n represent the bands of altitude, summer months and different types of land cover, respectively. A is the area, K_c is the crop coefficient and ET_0 is the reference evapotranspiration value calculated using the SAFRAN daily temperature. Thus, the summer ETP volume for the catchments considered in this work is obtained as the sum of the summer potential evapotranspiration associated with the 10 bands of altitude (Eqn III.4). Evapotranspiration above the summer 0°C isotherm (3750 m a.s.l.) is considered to be negligible. The glacier evaporation is considered negligible as it is usually small compared with the

other terms of the hydrological balance equation (Paterson, 1994a). Due to the frequent precipitation events during the summer season over the upper Arve catchment (60% of the summer days over the 1996–2004 period), the actual evapotranspiration (ETA) is expected to be equal to the potential evapotranspiration on most days (Konzelmann et al., 1997) (Eqn III.5).

$$ETA_{JJAS} = ETP_{JJAS} \quad (\text{III.5})$$

Three temperature time series (mean, maximum and minimum) from the SAFRAN reanalysis were used to calculate the ETA in order to know its range of interannual variability.

Table III.4: Reference K_c values for each type of land cover, for each summer month (JJAS), used in Eqn III.4

Land cover type	June	July	August	September
Urban fabrics	1.00	1.00	1.00	1.00
Sport and leisure facilities	1.00	1.00	1.00	1.00
Forest	1.20	1.20	1.20	1.18
Moors and heathland	0.50	0.50	0.50	0.50
Bare rocks	0.30	0.30	0.30	0.30
Sparsely vegetated areas	0.36	0.36	0.36	0.36

Six et al., 2009 have shown that, during the summer season, sublimation is <0.12 mm w.e. d^{-1} on the Saint-Sorlin glacier, located in the French Alps. Based on this result and in light of the relatively small distance (~ 100 km as the crow flies) to the Arve watershed, we assumed that sublimation is negligible compared with the other fluxes in our study area. Therefore, the S_{JJAS} in Eqn III.1 is set to zero.

The contribution of solid precipitation accumulated during the wintertime (ΔM_{snow}) to the summer discharge is calculated by considering the melting of the available snowpack that exists on 1 June outside of the glacierized areas. The presence of the snowpack and its thickness are quantified from the SAFRAN winter (October–May) snowfall data, MODIS images and in situ snow depth measurements. The following formula is used:

$$\Delta M_{snow} = \sum_{b=1}^{10} \left(Y(b) P_{snow\ ONDJFMAM}(b) \right) \quad (\text{III.6})$$

where the index b represents the elevation bands (Table III.3), $P_{snow\ ONDJFMAM}$ is the amount of winter (October–May) solid precipitation from the SAFRAN reanalysis (in mm w.e.) and Y is a multiplication factor indicating the percentage of the snow present on 1 June that can melt (in %). We assumed that there is negligible melt above the mean summer 0 °C isotherm (at 3750 m a.s.l.). MODIS images are used to identify the range of altitude characterized by the

presence of snow on 1 June outside of the glacierized areas. The available point measurements of snow depth (Fig. III.3) are used to validate the observation from the MODIS images and to quantify the snow depth at 1 June (in case of the presence of snow) in the part of the catchments up to 2550 m a.s.l. over the period 1996–2004. Once the altitude bands with snow on 1 June are identified, the Y is obtained by assuming a linear change with altitude and the complete melting of the existing percentage of snow. We estimate that the areas below 2350 m a.s.l. and above 3750 m a.s.l. do not represent a source of summer discharge ($Y_{1,2,3,4,10} = 0$) due to the absence of snow below 2350 m a.s.l. at the beginning of June and the absence of snow melt above 3750 m a.s.l. over the 1996–2004 period due to low temperatures (Table III.3). The contributing areas to the summer snow melt range from 2350 to 3750 m a.s.l., i.e. from the 5th to the 9th band of altitude (Table III.3). On the basis of the in situ measurements the Y value at the 5th band is estimated equal to 0.22 while it is set to 1 at the 9th band. Doing a linear interpolation between these two extreme values of Y , we obtained Y values equal to 0.415, 0.610 and 0.805 respectively for the 6th, 7th and 8th bands of altitude (Table III.3).

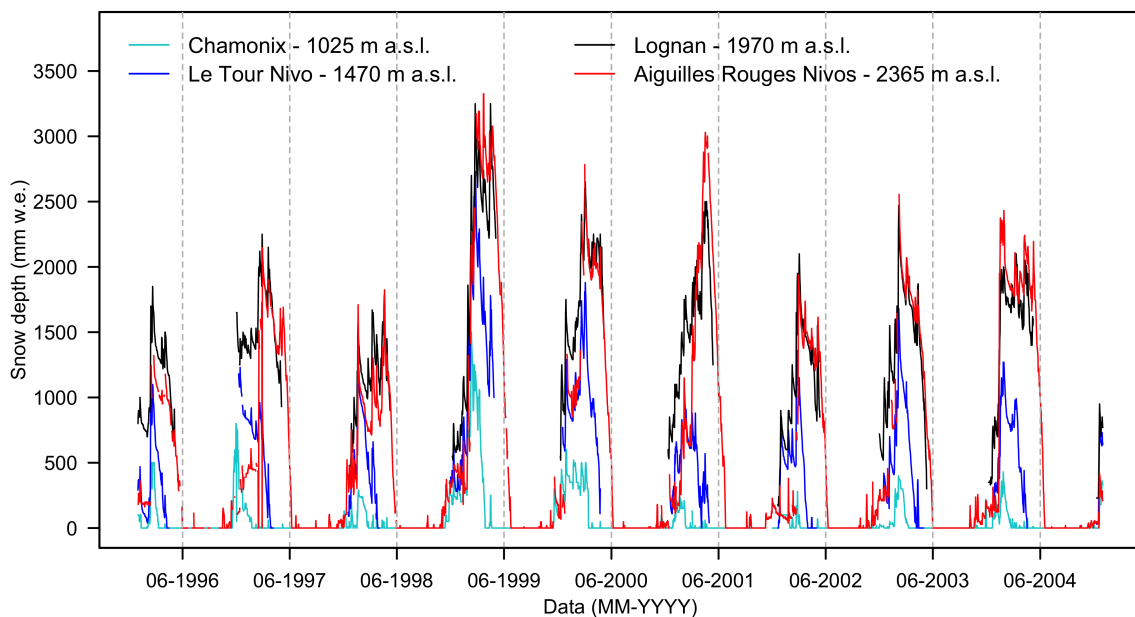


Figure III.3: Evolution of the point-scale snow depth measurements over the period 1996–2004, registered by four Météo-France meteorological stations at different altitudes. Grey vertical lines indicate 1 June of each year.

III.4.2 Glaciological method

In order to know the performance of the simulated glacier-wide summer surface mass balances using the hydrological method ($sSMB_{hydro}$) (Eqn III.1), we compared these balances with the 'observed' glacier-wide summer glaciological surface mass balances ($sSMB_{glacio}$) quantified for the Argentière and Mer de Glace-Leschaux glaciers (and their tributaries) as follows:

$$sSMB_{glacio} = aSMB_{glacio} + wSMB_{glacio} \quad (\text{III.7})$$

where $aSMB_{glacio}$ is the glacier-wide annual glaciological surface mass balance and $wSMB_{glacio}$ is the glacier-wide winter glaciological surface mass balance. $wSMB_{glacio}$ is obtained as follows. First, the glaciers are divided into different zones: seven for Argentière and nine for Mer de Glace-Leschaux, respectively ranging from 1.4 to 3.7 km² and 0.8 to 14.9 km² based on altitude, potential solar radiation and exposure (Fig. III.1b). Then, for the years when some $pwSMB$ measurements are missing (20% of the cases for Argentière and 27% for Mer de Glace-Leschaux), each missing stake measurement is estimated using a linear function with the next best fitting neighbouring stake. The fitting stake is chosen among the different neighbouring stakes on the base of the value of the determination coefficient (R^2 , that ranges from 0.70 to 0.97). Second, for each glacier and for each year, the complete $pwSMB$ dataset is interpolated with quadratic curves as a function of altitude (Réveillet et al., 2017). $wSMB_{glacio}$ (in m w.e. a⁻¹) is calculated as the sum of the products between the $pwSMB$ values at the mean altitude of the zone considered and its area, normalized by the area of the whole glacier considered in the year considered, to take the evolution of the glacier surface into account.

III.4.3 SAFRAN precipitation adjustment

Given that the SAFRAN reanalysis only partially represents the spatial variability of the meteorological conditions within a massif (Durand et al., 2009; Vionnet et al., 2016; Birman et al., 2017), we propose a correction of the SAFRAN precipitation values based on the comparison with the $pwSMB$ measurements (Gerbaux et al., 2005; Dumont et al., 2012; Réveillet et al., 2017). Glacier winter surface mass-balance observations have often been used to either replace precipitation measurements or to validate precipitation estimates at high altitudes (Bucher et al., 2004; Carturan et al., 2012). To capture the spatial variability in the amount of precipitation for the Arveyron d'Argentière and the Arveyron de la Mer de Glace catchments, the correction is done separately for the upper reaches of the two glacierized catchments over the 1996–2004 period. Below the mean altitude reached by the winter 0°C isotherm (at 2550 m a.s.l.), the SAFRAN values are not modified because melting processes can occur and therefore the winter surface mass-balance measurements can underestimate the winter solid precipitation. Conversely, SAFRAN values for higher elevation bands (from 2550 to 4300 m a.s.l.) are increased by an amount that is given by the difference between the trend lines for the SAFRAN winter precipitation and the $pwSMB$ measurements, located in the accumulation zone of the glaciers or at least above 2550 m, obtained using quadratic functions that best fit the data (Fig. III.4). The same precipitation adjustment is applied over the winter and the summer seasons.

In this study, we therefore, consider two SAFRAN precipitation datasets: the original

one (hereafter called 'original SAFRAN') and the adjusted one (hereafter called 'adjusted SAFRAN').

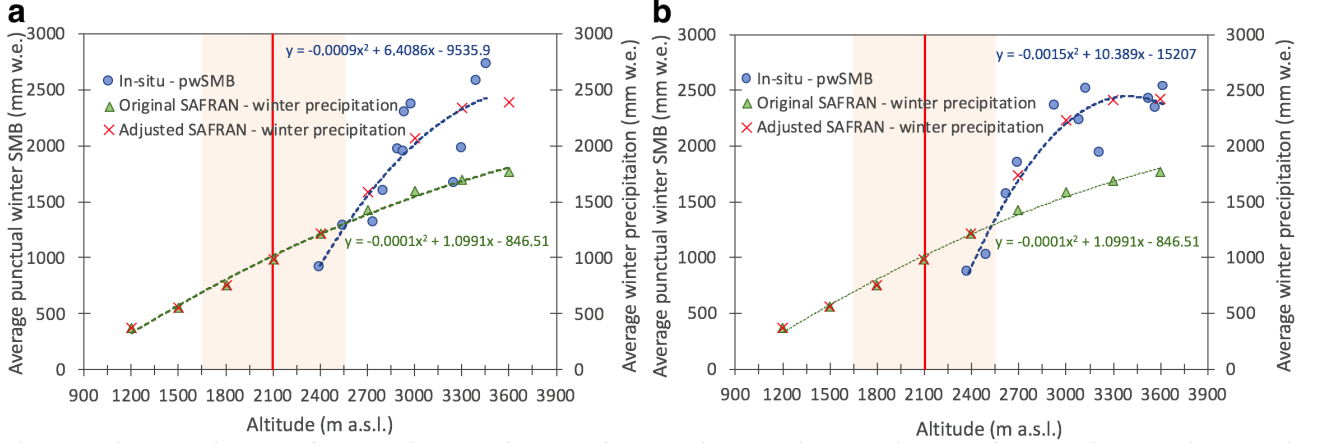


Figure III.4: Evolution with altitude of the point winter surface mass balance ($pwSMB$) of the (a) Argentière and (b) Mer de Glace-Leschaux glaciers and the winter precipitation of the SAFRAN reanalysis, averaged over the period 1996–2004. The dotted lines represent the trend lines of the original SAFRAN winter precipitation and the $pwSMB$ obtained using quadratic functions. The black crosses show the adjusted SAFRAN winter precipitation values. The grey area represents the altitude range reached by the 0°C isotherm during winter (over the period 1996–2004).

III.4.4 Uncertainty in the simulated and 'observed' glacier-wide summer surface mass balances

The standard uncertainty of the $sSMB_{hydro}$ ($\sigma_{sSMB_{hydro}}$), at the 68% level of confidence, is obtained as follows, assuming the errors are random and independent:

$$\sigma_{sSMB_{hydro}} = \sqrt{\sigma_{Q_{in-situ}}^2 + \sigma_{P_{tot}}^2 + \sigma_{ETA}^2 + \sigma_{\Delta M_{snow}}^2} \quad (\text{III.8})$$

where $\sigma_{Q_{in-situ}}$, $\sigma_{P_{tot}}$, σ_{ETA} and $\sigma_{\Delta M_{snow}}$ are, respectively, the standard uncertainties on the in situ runoff data, the total amount of summer precipitation, the actual evapotranspiration and the melting of the winter snow terms, all over the JJAS period, at the 68% level of confidence. $\sigma_{Q_{in-situ}}$ is quantified using the formulation described in the Manual on Stream Gauging (WMO, 2010), in ISO 1088 (International Organization for Standardization, 2007a) and ISO 748 (International Organization for Standardization, 2007b) and adapted to the gauging stations of our study. A 10% standard uncertainty was assumed reliable and conservative.

$\sigma_{P_{tot}}$ and $\sigma_{\Delta M_{snow}}$ are obtained by multiplying the daily standard uncertainty of the original SAFRAN massif precipitation (σ_p) for the summer and winter days, respectively. σ_p (in mm d^{-1}) is calculated as follows, considering the winter season:

$$\sigma_p = \frac{\sqrt{\sigma_{wP_{SAFRAN}}^2 + \sigma_{pwSMB}^2}}{\text{winter days}} \quad (\text{III.9})$$

where $\sigma_{wP_{SAFRAN}}$ and σ_{pwSMB} are the standard uncertainties of the original winter SAFRAN precipitation and the $pwSMB$ data, respectively. $\sigma_{wP_{SAFRAN}}$ is taken as equal to the difference between the trend lines of the SAFRAN winter precipitation and the $pwSMB$ measurements at the median altitude of the considered catchments (Table III.2). σ_{pwSMB} is considered as equal to the mean deviation of $pwSMB$ for the considered glacier from its quadratic trend line above the winter 0°C isotherm, over the period 1996–2004. These uncertainties are also applied to the adjusted SAFRAN precipitation values.

σ_{ETA} is quantified as half the range of the maximum to minimum ETA difference over the period 1996–2004. The standard uncertainty of the $sSMBglacio$ ($\sigma_{sSMBglacio}$), at the 68% level of confidence, is calculated as follows:

$$\sigma_{sSMBglacio} = \sqrt{\sigma_{aSMBglacio}^2 + \sigma_{wSMBglacio}^2} \quad (\text{III.10})$$

where $\sigma_{aSMBglacio}$ and $\sigma_{wSMBglacio}$ are the standard uncertainties of the $aSMBglacio$ and the $wSMBglacio$, respectively. $\sigma_{wSMBglacio}$ is taken as equal to the mean of the deviation of the $pwSMB$ data for the considered glacier from the quadratic line fitted to $pwSMB$ with their elevation, over the period 1996–2004. For the $\sigma_{aSMBglacio}$ value of both glaciers, we used the error quantified by Berthier et al., 2014 for the glaciological mass balance of the Argentière glacier, that is equal to ± 0.40 m w.e. a^{-1} .

It is important to note that the approach for the uncertainty estimation used in this paper is characterized by a significant degree of subjectivity, so one has to have in mind that the uncertainties could be slightly larger or slightly smaller.

III.5 Results

III.5.1 Glacier-wide summer surface mass balance from in situ glaciological measurements

Looking at the evolution of the $sSMBglacio$ (Fig. III.5a, c), it can be seen that the two glaciers considered here (with their tributaries) are characterized by almost the same interannual variability over the period 1996–2004. The mass loss of the Mer de Glace-Leschaux glacier (including all its tributaries) is slightly greater than that of the Argentière glacier (also including all its tributaries) over the entire period considered (-2.68 m w.e. a^{-1} vs -2.62 m w.e. a^{-1}), but the average difference between the two series can be considered within their measurement uncertainties (± 0.49 m w.e. a^{-1} for Argentière and ± 0.58 m w.e. a^{-1} for Mer de Glace-Leschaux)

(Table III.5). The amount of water provided by the two glaciers can be considered as similar and therefore these glaciers appear to be characterized by the same glaciological behaviour.

In addition, the $wSMB_{glacio}$ data for both glaciers, used to calculate $sSMB_{glacio}$ (Eq. III.7), reproduce similar interannual variations over the study period. The winter budget is equal to $+1.77$ m w.e. a^{-1} for Argentière and $+1.71$ m w.e. a^{-1} for Mer de Glace-Leschaux. The difference between these two series is smaller than their uncertainty (± 0.29 m w.e. a^{-1} for Argentière and ± 0.42 m w.e. a^{-1} for Mer de Glace-Leschaux).

Table III.5: Average values of the 'observed' ($sSMB_{glacio}$) and simulated ($sSMB_{hydro}$) glacier-wide summer surface mass balances of the Argentière (including its tributaries) and Mer de Glace-Leschaux (including its tributaries) glaciers over the period 1996–2004.

Glacier	$sSMB_{glacio}$ m w.e. a^{-1}	$sSMB_{hydro}$ m w.e. a^{-1}	
		Original SAFRAN	Adjusted SAFRAN
Argentière	-2.62 ± 0.49	-2.79 ± 0.67	-2.33 ± 0.67
Mer de Glace-Leschaux	-2.68 ± 0.58	-2.00 ± 0.66	-1.55 ± 0.66

III.5.2 Glacier-wide summer surface mass balance from hydrological data

Hereafter we present a quantification of each term of the hydrological balance equation (Eqn III.1) using both the original and adjusted SAFRAN reanalysis during the summer season (JJAS) over the period 1996–2004 for the Arveyron d'Argentière and Arveyron de la Mer de Glace catchments.

Over the period 1996–2004, the highest amounts of summer total precipitation occur in the 7th (between 2850 and 3150 m a.s.l.) and 8th band (between 3150 and 3450 m a.s.l.) of altitude for the Arveyron d'Argentière and Arveyron de la Mer de Glace catchments, respectively. Over this period, the discharge produced by the total summer precipitation for the two considered catchments is similar in relation to their size.

Over the study period, the average contribution to the outflow given by the total precipitation (original SAFRAN) equals 2.55 $m^3 s^{-1}$ (*i.e.* 0.84 m w.e. a^{-1}) and 6.20 $m^3 s^{-1}$ (*i.e.* 0.82 m w.e. a^{-1}) for the Arveyron d'Argentière and Arveyron de la Mer de Glace catchments, respectively. On average, the multiplication factors used for the SAFRAN precipitation adjustment are 1.3 for Arveyron d'Argentière and 1.4 for Arveyron de la Mer de Glace. For comparison, these values are slightly lower than those quantified by Gerbaux et al., 2005 (1.5) for the Argentière and Saint-Sorlin glaciers, Gottardi, 2009 (1.6) for solid precipitation on the French Alps and Dumont et al., 2012 (1.64) for the Saint-Sorlin glacier. It should be noted that the values for this factor depend on the calibration period and the site considered. On average,

over the study period, the discharges produced by total summer precipitation obtained from the adjusted SAFRAN are 20% (*i.e.* $0.51 \text{ m}^3 \text{ s}^{-1}$) and 24% (*i.e.* $1.50 \text{ m}^3 \text{ s}^{-1}$) higher than those obtained using the original SAFRAN reanalysis for the Arveyron d'Argentière and Arveyron de la Mer de Glace catchments, respectively. The difference of these rates is due to the different spatial distribution of precipitation over the two considered catchments.

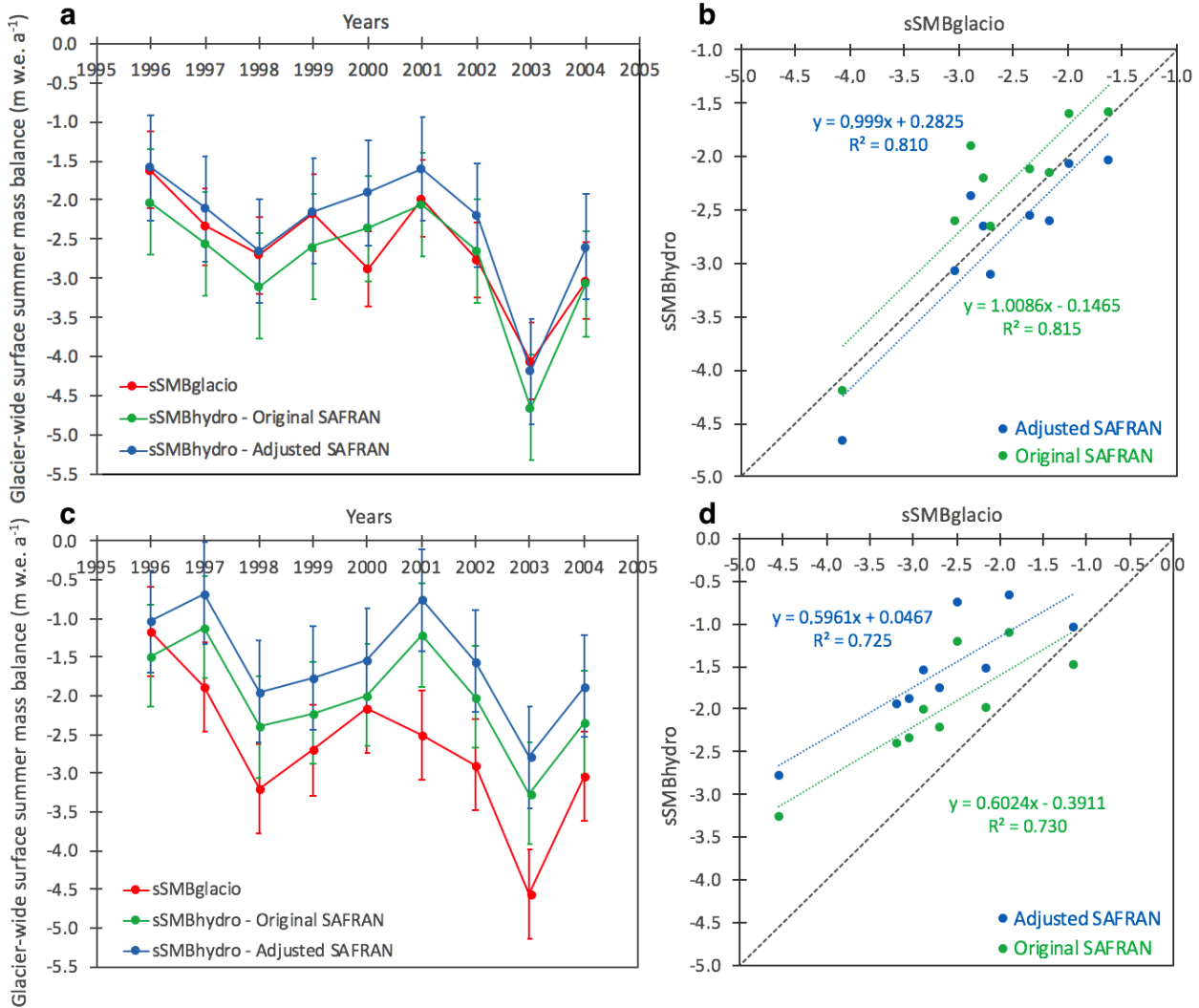


Figure III.5: Comparison between the 'observed' glacier-wide summer surface mass balances ($sSMB_{glacio}$) and the quantified balances ($sSMB_{hydro}$) using the original and adjusted SAFRAN data for (a) the Argentière (including its tributaries) and (c) Mer de Glace-Leschaux (including its tributaries) glaciers over the period 1996-.2004. Vertical bars represent the standard uncertainties. Correlations between the $sSMB_{glacio}$ dataset and the two estimates of $sSMB_{hydro}$ for (b) the Argentière and (d) Mer de Glace-Leschaux glaciers over the 1996-2004 are also presented. The dashed lines presented in (b) and (d) represent the bisector.

The highest values of summer ETA (Eqn III.5) are produced in the 4th band of altitude (between 1950 and 2250 m a.s.l.) for both the Arveyron d'Argentière ($0.03 \text{ m}^3 \text{ s}^{-1}$) and Arveyron de la Mer de Glace ($0.09 \text{ m}^3 \text{ s}^{-1}$) catchments. It is interesting to note that, on average, the

ETA rate (m w.e. a⁻¹) is 27.2% (*i.e.* 0.031 m w.e. a⁻¹) higher for Arveyron de la Mer de Glace, over the period 1996–2004. This could be because this catchment is characterized by a greater expanse of forested area related to Arveyron d’Argentière (3.7% *vs* 2.3%, respectively) and by a wider expanse of lower areas with higher temperature. The difference between the *ETA* for the two catchments remains constant over the whole period.

Over the study period, on average, the contribution to the discharge given by the winter snow melt (Eqn III.6) outside of the glacierized area during the summer months is estimated (original SAFRAN) to be equal to 0.6 m³ s⁻¹ (*i.e.* 0.42 m w.e. a⁻¹) and 1.1 m³ s⁻¹ (*i.e.* 0.31 m w.e. a⁻¹) for the Arveyron d’Argentière and Arveyron de la Mer de Glace catchments, respectively. These values increase by 30% (*i.e.* 0.18 m³ s⁻¹) for Arveyron d’Argentière and 34% (*i.e.* 0.36 m³ s⁻¹) for Arveyron de la Mer de Glace when the adjusted SAFRAN precipitation amounts are used instead of the original data.

After quantifying all the contributions, the glacier-wide summer surface mass balance based on hydrological data (Eqn III.1) can be estimated for each glacier using the original and adjusted SAFRAN reanalysis (Fig. III.6). Ice and snow melt from glacierized areas are clearly one of the main contributors to summer runoff. On average, the contributions of the *sSMBhydro* to the discharge, using the original (adjusted) SAFRAN values, are estimated to be 58% (49%) for Arveyron d’Argentière and 54% (42%) for Arveyron de la Mer de Glace. The amount of water loss through evapotranspiration represents ~6% (5%) of the summer total precipitation calculated using the original (adjusted) SAFRAN values for both the Arveyron d’Argentière and Arveyron de la Mer de Glace catchments. The contribution given by the summer total precipitation calculated with the original (adjusted) SAFRAN values represents 35% (42%) of the discharge for the Arveyron d’Argentière catchment and 41% (51%) for the Arveyron de la Mer de Glace catchment. The snow melt runoff (outside the glacier) represents 9% (11%) and 7% (9%) of the total summer discharge, respectively, for the Arveyron d’Argentière and Arveyron de la Mer de Glace catchments. The observed inter-annual variations in summer discharge from the two catchments are almost similar over the period 1996–2004 (not shown here).

The standard uncertainties of the terms involved in the hydrological balance equation are listed in Table III.6. The average standard uncertainties for *sSMBhydro* are equal to ± 1.06 m³ s⁻¹ (*i.e.* ± 0.67 m w.e. a⁻¹) for Argentière and ± 2.71 m³ s⁻¹ (*i.e.* ± 0.66 m w.e. a⁻¹) for Mer de Glace- Leschaux. The greatest errors affecting *sSMBhydro*, in terms of m³ s⁻¹, are introduced by precipitation and discharge measurements, *i.e.* 0.71 m³ s⁻¹ and 0.73 m³ s⁻¹ for Argentière and 2.14 m³ s⁻¹ and 1.51 m³ s⁻¹ for Mer de Glace-Leschaux (Fig. III.6 and Table III.6). The daily standard uncertainty estimated for precipitation is almost the same as that quantified by Quintana-Seguí et al., 2008 for the SAFRAN precipitation over France (2.3 mm d⁻¹ for the Arveyron d’Argentière and 2.4 mm d⁻¹ for the Arveyron de la Mer de Glace *vs* 2.4 mm d⁻¹).

III.6 Discussion

For the Argentière glacier, a small difference can be noted when comparing the average $sSMB_{hydro}$ and $sSMB_{glacio}$ values over the 1996–2004 period Fig. III.6a. The simulated values using the original SAFRAN reanalysis are more negative than the $sSMB_{glacio}$ values by 12% ($-2.79 \text{ m w.e. a}^{-1}$ vs $-2.62 \text{ m w.e. a}^{-1}$) while those obtained from the adjusted SAFRAN are less negative by 6% ($-2.33 \text{ m w.e. a}^{-1}$ vs $-2.62 \text{ m w.e. a}^{-1}$) (Table III.5). The evolution of the $sSMB_{hydro}$ values over the considered period is in good agreement with the $sSMB_{glacio}$ values, showing almost the same inter-annual variability (Fig. III.5a). The correlations between the $sSMB_{glacio}$ dataset and the two estimates of $sSMB_{hydro}$ are significant at 99% confidence interval according to the Pearson's test ($R^2 > 0.81$) (Fig. III.5 b). We can conclude that the difference between the $sSMB_{glacio}$ calculation and the two $sSMB_{hydro}$ estimates for the Argentière glacier is comprised in their measurement uncertainties, equal to $\pm 0.49 \text{ m w.e. a}^{-1}$ on the former and $\pm 0.67 \text{ m w.e. a}^{-1}$ on the latter (Table III.5). As a consequence, the two estimates of the summer surface mass balance using the hydrological and glaciological data are in good agreement.

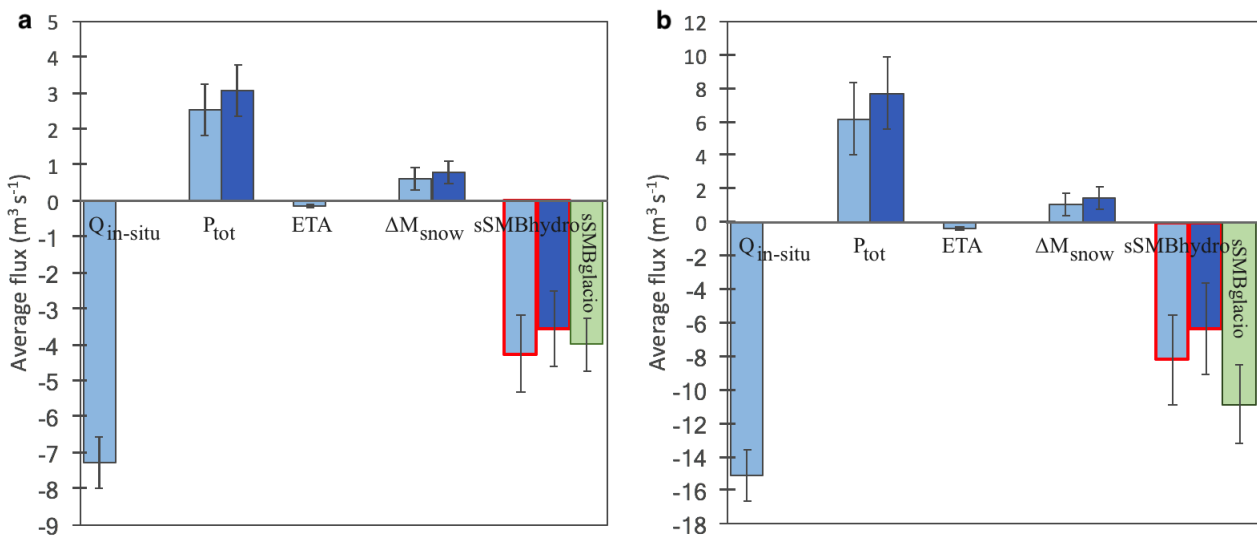


Figure III.6: Hydrological balance for the (a) Arveyron d'Argentière and (b) Arveyron de la Mer de Glace catchments. Light and dark blue bars represent the average summer flux of the variables involved in the hydrological balance equation (in situ stream outflow ($Q_{in-situ}$), total precipitation (P_{tot}), actual evapotranspiration (ETA) and snow melt runoff (ΔM_{snow})) calculated using the original and adjusted SAFRAN reanalysis, respectively, over the period 1996–2004. Red contours highlight the two $sSMB_{hydro}$ estimates for the glaciers considered. Green bars represent the $sSMB_{glacio}$ values. Vertical black lines represent the standard uncertainties.

In the case of the Mer de Glace-Leschaux glacier, the $sSMB_{hydro}$ values quantified from the original and adjusted SAFRAN data are less negative than the $sSMB_{glacio}$ values by 24% ($-2.00 \text{ m w.e. a}^{-1}$ vs $-2.68 \text{ m w.e. a}^{-1}$) and 41% ($-1.55 \text{ m w.e. a}^{-1}$ vs $-2.68 \text{ m w.e. a}^{-1}$), respectively

Table III.6: Standard uncertainties (σ) ($\text{m}^3 \text{s}^{-1}$ and m w.e. a^{-1}) for the variables involved in the hydrological balance equation ($Q_{in-situ}$, P_{tot} , ETA , ΔM_{snow}), the simulated glacier-wide summer surface mass balance ($sSMBhydro$) obtained in the case of the original and the adjusted SAFRAN reanalysis, the glacier-wide winter surface mass balance ($wSMBglacio$), the glacier-wide annual surface mass balance ($aSMBglacio$) and the 'observed' glacier-wide summer surface mass balance ($sSMBglacio$).

	Arv. d'Argentière / Argentière				Arv. De la Mer de Glace / Mer de Glace-Leschaux			
	Original SAFRAN		Adjusted SAFRAN		Original SAFRAN		Adjusted SAFRAN	
	$\text{m}^3 \text{s}^{-1}$	m w.e. a^{-1}	$\text{m}^3 \text{s}^{-1}$	m w.e. a^{-1}	$\text{m}^3 \text{s}^{-1}$	m w.e. a^{-1}	$\text{m}^3 \text{s}^{-1}$	m w.e. a^{-1}
$\sigma_{Q_{in-situ}}$	0.73	0.24	–	–	1.51	0.20	–	–
$\sigma_{P_{tot}}$	0.71	0.23	0.71	0.23	2.14	0.28	2.14	0.28
σ_{ETA}	0.03	0.02	–	–	0.08	0.02	–	–
$\sigma_{P_{\Delta M_{snow}}}$	0.30	0.20	0.30	0.20	0.68	0.20	0.68	0.20
$\sigma_{sSMBhydro}$	1.06	0.67	1.06	0.67	2.71	0.66	2.71	0.66
$\sigma_{aSMBglacio}$	0.20	0.40	–	–	0.54	0.40	–	–
$\sigma_{wSMBglacio}$	0.22	0.29	–	–	0.86	0.42	–	–
$\sigma_{sSMBglacio}$	0.75	0.49	–	–	2.36	0.58	–	–

(Table III.5). As for the Argentière glacier, the correlations between the $sSMBglacio$ dataset and the two estimates of $sSMBhydro$ for Mer de Glace-Leschaux are significant at 99% confidence (Pearson's test) ($R^2 > 0.72$) (Fig. III.5d). In this case, although the uncertainty ranges overlap ($\pm 0.66 \text{ m w.e. a}^{-1}$ on the $sSMBhydro$ data and $\pm 0.58 \text{ m w.e. a}^{-1}$ on the $sSMBglacio$ data) (Fig. III.5c), the marked difference between the $sSMBhydro$ and $sSMBglacio$ values probably also results from another source. It could be attributed to the presence of aquifers and subterranean fluxes in the Arveyron de la Mer de Glace catchment that prevents the transfer of the totality of the liquid water to the outlet of the catchment. Thus, we can hypothesize that the groundwater term (see Eqn III.3) cannot be neglected in the Arveyron de la Mer de Glace catchment. We might expect that the measured discharge from the Arveyron de la Mer de Glace catchment underestimates the real water production of the catchment, leading to an underestimation of the $sSMBhydro$ value for the Mer de Glace-Leschaux glacier. By observing the network of fractures located in the upper Arve watershed (Fig. III.1d), we can notice that they are mainly concentrated in the Arveyron de la Mer de Glace catchment. They are NE-SW and N-S oriented and can drive the subterranean fluxes southward, outside of the topographic catchment. The abundance of open fractures actually leads to a relatively higher permeability of the ground, compared with that of undisturbed crystalline rocks (Kilchmann S., 2001). The real existence of deep large groundwater fluxes within the Mont Blanc massif has already been demonstrated through studies carried out on water inflows during the drilling of the Mont Blanc road tunnel (Maréchal, 1998, 2000, 2012; Rolland et al., 2003). The zones characterized by high water inflows are accompanied by a decrease in the water temperature, due to the large

cold water infiltration from the glaciers. The water inflows are also recharged by snow melt at the beginning of summer on the Glacier du Gèant and more probably on the Glacier de Toule (Maréchal, 2000), which are located in the Arveyron de la Mer de Glace catchment. On the other hand, observing the geological map (Fig. III.1d), it can be noted that in the lower part of the Arveyron de la Mer de Glace catchment there is a significant amount of alluvial soils that do not exist in the Arveyron d'Argentière catchment, which likely facilitates the movement of groundwater into local shallow aquifers.

The adjustment of precipitation does not lead to a clear improvement of the computation of the *sSMBhydro* (Figs. III.5 and III.6). For the Argentière glacier the two estimates of the summer surface mass balance, with and without precipitation adjustment, are respectively a little higher and a little lower than what the glaciological data suggest. In the case of Mer de Glace glacier, it seems that the adjustment leads in the wrong direction compared with the glaciological values. This simply means that this catchment might lose an important water amount through groundwater flows. Since SAFRAN reanalysis yields an underestimation of winter precipitation, the adjustment is made to reproduce the observed spatial distribution of the winter accumulation.

III.7 Conclusion

The comparison between the glaciological summer mass balances and the runoff measurements shows that the water provided by the two glaciers, including snow and ice melt, can be considered as the main contributor of summer runoff. After the quantification of all components of the summer hydrological balance equation for each study catchment, it can be seen that the contributions of the simulated glacier-wide summer surface mass balance obtained using the original and adjusted SAFRAN data to the discharge are estimated to be 58% 49% for the Arveyron d'Argentière catchment and 54% and 42% for the Arveyron de la Mer de Glace catchment. In the two catchments, the volume of evapotranspiration remains small and does not strongly impact the hydrological balance.

The spatial distribution of precipitation within the considered catchments is adjusted using in situ winter mass balance measurements. The multiplication factors applied to the original SAFRAN data, estimated from the point winter glaciological surface mass-balance measurements, revealed that the precipitation amount that falls over the Arveyron de la Mer de Glace catchment is slightly higher than that over the Arveyron d'Argentière catchment on average (1.4 vs 1.3, respectively).

The standard uncertainty of the Argentière glacier-wide summer surface mass balance based on hydrological data are equal to ± 0.67 m w.e. a^{-1} over the 1996–2004 period. The differences between the glacier-wide summer glaciological surface mass balance and the two estimates of the

hydrological glacier-wide summer surface mass balance, computed with and without adjusted precipitation values, are not significant and can be justified by the measurement uncertainties. In addition, the summer mass balances quantified from the hydrological and glaciological data show almost the same interannual variability. In the case of the Mer de Glace-Leschaux glacier, the average error of the glacier-wide summer surface mass balance based on hydrological data are equal to ± 0.66 m w.e. a^{-1} . The two estimates of the glacier-wide summer surface mass balance based on hydrological data are less negative than the summer mass balances quantified from glaciological data. This difference cannot be explained by the measurement uncertainties alone and therefore it can be hypothesized that in the Arveyron de la Mer de Glace catchment the groundwater term of the hydrological balance equation cannot be neglected and that the measured discharge underestimates the real water production of the catchment. The presence of aquifers and subterranean fluxes could prevent the transfer of all of the liquid water to the outlet, leading to an underestimation of the glacier-wide summer surface mass balance for Mer de Glace-Leschaux. Further investigations are needed in order to quantify these subterranean water fluxes.

The precipitation adjustment does not improve the computation of the glacier-wide summer surface mass balance based on the hydrological data, for both Argentière and Mer de Glace glaciers. The results point out the important loss of water through groundwater flows in the Arveyron de la Mer de Glace catchment. Substantially, the adjustment of the SAFRAN reanalysis allows for a better reproduction of the spatial distribution of the winter accumulation.

In essence, this study underlines the importance of estimating the groundwater fluxes and taking them into account when they are not negligible, for a comprehensive assessment of the present and future hydro-glaciological behaviour of a catchment.

Acknowledgments

This study was conducted in the context of a research project to develop a flood forecasting system in the Arve catchment (funded by the SM3A). The authors acknowledge the French glacier observatory GLACIOCLIM (<https://glacioclim.osug.fr>) and the Labex OSUG@2020 (Investissements d'avenir – ANR10 LABX56). We thank CNRM/CEN (Météo-France and CNRS) for providing the SAFRAN reanalysis data and in situ snow depth data; Frederic Gottardi (EDF/DTG) for providing the hydrological data. We are grateful to R. Ranzi, O. Laarman and C. Coulaud for fruitful discussions and to S. Morin for his constructive and useful comments. We thank all those who collected data from field measurements on the two glaciers as well as meteorological and snow observations used for this study. Finally, we are very grateful to the two anonymous reviewers for their comments and suggestions that have improved greatly the quality of the manuscript.

Chapter IV

Multi-criteria calibration of distributed temperature index models in a highly glacierized alpine catchment under climate variability

This chapter consists in a paper in preparation for Water Resources Research:

Viani, A.^{1,2}, Condom, T.¹, Vincent, C.¹, Rabatel, A.¹, Gouttevin, I.³, Simon, G.⁴, Sicart, J.E.¹ and Ranzi, R.². Multi-criteria calibration of distributed temperature index models in a highly glacierized alpine catchment under climate variability. *In preparation*.

¹ University of Grenoble Alpes, CNRS, IRD, Institut des Géosciences de l'Environnement (IGE) - UMR 5001, Grenoble, France; ² Department of Civil Engineering, Architecture, Land, Environment and Mathematics (DICATAM), University of Brescia, Brescia, Italy; ³ Météo-France - CNRS, CNRM UMR 3589, Centre d'Études de la Neige (CEN), Grenoble, France; ⁴ Centre d'Études Spatiales de la Biosphère (CESBIO), UPS/CNRS/IRD/CNES, Toulouse, France.

Summary of the research paper

Paper 3

Viani, A., Condom, T., Rabatel, A., Vincent, C., Gouttevin, I., Simon, G., Sicart, J.E., and Ranzi, R.. **Multi-criteria calibration of distributed temperature index models in a highly glacierized alpine catchment under climate variability.** *In preparation for Water Resources Research.*

The purpose of this work is to identify the best suitable simple model allowing the simulation of the hydro-glaciological processes and the subglacial discharge in the Arveyron d'Argentière catchment (French Alps) with a glacial coverage of 49% (in 2003). In addition, the importance of the choice of the calibration method and the short and long-term temporal stability of the considered models have been assessed. The classical degree-day method (DD) and the enhanced temperature index model with the inclusion of the potential clear-sky direct solar radiation (HTI) coupled with a linear reservoir discharge model are used. Simulations are run at daily time step, with a spatial resolution of 5 m. The calibration is carried out against discharge only and with a multi-criteria approach considering the discharge, the snow cover area and the glacier-wide annual mass balance, over the 2000–2003 period. Validation is made over different subperiods according to data availability within the 1960–2009 period. This study is based on long dataset of in situ or remote sensing glaciological, meteorological, hydrological and snow cover area data. The computation of the glacier contribution to the total discharge and the simulated uncertainties are also carried out.

The main conclusions are the follows:

- Generally, both the calibrated DD and HTI models exhibit a very good performance in simulating the variables considered, but the simulations tend:
 - to overestimate the discharge production at the beginning of the melt season (May–June). This may be mainly because the cold content of the snowpack is not included in the models' structure.
 - to overestimate the observed snow cover area in June.
 - to underestimate the snow line altitude.
- The glacier discharge is one the most important component of the total discharge, representing on average 63% of the total water production of the catchment over the 1960–2004 period (result in agreement with [Viani et al., 2018](#)).

- Results underline the suitability of both models in simulating the subglacial water production.
- Unlike [Pellicciotti et al., 2005](#), [Hock, 1999](#) and [Gabbi et al., 2014](#), in our catchment the inclusion of the clear sky solar radiation in a temperature index model does not seem to improve considerably the model performance in simulating the hydro-glaciological variables considered over calibration and validation periods.
- The use of a multi-calibration approach could help to reduce the uncertainty in the simulations and to obtain a robust model increasing the confidence in its physical relevance.
- The short-term stability both of the DD and HTI models is pointed out, since their performance does not deteriorate significantly using set of parameters coming from different calibration years, characterized by distinct climate conditions.
- Our results reveal a long-term stability of the DD and HTI models in simulating the daily discharge and the annual water volume production over 1960–2004.
- We suggest the use of a classical degree day model calibrated with a multi criteria approach to simulate the hydro-glaciological behavior of a highly glacierized catchment and to study the long-term impact of the climate variability on the discharge.

Abstract

We identify the best suitable simple model allowing the simulation of the hydro-glaciological processes and the subglacial discharge on a daily time scale in the Arveyron d'Argentière catchment (French Alps) with a glacial coverage of 49% (in 2003). In addition, the importance of the choice of the calibration method and the short and long-term temporal stability of the considered models have been assessed. Two different distributed melt models are considered: the classical degree-day model and the enhanced temperature index one with the inclusion of the potential clear-sky direct solar radiation. Both have been coupled with a linear reservoir discharge model for routing the ice and snow melt runoff to the basin's outlet. The calibration is carried out against discharge only and with a multi-criteria approach considering the discharge, the snow cover area and the glacier-wide annual mass balance, over the 2000–2003 period at daily time step. Validation is made over different subperiods according to data availability within the 1960–2009 period. This study is based on long dataset of in situ or remote sensing glaciological, meteorological, hydrological and snow cover area data. Our findings reveal that the multi-calibration of a conceptual model against the discharge only results in an increase in the performance that is generally not significant compared to the measurement uncertainties but could help to reduce the uncertainty in the simulations. Simulations over the long term (1960–2004) show that both models agree with the observed discharge values, indicating that their melt relationships are robust in time and thus suitable for modeling discharge in the long term. The models' suitability in simulating the subglacial discharge is highlighted. In contrast with results of previous studies, in our catchment the inclusion of the clear sky solar radiation in a melt model does not seem to improve considerably the performance of the simulations over calibration and validation periods.

KEYWORDS: Temperature index models; Multi-criteria calibration; Glacierized catchment; Discharge; Glacier-wide surface mass balance; Snow Cover Area.

IV.1 Introduction

Being the 'water tower' of Europe, the Alps are crucial for supplying runoff for large part of the continent (Viviroli and Weingartner, 2004; Viviroli et al., 2007). Their snow fields and glaciers provide indispensable water resources for municipal and industrial water uses, irrigation and hydropower production (Barnett et al., 2005; Viviroli et al., 2011). The Alpine region is extremely sensitive to global climate changes (*e.g.*, Beniston et al., 2018); it appears among the most severely and rapidly impacted ecosystem (Zemp et al., 2009; Loarie et al., 2009; Gobiet

et al., 2014). Particularly, marked changes in the hydrological cycle of partially glacierized catchments have been documented (Birsan et al., 2005; Huss et al., 2008; Casassa et al., 2009; Pellicciotti et al., 2010; Bard et al., 2015). Indeed, glaciers affect the catchment hydrology even for low percentages of glacier coverage and constitute an important water reservoir in the form of snow and ice (Jansson et al., 2003). In glacier-fed catchments, the long term glacier shrinkage is expected to be accompanied by a decrease in the discharge after a transient phase of increase discharge until reached a so-called “peak water” (Braun et al., 2000; Barnett et al., 2005; Huss and Hock, 2018). These changes affect the availability of water resources and their management, and may influence the production of the hydropower energy (Schaeffli et al., 2007). For these reasons, understanding the sensitivity of the hydrological regime, the melt water runoff and the glaciers to the climate variability is a key issue for the management of the water resources within the next decades.

Hydro-glaciological models may help improving our understanding of hydrological processes in glacierized catchments (Hock and Noetzli, 1997). Such models are commonly based on two components: a surface mass balance model to simulate accumulation and ablation processes, and a runoff model (World Meteorological Organisation, 1986). To simulate ablation, melt models can be classified in two categories: empirical (*e.g.* temperature index models, Martinec and Rango, 1986; Hock, 2003; Bocchiola et al., 2018) and physically based (*e.g.* Obled and Rosse, 1977; Ranzi et al., 2010; Réveillet et al., 2018). The former requires only air temperature as input and assumes a linear relationship between air temperature and melt rates, whereas the latter includes all energy fluxes at the glacier surface, requiring a large amount of data available on gridded mesh, such as meteorological forcing, surface properties, etc.. Due to their simplicity, the temperature index models are not able to accurately represent the spatial variability of melt rates over the glacier surface because the terrain effects are not considered. To overcome this drawback, enhanced temperature index models have been developed by including others input variables such as potential solar radiation, surface albedo and short-wave radiation to the air temperature (*e.g.* Oerlemans, 2001; Pellicciotti et al., 2005; Réveillet et al., 2017).

Several studies have compared the performance of these different melt models. Hock, 1999 showed that the inclusion of the potential clear-sky solar radiation allows better simulations of the diurnal discharge fluctuations and the spatial distribution of melt rates. At punctual scale, Pellicciotti et al., 2005 stated the improvement of the modeling performance considering the incoming shortwave radiation and albedo compared to the other temperature index models. On contrary, Carenzo et al., 2009 showed that the melt simulations obtained considering the incoming shortwave radiation and albedo are comparable to those generating only with the inclusion of the potential solar radiation. According to Réveillet et al., 2017 and Bouamri et al., 2018 the use of a classical temperature index model is sufficient to accurately simulate the glacier-wide annual surface mass balance and the temporal variation in the snowmelt. None of these studies used a multi-calibration model’s approach. A single-variable calibration

could be inadequate to accurately estimate the models' internal variables (Madsen, 2003). Several studies have demonstrated the need to perform a multi-objective calibration to well represent the hydrological processes, to reduce the uncertainties and to increase the confidence in the physical relevance of the models (Gupta et al., 1998; Kuczera and Mroczkowski, 1998; Bergström et al., 2002; Şorman et al., 2009). Furthermore, it may result in the reduction of the equifinality problem and allow to obtain a robust parameters values (Ragettli and Pellicciotti, 2012). According to these studies, a question about the most suitable models to simulate the hydro-glaciological processes and the subglacial discharge in a highly glacierized catchments is still open.

In addition, the long-term stability of temperature index models is rarely discussed in literature. Gabbi et al., 2014 showed that the use of a temperature index model and the enhanced ones including potential clear-sky solar radiation tend to simulate too positive glacier surface mass balance over several decades. This finding is in agreement with Huss et al., 2009. Both studies pointed out the temporal changes in the relationship between melt and temperature and thus the inability of temperature index models to be used for future projection.

In this context, the purpose of this study is to assess the importance of the choice of the calibration method and identify the best suitable simple model allowing the simulation of the hydro-glaciological processes in a highly glacierized area. The work is focused on the Arveyron d'Argentière catchment, located in the upper part of the Arve watershed (French Alps) with a glacial coverage of 49% (in 2003). Two different distributed melt models are considered: the classical degree-day method (DD) and the enhanced temperature index model with the inclusion of the potential clear-sky direct solar radiation (the HTI model by Hock, 1999). Both have been coupled with a linear reservoir discharge model. Precisely, our aims are: (i) to assess the performance of the considered models when calibrated against discharge only and with a multi-criteria approach considering discharge, snow cover area and glacier-wide annual surface mass balance; (ii) to identify the best suitable simple model allowing the simulation of the hydro-glaciological processes and the subglacial discharge at the catchment/glacier scale at daily resolution; and (iii) to evaluate their short and long-term temporal stabilities, over the 2000–2003 and 1960–2009 periods, respectively. This study is based on long dataset of in situ or remote sensing glaciological, meteorological and snow cover area data. The models' calibration is carried out over the 2000–2003 period at daily time step, whereas the validation is made over different subperiods according to data availability within the 1960–2009 period. The computation of the glacier contribution to the total discharge and the simulated uncertainties are carried out. The evaluation of the model's ability in simulating the subglacial runoff is a rare opportunity made possible by the subglacial observatory beneath the Argentière glacier, where the sliding velocities and the summer subglacial runoff have been measured continuously since 2000.

IV.2 Study site

Arveyron d'Argentière catchment is located in the upper part of the Arve River catchment (French Alps), between the Mont Blanc and Aiguilles Rouges massifs (Fig. IV.1). It has an area of 32.2 km², with elevations ranging from 1363 to 4079 m a.s.l. (Fig. IV.1). Its median elevation is 2880 m a.s.l. and the average slope is 29°. According to the Corine Land Cover maps in 2000 (Bossard et al., 2000), 44% of the catchment is covered with bare rocks, whereas forested and vegetated areas represented only 4% of the entire area.

In 2003, the 49% of the catchment area was covered by Glacier d'Argentière (11.4 km² in 2003) and its tributaries (Fig. IV.1). The main ones are Glacier des Améthystes (1.3 km² in 2003) and Glacier du Tour Noir (1.2 km² in 2003). Glacier d'Argentière belongs to the GLACIOCLIM observatory (<https://glacioclim.osug.fr>) and it is monitored since 1975 for continuous surface mass balance measurements (Vincent et al., 2009). It extends from an altitude of 1455 to 3738 m a.s.l. with a length of ~10 km. It faces north, except for a large part of the accumulation area (south-orientated tributaries). Its equilibrium-line altitude (ELA) ranges between 2430 and 2914 m a.s.l. over the 1984–2014 period, with a mean value of 2772 m a.s.l. (Rabatel et al., 2013). Since 1993 systematic winter and summer mass-balance measurements have been performed on the entire glacier surface: 39 sites have been selected at various elevations representative of the whole surface, distributed over both the ablation (30 sites) and the accumulation areas (9 sites) (Fig. IV.1). A subglacial observatory has been set up at 2173 m a.s.l. to continuously monitor the sliding movement and the subglacial runoff (Moreau, 1995; Vincent and Moreau, 2016) (Fig. IV.1).

The streamflow produced by the Arveyron d'Argentière is affected by water withdraws. Upstream of the hydrological gauging station of this catchment (at 2060 m a.s.l.), waters coming from the Argentière glacier are collected by subterranean tunnels carved into the mountain, managed by Electricité d'Emosson S.A., and routed to the Emosson lake (Switzerland) for electricity production. These water extractions represent ~ 78% of the water production of the catchment on average over the 1983–2004 period.

IV.3 Data

IV.3.1 Meteorological data

An automatic weather station (AWS) is located on the moraine of the Argentière glacier at ~ 2400 m a.s.l. since 2010. As these data do not cover the study period, we only used the shortwave radiation data to estimate the atmosphere transmissivity (Section IV.4.1.1). Air temperature and precipitation amount are taken from the SAFRAN reanalysis, available over the 1958–2013 period. SAFRAN (Système d'Analyse Fournissant des Renseignements Adaptés

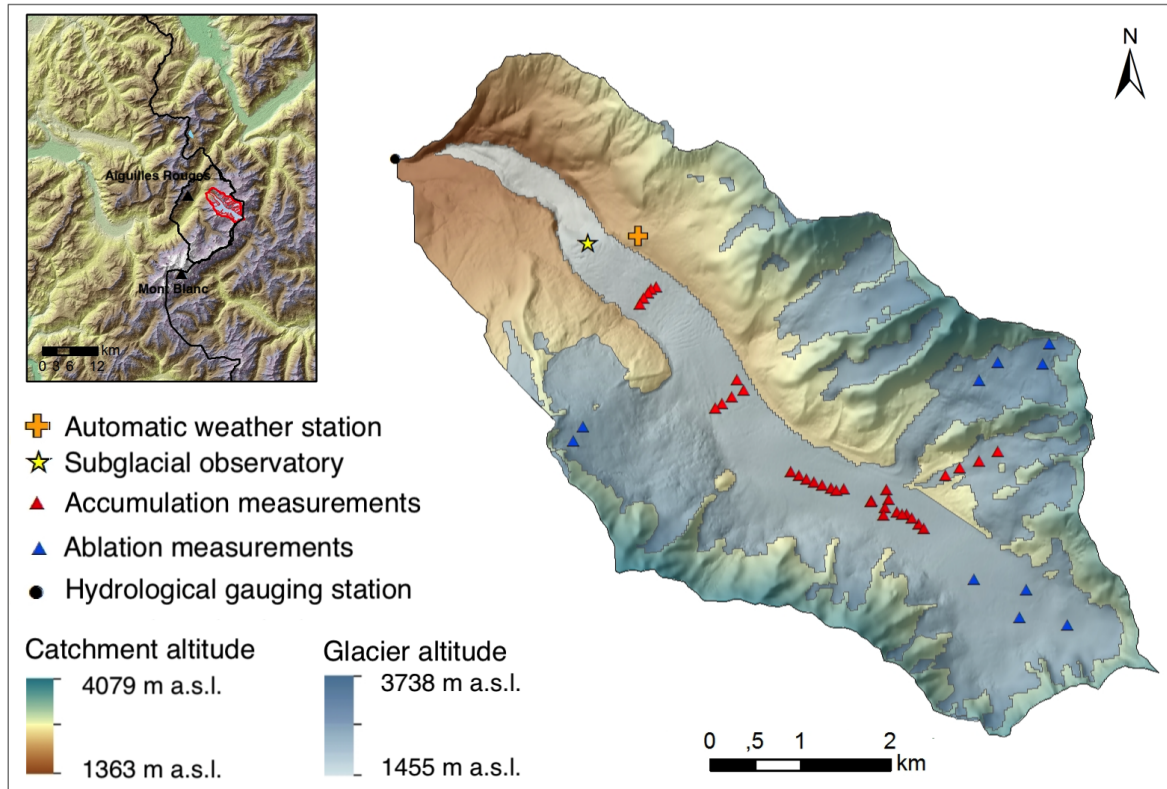


Figure IV.1: Location and altimetry of the Arveyron d'Argentière catchments and its glacier cover (in 2003, [Gardent et al., 2014](#); [Rabatel et al., 2016](#)). The black point indicates the hydrological gauging station; the orange cross the automatic weather station on the moraine of the glacier and the yellow star the subglacial observatory. The triangles represent the network of the in-situ surface mass-balance measurements in both the accumulation (blue) and ablation (red) areas.

à la Nivologie, [Durand et al., 1993, 2009](#)) is a mesoscale atmospheric analysis system for near-surface atmospheric variables. It combines the observed information with a preliminary estimation from numerical weather forecasting models (ARPEGE - Action Recherche Petite Echelle Grande Echelle French ([Courtier et al., 1991](#)) or ECMWF - European Centre for Medium-range Weather Forecasts ([Hagemann et al., 2005](#)), providing meteorological data at 300 m altitude steps from 1200 m to 3600 m a.s.l. for 23 mountain ranges of the French Alps, *e.g.* Mont Blanc massif. Furthermore, temperature data from 6 temporary stations located in the Mont Blanc massif between 2250–2830 m a.s.l. are used to verify the accuracy of the summer environmental lapse rates estimated by SAFRAN reanalysis in the Arveyron d'Argentière catchment over the summer season (JJA).

To justify the use of the reanalysis, we compared the meteorological data (precipitation and temperature) provided by SAFRAN and the meteorological station located at Chamonix (Météo-France), downslope in the Arve valley. The results show a high agreement between the two datasets. For example, over the 1983–2009 period, correlations between the daily temperature or precipitation values of the two datasets are significant at 99% confidence interval

according to the Pearson's test, with R^2 equals to 0.94 and 0.90, respectively.

IV.3.2 Hydrological data

Because of the water withdrawals below the Argentière glacier, the total discharge of the Arveyron d'Argentière was obtained by adding the data measured at the extraction point to the stream discharge values registered by the gauging station located at the outlet of the catchment (Fig. IV.1). The available data over the 1955–2004 period are mainly concentrated from May to October as the sensors are removed during winter. These data are assumed to be affected by a 10% standard uncertainty (Viani et al., 2018). The amount of water withdrawals is provided by Electricité d'Emosson S.A. whereas the measured discharges by Électricité de France (EDF), both at daily time scale.

In addition, mean daily subglacial runoff produced by the Argentière Glacier is used to demonstrate the ability of the calibrated hydro-glaciological models to reproduce the interannual variability of the subglacial water production. Since 2000, it is measured during each summer using an Endress Hauser sensor in the gallery (2060 m a.s.l) located in the subglacial observatory built under the glacier (Fig. IV.1). It has an accuracy of $\pm 0.1 \text{ m}^3\text{s}^{-1}$ and a frequency of 15 min (Vincent and Moreau, 2016).

IV.3.3 Glaciological data

Glacier-wide annual surface mass balance (aSMB) of Argentière are available since 1975 (Vincent et al., 2009). These have been obtained using a linear model (Lliboutry, 1974) combined with the geodetic method. The uncertainty in the glacier-wide annual surface mass balance is estimated as $\pm 0.40 \text{ m w.e. yr}^{-1}$ (Berthier et al., 2014). Furthermore, point measurements of the annual (paSMB) surface mass balance over the accumulation and ablation areas of Argentière and its main tributaries are available since 1995 (Six and Vincent, 2014). These data are determined from snow cores and wood stakes inserted in the ice (Fig. IV.1). Uncertainties of these point measurements have been assessed to $\pm 0.21 \text{ m w.e. yr}^{-1}$ for accumulation and ± 0.14 or $\pm 0.27 \text{ m w.e. yr}^{-1}$ for ablation depending on the surface concerned, *i.e.* ice or firn respectively (Thibert et al., 2008). Furthermore, glacier-wide summer surface mass balances of Argentière quantified for each year of the 1996–2004 period are used. These have been quantified as the difference between the annual and the winter glacier-wide surface mass balances (see details in Viani et al., 2018) and are affected by an uncertainty of $\pm 0.49 \text{ m w.e. yr}^{-1}$. In addition, the equilibrium-line altitude (ELA) values available over the 1984–2014 period are considered. ELAs were inferred from the end-of-summer snow line altitude (SLA) computed from satellite images acquired by Landsat, SPOT and ASTER (Rabatel et al., 2016). The uncertainty of the estimated SLA ranges from ± 15 to $\pm 60 \text{ m}$, depending on the year (Rabatel

et al., 2016).

IV.3.4 Snow cover area data

The ‘‘Snow Cover Daily Tile’’ from Aqua (MYD10A1) and Terra (MOD10A1) MODIS snow products version 5 are used to generate a daily gap-filled time series of the extent of the snow cover area with a horizontal resolution of 500 m since 2000 (Gascoïn et al., 2015). The used gap-filling algorithm is derived from Parajka and Blöschl, 2008a and Gafurov and Bárdossy, 2009 and consists in a (i) Aqua/Terra combination; (ii) spatial and (iii) temporal deduction; and (iv) reclassification of no-data pixel using a classification tree based on geographic position and the topographic characteristics (see details in Gascoïn et al., 2015).

IV.3.5 Grid data

The RGE ALTI DEM provided by the French National Geographic Institute (IGN, Institut Géographique National, France) with a horizontal resolution of 5 m is served as input for the modelling and is used to compute the mask for potential solar radiation. Glacier outlines obtained using topographic maps, LANDSAT and ASTER satellite images in 2003 (Gardent et al., 2014; Rabatel et al., 2016) are used to provide model boundary condition for the delimitation of the glacierized areas.

IV.4 Methods and model' setup

IV.4.1 Model description

The snow and ice melts are computed from two distributed temperature index models available in the literature: (i) the classical degree-day method (DD) and (ii) the enhanced temperature index method (HTI) proposed by Hock, 1999 including the potential clear-sky direct solar radiation. A discharge distributed model (DR) is coupled to the melt models mentioned above to simulate the discharge production of the catchment.

IV.4.1.1 Melt model

The DD (Braithwaite and Olesen, 1989) is based solely on the air temperature and linearly relates melt rates (M , mm w.e. d^{-1}) to air temperature by different factors of proportionality for snow and ice surfaces:

$$M = \begin{cases} \frac{1}{n}DDF_{ice/snow}T & T > 0^\circ C \\ 0 & T \leq 0^\circ C \end{cases} \quad (IV.1)$$

where $DDF_{ice/snow}$ is the degree-day factor for ice or snow (mm w.e. $d^{-1} \text{ } ^\circ\text{C}^{-1}$), T the mean daily air temperature ($^\circ\text{C} \text{ d}^{-1}$) and n the number of time steps per day (here $n = 1$). DDF_{ice} and DDF_{snow} are assumed constant in space and time, thus the spatial distribution of melt rates varies as function of the elevation, neglecting the topographic effects of the terrain.

The HTI (Hock, 1999) incorporates the potential clear-sky direct solar radiation to take into account the spatial variability of the melt rate due to slope, aspect and shading.

$$M = \begin{cases} (\frac{1}{n}MF + \alpha_{ice/snow}I_{pot}T) & T > 0 \text{ } ^\circ\text{C} \\ 0 & T \leq 0 \text{ } ^\circ\text{C} \end{cases} \quad (\text{IV.2})$$

where MF (mm w.e. $d^{-1} \text{ } ^\circ\text{C}^{-1}$) is the melt factor, $\alpha_{ice/snow}$ (mm w.e. $\text{m}^2 \text{ d}^{-1} \text{ } ^\circ\text{C}^{-1}$) the radiation coefficient different for the surfaces cover by ice or snow, I_{pot} the potential clear-sky direct solar radiation at the ice or snow surfaces ($\text{W} \text{ m}^{-2}$) and T the mean daily air temperature ($^\circ\text{C} \text{ d}^{-1}$). I_{pot} is calculated from a DEM as a function of top of atmosphere solar radiation, topographic characteristics of the study area, atmospheric transmissivity and solar geometry. The reduction of the I_{pot} due to clouds is neglected to avoid additional input data. The atmospheric transmissivity is assumed constant and is computed from the clear-sky days during the summer months (JJA) as the mean of the ratio between the shortwave incoming radiation at the AWS on the moraine of Glacier d'Argentière and the top of the atmosphere (TOA) solar insolation. The cosine of the solar zenith is approximated as function of latitude, hour angle and solar declination, which is expressed as a function of the day of the year (Iqbal, 1983). The assumption of a constant value for the atmospheric transmissivity is considered sufficiently accurate, as the computed direct solar radiation is not interpreted as an energy available for melt but it represents an index which is scaled by the empirical coefficient α (Eqn. IV.2).

IV.4.1.2 Discharge routing

The discharge over the studied area is obtained as the sum of the melt and rain water using a linear reservoir model. This approach assumes the linear relationship between the reservoir's volume and its outflow at any time t . The factor of proportionality is the storage coefficient (k) that has a dimension of time and indicates the speed at which the water is routed downstream.

The catchment has been divided in four linear reservoirs, associated at four different surface covers: firn, snow, ice and rock. Each one is characterized by a value of k assumed constant in time (Hock and Noetzli, 1997). The total daily discharge (Q) at the time t is given by:

$$Q(t) = \sum_{i=1}^4 (Q_i(t-1) \exp(-\frac{1}{k_i}) + P_i(t) - P_i \exp(-\frac{1}{k_i})) + Q_5 \quad (\text{IV.3})$$

where $P(t)$ is the rate of water inflow to the reservoir i , equivalent to the sum of meltwater

and rain and Q_5 a small constant representing the ground water runoff (Baker et al., 1982). Q_5 is taken equal to $0.3 \text{ m}^3 \text{ s}^{-1}$ (Viani et al., 2018). The firn reservoir is defined as the area above the ELA. The snow reservoir refers to the snow-covered area, whereas the ice reservoir to that characterized by exposed ice (not in the firn area and not snow-covered). The rock reservoir consists in the part of the catchment outside the glacier but not snow-covered. The size of the snow reservoir changes according to the evolution of the snow line altitude (SLA), considering the growth of the ice reservoir when the SLA rises.

The glacier discharge is defined as the fraction of the outflows coming from the glacierized area, considering the melting of ice, snow, firn and from the rainfall precipitated on the surface of the glacier.

Sublimation and evapotranspiration losses are neglected in the model. These processes are considered to be negligible compared with the other fluxes in our study area (Six et al., 2009; Viani et al., 2018).

IV.4.2 Model forcing and data preprocessing

The two models require the same inputs: (i) climate data representative of the modeled area; and (ii) grid data providing boundary and initial conditions. The models are forced with daily temperature and precipitation values. The grid files contain terrain information provided by a DEM of the drainage basin. DEMs containing the glacier outline and the extent of the firn area are requested to assign the melt factor for ice or snow after the initial snow cover has melted away. Furthermore, for the initialization the models need a grid containing initial snow water equivalent. Simulations are run at daily time step, with a spatial resolution of 5 m.

Changes in the glacier geometry are not accounted over the historical period of analysis, as done by Zhang et al., 2016 and Lecourt, 2018. Naz et al., 2014 demonstrate that the use of static glacial contours is justified by the high complexity, uncertainty and computational cost of the glacier evolution models. Furthermore, they show that the difference in the performance of the static and dynamic ice model configurations is modest over a period of several decades.

Temperature values are extrapolated over the study site using a mean annual fixed altitudinal gradient of $0.6^\circ\text{C}/100 \text{ m}$. This is in agreement with the values adopted by Vincent, 2002 and Vincent and Moreau, 2016 over the same site.

Relying on Viani et al., 2018, precipitation is assumed to increase linearly with elevation and two different lapse rate values are used in order to avoid unrealistically high precipitation in the highest part of the study area. Therefore, precipitation is expected to increase by $3\%/100 \text{ m}$ for altitude below 2550 m a.s.l. and by $1.8\%/100 \text{ m}$ above (Viani et al., 2018). The precipitation phase (rain and snow) is discriminated according to an air temperature threshold T_t . One degree below (above) T_t all precipitation is assumed to fall as snow (rain). Within the 2°C range the amount of rain and snow is obtained using a linear interpolation (Fig. IV.2).

T_t is considered constant and equals to 2°C , on the base of the precipitation phases provided by SAFRAN reanalysis (Fig. IV.2). This threshold value is in agreement with L'hôte et al., 2005, Kienzle, 2008 and Gouttevin et al., 2017. Over the 1960–2010 period, the available data show that the year-to-year variability of T_t is less than 2°C (not depicted here), which justifies the use of a constant value. In addition, Grossi et al., 2017 showed that T_t of 1°C is an appropriate threshold temperature for rain/snow partitioning of precipitation in the Italian Alps thus confirming the assumption adopted by several DD models as those of the World Meteorological Organisation, 1986 intercomparison.

The obtained transmissivity value needed for the HTI model (Section IV.4.1.1) is equal to 0.734. This value agrees with Oke, 1987 that showed that transmissivity generally varies between 0.6 and 0.9. The uncertainty on the atmospheric transmissivity leads to a maximum difference in the melt rate estimation of 0.07%.

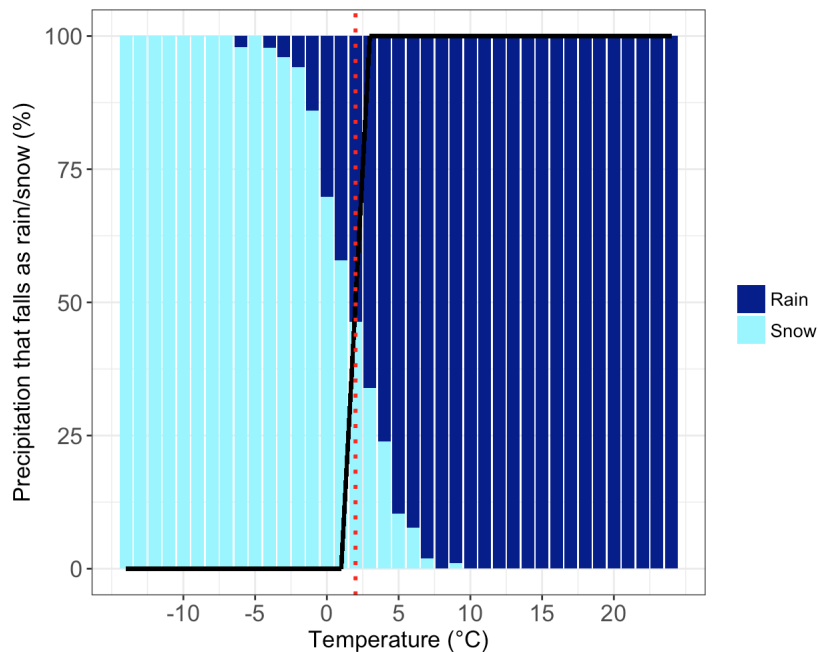


Figure IV.2: Percentage of occurrence of snowfall and rainfall as function of the 1°C daily air temperature categories over the 1980–2010 period using the meteorological data provided by SAFRAN reanalysis. The red dotted line indicates the air temperature threshold T_t at 2°C chosen to discriminate the precipitation phase, whereas the black solid line indicates the linear rain threshold schemes used in the current study.

IV.4.3 Sensitivity analysis

The parameters that have to be calibrated are the following: two degree-day factors for the DD model (DDF_{ice} , DDF_{snow}), one melt factor and two radiation coefficients for the HTI (MF , α_{ice} , α_{snow}) and four linear reservoir coefficients (k_{firn} , k_{snow} , k_{ice} , k_{rock}) for the DR model (Table IV.1).

For each hydro-glaciological model (melt model coupled with the discharge routing model), a sensitivity analysis “one-at-a-time” is performed over the year 2000 to identify the sensitive parameters (Hamby, 1994). A simulation is carried out by varying the considered parameters from the minimum to the maximum values of their intervals range (Table IV.2, Hoffman and Gardner, 1983). The impact of this change on the (i) discharge during summer (Q_{JJA}), (ii) snow cover area over the summer (SCA_{JJA}), the months of May (SCA_{May}) and October (SCA_{Oct}) and (iii) glacier-wide annual surface mass balance (aSMB) is evaluated using the sensitivity index (SI) calculated as follows:

$$SI = \frac{P_{\max} - P_{\min}}{P_{\max}} 100 \quad (\text{IV.4})$$

where P_{\max} and P_{\min} represent the maximum and the minimum values of the output variables, respectively, resulting from varying the input parameters over their entire range (Hoffman and Gardner, 1983). This method does not allow us to consider the interaction between the different parameters but just to identify those that can have a strong impact on the model outputs.

The results of the sensitivity analysis are shown in Table XX2. The DD and HTI models appear to be sensitive to the degree-days and melt factors and to the radiation coefficients, respectively. It is logical since these parameters control the melt processes into the models. Their variation results in a change higher than 92% in the aSMB and higher than 13% in the Q_{JJA} . Regarding the storage coefficient, the results are relatively insensitive to the choice of the k_{snow} , k_{ice} and k_{rock} : the resulting changes are less than 0.4% in the summer discharge. On the contrary, k_{firn} has a stronger impact comparing to the others: its changes results in a SI equal to 4% on the summer discharge.

Table IV.1: Models parameters, their intervals and the corresponding increments used for their calibration.

Model	Parameters	Unit	Range values	Δ	References
HTI	MF	mm d ⁻¹ °C ⁻¹	1–5	0.5	
	α_{snow}	mm m ² h ⁻¹ W ⁻¹ °C ⁻¹	1 10 ⁻⁴ – 8 10 ⁻⁴	1 10 ⁻⁴	Hock, 1999; Gabbi et al., 2014;
	α_{ice}	mm m ² h ⁻¹ W ⁻¹ °C ⁻¹	3 10 ⁻⁴ – 1 10 ⁻³	1 10 ⁻⁴	Réveillet et al., 2017
DD	DDF_{snow}	mm d ⁻¹ °C ⁻¹	2–7	0.1	Hock, 1999, 2003;
	DDF_{ice}	mm d ⁻¹ °C ⁻¹	5–11	0.1	Braithwaite and Zhang, 2000
DR	k_{firn}	h	100–500	50	
	k_{snow}	h	10–80	10	Oerter et al., 1981; Baker et al., 1982;
	k_{ice}	h	1–30	5	Noetzli 1996
	k_{rock}	h	5–200	35	

HTI=the enhanced temperature index method; DD=classical degree-day method; DR= discharge model; DDF_{snow} , DDF_{ice} = degree-day factors for snow and ice; MF = melt factor; α_{snow} , α_{ice} = radiation coefficients for snow and ice; k_{firn} , k_{snow} , k_{ice} , k_{rock} = storage coefficients for firn, snow, ice and rock surface covers.

Table IV.2: Sensitivity index (%), Eqn. IV.4) on the summer discharge (Q_{JJA}), glacier-wide annual surface mass balance ($aSMB$) values, snow cover area over summer (SCA_{JJA}), May (SCA_{May}) and October (SCA_{Oct}). The most sensitive parameters are marked with an asterisk.

Parameter	Q_{JJA} (%)	$aSMB$ (%)	SCA_{JJA} (%)	SCA_{May} (%)	SCA_{Oct} (%)
DDF_{snow}^*	47.46	507.26	31.79	6.55	2.55
DDF_{ice}^*	17.81	-195.80	0.35	0.00	0.14
MF^*	52.72	259.24	27.40	4.76	3.02
α_{snow}^*	24.08	-152.19	24.80	5.08	0.53
α_{ice}^*	12.74	-92.33	0.26	0.00	0.05
k_{firm}^*	4.35	0.00	0.00	0.00	0.00
k_{snow}	0.23	0.00	0.00	0.00	0.00
k_{ice}	0.12	0.00	0.00	0.00	0.00
k_{rock}	0.40	0.00	0.00	0.00	0.00

IV.4.4 Fixing the not-sensitive parameters

In order to select the values of the insensitive parameters, *i.e.* k_{snow} , k_{ice} and k_{rock} (Section IV.4.3), different simulations are carried out combining their different values according to Table IV.1, taking unaltered the other input parameters. The set of k values associated to the highest Kling-Gupta Efficiency (KGE, Gupta et al., 2009) between the calculated and observed discharge has been chosen. Only the performance on the discharge is evaluated since the changes in k_{snow} , k_{ice} and k_{rock} have no impact on the other variables considered (Table IV.2). The chosen values are the following: $k_{ice}=16$ h; $k_{snow}=35$ h; $k_{rock}=50$ h. They are of the same order of magnitude of those used by Hock and Noetzli, 1997 and Baker et al., 1982 for the Storglaciaren (Sweden) and Vernagtfiner (Austria) glaciers, respectively.

IV.4.5 Models calibration, validation and evaluation metrics

The sensitive parameters are: DDF_{ice} and DDF_{snow} for the DD model, MF , α_{ice} , α_{snow} for the HTI model and k_{firm} for the DR model. To determine their values, the calibration is first carried out against discharge (Q) only and in a second step with a multi-criteria approach considering the discharge (Q), the snow cover area (SCA) and the glacier-wide annual mass balance ($aSMB$). The calibration process has been done over the 2000–2003 period (Table IV.3). The total discharge measurements are used for the evaluation of the simulated discharge from May to October, accordingly to data availability. The simulated SCA is compared to the daily SCA derived from the MODIS gap-filled product. This evaluation is done excluding the winter months (from October to February) during which the daily SCA retrieved from optical satellite imagery exhibits large artefacts mostly due to the correction of shadows (Davaze et al., 2018).

For instance, during winter Arveyron d'Argentière exhibits a severe drop of its SCA, reaching values as low as in the snowmelt season, such as in June. The simulated aSMB is evaluated in comparison with the values obtained using the linear model adjusted by the geodetic method, and whereas the simulated surface mass balance gradient with elevation is evaluated using stakes measurements. The parameters intervals and the corresponding increments employed for the calibration are listed in the Table [IV.1](#): only physically reasonable combinations are tested, *i.e.* with a physical consistency between DDF_{ice} and α_{ice} and DDF_{snow} and α_{snow} .

The optimal set of parameters of each model is the one maximizing the KGE on the discharge in the case of single calibration and the following objective function (KGE_{TOT}) for the multi-criteria approach.

$$KGE_{TOT} = w_1 KGE_Q + w_2 KGE_{SCA} + w_3 KGE_{aSMB} - w_4 |V_Q| \quad (IV.5)$$

$$V_Q = \frac{\sum_{i=1}^N (Q_{obs,i} - Q_{sim,i})}{\sum_{i=1}^N Q_{obs,i}} \quad (IV.6)$$

where KGE_Q , KGE_{SCA} and KGE_{aSMB} are the Kling-Gupta Efficiency related to Q, SCA and aSMB, respectively. V_Q is the accumulated relative volume error, computed between the observed (Q_{obs}) and simulated (Q_{sim}) discharge (Eqn. [IV.6](#)). The index i refers to a given point in a dataset of length N . w_1 , w_2 , w_3 and w_4 are the weights of the different terms of the Eqn. [IV.5](#). In order to ensure that one variable does not dominate over the others during the calibration process even when their numbers are different, the weight values have been identified by a sensitivity analysis. w_1 and w_2 are both taken equal to 0.425, w_3 is specified as 0.15 and w_4 0.1 as proposed by [Lindström, 1997](#) and [Bergström et al., 2002](#). A KGE_{TOT} of 1 indicates the perfect fit.

For the validation, in addition to Q, SCA and aSMB, two other variables are considered: the snow line altitude (SLA) and the glacier-wide summer surface mass balance (sSMB). The first is validated against the SLA inferred by satellite images at the end-of-summer while the second against the sSMB estimated with a glaciological method. Furthermore, the observed and simulated aSMB gradients according to elevation are compared. The suitability of the calibrated models in reproducing the subglacial discharge ($Q_{subglacial}$) of the Argentière glacier is also tested. Different validation periods are considered, according with the data availability (Table [IV.3](#)).

The performances of the models are assessed by the agreement between simulated and measured variables using the three goodness-of-fit criterions: the KGE and Root Mean Square Error (RMSE) and the determination coefficient (R^2). KGE and R^2 have been applied only to the variables available at daily time scale (*i.e.* Q and SCA). The spatial similarity between the observed and simulated SCA is evaluated using the Jaccard index (J). It is defined as the

ratio between the size of the intersection and the size of the union of the considered samples, *i.e.* the observed and the simulated SCA. The index values range from 0 to 1, with a value of 1 representing a perfect match between the observed and simulated data. The Jaccard index is calculated at daily time step, *i.e.* one value for each available snow cover map. Since the spatial resolution of the hydrological model and the MODIS data sources of the SCA product are not the same, the grid simulations have been aggregate at 500 m-resolution for the comparison.

Table IV.3: Time periods used for the DD and HTI models' calibration and validation.

Type	Period	Variables					
		Q	SCA	aSMB	sSMB	SLA	Q _{subglacial}
Calibration	2000–2003	X	X	X			
Validation	2004	X	X	X		X	X
Validation	1984–1999	X		X		X	
Validation	2005–2009		X	X		X	
Validation	2003						X
Validation	1996–2004				X		
Validation	1960–1984	X					

Q=Discharge; SCA=Snow Cover Area; aSMB=glacier-wide annual surface mass balance; sSMB=glacier-wide summer surface mass balance; SLA=Snow Line Altitude; Q_{subglacial}=Subglacial discharge.

IV.4.6 Temporal stability of the models' parameters

To study the variability of the DD and HTI models' parameters induced by the calibration period and to investigate their influence on the models' performance, different parameter sets are determined for each individual year over the 2000–2003 period and for each models. They are compared with the values of the parameters calibrated over the entire period. These years are selected since they are characterized by different meteorological conditions. Furthermore, the short-term temporal stability of the parameters is quantified by computing the absolute mean difference between the simulated and observed variables, *i.e.* Q, SCA, SLA and aSMB, for each set of parameters over the period 2000–2003 (Table IV.3). The long-term stability on discharge and glacier-wide annual mass balance simulations is evaluated observing the models' performance over the 1960–2004 and 1984–2009 periods respectively, accordingly with data availability.

IV.4.7 Simulations uncertainties

In general, the model uncertainties are associated with input data, parameter values, initial conditions and model structure (Pechlivanidis et al., 2011). In the current study, we focus on the uncertainties of the simulated variables due to the input parameters. They are estimated

using the Monte Carlo approach (Ronen, 1988; Sobol', 1994; Beven, 2009), as is done in previous studies (Machguth et al., 2008; Diaz-Ramirez et al., 2012; Khoi and Thom, 2015; Réveillet et al., 2017). The performed steps are the following:

- (i) Definition of a domain of possible inputs parameters for the DD and HTI models (Table IV.1).
- (ii) Generation of all the physically reasonable combinations of the input parameters associated with values of the considered objective function (Section IV.4.5) higher than 0.8 assuming the independence between each parameter and using a uniform probability distribution;
- (iii) Independent random simulations of Q, SCA, aSMB, sSMB and SLA are run over and over using a different set of inputs. The uncertainties of each variables are taken as the highest difference between the values provided by the different random simulations at each time step, *i.e.* at daily scale for the Q and SCA whereas at annual scale for aSMB, sSMB and SLA.

IV.5 Results and discussion

IV.5.1 Single vs. multi calibration approach

Table IV.4 lists the performance of the DD and HTI models when calibrated against Q only and using a multi-criteria approach. The multi-criteria approach leads to a slight reduction in the accuracy of the simulated Q over the calibration period in comparison to that obtained with a single-variable calibration, for the two models. The value of the KGE_Q is decreased by 1.4% (0.6%) whereas the $RMSE_Q$ is increased by 1.1% (0.6%) using the DD (HTI) model. These changes are not significant with regard to the measurement uncertainties. The simulation of SCA is improved by calibrating the model against SCA and aSMB in addition to Q; this performance increase is more pronounced with the DD model than the HTI one. The results show an increase in the accuracy of the SLA and aSMB simulations using a multi-criteria approach compared to the single-variable calibration; $RMSE_{SLA}$ and $RMSE_{aSMB}$ are reduced by 27.3% (17.9%) and 36.5% (15%) using DD (HTI), over the calibration period. For the aSMB this increase is not significant with regard to the measurement uncertainties whereas for the SLA the improvement could be significant depending on the year considered. The variation of the performances of the considered variables over the validation periods agrees with what occurs over the calibration one.

The results show that the performance in SLA and aSMB carried out with a multi-criteria approach are higher than the reduction on the performance in the Q simulation. The use of

the multi-criteria calibration against the single-variable ones results in a performance increase that is generally not significant compared to the measurement uncertainties. However, it leads to an improvement in simulating all the considered variables (except for Q) over both the validation and the calibration periods. Therefore, the multi-criteria approach could help to reduce the uncertainty in the simulations and to obtain a robust model increasing the confidence in its physical relevance (Gupta et al., 1998; Seibert, 2000). This result tends to confirm that in a conceptual model, an accurate simulation of the Q could not ensure an equally accuracy in the estimation of the other variables, such as aSMB, SCA and SLA. Indeed, models can “work well for a wrong reason”, *i.e.* an error in the description of one process may be compensated by an error in another part of the model (Klemes, 1982; Klemes, 1986). In addition, the multi-criteria calibration allows to reduce the equifinality problem, by which several combinations of model parameters result in the same model performance (Beven, 1996; Finger et al., 2011). Based on this finding, the results presented hereafter will refer only to simulation obtained with DD and HTI models, calibrated with a multi-criteria approach.

Table IV.4: Changes (Δ) of the evaluation metrics of the multi-criteria simulations against the single-variable ones, obtained using DD and HTI models, over calibration and validation periods. The given values are in %.

Evaluation Metrics	Model	Calibration	Validation		
		2000–2003	1984–1999	2004	2005–2009
ΔKGE_Q (%)	DD	-1.4	-1.3	0.4	-
	HTI	-0.6	0.0	0.9	-
$\Delta RMSE_Q$ (%)	DD	1.1	4.6	-0.8	-
	HTI	0.6	-0.7	-1.8	-
ΔKGE_{SCA} (%)	DD	6.3	-	10.8	8.6
	HTI	0.2	-	4.1	-0.2
$\Delta RMSE_{SCA}$ (%)	DD	-5.3	-	-8.9	-6.8
	HTI	-0.7	-	-6.8	-0.2
$\Delta RMSE_{SLA}$ (%)	DD	-27.3	-	-29.6	-23.0
	HTI	-17.9	-	-20.5	-9.6
$\Delta RMSE_{aSMB}$ (%)	DD	-36.5	-9.2	5.9	-7.7
	HTI	-15.0	-7.5	-6.3	0.9

IV.5.2 Performance of the models calibrated with a multi-criteria approach

When the calibration occurs over a short period, *i.e.* seasonal or yearly scale, the set of obtained parameters may be influenced by the specific meteorological condition that characterized the period considered (Carenzo et al., 2009; Gabbi et al., 2014). In this study the problem

is overcome choosing a calibration period that is relative short (4 years, 2000–2003) but characterized by very different meteorological conditions, with precipitation and temperature values spanning over a large range.

IV.5.2.1 Total discharge, glacier runoff contribution and subglacial hydrology

The DD and HTI models show a good performance in simulating the daily discharge values over both the calibration and validation periods (Table IV.5). The values of KGE_Q do not vary considerably from one model to the other; they exhibit a maximum absolute difference of 0.08 (0.05) for DD (HTI) over the 1960–2004 period. Both models show a slight drop in KGE_Q and $RMSE_Q$ values passing from the calibration to the validation. The correlations between the simulated and observed daily values are significant at 99% confidence interval according to the Pearson's test, with R^2 of 0.76 and 0.75 for DD and HTI, respectively (Fig. IV.3a). These performances are of the same magnitude of that obtained for the same catchment by Lecourt, 2018 (R^2 of 0.73), using a model with physical basis over the 1995–2004 period (SURFEX/ISBA-Crocus snowpack model coupled with a conceptual model of discharge routing). Both models are able to capture the seasonal and inter-annual variability of discharge (Fig. IV.3b). The annual values of KGE_Q range from 0.604 to 0.908. The simulations tend to overestimate the discharge production at the beginning of the melt season (May-mid June). This may be mainly because the cold content of the snowpack is not included in the models' structure (Valéry et al., 2014). The timing of the high flows is well captured but sometimes they tend to be underestimated. This underestimation has been already observed by Hock and Noetzli, 1997 and Hock, 1999 applying both a temperature index models and an energy balance one. It could be attributed to the assumption of the constant values of k , since they are expected to vary with time (Gurnell, 1993). Furthermore, an error in the discharge measurement or an underestimation of the melt processes or the amount of precipitation could influence the results. The models well reproduce the discharge cumulative density function (CDF) (Fig. IV.3c). In addition, the observed and the simulated mean discharge season cycles computed over the 1960–2004 period show a good correspondence (R^2 of 0.98 and 0.97 for DD and HTI, respectively); here again, the overestimation of the snow melt over May-mid June is visible (Fig. IV.3d).

The annual discharge volume production of the catchment is well represented by both DD and HTI models, all over the considered period, showing both a KGE of 0.78 (Fig. IV.4). The difference between the observed and simulated values is almost comprised in their respective uncertainties. The glacier discharge is one the most important component of the total discharge, representing on average 63% of the total water production of the catchment over the 1960–2004 period. The proportion of their contribution varies greatly among the years, ranging from a minimum of 45% to a maximum of 81%. These findings are also in agreement with Lecourt, 2018 and Viani et al., 2018. In addition, the glacier contribution reaches its maximum at the

end of July/beginning of August, in each year.

These results allow saying that the inclusion of the clear sky solar radiation in a temperature index model does not seem to improve the discharge simulation at daily time scale in terms of the used evaluation metrics over calibration and validation period and from visual inspection of the discharge hydrograph (Table IV.5, Fig IV.3).

In addition, the DD and HTI models are able to reproduce the seasonal variability of the mean subglacial water production observed in the subglacial observatory over the years 2003 and 2004. The performance at daily time scale cannot be evaluated in details since, according to Vincent and Moreau, 2016 the measured data are affected by some artefacts (Fig IV.5). Our results allow to state that temperature index models can be used to obtain subglacial discharge when no measurements are available for a qualitative analysis. At seasonal scale, these data could be used to infer information regarding the ice-sliding velocity, since its oscillations are similar to those of the subglacial discharge (Vincent and Moreau, 2016). Furthermore, this simulation could be useful for the stakeholder in charge of the planning and managing water resources and the hydro-electricity producer; they allow having an estimation of the evolution of the subglacial water production.

Table IV.5: Performance of the DD and HTI models calibrated with a multi-criteria approach, over the calibration and validation periods.

Evaluation Metrics	Model	Calibration			Validation		
		2000–2003	2004	1960–1983	1984–1999	2005–2009	1996–2004
KGE _Q (-)	DD	0.869	0.831	0.840	0.788	-	-
	HTI	0.868	0.835	0.840	0.812	-	-
RMSE _Q (m ³ s ⁻¹)	DD	1.79	1.87	1.92	2.21	-	-
	HTI	1.86	1.85	1.94	2.07	-	-
KGE _{SCA} (-)	DD	0.794	0.646	-	-	0.770	-
	HTI	0.815	0.710	-	-	0.800	-
RMSE _{SCA} (% d ⁻¹)	DD	13.7	14.7	-	-	12.8	-
	HTI	13.4	13.2	-	-	12.4	-
Jaccard [-]	DD	0.821	0.818	-	-	0.800	-
	HTI	0.821	0.819	-	-	0.800	-
RMSE _{SLA} (m a.s.l.)	DD	133.6	131.0	-	-	135.7	-
	HTI	117.9	120.0	-	-	130.6	-
RMSE _{aSMB} (m w. e. yr ⁻¹)	DD	0.13	0.56	-	0.58	0.30	-
	HTI	0.16	0.59	-	0.56	0.32	-
RMSE _{sSMB} (m w. e. yr ⁻¹)	DD	-	-	-	-	-	0.62
	HTI	-	-	-	-	-	0.65

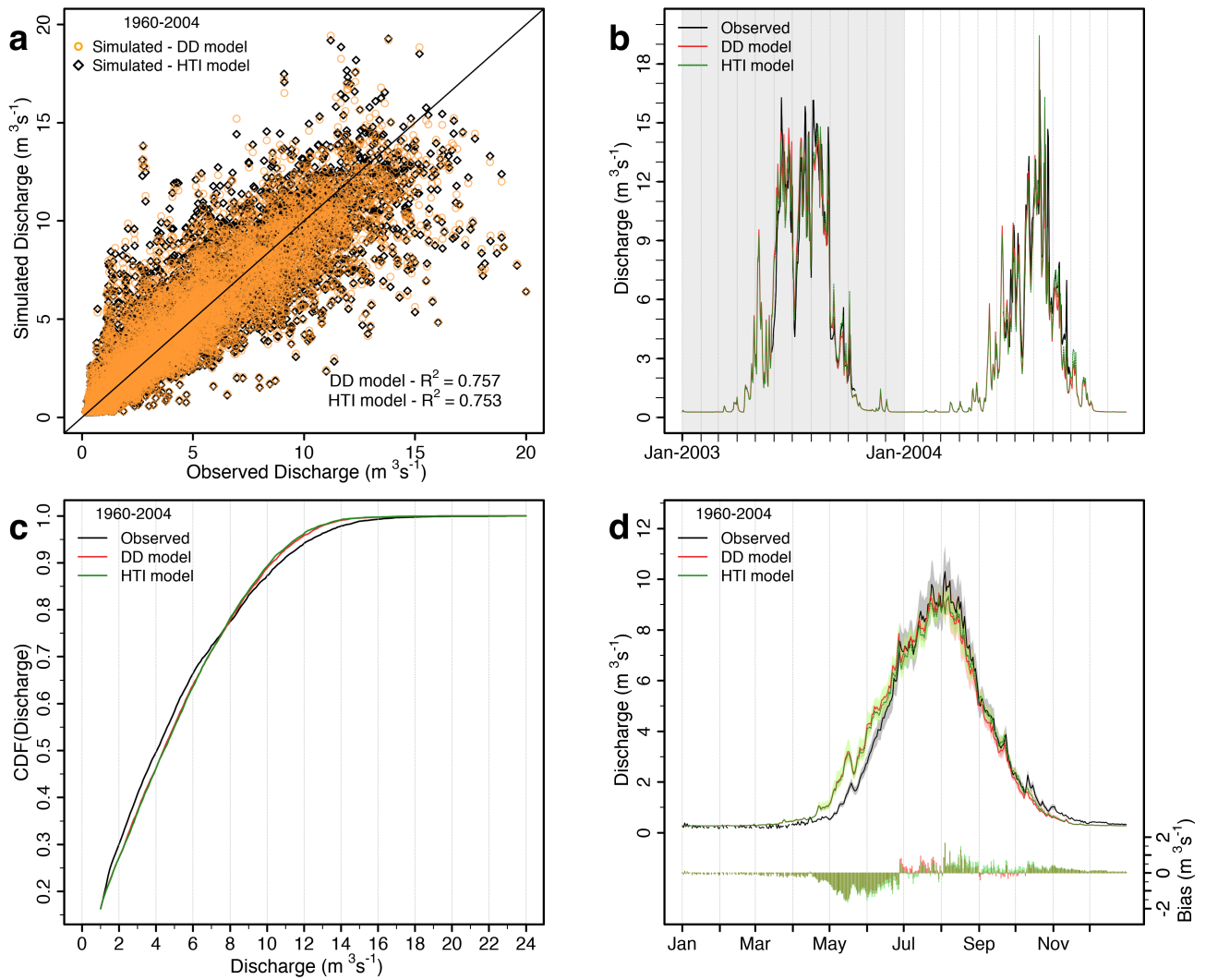


Figure IV.3: (a) Correlation between observed and simulated daily discharge values over the 1960–2004 period; (b) Evolution of the observed and simulated discharge over the years 2003 and 2004. The gray box indicates the calibration year; observed and simulated (c) discharge cumulative density function (CDF) and (d) mean daily discharge, over the 1960–2004 period. In figure (d) the colored areas represent the uncertainty of the discharge seasonal cycle (Section IV.4.7) and the bias between the observed and simulated values are drawn. In all figures the simulated values are obtained with DD and HTI models, calibrated with a multi-criteria approach.

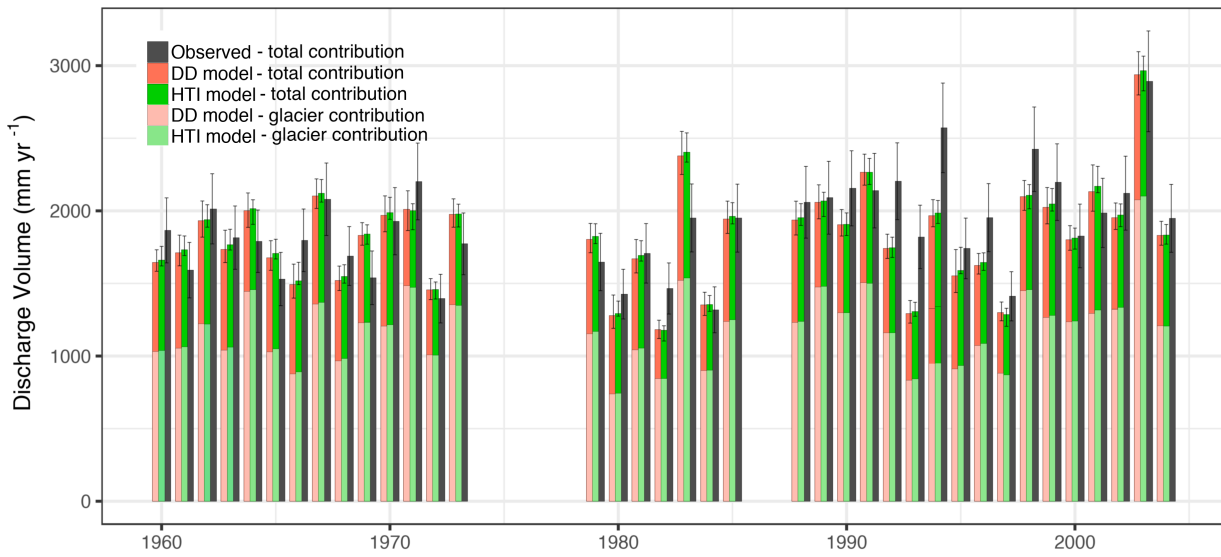


Figure IV.4: Observed and simulated discharge volume production with DD and HTI models of the Arveyron d’Argentière catchment over the 1960–2004 period. Light colors indicate the simulated annual glacier contribution on the catchment discharge volume production. The black bars match the uncertainties on the observed and simulated values.

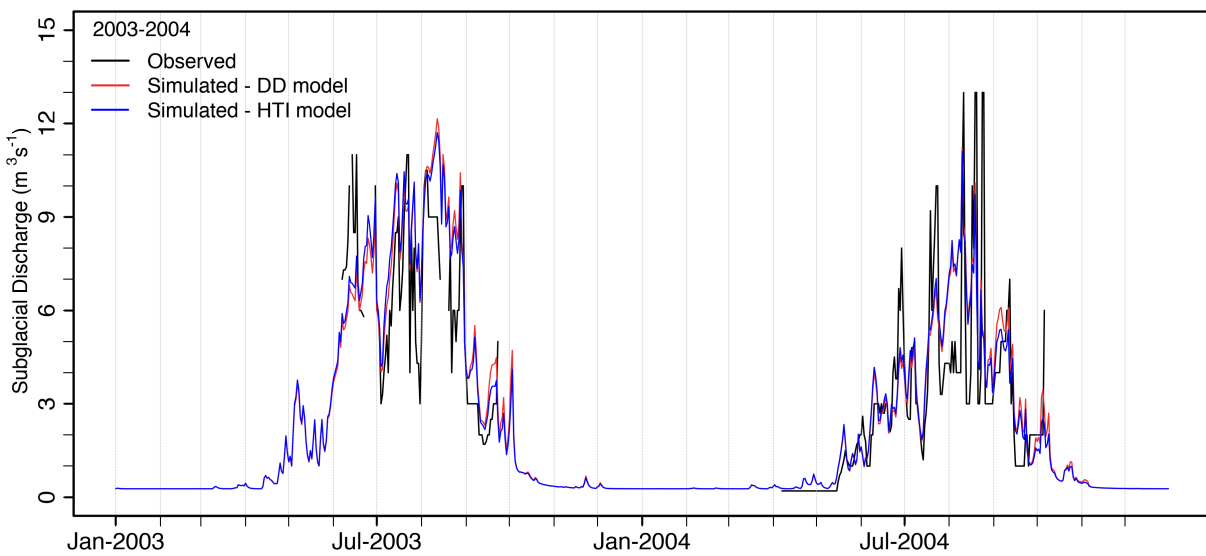


Figure IV.5: Observed and simulated subglacial discharge with DD and HTI models produced by the Argentière glacier, over the years 2003 and 2004.

IV.5.2.2 Glacier-wide surface mass balances and snow line altitude

The glacier-wide annual SMB and its interannual variability are simulated by both the DD and HTI models with similar performances over the calibration and validation periods (Fig IV.6a, Table IV.5). Generally, the obtained values of $RMSE_{aSMB}$ do not vary consider-

ably from one model to the other over the considered simulation periods (Table IV.5). The $\text{RMSE}_{\text{aSMB}}$ computed over the 1984–2009 period equals $0.50 \text{ m w.e. yr}^{-1}$ ($0.48 \text{ m w.e. yr}^{-1}$) with DD (HTI) model. In addition, the simulated glacier-wide summer SMB tends to underestimate the glaciological values, but the difference is most of the time included in the measurement uncertainties (Fig. IV.6b, Table IV.5). The interannual variability of the observations is well simulated by the two models.

This overall agreement must not hide some exceptions as for the hydrological years 1984/1985 and 1986/1987 where the simulations show too negative glacier-wide annual SMB values in comparison with the observations (Fig. IV.6a). In these years the observed values are comparable to the one in 1994/1995, conversely matched perfectly by the two models. This difference in simulations may result from different input conditions characterizing the considered years; it seems that the years 1984/1985 and 1986/1987 are characterized by a higher ablation in summer and a lower accumulation during winter in comparison to what occurred in 1994/1995. It underlines that the forcing data may represent a considerable source of uncertainties in the simulations. Uncertainty in precipitation estimates could hide the ability of the models to accurately predict the variables such as the discharge production, runoff volumes and the glacier surface mass balance (Ralph et al., 2005). In high-altitude complex terrains such as the high mountain areas, having an accurate estimation of precipitation amounts is challenging because of their high spatial variability and the bias that can affect the precipitation gauges due to the under catch of snow and rain, as well as gauge icing (Sieck et al., 2007; Rasmussen et al., 2012; Grossi et al., 2017). This issue represents one of the major challenges for the hydrological modeling. Several studies in the past attempted to identify the causes and quantify the magnitude of the errors affecting the gauge catch (Kurtyka, 1953; Israelsen, 1967; Larson and Peck, 1974). Recently, to reduce the uncertainty in precipitation estimates for mountain environments, the inference of the precipitation from streamflow observations using a Bayesian approach (Kirchner, 2009; Henn et al., 2015) and the combination of the rain gauge measurements with high-resolution radar field surveys (Borga, 2002; Cole and Moore, 2008; Goudenhoofd and Delobbe, 2009) have been proposed.

At glacier scale our analysis indicates that both DD and HTI models are suited to simulate the glacier-wide annual SMB not only over the calibration period but all over the considered 26 years (1984–2009). This suggests that at the glacier scale the temperature gradient related to elevation has the greatest impact on the spatial variability of ice and snowmelt compared to solar radiation; which is in agreement with Réveillet et al., 2017. According to Heynen et al., 2013 this is particularly suitable for glaciers spanning a wide elevation range. Our finding is in contrast with Gabbi et al., 2014 that concluded that the DD and HTI models are only able to reproduce the SMB changes of the most recent years (~ 6 years) but they tend to simulate too positive mass balance in the previous period. Furthermore, our results contradict Hock, 1999 and Pellicciotti et al., 2005 who showed an improvement in the modeling performance using a

HTI model compared to a DD one at point and glacier scales, respectively.

There is no marked difference between the spatial distribution of the mass balance simulated by the DD and HTI models. Indeed, the melt rate induced by the higher values of solar radiation is compensated by the altitude since the part of the Argentière glacier that is south exposed (submit to a higher values of solar radiation) is located at a higher altitude compared to the north exposed one. This particular morphology could explain also the generally similar performance of the two considered models at glacier and catchments scales.

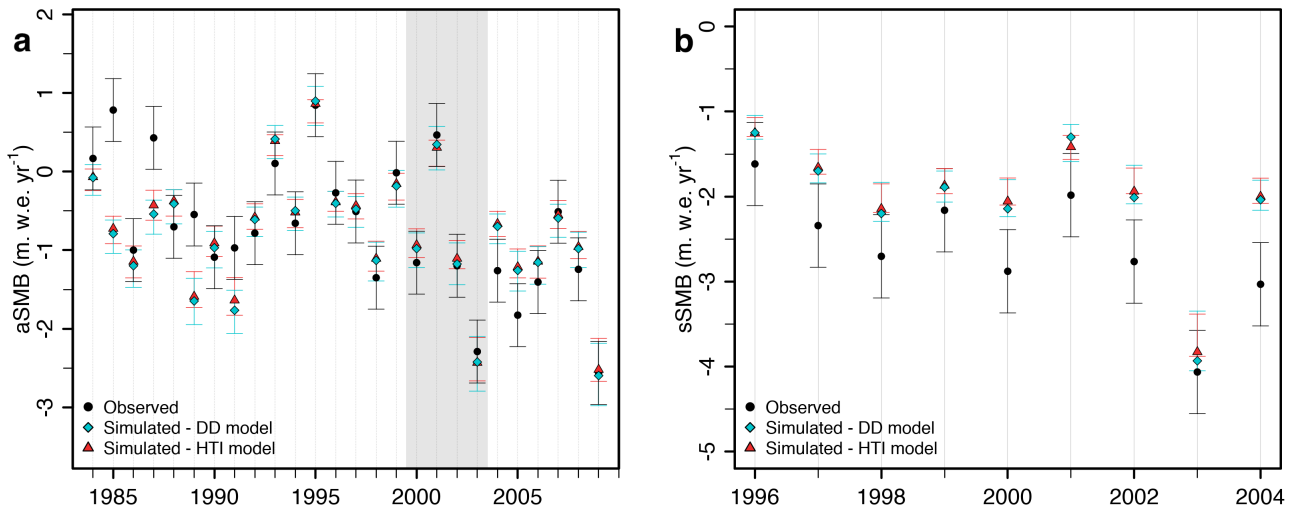


Figure IV.6: Evolution of the observed and simulated (a) aSMB and (b) aSMB with DD and HTI models, calibrated with a multi-criteria approach over the periods 1983–2009 and 1996–2004, respectively. The gray box indicates the calibration period.

The consistence in reproducing the annual SMB as function of altitude is important for the model evaluation, since it could be an indicator of the degree of accuracy of the simulated snow and ice accumulation and ablation processes (Schaeffli et al., 2005). Both DD and HTI models are able to well reproduce the altitudinal SMB distribution above 2300 m a.s.l. for each investigated year over the 1995–2009 period (Fig. IV.7). Below this altitude, the two models tend to overestimate the ablation compared to the observations, for all the investigated period. This is probably due to the thick layer of debris cover on the lowermost part of the Argentière Glacier (*i.e.* below the ice fall located ~ 2300 m a.s.l.) that reduce the melt of the ice beneath it, but that is not consider by the models (Fyffe et al., 2019). The difference between the simulations and the observed measure (at ~ 1800 m a.s.l.) tends to increase with time, which matches the increase in debris coverage. The overestimation of the ablation below 2300 m a.s.l by the DD model compared to the HTI could be due the fact that the glacier’s tongue is located in a “canyon” with important shadowing that is considered in the HTI model and not in the DD, because of the assumption on the values of the DDFs, taken constant in space and in time. We can assume that the simulations done by the HTI are more accurate, but to

validate this hypothesis it would be needed to test the models on a debris-free glacier where more measurements are available at lower elevation.

Despite the interannual variability of the SLA is well simulated, generally both models tend to underestimate it over the 1984–2009 period (Fig. IV.8). The $RMSE_{SLA}$ associated to the simulations of the HTI model are always smaller than those obtained with the DD one, but their difference is not considered significant (Table IV.5). The $RMSE_{SLA}$ values equal 140 and 133 m a.s.l. with DD and HTI models, respectively. In addition, the DD and HTI models are able to reproduce the typical linear relationship between the ELA and the annual SMB (Braithwaite, 1984; Paterson, 1994b) showing a R^2 of 0.70 and 0.79, respectively. On these bases, as for the discharge, the use of the HTI model does not seem to improve the simulation of both the temporal evolution of the surface annual and summer mass balance and the SLA. Indeed, a DD model is sufficient for the simulations at glacier scale (e.g. Vincent, 2002).

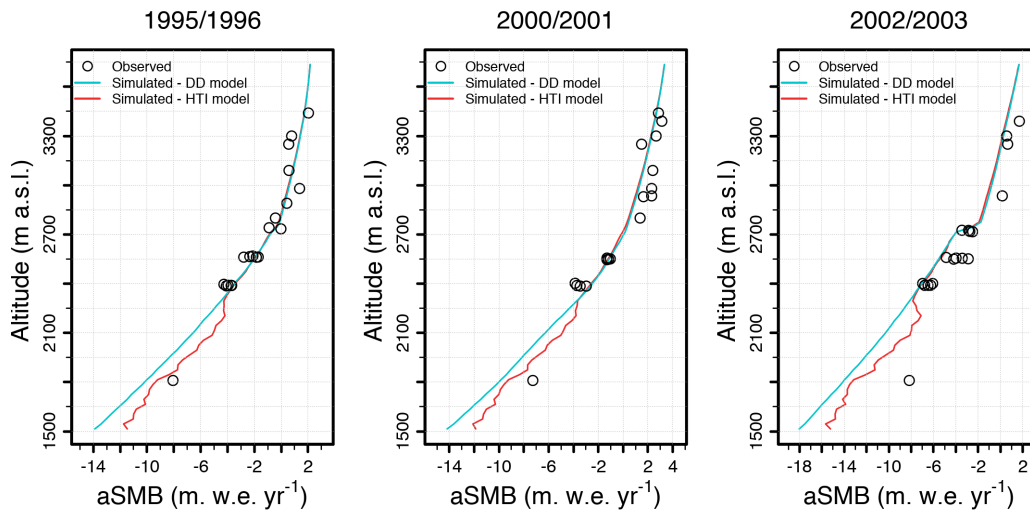


Figure IV.7: Observed and simulated annual surface mass balance (aSMB) with DD and HTI models as function of altitude for the hydrological year 1995/1996, 2000/2001, and 2002/2003.

IV.5.2.3 Snow Cover Area

Both DD and HTI models are able to reproduce the SCA evolution derived from MODIS data. The difference between the performances of the models is almost negligible (Table IV.5); the values of KGE_{SCA} and $RMSE_{SCA}$ are comparable over both the calibration and validation periods. Values of the annual KGE_{SCA} vary from 0.70 to 0.91 over the 2000–2009 period. Generally, during the month of June, both simulations tend to overestimate the observed SCA (e.g. Fig. IV.9a). For the other months, the evolution of the SCA is better represented. In addition, the SCA temporal variability is well reproduced. The observed and simulated daily values are well correlated, showing a R^2 of 0.74 for DD model and 0.75 for HTI ones, over the 2000–2009 period (Fig. IV.9b).

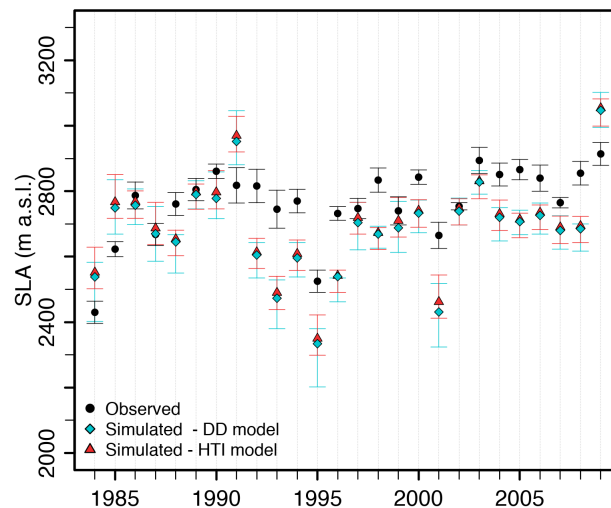


Figure IV.8: Evolution of the observed and simulated SLA with DD and HTI models, calibrated with a multi-criteria approach over the 1983–2009 period.

The evaluation of the spatial consistency between simulations and observations showed that the variability of the SCA spatial pattern is well represented (Fig. IV.9c). The higher values of Jaccard index occur in seasons having high levels of snow accumulation where the larger area is covered by snow, whereas the lower values in July. In summer the simulation performances decline; the mean value of the Jaccard index equals 0.810 for the DD and HTI models over the 2000–2009 period.

The performances of our simulations are comparable with those obtained by Revuelto et al., 2018 using a model with physical basis (SURFEX/ISBA-Crocus snowpack model). In addition, since the improvement in capturing the spatial distribution and the evolution of the SCA obtained with the introduction of the clear-sky solar radiation is irrelevant compared to the DD model, the use of the DD model is suggested to describe the evolution of the snow pack. These results are in agreement with those of Bouamri et al., 2018, who suggested that a simple DD model, when calibrated on a period long enough, offers performance comparable and even superior to some enhanced models. Several studies demonstrated the usefulness of the MODIS satellite images in improving the hydrological modeling (Parajka and Blöschl, 2008a,c; Thirel et al., 2013), but the accuracy of the evaluation of the models' performance in simulating the spatial distribution of the snow pack could be limited by the horizontal resolution of these satellite images.

IV.5.3 Temporal stability of the models

The calibration of the parameters of the DD and HTI models done over each individual year shows that most of them fluctuate from year to year; their variation in comparison with the respectively values calibrated over the 2000–2003 period is not negligible (Table IV.6).

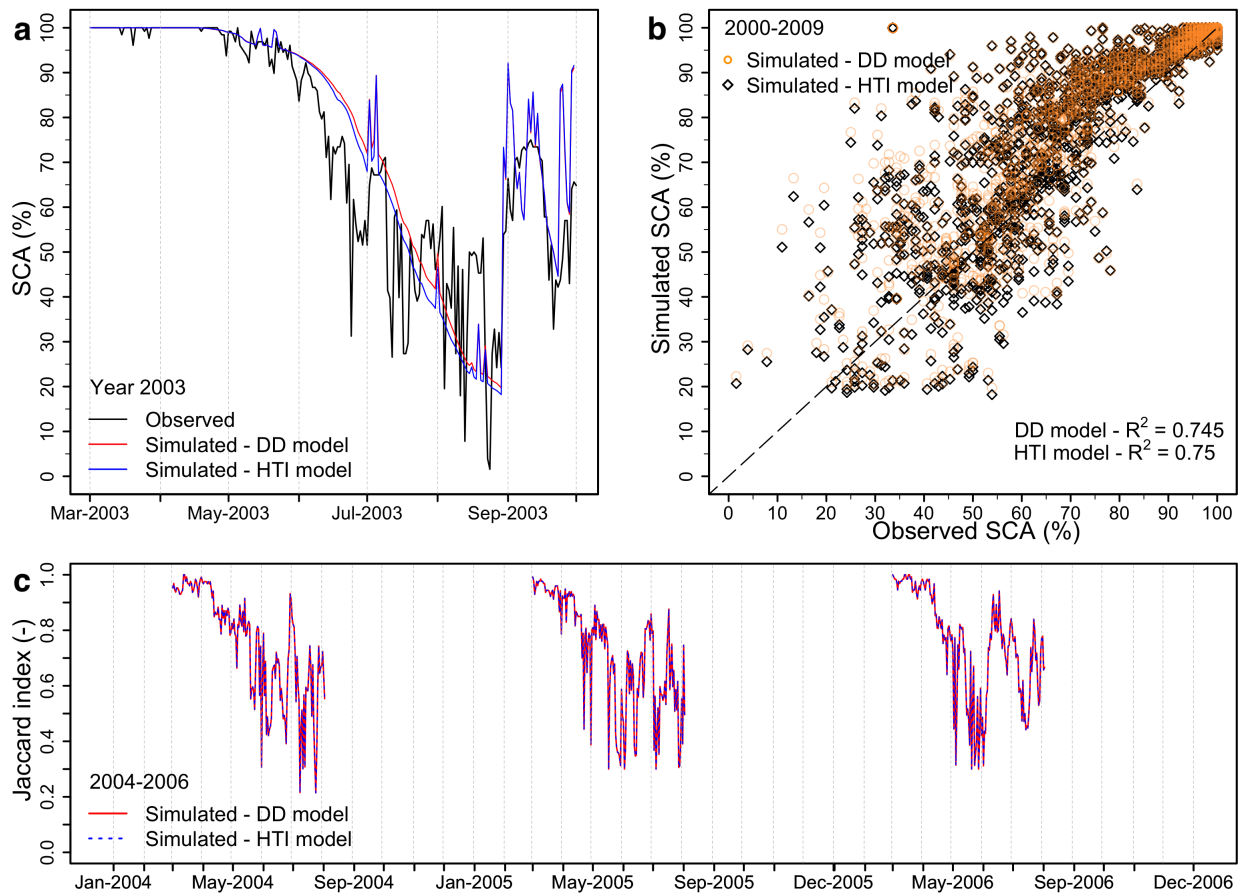


Figure IV.9: (a) Evolution of the observed and simulated daily SCA over the year 2003; (b) Correlation between observed and simulated SCA at daily time scale over the 2000–2009 period, from March to September. The simulated values are obtained with DD and HTI models, calibrated with a multi-criteria approach; (c) Evolution of the Jaccard index over the 2004–2006 period.

Regarding the DD model, the yearly calibrated DDF_{snow} and DDF_{ice} have a coefficient of variation of 5.5% and 22.3%, respectively, ranging from 4.4 to 5 mm d⁻¹ °C⁻¹ and from 5.2 to 9 mm d⁻¹ °C⁻¹. In the case of HTI, the yearly calibrated MFs agree with that obtained over all the period considered. α_{snow} ranges between $3 \cdot 10^{-4}$ and $8 \cdot 10^{-4}$ mm m² h⁻¹ W⁻¹ °C⁻¹ whereas α_{ice} from $1 \cdot 10^{-4}$ to $2 \cdot 10^{-4}$ mm m² h⁻¹ W⁻¹ °C⁻¹, with a variation coefficient equals to 36% and 40%, respectively. In addition, the value of the k_{firn} does not fluctuate, both from year to year and compared to the multi-yearly calibrated value. The year 2001 is characterized by lower values of DDF_{ice} and α_{snow} . They compensate for a greater winter accumulation compared to the other considered years. The mean values of each yearly calibrated melt parameters over the years 2000, 2001 and 2003, are very similar to the multi-yearly calibrated ones.

The variation in the period of calibration of the model parameters does not result in significant changes in model performance both for the DD and HTI models (Table IV.7). The yearly calibration leads to a slight reduction of the KGE_{TOT} in comparison to that of the multi-yearly calibration. Its value decrease by up to 0.1. Results indicate that the values of the mean abso-

lute difference between the simulated and observed Q, SCA and SLA calculated for each set of parameters obtained with a yearly and multi-yearly calibration do not change a lot, having a coefficient of variation of 3, 4 and 14%, respectively. The difference in aSMB exhibits a greater variability, with a coefficient of variation of 40% (31%) for DD (HTI) model. The highest mean absolute difference between the simulated and observed aSMB occurs in 2001.

These results show the short-term stability both of the DD and HTI models, since their performance does not deteriorate significantly using set of parameters coming from different calibration years, characterized by distinct climate conditions. This also indicates that comparable results can be achieved by different parameter sets (equifinality problem, [Beven, 1996](#)). This problem can be reduced by basing calibration on a period including different climate meteorological conditions ([Gabbi et al., 2014](#)) and using numerous and different observed measurements (multi criteria approach).

There are indications on the long-term instability of the parameters of classical temperature index models, because of the changes in the relation between positive air temperature and melt ([Pellicciotti et al., 2005](#); [Huss et al., 2009](#); [Gabbi et al., 2014](#)). This implies that they have to be recalibrated over different subperiods in order to well reproduce the observed data over several decades. In contrast, our results show the long-term stability of the DD and HTI models in simulating the daily discharge and the annual volume production over long period (45 years) (Table [IV.5](#)). The period investigated for the evolution of the glacier-wide annual surface mass balance and the SLA spans only over three decades, according to data availability. The good performance of both models without the need of further recalibrations suggests a long-term stability of the parameters also for the simulation of these variables (Table [IV.5](#)). Nevertheless, a study should be performed over a longer time period to state a real conclusion.

Table IV.6: Values of the parameters of the DD and HTI models calibrated over yearly and multi-yearly periods, using a multi-criteria approach. The fixed not-sensitive parameters are marked with an asterisk.

Year	DD		MF	HTI		DR			
	DD_{snow} mm d ⁻¹ °C ⁻¹	DD_{ice} mm d ⁻¹ °C ⁻¹		α_{snow} mm m ² h ⁻¹ W ⁻¹	α_{ice} mm m ² h ⁻¹ W ⁻¹	k_{firn} h	k_{ice}^* h	k_{snow}^* h	k_{rock}^* h
2000	4.6	8.6	4.0	8 10 ⁻⁴	1 10 ⁻⁴	300	16	35	50
2001	4.8	5.2	4.0	3 10 ⁻⁴	1 10 ⁻⁴	300	16	35	50
2002	5.0	8.2	4.0	6 10 ⁻⁴	2 10 ⁻⁴	300	16	35	50
2003	4.4	9.0	4.0	7 10 ⁻⁴	1 10 ⁻⁴	300	16	35	50
2000–2003	4.4	8.6	4.0	7 10⁻⁴	1 10⁻⁴	300	16	35	50

Table IV.7: Absolute average difference between the simulated and observed variables (*i.e.* discharge (Q), snow cover area (SCA), snow line altitude (SLA) and glacier-wide annual surface mass balance (aSMB)) and the values of the objective function (KGE_{TOT}) obtained using either annually or multi-yearly calibrated model parameters (Section 4.3), over the 2000–2003 period for both the DD and HTI models.

Calibration year	Q		SCA		SLA		aSMB		KGE _{tot}	
	[m ³ s ⁻¹ d ⁻¹]		[%]		[m a.s.l. yr ⁻¹]		[m w.e. yr ⁻¹]		[-]	
	DD	HTI	DD	HTI	DD	HTI	DD	HTI	DD	HTI
2000	1.38	1.39	7.8	7.8	112	112	0.16	0.16	0.789	0.789
2001	1.49	1.46	7.7	7.9	101	114	0.30	0.30	0.786	0.783
2002	1.45	1.50	7.5	7.6	88	81	0.23	0.22	0.783	0.787
2003	1.35	1.37	8.1	7.8	124	113	0.13	0.15	0.880	0.886
2000–2003	1.34	1.37	8.1	7.8	125	113	0.11	0.15	0.879	0.886

IV.6 Conclusion

In this study a classical degree-day method (DD) and an enhanced temperature index model (HTI) which includes the potential clear-sky direct solar radiation have been used to simulate the hydrological processes of the Arveyron d’Argentière, a highly glacierized catchment, located along the Arve River in the French Alps. The importance of the choice of the calibration method and temporal stability (over short and long-term) of the models has been evaluated. The main findings of the study are:

1. The calibration of a conceptual model considering discharge, snow cover area and glacier-wide annual mass balance against the discharge only results in an increase in the performance that is generally not significant compared to the measurement uncertainties. However, the multi-calibration approach leads to an improvement in simulating all the considered variables (except for the discharge) over both the validation and the calibration periods. This suggests that the use of a multi-calibration approach could help to reduce the uncertainty in the simulations and to obtain a robust model increasing the confidence in its physical relevance. Furthermore, it allows identifying only one set of optimum parameters, reducing the equifinality problem.
2. Both the calibrated DD and HTI models exhibit a very good performance in simulating the daily discharge, the annual water volume production, the snow cover area and the glacier-wide surface mass balance both over the calibration (2000–2003) and validation (within the 1960–2009) periods. On the contrary, generally they tend to underestimate the snow line altitude over all the considered period.
3. The simulations are consistent with the mean values of the subglacial water production observed in the observatory of the Argentière glacier over the years 2003 and 2004. There-

fore, we highlight the suitability of both models to obtained subglacial discharge for period or/and glacier where no measurements are available for a qualitative analysis.

4. The multi-calibration of the DD and HTI models over each individual year of the 2000–2003 period shows that the parameters values fluctuate from year to year and their variation in comparison with the respectively values optimized over all the calibration period is generally not negligible. However, we concluded about a short-term stability of both models, since their performances do not deteriorate significantly using set of parameters coming from different calibration years characterized by distinct climate conditions.
5. Our results reveal a long-term stability of the DD and HTI models in simulating the daily discharge and the annual volume production over 1960–2004. In contrast to [Huss et al., 2009](#) and [Gabbi et al., 2014](#), the good performance in reproducing the glacier-wide annual surface mass balance over 1983–2009 suggests a long-term stability of the parameters also regarding this variable; however, the validation over a longer time period is needed to state a real conclusion.

Our results show that the inclusion of the clear sky solar radiation in a temperature index model does not seem to improve considerably the performance of the simulations over calibration and validation periods. As consequences, we suggest the use of a classical degree day model calibrated with a multi-criteria approach to simulate the hydro-glaciological behavior and the subglacial water production of a highly glacierized catchment and to study the long-term impact of the climate variability on the discharge. Given its simplicity and its effectiveness for discharge simulation, this model may be used in the context concerning the water resources management and for projecting discharge volume production under different climate scenario.

Further developments

One limitation of this study is the fact that I did not take into account the evolution of the glacier surface area and its thickness. [Rabatel et al., 2016](#) and [Rabatel et al., 2013](#) showed that over the 1979–2011 period, the subtraction of two DEMs of the Argentière glacier at ~ 3050 m a.s.l. matches the vertical accuracy of the DEMs, whereas at lower altitude the maximum drop in glacier surface elevation is between 100 and 130 m. Future work will be done to address this point: the models will be forced with different DEMs to take in account the glacier evolution over the 1960–2009 period.

I am surprised by the fact that the results do not show difference in the ability of the two models in reproducing the annual SMB as function of altitude (Section [IV.5.2.2](#), Fig. [IV.6](#)) above 2300 m a.s.l. for each investigated year over the 1995–2009 period. I would have expected more contrast among the two different simulations, *i.e.* an overestimation of the melt rate by the classical degree day model since it neglects the effects of surrounding topography. This result deserves some attention. It will be worth to check the grid file of the used potential clear-sky direct solar radiation and the values of the simulated glacier surface mass balance along the glacier, for a better understanding.

Generally, both models tend to underestimate the SLA over the simulation periods (Section [IV.5.2.2](#), Fig. [IV.8](#)). This evaluation needs some refinements. The simulated SLA values presented in this paper are extracted on the basis of the simulated SCA data and the hypsometric curve of the entire catchment. It is worth trying to extract the simulated SLA in other ways, and to compare them with each other, since the SLA used for the validation was delineated on the central part of the glaciers from satellite images. Precisely, I could extract the SLA on the base of the simulated SCA data and the hypsometric curve of the glacier only, and retrieve it from the simulated ELA of the considered glacier, with and without take in to account the main glacier tributaries.

Conclusion and perspectives

1 Conclusion

This research is motivated by the importance of understanding the sensitivity of the hydrological regime, the melt water runoff and the glaciers' evolution to the climate variability in high-alpine catchments. Changes in the hydrological regime affect the availability of the water resource posing new challenges for their management. The studies of the interaction between glaciers, climate and hydrology are not so many because of the few time series long enough for climatological studies available in highly glacierized areas.

This thesis is focused on the Arve watershed, covering a surface of 1958 km² in the French Alps, composed by five nested catchments (*i.e.* Arveyron d'Argentière, Arveyron de la Mer de Glace, Arve at Pont des Favrands, Arve at Sallanches and Arve at Bout du Monde) characterized by various percentages of glacier cover ranging from 53 to 5% (in 2003). The objectives are: (1) to characterize the current and future glacier's influence on the discharge seasonal cycle of the five nested catchments located in the Arve River valley; (2) to show the importance of considering the groundwater fluxes to calculate future runoff in two highly glacierized catchments (Arveyron d'Argentière and Arveyron de la Mer de Glace); and (3) to identify the best suitable simple model allowing the simulation of the hydro-glaciological processes and the subglacial discharge in the Arveyron d'Argentière.

The specific conclusions are given in each research paper reported in the respective chapters; the main findings of this thesis can be summarized as follows:

1. The trend analysis on the discharge values points out a contrasting behaviour among the catchments characterized by different glacier covers, showing an increase in highly glacierized catchments and a decrease in the low glacierized ones. This difference may be influenced by the changes in land use and in the evapotranspiration losses, but further investigations are needed to quantify each process. Moving from 1960–2004 to 1983–2004 periods, the magnitude of the increasing trend on the discharge registered at Arveyron d'Argentière and Arveyron de la Mer de Glace became less pronounced. This finding underlines the relationship between the discharge and glacier changes in a highly glacierized catchments. The results suggest that the Mer de Glace glacier could have already passed or would be currently passing the phase of enhanced contribution to the total discharge; meaning that the increase in melt rate does not compensate the reduction in glacier's surface area. Last, glaciers do not seem to strongly affect the regime of the low

glacierized catchments when the glacierized area is less than 20%. However, at this scale the anthropogenic impacts may mask the influence of the glaciers. Under future climate condition, in the mid-21st century, the peak of the discharge seasonal cycle is projected to decrease in average by 14% and 36% for Arveyron d'Argentière and Arveyron de la Mer de Glace, respectively, and to occur approximately 10 days later compared with the historical period. The annual runoff would be reduced by 16% for Arveyron d'Argentière and 31% for Arveyron de la Mer de Glace. Furthermore, an earlier snowmelt season, a decrease in the discharge in late summer and a reduction in the seasonal snow cover would be expected.

2. The estimation of the glacier-wide summer surface mass balance of Argentière and Mer de Glace-Leschaux glaciers using the hydrological method allows to underline the importance of considering the groundwater transfers to represent and predict the hydro-glaciological behaviour of a catchment. Estimates of the Argentière glacier-wide summer surface mass are in good agreement with the glaciological values: they show almost the same inter-annual variability. From the marked difference between the hydrological and glaciological glacier-wide summer surface mass balances for the Mer de Glace-Leschaux glacier, we suspect a significant role of groundwater fluxes in the hydrological balance. We therefore suggest some caution in the use of calibrated/validated hydro-glaciological models against glaciological and/or altimetric measurements of glacier mass balance to calculate future runoff when groundwater fluxes are not negligible, as they are not accounting for inter-basin transfer of water volumes. The hydrological glacier-wide summer surface mass balance has been obtained with an uncertainty of ± 0.67 m w.e. yr^{-1} at Argentière and ± 0.66 m w.e. yr^{-1} at Mer de Glace-Leschaux.
3. The results show the suitability of a classical degree day model in simulating the hydro-glaciological behaviour and the subglacial discharge of a highly glacierized catchment. The use of a multi-calibration approach considering the discharge, the snow cover area and the glacier-wide annual mass balance is recommended since it allows to reduce the uncertainty in the simulations and to obtain a robust model increasing the confidence in its physical significance. In addition, the temporal long-term stability of this model in simulating the daily discharge and the annual volume production is shown. The classical degree day model may be used in the context of the water resources management and for projecting discharge volume production under different climate scenarios.

This thesis has underlined the importance of the investigation of all the available dataset (meteorological, glaciological, hydrological, snow cover data) and the computation of their uncertainties before performing a hydrological modelling. This allows to improve the knowledge on the physical processes occurring in the considered catchment. It is an essential aspect, since

the comprehension of the hydrological behaviour of an area under the present climate condition is fundamental for understanding its future hydrological regime under a changing climate. Furthermore, this research can be used to complete the results of previous studies providing evidence on the temporal and spatial changes in the discharge seasonal cycle in high-alpine glacierized catchments. In addition, the suitability of a conceptual model in simulating the subglacial discharge is an important result, since two hydropower plants are strongly dependent on the subglacial water generated by the Argentière and Mer de Glace glaciers. Given its temporal transferability in simulating the discharge, the considered model calibrated could be used to predict changes in the glacier's water production. Finally, this study could represent a step to address the gaps in the knowledge concerning the assessment of the subsurface fluxes dynamic.

2 Outlook for further research

Hereafter some research directions for future work in the high-alpine region are given.

Analysis of the evolution of the glacier annual mass balance as a function of altitude.

Several studies have focused on the changes in the elevation dependence of the mass balance of the Asiatic glaciers. For the entire Pamir region and the Abramov glacier, the results demonstrate a weak tendency towards more accumulation at higher elevation but also more ablation during the past few decades comparing to the 1970s (Khromova et al., 2006, 2014; Barandun et al., 2015). On contrary, for high-elevation glaciers in the Karakoram region, Gardelle et al., 2013 and Mandal et al., 2014 reveal a reduction in the sensitivity of the glacier annual surface mass balance gradients to air temperature changes due to an increase in winter snowfall compensated by the increase in summer melt rates. These evaluations could be done also on the alpine glaciers. The classical degree day model calibrated in this study (Chapter IV) could be used to provide time series of the Argentière glacier annual mass balance since 1960.

Assessment of the sensitivity of the hydro-glaciological models to precipitation uncertainties.

The problem to obtain an accurate estimation of precipitation in mountain region, due to their high spatial variability and the bias that can affect the precipitation gauges due to the under catch of snow and rain as well as gauge icing, is largely discussed in the literature (*e.g.* Sevruk, 1983, 1987; Schaeffi et al., 2005; Immerzeel et al., 2015; Chen et al., 2017; Grossi et al., 2017; Réveillet et al., 2017). Therefore, it is worth investigating the propagation of uncertainties from the precipitation forcing on the resulting streamflow, testing different hydro-glaciological models. In the French region, in addition to the SAFRAN reanalysis used in this thesis, SPAZM datasets (SPAtialisation en Zones de Montagne, Gottardi, 2009) with a spatial resolution of 1 km could be considered. Furthermore, on the European Alps, a daily

precipitation dataset with a grid spacing of 5 km is available (Isotta et al., 2013). It was developed as part of the EU funded EURO4M (European Reanalysis and Observations for Monitoring) (Innovation International, 2011) project.

The use of a physically based model including the glacier dynamic to simulate the hydro-glaciological processes in the Arveyron d'Argentière catchment. The DHSVM (Distributed Hydrology Soil-Vegetation model, Wigmosta et al., 1994) coupled with the GDM (Glacier Dynamics Model, Jarosch et al., 2013) could be used to investigate more in details the hydro-glaciological behaviour of this area in actual climate conditions and to predict its future behavior (Naz et al., 2014). In literature several studies have adopt a parametrized glacier geometry change, *i.e.* the Δh -parametrization (Huss et al., 2010) or an empirical area-volume scaling (Bahr et al., 2015) to simulate the glacier dynamic. Another solution could be the use of a finite element model, such as Elmer/Ice model (Gagliardini et al., 2013); then it could be coupled with a hydrological model. These simulations could be compared with those obtained in this thesis using a conceptual model (Chapter IV).

Assessment of the hydrological processes at regional scale. This investigation could be done using available in-situ measurements and remote sensing data. For instance, changes in evapotranspiration could be inferred from the NDVI and observing the evolution of the forested areas using Landsat satellite imagery or directly evaluated with the MOD16A2 product. The precipitation could be investigated using CHIRPS (Climate Hazards Group InfraRed Precipitation with Station data, Funk et al., 2015) and the GPM (Global Precipitation Measurement, Huffman et al., 2014) data. In addition, for a better understanding an improvement in a precipitation product all over the alpine arc based on the available winter accumulation measurement on the glaciers and on the gradient inferred from the high-resolution meteorological forecasting like AROME (Seity et al., 2011) could be carried out.

Bibliography

- Abdul Aziz, O. and Burn, D. (2006), 'Trends and variability in the hydrological regime of the Mackenzie River Basin', *Journal of Hydrology* **319**, 282–294. doi: 10.1016/j.jhydrol.2005.06.039.
- Allen, R., Pereira, L., Raes, D. and Smith, M. (1998), Crop Evapotranspiration-Guidelines for Computing Crop Water Requirements. FAO Irrigation and Drainage Paper 56. Food and Agriculture Organization of the United Nations (FAO), Rome., Technical report.
- Amundson, J. M., Truffer, M. and Lüthi, M. P. (2006), 'Time-dependent basal stress conditions beneath Black Rapids Glacier, Alaska, USA, inferred from measurements of ice deformation and surface motion', *Journal of Glaciology* **52**(178), 347–357. doi: 10.3189/172756506781828593.
- Armstrong, T., Roberts, B. and Swithinbank, C. (1973), 'Illustrated glossary of snow and ice. Second edition. Cambridge, Scott Polar Research Institute. (SPRI Special Publication 4.)'.
- Auer, I., Böhm, R., Jurkovic, A., Lipa, W., Orlik, A., Potzmann, R., Schöner, W., Ungersböck, M., Matulla, C., Briffa, K., Jones, P., Efthymiadis, D., Brunetti, M., Nanni, T., Maugeri, M., Merciali, L., Mestre, O., Moisselin, J.-M., Begert, M., Müller-Westermeier, G., Kveton, V., Bochnicek, O., Stastny, P., Lapin, M., Szalai, S., Szentimrey, T., Cegnar, T., Dolinar, M., Gajic-Capka, M., Zaninovic, K., Majstorovic, Z. and Nieplova, E. (2006), 'HISTALP—historical instrumental climatological surface time series of the Greater Alpine Region', *International Journal of Climatology* **27**(1), 17–46. doi: 10.1002/joc.1377.
- Baccolo, G., Delmonte, B., Albani, S., Baroni, C., Cibin, G., Frezzotti, M., Hampai, D., Marcelli, A., Revel, M., Salvatore, M. C., Stenni, B. and Maggi, V. (2018), Atmospheric dust fluxes from the Antarctic ice core Talos Dome, PANGAEA. doi: 10.1594/PANGAEA.890896.
- Bahr, D. B., Pfeffer, W. T. and Kaser, G. (2015), 'A Review of Volume-Area Scaling of Glaciers', *Reviews of Geophysics* **53**, 95–140. doi: 10.1002/2014RG000470.
- Baker, D., Escher-Vetter, H., Moser, H., Oerter, H. and Reinwarth, O. (1982), 'A glacier discharge model based on results from field studies of energy balance, water storage and flow. in: Hydrological Aspects of Alpine and High-Mountain Areas, edited by: Glenn, J. W., IAHS Publ. no. 138, Wallingford, Oxfordshire UK, 103–112'.
- Baraer, M., Mark, B. G., McKenzie, J. M., Condom, T., Bury, J., Huh, K. I., Portocarrero, C., Gómez, J. and Rathay, S. (2012), 'Glacier recession and water resources in Peru's Cordillera Blanca', *Journal of Glaciology* **58**(207), 134–150. doi: 10.3189/2012JoG11J186.
- Barandun, M., Huss, M., Sold, L., Farinotti, D., Azisov, E., Salzmann, N., Usabaliev, R., Merkushev, A. and Hoelzle, M. (2015), 'Re-analysis of seasonal mass balance at Abramov glacier 1968–2014', *Journal of Glaciology* **61**(230), 1103–1117. doi: 10.3189/2015JoG14J239.
- Bard, A., Renard, B., Lang, M., Giuntoli, I., Korck, J., Koboltschnig, G., Janža, M., D'Amico, M. and

- Volken, D. (2015), 'Trends in the hydrologic regime of Alpine rivers', *Journal of Hydrology* **529**(Part 3), 1823–1837. doi: 10.1016/j.jhydrol.2015.07.052.
- Barnett, T. P., Adam, J. C. and Lettenmaier, D. P. (2005), 'Potential impacts of a warming climate on water availability in snow-dominated regions.', *Nature* **438**(7066), 303–309. doi: 10.1038/nature04141.
- Barry, R. (2001), 'Mountain Weather & Climate. Routledge'.
- Bartholomäus, T., Anderson, R. and Anderson, S. (2008), 'Response of glacier basal motion to transient water storage', *Nat. Geosci.* **1**(1), 33–37. doi: 10.1038/ngeo.2007.52.
- Bartlett, M. S. (1935), 'Some Aspects of the Time-Correlation Problem in Regard to Tests of Significance', *Journal of the Royal Statistical Society* **98**(3), 536–543.
- Bauder, A. (2017), 'The Swiss Glaciers 2013/14 and 2014/15', p. 144. doi: 10.18752/glrep 135-136.
- Bauder, A., Funk, M. and Huss, M. (2007), 'Ice-volume changes of selected glaciers in the Swiss Alps since the end of the 19th century', *Annals of Glaciology* **46**, 145–149. doi: 10.3189/172756407782871701.
- Bénévent, E. (1926), 'Documents sur le climat des Alpes françaises. Étude critique', *Revue de Géographie Alpine* **14**(4), 681–764. doi: 10.3406/rga.1926.5004.
- Beniston, M. (2003), 'Climatic change in mountain regions: A review of possible impacts', *Climatic Change* **59**(1-2), 5–31. doi: 10.1023/A:1024458411589.
- Beniston, M., Farinotti, D., Stoffel, M., Andreassen, L. M., Coppola, E., Eckert, N., Fantini, A., Giacomoni, F., Hauck, C., Huss, M., Huwald, H., Lehning, M., López-Moreno, J.-I., Magnusson, J., Marty, C., Morán-Tejeda, E., Morin, S., Naaim, M., Provenzale, A., Rabatel, A., Six, D., Stötter, J., Strasser, U., Terzago, S. and Vincent, C. (2018), 'The European mountain cryosphere: a review of its current state, trends, and future challenges', *The Cryosphere* **12**(2), 759–794. doi: 10.5194/tc-12-759-2018.
- Bergstrom, S. (1995), 'The HBV Model. In Computer Models of Watershed Hydrology, Singh VP (ed). Water Resources Publications: Colorado', pp. 443 – 476.
- Bergström, S., Lindström, G. and Pettersson, A. (2002), 'Multi-variable parameter estimation to increase confidence in hydrological modelling', *Hydrological Processes* **16**(2), 413–421. doi: 10.1002/hyp.332.
- Berthier, E., Arnaud, Y., Vincent, C. and Rémy, F. (2006), 'Biases of SRTM in high-mountain areas: Implications for the monitoring of glacier volume changes', *Geophysical Research Letters* **33**(8), 1–5. doi: 10.1029/2006GL025862.
- Berthier, E. and Vincent, C. (2012), 'Relative contribution of surface mass-balance and ice-flux changes to the accelerated thinning of Mer de Glace, French Alps, over 1979-2008', *Journal of Glaciology* **58**(209), 501–512. doi: 10.3189/2012JoG11J083.
- Berthier, E., Vincent, C., Magnússon, E., Gunnlaugsson, P., Pitte, P., Le Meur, E., Masiokas, M., Ruiz,

- L., Pálsson, F., Belart, J. M. C. and Wagnon, P. (2014), 'Glacier topography and elevation changes derived from Pléiades sub-meter stereo images', *Cryosphere* **8**(6), 2275–2291. doi: 10.5194/tc-8-2275-2014.
- Beven, K. (1996), 'Equifinality and Uncertainty in Geomorphological Modelling, in B L Rhoads and C E Thorn (Eds.), *The Scientific Nature of Geomorphology*, Wiley: Chichester, 289-313'.
- Beven, K. (2009), 'Environmental modelling: an uncertain future? Routledge, London, 1-310 pp'.
- Bindschadler, R. (1983), 'The importance of pressurized subglacial water in separation and sliding at the glacier bed', *Journal of Glaciology* **29**(1), 3–19.
- Birman, C., Karbou, F., Mahfouf, J.-F., Lafaysse, M., Durand, Y., Giraud, G., Mérindol, L. and Hermozo, L. (2017), 'Precipitation Analysis over the French Alps Using a Variational Approach and Study of Potential Added Value of Ground-Based Radar Observations', *Journal of Hydrometeorology* **18**(5), 1425–1451. doi: 10.1175/JHM-D-16-0144.1.
- Birsan, M.-V., Molnar, P., Burlando, P. and Pfaundler, M. (2005), 'Streamflow trends in Switzerland', *Journal of Hydrology* **314**, 312–329. doi: 10.1016/j.jhydrol.2005.06.008.
- Blake, E., Fischer, U. and Clarke, G. (1994), 'Direct measurement of sliding at the glacier bed', *J. Glaciol.* **40**(1), 595–599.
- Bliss, A., Hock, R. and Radić, V. (2014), 'Global response of glacier runoff to twenty-first century climate change', *Journal of Geophysical Research: Earth Surface* **119**(4), 717–730. doi: 10.1002/2013JF002931.
- Bocchiola, D. and Diolaiuti, G. (2010), 'Evidence of climate change within the adamello glacier of italy', *Theoretical and Applied Climatology* **100**, 351 – 369. doi: <https://doi.org/10.1007/s00704-009-0186-x>.
- Bocchiola, D., Soncini, A., Diolaiuti, G., Smiraglia, C., Mauro, V., Franzini, C. and Meinardi, A. (2018), 'Idrostellvio: a hydrometric network for the lombardo stelvio park area 2011-2015. results from measurements and models', *L'Acqua* **4**, 45 – 58.
- Boehm, R. (1975), 'Lufttemperaturen bei Schneefall von grösserer Ergiebigkeit in Wien, Wetteru. Leben', **27**((1-2)), 133–137.
- Bontron, G. (2004), 'Prèvision quantitative des prècipitations : adaptation probabiliste par recherche d'analogues - utilisation des rèanalyses NCEP/NCAR et application aux prècipitations du sud- est de la France. Thèse de doctorat, INPG'.
- Borga, M. (2002), 'Accuracy of radar rainfall estimates for streamflow simulation', *Journal of Hydrology* **267**(1-2), 26–39. doi: 10.1016/S0022-1694(02)00137-3.
- Bossard, M., Feranec, J. and Otahel, J. (2000), *CORINE land cover technical guide – Addendum 2000*, Technical report No 40.
- Bouamri, H., Boudhar, A., Gascoin, S. and Kinnard, C. (2018), 'Performance of temperature and radiation index models for point-scale snow water equivalent (SWE) simulations in the Moroccan High

- Atlas Mountains', *Hydrological Sciences Journal* **0**(0), 1–19. doi: 10.1080/02626667.2018.1520391.
- Braithwaite, R. (1984), 'Can the mass balance of a glacier be estimated from its equilibrium-line altitude?', *Journal of Glaciology* · **30 No. 106**(January 1984), 364–368.
- Braithwaite, R. J. and Zhang, Y. (2000), 'Sensitivity of mass balance of five Swiss glaciers to temperature changes assessed by tuning a degree-day model', *Journal of Glaciology* **46**(152), 7–14. doi: 10.3189/172756500781833511.
- Braithwaite, R. and Olesen, O. (1989), 'Calculation of glacier ablation from air temperature. Springer Netherlands, West Greenland', pp. 219–233.
- Braun, L. (1985), 'Simulation of snowmelt-runoff in lowland and lower alpine regions of Switzerland. Dissert. Zurcher Geographische Schriften, Heft 21. (ETH) Zurich'.
- Braun, L. N., Weber, M. and Schulz, M. (2000), 'Consequences of climate change for runoff from Alpine regions', *Annals of Glaciology* **31**, 19–25. doi: 10.3189/172756400781820165.
- Bretherton, C. S., Widmann, M., Dymnikov, V. P., Wallace, J. M. and Bladé, I. (1999), 'The Effective Number of Spatial Degrees of Freedom of a Time-Varying Field', *Journal of Climate* **12**(7), 1990–2009. doi: 10.1175/1520-0442(1999)012<1990:TENOSD>2.0.CO;2.
- Bucher, K., Kerschner, H., Lumasegger, M., Mergili, M. and Rastner, P. (2004), Spatial Precipitation Modelling for the Tyrol Region, Technical report.
- Carenzo, M., Pellicciotti, F., Rimkus, S. and Burlando, P. (2009), 'Assessing the transferability and robustness of an enhanced temperature-index glacier-melt model', *Journal of Glaciology* **55**(190), 258–274. doi: 10.3189/002214309788608804.
- Carturan, L., Baroni, C., Brunetti, M., Carton, A., Dalla Fontana, G., Salvatore, M. C., Zanoner, T. and Zuecco, G. (2016), 'Analysis of the mass balance time series of glaciers in the Italian Alps', *The Cryosphere* **10**(2), 695–712. doi: 10.5194/tc-10-695-2016.
- Carturan, L., Fontana, G. and Borga, M. (2012), 'Estimation of winter precipitation in a high-altitude catchment of the Eastern Italian Alps: validation by means of glacier mass balance observations', *Geogr. Fis. Dinam. Quat.* **35**(1), 37–48. doi: 10.4461/GFDQ.2012.35.4.
- Casassa, G., Paulina, L., Pouyaud, B. and Escobar, F. (2009), 'Detection of changes in glacial run-off in alpine basins : examples from North America , the Alps , central Asia and the Andes', **41**, 31–41. doi: 10.1002/hyp.
- Chen, J. and Ohmura, A. (1990), 'On the influence of Alpine glaciers on runoff', *Hydrology in Mountainous Regions*. (193), 117–126.
- Chen, Y., Li, W., Fang, G. and Li, Z. (2017), 'Review article: Hydrological modeling in glacierized catchments of central Asia – status and challenges', *Hydrol. Earth Syst. Sci.* **21**(2), 669–684. doi: 10.5194/hess-21-669-2017.
- Church, J. and others, . (2013), Sea level change, in B. V. Stocker TF, Qin D, Plattner G-K, Tignor M, Allen SK, Boschung J, Nauels A, Xia Y and M. PM, eds, 'Climate change 2013: the physical science

- basis. Contribution of working group I to the fifth assessment report of the intergovernmental panel on climate change', Cambridge University Press, Cambridge, United Kingdom and New York, NY, USA, pp. 1137– 1216. doi: 10.1017/CBO9781107415324.026.
- Cogley, G. J. (2009), 'Geodetic and direct mass-balance measurements: comparison and joint analysis', *Annals of Glaciology* **50**(50), 96–100. doi: 10.3189/172756409787769744.
- Cogley, J., Hock, R., Rasmusse, L., Arendt, A., Bauder, A., Braithwaite, R., Jansson, P., Kaser, G., Möller, M., Nicholson, L. and Zemp, M. (2011), 'Glossary of Glacier Mass Balance and Related Terms, IHP-VII Technical Documents in Hydrology No. 86, IACS Contribution No. 2, UNESCO-IHP, Paris'.
- Cole, S. J. and Moore, R. J. (2008), 'Hydrological modelling using raingauge- and radar-based estimators of areal rainfall', *Journal of Hydrology* **358**(3), 159–181. doi: <https://doi.org/10.1016/j.jhydrol.2008.05.025>.
- community Members, E., Augustin, L., Barbante, C., Barnes, P. R. F., Marc Barnola, J., Bigler, M., Castellano, E., Cattani, O., Chappellaz, J., Dahl-Jensen, D., Delmonte, B., Dreyfus, G., Durand, G., Falourd, S., Fischer, H., Flückiger, J., Hansson, M. E., Huybrechts, P., Jugie, G., Johnsen, S. J., Jouzel, J., Kaufmann, P., Kipfstuhl, J., Lambert, F., Lipenkov, V. Y., Littot, G. C., Longinelli, A., Lorrain, R., Maggi, V., Masson-Delmotte, V., Miller, H., Mulvaney, R., Oerlemans, J., Oerter, H., Orombelli, G., Parrenin, F., Peel, D. A., Petit, J.-R., Raynaud, D., Ritz, C., Ruth, U., Schwander, J., Siegenthaler, U., Souchez, R., Stauffer, B., Peder Steffensen, J., Stenni, B., Stocker, T. F., Tabacco, I. E., Udisti, R., van de Wal, R. S. W., van den Broeke, M., Weiss, J., Wilhelms, F., Winther, J.-G., Wolff, E. W. and Zucchelli, M. (2004), 'Eight glacial cycles from an Antarctic ice core', *Nature* **429**, 623.
- Confortola, G., Soncini, A. and Bocchiola, D. (2013), 'Climate change will affect water resources in the alps: a case study in italy', *Journal of Alpine Research* **110**(3), 1 – 19. doi: <https://doi.org/10.4000/rga.2176>.
- Corbin, P. and Oulianoff, N. (1930), 'Notice explicative de la Carte Geologique du Massif du Mont Blanc (partie francaise) a l'échelle du 1/20 000- Feuille Vallorcine.', *Notice + carte géologique au 1/20 000* .
- Courault, T. and Monestiez, P. (1999), 'Spatial interpolation of air temperature according to atmospheric circulation patterns in southeast france', *International Journal of Climatology* **99**, 365–378.
- Courtier, P., Freydier, C., Geleyn, J.-F., Rabier, F. and Rochas, M. (1991), The Arpege project at Meteo France, in 'Seminar on Numerical Methods in Atmospheric Models, 9-13 September 1991', Vol. II, ECMWF, ECMWF, Shinfield Park, Reading, pp. 193–232.
- Dahlke, H., Lyon, S., Stedinger, J., Rosqvist, G. and Jansson, P. (2012), 'Contrasting trends in floods for two sub-arctic catchments in northern Sweden – does glacier presence matter?', *Hydrology and Earth System Sciences* **16**(7), 2123–2141. doi: 10.5194/hess-16-2123-2012.
- Danneberg, J. (2012), 'Changes in runoff time series in Thuringia, Germany - Mann-Kendall trend test

- and extreme value analysis', *Advances in Geosciences* **31**, 49–56. doi: 10.5194/adgeo-31-49-2012.
- Davaze, L., Rabatel, A., Arnaud, Y., Sirguey, P., Six, D., Letreguilly, A. and Dumont, M. (2018), 'Monitoring glacier albedo as a proxy to derive summer and annual surface mass balances from optical remote-sensing data', *The Cryosphere* **12**(1), 271–286. doi: 10.5194/tc-12-271-2018.
- Diaz-Ramirez, J., Camacho, R., McAnally, W. and Martin, J. (2012), 'Parameter uncertainty methods in evaluating a lumped hydrological model', *Obras y Proyectos* **12**, 42–56.
- Dingman, S. (2002), 'Physical Hydrology. Prentice-Hall: New Jersey; 646'.
- Diolaiuti, G., Bocchiola, D., D'agata, C. and Smiraglia, C. (2012), 'Evidence of climate change impact upon glaciers' recession within the italian alps: the case of lombardy glaciers', *Theoretical and Applied Climatology* **109**(3-4), 429 – 445. doi: <https://doi.org/10.1007/s00704-012-0589-y>.
- Djrboua, A. (2001), 'Prédetermination des pluies et crues extrêmes dans les Alpes franco-italiennes, prévision quantitative des pluies journalières par la méthode des analogues. Thèse de doctorat, INPG.'.
- Duband, D. (1970), 'Reconnaissance dynamique de la forme des situations météorologiques. Application à la prévision quantitative des précipitations. Thèse de doctorat, Faculté des Sciences de Paris'.
- Dubois, J. (1992), Typologie des aquifères du cristallin: exemple des massifs des Aiguilles rouges et du Mont-blanc (France, Italie et Suisse), PhD thesis, École polytechnique fédérale de Lausanne.
- Dumont, M., Durand, Y., Arnaud, Y. and Six, D. (2012), 'Variational assimilation of albedo in a snowpack model and reconstruction of the spatial mass-balance distribution of an alpine glacier', *Journal of Glaciology* **58**(207), 151–164. doi: 10.3189/2012JoG11J163.
- Durand, Y. (1985), The use of satellite data in the French high resolution analysis, in 'Workshop on High Resolution Analysis, 24-26 June 1985', ECMWF, ECMWF, Shinfield Park, Reading, pp. 89–128.
- Durand, Y., Brun, E., Mérindol, L., Guyomarc'h, G., Lesaffre, B. and Martin, E. (1993), 'A meteorological estimation of relevant parameters for snow models', *Annals of Glaciology* **18**, 65–71. doi: 10.1017/S0260305500011277.
- Durand, Y., Giraud, G., Brun, E., Mérindol, L. and Martin, E. (1999), 'A computer-based system simulating snowpack structures as a tool for regional avalanche forecasting', *Journal of Glaciology* **45**(151), 469–484. doi: 10.3189/S0022143000001337.
- Durand, Y., Laternser, M., Giraud, G., Etchevers, P., Lesaffre, B. and Mérindol, L. (2009), 'Reanalysis of 44 Yr of Climate in the French Alps (1958–2002): Methodology, Model Validation, Climatology, and Trends for Air Temperature and Precipitation', *Journal of Applied Meteorology and Climatology* **48**(3), 429–449.
- EDF (2012), 'Dèplacement du captage sous-glaciaire de l'aménagement hydroélectrique des Bois', p. 14.
- EDF (2016), 'Les bois, une centrale entièrement souterraine. retrieved from <https://www.youtube.com/watch?v=7udgr7ffrc8>'.

- EEA (2007), CLC2006 technical guidelines, Technical Report No. 2007/17. doi: 10.2800/12134.
- EEA (2009), ‘Regional climate change and adaptation — The Alps facing the challenge of changing water resources’, (8), 1–143. doi: 10.2800/12552.
- European Commission (2009), ‘Adapting to climate change: Towards a European framework for action. White paper. COM(2009), 147/4 final.’.
- Farinotti, D., Usselman, S., Huss, M., Bauder, A. and Funk, M. (2012), ‘Runoff evolution in the Swiss Alps: projections for selected high-alpine catchments based on ENSEMBLES scenarios’, *Hydrological Processes* **26**(13), 1909–1924. doi: 10.1002/hyp.8276.
- Finger, D., Pellicciotti, F., Konz, M., Rimkus, S. and Burlando, P. (2011), ‘The value of glacier mass balance, satellite snow cover images, and hourly discharge for improving the performance of a physically based distributed hydrological model’, *Water Resources Research* **47**(7), 1–14. doi: 10.1029/2010WR009824.
- Fountain, A. G. and Walder, J. S. (1998), ‘Water flow through temperate glaciers’, *Reviews of Geophysics* **36**(3), 299–328. doi: 10.1029/97RG03579.
- Fu, P. and Rich, P. M. (1999), Design and Implementation of the Solar Analyst: an ArcView Extension for Modeling Solar Radiation at Landscape Scales. Proceedings of the Nineteenth Annual ESRI User Conference, number February.
- Fu, P. and Rich, P. M. (2002), ‘A geometric solar radiation model with applications in agriculture and forestry’, *Computers and Electronics in Agriculture* **37**(1), 25–35. doi: [https://doi.org/10.1016/S0168-1699\(02\)00115-1](https://doi.org/10.1016/S0168-1699(02)00115-1).
- Funk, C., Peterson, P., Landsfeld, M., Pedreros, D., Verdin, J., Shukla, S., Husak, G., Rowland, J., Harrison, L., Hoell, A. and Michaelsen, J. (2015), ‘The climate hazards infrared precipitation with stations - A new environmental record for monitoring extremes’, *Scientific Data* **2**, 1–21. doi: 10.1038/sdata.2015.66.
- Fyffe, C., Brock, B., Kirkbride, M., Mair, D., Arnold, N., Smiraglia, C., Diolaiuti, G. and Diotri, F. (2019), ‘Do debris-covered glaciers demonstrate distinctive hydrological behaviour compared to clean glaciers?’, *Journal of Hydrology* **570**, 584 – 597. doi: <https://doi.org/10.1016/j.jhydrol.2018.12.069>.
- Gabbi, J., Carenzo, M., Pellicciotti, F., Bauder, A. and Funk, M. (2014), ‘A comparison of empirical and physically based glacier surface melt models for long-term simulations of glacier response’, *Journal of Glaciology* **60**(224), 1199–1207. doi: 10.3189/2014JoG14J011.
- Gabbi, J., Farinotti, D., Bauder, A. and Maurer, H. (2012), ‘Ice volume distribution and implications on runoff projections in a glacierized catchment’, *Hydrology and Earth System Sciences* **16**(12), 4543–4556. doi: 10.5194/hess-16-4543-2012.
- Gafurov, A. and Bárdossy, A. (2009), ‘Cloud removal methodology from MODIS snow cover product’, *Hydrology and Earth System Sciences* **13**(7), 1361–1373. doi: 10.5194/hess-13-1361-2009.
- Gagliardini, O., Zwinger, T., Gillet-Chaulet, F., Durand, G., Favier, L., de Fleurian, B., Greve, R.,

- Malinen, M., Martín, C., Råback, P., Ruokolainen, J., Sacchetti, M., Schäfer, M., Seddik, H. and Thies, J. (2013), 'Capabilities and performance of Elmer/Ice, a new-generation ice sheet model', *Geosci. Model Dev.* **6**(4), 1299–1318. doi: 10.5194/gmd-6-1299-2013.
- Garavaglia, F., Gailhard, J., Paquet, E., Lang, M., Garçon, R. and Bernardara, P. (2010), 'Introducing a rainfall compound distribution model based on weather patterns sub-sampling', *Hydrology and Earth System Sciences* **14**(6), 951–964. doi: 10.5194/hess-14-951-2010.
- Gardelle, J., Berthier, E., Arnaud, Y. and Kääb, A. (2013), 'Region-wide glacier mass balances over the Pamir-Karakoram-Himalaya during 1999–2011', *The Cryosphere* **7**(4), 1263–1286. doi: 10.5194/tc-7-1263-2013.
- Gardent, M., Rabatel, A., Dedieu, J. P. and Deline, P. (2014), 'Multitemporal glacier inventory of the French Alps from the late 1960s to the late 2000s', *Global and Planetary Change* **120**, 24–37. doi: 10.1016/j.gloplacha.2014.05.004.
- Gascoin, S., Hagolle, O., Huc, M., Jarlan, L., Dejoux, J.-F., Szczypta, C., Marti, R. and Sánchez, R. (2015), 'A snow cover climatology for the Pyrenees from MODIS snow products', *Hydrology and Earth System Sciences* **19**(5), 2337–2351. doi: 10.5194/hess-19-2337-2015.
- Gerbaux, M., Genthon, C., Etchevers, P., Vincent, C. and Dedieu, J. (2005), 'Surface mass balance of glaciers in the French Alps: distributed modeling and sensitivity to climate change', *Journal of Glaciology* **51**(175), 561–572. doi: 10.3189/172756505781829133.
- Giuntoli, I., Renard, B. and Lang, M. (2012), *Floods in France*.
- Gleick, P. H. and Palaniappan, M. (2010), 'Peak water limits to freshwater withdrawal and use', *Proceedings of the National Academy of Sciences* **107**(25), 11155–11162. doi: 10.1073/pnas.1004812107.
- Gobiet, A., Kotlarski, S., Beniston, M., Heinrich, G., Rajczak, J. and Stoffel, M. (2014), '21st century climate change in the European Alps—A review', *Science of The Total Environment* **493**, 1138–1151. doi: <https://doi.org/10.1016/j.scitotenv.2013.07.050>.
- Gottardi, F. (2009), Statistical estimation of precipitation over french mountain ranges, Theses, Institut National Polytechnique de Grenoble - INPG.
- Goudenhoofdt, E. and Delobbe, L. (2009), 'Evaluation of radar-gauge merging methods for quantitative precipitation estimates', *Hydrol. Earth Syst. Sci.* **13**(2), 195–203. doi: 10.5194/hess-13-195-2009.
- Gouttevin, I., Turko, M., Branger, F., Leblois, E. and Sicart, J. (2017), 'Amélioration de la modélisation hydrologique distribuée en conditions naturelles dans les Alpes. Rapport Final. Action Neige 2016-2017', p. 58.
- Gray, D. and Prowse, T. (1993), 'Snow and floating ice. In Handbook of Hydrology, Maidment DR (ed). McGraw-Hill: New York; 71–758'.
- Grossi, G., Caronna, P. and Ranzi, R. (2013), 'Hydrologic vulnerability to climate change of the Mandrone glacier (Adamello-Presanella group, Italian Alps)', *Advances in Water Resources* **55**, 190–203. doi: <https://doi.org/10.1016/j.advwatres.2012.11.014>.

- Grossi, G., Lendvai, A., Peretti, G. and Ranzi, R. (2017), 'Snow precipitation measured by gauges: Systematic error estimation and data series correction in the central Italian Alps', *Water* **9**(7), 1–14. doi: 10.3390/w9070461.
- Guilbaud, S. (1997), 'Prévision quantitative des précipitations journalières par une méthode statistico-dynamique des recherche d'analogues - Application à des bassins du pourtour méditerranéen. Thèse de doctorat, INPG'.
- Gupta, H. V., Kling, H., Yilmaz, K. K. and Martinez, G. F. (2009), 'Decomposition of the mean squared error and NSE performance criteria: Implications for improving hydrological modelling', *Journal of Hydrology* **377**(1), 80–91. doi: <https://doi.org/10.1016/j.jhydrol.2009.08.003>.
- Gupta, H. V., Sorooshian, S. and Yapo, P. O. (1998), 'Toward improved calibration of hydrologic models: Multiple and noncommensurable measures of information', *Water Resources Research* **34**(4), 751–763. doi: 10.1029/97WR03495.
- Gurnell, A. M. (1993), 'How many reservoirs? An analysis of now recessions from a glacier basin.', *Journal of Glaciology* **39**(132), 409–414.
- Haerberli, W. (1995), 'Glacier Fluctuations and Climate Change Detection', *Geogr. Fis. Dinam. Quat.* **18**, 191–199.
- Haerberli, W. (2005), Mountain Glaciers in Global Climate-related Observing Systems, in R. M. Huber U.M., Bugmann H.K.M., ed., 'Global Change and Mountain Regions. Advances in Global Change Research, vol 23', Vol. 23, Springer, Dordrecht, pp. 169–175.
- Hagemann, S., Arpe, K. and Bengtsson, L. (2005), 'Validation of the hydrological cycle of ERA-40', Shinfield Park, Reading.
- Hall, D., Riggs, G. and Salomonson, V. (2004), 'Updated daily. MODIS/ Terra Snow Cover Daily L3 Global 500 m Grid V005.Boulder, Colorado USA: National Snow and Ice Data Center. Digital media'.
- Hamby, D. (1994), 'A review of techniques for parameter sensitivity analysis of environmental models', *Environ Monit Assess.* **32**(2), 135–154. doi: 10.1007/BF00547132.
- Harpold, A. A., Kaplan, M. L., Klos, P. Z., Link, T., McNamara, J. P., Rajagopal, S., Schumer, R. and Steele, C. M. (2017), 'Rain or snow: hydrologic processes, observations, prediction, and research needs', *Hydrology and Earth System Sciences* **21**(1), 1–22. doi: 10.5194/hess-21-1-2017.
- Helsel, D. R. and Hirsch, R. M. (1992), *Statistical Methods in Water Resources*, Elsevier.
- Henn, B., Clark, M. P., Kavetski, D. and Lundquist, J. D. (2015), 'Estimating mountain basin-mean precipitation from streamflow using Bayesian inference', *Water Resources Research* **51**(10), 8012–8033. doi: 10.1002/2014WR016736.
- Heynen, M., Pellicciotti, F. and Carenzo, M. (2013), 'Parameter sensitivity of a distributed enhanced temperature-index melt model', *Annals of Glaciology* **54**(63), 311–321. doi: 10.3189/2013AoG63A537.

- Hochenbaum, J., Vallis, O. and Kejariwal, A. (2017), ‘Automatic Anomaly Detection in the Cloud Via Statistical Learning’, *ArXiv e-prints* .
- Hock, R. (1999), ‘A distributed temperature-index ice- and snowmelt model including potential direct solar radiation’, *Journal of Glaciology* **45**(149), 101–111. doi: 10.1017/S0022143000003087.
- Hock, R. (2003), ‘Temperature index melt modelling in mountain areas’, *Journal of Hydrology* **282**(1), 104–115. doi: [https://doi.org/10.1016/S0022-1694\(03\)00257-9](https://doi.org/10.1016/S0022-1694(03)00257-9).
- Hock, R. and Noetzli, C. (1997), ‘Areal melt and discharge modelling of Storglaciären, Sweden’, *Annals of Glaciology* **24**, 211–216.
- Hoffman, E. and Gardner, R. (1983), ‘Evaluation of Uncertainties in Environmental Radiological Assessment Models’, in: Till, J.E.; Meyer, H.R. (eds) *Radiological Assessments: a Textbook on Environmental Dose Assessment*. Washington, DC: U.S. Nuclear Regulatory Commission; Report No. NUREG/CR-’.
- Hooke, R. L., Pohjola, V. A., Jansson, P. and Kohler, J. (1992), ‘Intra-seasonal changes in deformation profiles revealed by borehole studies, Storglaciären, Sweden’, *Journal of Glaciology* **38**(130), 348–358. doi: 10.3189/S0022143000002239.
- Hooke, R., Laumann, T. and Kohler, J. (1990), ‘Subglacial water pressures and the shape of subglacial conduits.’, *Journal of Glaciology* **36**(122), 67–71.
- Horton, P., Schaefli, B., Mezghani, A., Hingray, B. and Musy, A. (2006), ‘Assessment of climate-change impacts on alpine discharge regimes with climate model uncertainty’, *Hydrological Processes* **20**(10), 2091–2109. doi: 10.1002/hyp.6197.
- Hubbard, A., Blatter, H., Nienow, P., Mair, D. and Hubbard, B. . (1998), ‘Comparison of a three-dimensional model for glacier flow with field data from haut Glacier d’Arolla, Switzerland.’, *Journal of Glaciology* **44**(147), 368–378.
- Huffman, G., Bolvin, D., Braithwaite, D., Hsu, K., Joyce, R. and Xie, P. (2014), ‘Integrated multi-satellite retrievals for gpm (imerg), version 4.4. nasa’s precipitation processing center, accessed 31 march, 2015, <ftp://arthurhou.pps.eosdis.nasa.gov/gpmdata/>’.
- Huss, M. (2011), ‘Present and future contribution of glacier storage change to runoff from macroscale drainage basins in Europe’, *Water Resources Research* **47**(7). doi: 10.1029/2010WR010299.
- Huss, M. (2013), ‘Density assumptions for converting geodetic glacier volume change to mass change’, *The Cryosphere* **7**(3), 877–887. doi: 10.5194/tc-7-877-2013.
- Huss, M., Farinotti, D., Bauder, A. and Funk, M. (2008), ‘Modelling runoff from highly glacierized alpine drainage basins in a changing climate’, *Hydrological Processes* **22**(19), 3888–3902. doi: 10.1002/hyp.7055.
- Huss, M., Funk, M. and Ohmura, A. (2009), ‘Strong Alpine glacier melt in the 1940s due to enhanced solar radiation’, *Geophys. Res. Lett.* **36**(L23501), 1–5. doi: 10.1029/2009GL040789.
- Huss, M. and Hock, R. (2018), ‘Global-scale hydrological response to future glacier mass loss’, *Nature*

- Climate Change* **8**(2), 135–140. doi: 10.1038/s41558-017-0049-x.
- Huss, M., Joutet, G., Farinotti, D. and Baumer, A. (2010), ‘Future high-mountain hydrology: A new parameterization of glacier retreat’, *Hydrology and Earth System Sciences* **14**(5), 815–829. doi: 10.5194/hess-14-815-2010.
- Immerzeel, W. W., van Beek, L. P. H. and Bierkens, M. F. P. (2010), ‘Climate Change Will Affect the Asian Water Towers’, *Science* **328**(5984), 1382–1385. doi: 10.1126/science.1183188.
- Immerzeel, W. W., van Beek, L. P. H., Konz, M., Shrestha, A. B. and Bierkens, M. F. P. (2012), ‘Hydrological response to climate change in a glacierized catchment in the Himalayas’, *Climatic Change* **110**(3-4), 721–736. doi: 10.1007/s10584-011-0143-4.
- Immerzeel, W. W., Wanders, N., Lutz, A. F., Shea, J. M. and Bierkens, M. F. P. (2015), ‘Reconciling high-altitude precipitation in the upper Indus basin with glacier mass balances and runoff’, *Hydrol. Earth Syst. Sci.* **19**(11), 4673–4687. doi: 10.5194/hess-19-4673-2015.
- Innovation International (2011), ‘Environment Monitoring a changing climate. In Confronting the Pressures on Ecosystem Services. International Innovation. August 2011, 16–18. Available at www.research-europe.com/index.php/international-innovation/.’.
- International Organization for Standardization (2007a), ‘ISO 1088:2007. Hydrometry: Velocity-area methods using current-meters : collection and processing of data for determination of uncertainties in flow measurement. Geneva: International Organization for Standardization.’.
- International Organization for Standardization (2007b), ‘ISO 748:2007. Measurement of liquid flow in open channels using current-meters or floats. Geneva: International Organization for Standardization.’.
- Iqbal, M. (1983), ‘An Introduction to Solar Radiation’, p. 390.
- Isoard, S., McCallum, S. and Hain, B. (2009), ‘Vulnerability and adaptation to water scarcity in the European Alps’, *IOP Conference Series: Earth and Environmental Science* **6**(36), 362008.
- Isotta, F. A., Frei, C., Weingartner, V., Perčec Tadić, M., Lassègues, P., Rudolf, B., Pavan, V., Cacciamani, C., Antolini, G., Ratto, S. M., Munari, M., Micheletti, S., Bonati, V., Lussana, C., Ronchi, C., Panettieri, E., Marigo, G. and Vertačnik, G. (2013), ‘The climate of daily precipitation in the Alps: development and analysis of a high-resolution grid dataset from pan-Alpine rain-gauge data’, *International Journal of Climatology* **34**(5), 1657–1675. doi: 10.1002/joc.3794.
- Israelsen, C. (1967), ‘Reliability of can-type precipitation gage measurements, Tech. Rep. 2, pp 1-74, Utah Water Res. Lab., Utah State Univ., Logan’.
- Jabot, E. (2013), ‘Etude de la fonte nivale et des températures en vue de la prévision hydrologique : du ponctuel au spatial. Sciences de la Terre. Université de Grenoble, 2012. Français.’.
- Jamier, D. (1975), ‘Etude de la fissuration, de l’hydrologie et de la géochimie des eaux profondes des massifs de l’Arpille et du Mont Blanc’, *Tectonics. Université de Lausanne, French* .
- Jansson, P., Hock, R. and Schneider, T. (2003), ‘The concept of glacier storage: a review’, *Journal of*

- Hydrology* **282**(1), 116–129. doi: [https://doi.org/10.1016/S0022-1694\(03\)00258-0](https://doi.org/10.1016/S0022-1694(03)00258-0).
- Jansson, P., Kohler, J. and Pohjola, V. A. (1996), ‘Characteristics of basal ice at Engabreen, northern Norway’, *Annals of Glaciology* **22**, 114–120. doi: 10.3189/1996AoG22-1-114-120.
- Jarosch, A. H., Schoof, C. G. and Anslow, F. S. (2013), ‘Restoring mass conservation to shallow ice flow models over complex terrain’, *The Cryosphere* **7**(1), 229–240. doi: 10.5194/tc-7-229-2013.
- Johannesson, T. (1997), ‘The response of two Icelandic glaciers to climatic warming computed with a degree-day glacier mass-balance model coupled to a dynamic glacier model’, *Journal of Glaciology* **43**(144), 321–327.
- Jost, G., Moore, R. D., Menounos, B. and Wheate, R. (2012), ‘Quantifying the contribution of glacier runoff to streamflow in the upper Columbia River Basin, Canada’, *Hydrology and Earth System Sciences* **16**(3), 849–860. doi: 10.5194/hess-16-849-2012.
- Kaser, G., Großhauser, M. and Marzeion, B. (2010), ‘Contribution potential of glaciers to water availability in different climate regimes’, *Proceedings of the National Academy of Sciences* **107**(47), 20223–20227. doi: 10.1073/pnas.1008162107.
- Kendall, M. (1975), *Rank Correlation Methods*, Charles Griffin, London.
- Kendall, M. and Stuart, A. (1961), ‘The advanced theory of statistics’.
- Khoi, D. N. and Thom, V. T. (2015), ‘Parameter uncertainty analysis for simulating streamflow in a river catchment of Vietnam’, *Global Ecology and Conservation* **4**, 538–548. doi: <https://doi.org/10.1016/j.gecco.2015.10.007>.
- Khromova, T., Nosenko, G., Kutuzov, S., Muraviev, A. and Chernova, L. (2014), ‘Glacier area changes in Northern Eurasia. Environ’, *Environ. Res. Lett.* **9**(1), 015 003. doi: 10.1088/1748-9326/9/1/015003.
- Khromova, T., Osipova, G., Tsvetkov, D., Dyurgerov, M. and Barry, R. (2006), ‘Changes in glacier extent in the eastern Pamir, Central Asia, determined from historical data and ASTER imagery’, *Remote Sens. Environ.* **102**, 24.
- Kienzle, S. (2008), ‘A new temperature based method to separate rain and snow’, *Hydrol. Process* **22**, 2267–2274. doi: 10.1002/hyp.
- Kilchmann S. (2001), Typology of recent groundwaters from different aquifer environments based on geogenic tracer elements, PhD thesis, Ph.D. Thesis No. 2411. École polytechnique fédérale de Lausanne.
- Kirchner, J. W. (2009), ‘Catchments as simple dynamical systems: Catchment characterization, rainfall-runoff modeling, and doing hydrology backward’, *Water Resources Research* **45**(2), 1–34. doi: 10.1029/2008WR006912.
- Kirkpatrick, S., Gelatt, C. D. and Vecchi, M. P. (1983), ‘Optimization by Simulated Annealing’, *Science* **220**(4598), 671–680.
- Kleman, J. and Glasser, N. F. (2007), ‘The subglacial thermal organisation (STO) of ice sheets’,

- Quaternary Science Reviews* **26**(5), 585–597. doi: <https://doi.org/10.1016/j.quascirev.2006.12.010>.
- Klemeš, V. (1982), ‘Empirical and causal models in hydrology, in Scientific Basis of Water Resource Management, pp. 95-104. National Academy Press, Washington, D.C.’.
- Klemes, V. (1986), ‘Operational testing of hydrological simulation models’, *Hydrological Sciences Journal* **31**(1), 13–24. doi: 10.1080/02626668609491024.
- Koboltschnig, G., Schöner, W., Zappa, M., Kroisleitner, C. and Holzmann, H. (2008), ‘Runoff modelling of the glacierized Alpine Upper Salzach basin (Austria): multi-criteria result validation’, *Hydrological Processes* **22**(19), 3950–3964. doi: 10.1002/hyp.7112.
- Konzelmann, T., Calanca, P., Müller, G., Menzel, L. and Lang, H. (1997), ‘Energy Balance and Evapotranspiration in a High Mountain Area during Summer.’, *Journal of Applied Meteorology* **36**, 966–973. doi: 10.1175/1520-0450(1997)036<0966:EBAEIA>2.0.CO;2.
- Kuczera, G. and Mroczkowski, M. (1998), ‘Assessment of hydrologic parameter uncertainty and the worth of multiresponse data’, *Water Resources Research* **34**(6), 1481–1489. doi: 10.1029/98WR00496.
- Kuhn, M. (1989), ‘The response of the equilibrium line altitude to climatic fluctuations: theory and observations. in oerlemans j ed. *glacier fluctuations and climatic change. kluwer academic publishers, dordrecht*, 407–417’.
- Kurtyka, J. (1953), ‘Precipitation measurements study, Rep. Invest. 20, pp 1-178, State Water Surv. Div., Urbana, Ill.’.
- Lachapelle, E. (1962), ‘Assessing glacier mass budgets by reconnaissance aerial photography’. doi: 10.1017/S0022143000027593.
- Lang, M., Renard, B., Sauquet, E., Bois, P., Dupeyrat, A., Laurent, C., Mestre, O., Niel, H., Neppel, L. and Gailhard, J. (2006), *A national study on trends and variations of French floods and droughts*, IAHS Publ. 308. IAHS Press, Wallingford, UK.
- Larson, L. W. and Peck, E. L. (1974), ‘Accuracy of precipitation measurements for hydrologic modeling’, *Water Resources Research* **10**(4), 857–863. doi: 10.1029/WR010i004p00857.
- Leavesley, G., Lichty, R., Troutman, B. and Saindon, L. (1983), ‘Precipitation-Runoff Modeling System: User’s Manual. Water Resources Investigations Report 83 – 4238, US Geological Survey, Denver, Colorado.’.
- Lecourt, G. (2018), ‘Modélisation à bases physiques de l’hydrologie de l’Arve à Chamonix et application à la prévision des crues. Toulouse’, p. 207pp.
- Lefeuvre, P.-M. (2016), ‘Subglacial Processes and Subglacial Hydrology. University of Oslo, Norway’.
- Lefeuvre, P.-M., Jackson, M., Lappégard, G. and Hagen, J. O. (2015), ‘Interannual variability of glacier basal pressure from a 20 year record’, *Annals of Glaciology* **56**(70), 33–44. doi: 10.3189/2015AoG70A019.
- L’hôte, Y., Chevallier, P., Coudrain, A., Lejeune, Y. and Etchevers, P. (2005), ‘Relationship between

- precipitation phase and air temperature: comparison between the Bolivian Andes and the Swiss Alps', *Hydrological Sciences Journal* **50**(6), 988–887. doi: 10.1623/hysj.2005.50.6.989.
- Lindström, G. (1997), 'A Simple Automatic Calibration Routine for the HBV Model', *Hydrology Research* **28**(3), 153. doi: 10.2166/nh.1997.0009.
- Lins, H. F. and Slack, J. R. (1999), 'Streamflow trends in the United States', *Geophysical Research Letters* **26**(2), 227–230. doi: 10.1029/1998GL900291.
- Littmann, T. (2000), 'An empirical classification of weather types in the mediterranean basin and their interrelation with rainfall', *Theor. Appl. Climatol.* **66**, 161–171.
- Lliboutry, L. (1965), 'Traité de glaciologie. Tome II: Glaciers, variations du climat, sols gelés, Paris, Masson et Cie.'
- Lliboutry, L. (1974), 'Multivariate Statistical Analysis of Glacier Annual Balances', *Journal of Glaciology* **13**(69), 371–392. doi: 10.3189/S002214300023169.
- Loarie, S. R., Duffy, P. B., Hamilton, H., Asner, G. P., Field, C. B. and Ackerly, D. D. (2009), 'The velocity of climate change', *Nature* **462**, 1052.
- Machguth, H., Purves, R. S., Oerlemans, J., Hoelzle, M. and Paul, F. (2008), 'Exploring uncertainty in glacier mass balance modelling with Monte Carlo simulation', *The Cryosphere* **2**(2), 191–204. doi: 10.5194/tc-2-191-2008.
- Madsen, H. (2003), 'Parameter estimation in distributed hydrological catchment modelling using automatic calibration with multiple objectives', *Advances in Water Resources* **26**(2), 205–216. doi: 10.1016/S0309-1708(02)00092-1.
- Mandal, A., Ramanathan, A. and Angchuk, T. (2014), 'Assessment of Lahaul-Spiti (western Himalaya, India) Glaciers – an overview of mass balance and climate.', *J. Earth Sci. Climatic Change* **11**(2). doi: 10.4172/2157-7617.S11-003.
- Mann, H. B. (1945), 'Nonparametric Tests Against Trend', *Econometrica* **13**(3), 245–259.
- Maragno, D., Diolaiuti, G., D'agata, C., Mihalcea, C., Bocchiola, D., , E. B. J., Riccardi, A. and Smiraglia, C. (2009), 'New evidence from italy (adamello group, lombardy) for analysing the ongoing decline of alpine glaciers', *Geografia Fisica e Dinamica Quaternaria* **32**, 31 – 39.
- Maréchal, J. (1998), Les circulations d'eau dans les massifs cristallins alpins et leurs relations avec les ouvrages souterrains, PhD thesis, Ph.D. Thesis No. 1796. École polytechnique fédérale de Lausanne.
- Maréchal, J. (2000), 'Massif du Mont-Blanc : identification d'une structure hydrogéologique majeure', *La Houille Blanche - Revue internationale de l'eau* **6**, 78–86.
- Maréchal, J. (2012), 'Les tunnels alpins : observatoires de l'hydrogéologie des grands massifs montagneux', *La Houille Blanche, Société Hydrotechnique de France* **1**, 44–50. doi: 10.1051/lhb/2012007.
- Martinec, J. and Rango, A. (1986), 'Parameter values for snowmelt runoff modelling', *Journal of Hydrology* **84**(3), 197 – 219. doi: 10.1016/0022-1694(86)90123-X.

- Marzeion, B., Jarosch, A. H. and Hofer, M. (2012), 'Past and future sea-level change from the surface mass balance of glaciers', *The Cryosphere* **6**(6), 1295–1322. doi: 10.5194/tc-6-1295-2012.
- Meier, M. F. (1980), 'Remote sensing of snow and ice / La télédétection de neige et de glace', *Hydrological Sciences Bulletin* **25**(3), 307–330. doi: 10.1080/02626668009491937.
- Moreau, L. (1995), Comportement d'un glacier tempéré sur son lit rocheux, thesis, University of Grenoble, Institut de Géographie Alpine, Grenoble.
- Morton, F. (1983), 'Operational estimates of areal evapotranspiration and their significance to the science and practice of hydrology', *Journal of Hydrology* **66**(1), 1–76. doi: [https://doi.org/10.1016/0022-1694\(83\)90177-4](https://doi.org/10.1016/0022-1694(83)90177-4).
- Motiee, H. and McBean, E. (2009), 'An assessment of long-term trends in hydrologic components and implications for water levels in Lake Superior', *Hydrology Research* **40**(6), 564. doi: 10.2166/nh.2009.061.
- Mottier, J. (1970), 'L'aménagement hydro-électrique franco-suisse d'Emosson', *Bulletin technique de la Suisse romande* pp. 249–266.
- Naz, B. S., Frans, C. D., Clarke, G. K. C., Burns, P. and Lettenmaier, D. P. (2014), 'Modeling the effect of glacier recession on streamflow response using a coupled glacio-hydrological model', *Hydrology and Earth System Sciences* **18**(2), 787–802. doi: 10.5194/hess-18-787-2014.
- Noetzli, C. (1996), 'Die Simulation des Abflusses am Storglaciären, Nordschweden mit einem Linearspeichermodell. (M.Sc. thesis, Eidgenössische Technische Hochschule, Zürich. Geographisches Institut.)'.
- Nye, J. F. (1976), 'Water Flow in Glaciers: Jökulhlaups, Tunnels and Veins', *Journal of Glaciology* **17**(76), 181–207. doi: 10.3189/S002214300001354X.
- Obled, C., Bontron, G. and Garçon, R. (2002), 'Quantitative precipitation forecasts: a statistical adaptation of model outputs through an analogues sorting approach', *Atmospheric Research* **63**(3), 303–324. doi: [https://doi.org/10.1016/S0169-8095\(02\)00038-8](https://doi.org/10.1016/S0169-8095(02)00038-8).
- Obled, C. and Good, W. (1980), 'Recent developments in avalanche forecasting by statistical techniques : a methodological review and some applications to the parsenn area (davos-switzerland)', *Journal of Glaciology* **92**, 315–346.
- Obled, C. and Rosse, B. (1977), 'Mathematical models of a melting snowpack at an index plot', *Journal of Hydrology* **32**(1), 139 – 163. doi: 0.1016/0022-1694(77)90123-8.
- Oerlemans, J. (1986), 'Glaciers as indicators of a carbon dioxide warming', *Nature* **320**(6063), 607–609. doi: 10.1038/320607a0.
- Oerlemans, J. (2001), 'Glaciers and climate change. AA Balkema, Lisse'.
- Oerlemans, J. and Fortuin, J. P. F. (1992), 'Sensitivity of Glaciers and Small Ice Caps to Greenhouse Warming', *Science* **258**(5079), 115–117. doi: 10.1126/science.258.5079.115.
- Oerter, H., Baker, D., Moser, H. and Reinwarth, O. (1981), 'Glacial-Hydrological Investigations at the Vernagtferner Glacier as a Basis for a Discharge Model', *Hydrology Research* **12**(4-5), 335. doi:

- 10.2166/nh.1981.0027.
- Ohmura, A., Kasser, P. and Funk, M. (1992), 'Climate at the Equilibrium Line of Glaciers', *Journal of Glaciology* **38**(130), 397–411. doi: 10.3189/S0022143000002276.
- Oke, T. (1987), 'Boundary Layer Climates. ISBN 0-415-04319-0'.
- Østrem, G. (1975), 'ERTS data in glaciology – an effort to monitor glacier mass balance from satellite imagery', *J. Glaciol.* **15**(73), 403–415.
- Oudin, L., Hervieu, F., Michel, C., Perrin, C., Andréassian, V., Anctil, F. and Loumagne, C. (2005), 'Which potential evapotranspiration input for a lumped rainfall-runoff model? Part 2 - Towards a simple and efficient potential evapotranspiration model for rainfall-runoff modelling', *Journal of Hydrology* **303**(1-4), 290–306. doi: 10.1016/j.jhydrol.2004.08.026.
- Paquet, J., Gailhard, J. and Garçon, R. (2006), 'Évolution de la méthode du gradex : approche par type de temps et modélisation hydrologique', *La Houille Blanche* **5**, 80–90.
- Parajka, J. and Blöschl, G. (2008a), 'Spatio-temporal combination of MODIS images – potential for snow cover mapping', *Water Resources Research* **44**(3). doi: 10.1029/2007WR006204.
- Parajka, J. and Blöschl, G. (2008b), 'The value of MODIS snow cover data in validating and calibrating conceptual hydrologic models', *Journal of Hydrology* **358**(3), 240–258. doi: <https://doi.org/10.1016/j.jhydrol.2008.06.006>.
- Parajka, J. and Blöschl, G. (2008c), 'The value of MODIS snow cover data in validating and calibrating conceptual hydrologic models', *Journal of Hydrology* **358**(3), 240–258. doi: <https://doi.org/10.1016/j.jhydrol.2008.06.006>.
- Paterson, W. (1994a), *The physics of glaciers*, 3th edn, Butterworth-Heinemann, Oxford.
- Paterson, W. (1994b), *The physics of glaciers*, 3th edn, Butterworth-Heinemann, Oxford.
- Paul, F. and Haeberli, W. (2008), 'Spatial variability of glacier elevation changes in the Swiss Alps obtained from two digital elevation models', *Geophysical Research Letters* **35**(21). doi: 10.1029/2008GL034718.
- Pechlivanidis, I. G., Jackson, B. M., McIntyre, N. R. and Wheeler, H. S. (2011), 'Catchment scale hydrological modelling: a review of model types, calibration approaches and uncertainty analysis methods in the context of recent developments in technology and applications', *Global Nest Journal* **13**(3), 193–214.
- Pekárová, P., Miklánek, P. and Pekár, J. (2003), 'Spatial and temporal runoff oscillation analysis of the main rivers of the world during the 19th?20th centuries', *Journal of Hydrology* **274**, 62–79. doi: 10.1016/S0022-1694(02)00397-9.
- Pellicciotti, F., Bauder, A. and Parola, M. (2010), 'Effect of glaciers on streamflow trends in the Swiss Alps', *Water Resources Research* **46**(W10522), 1–16. doi: 10.1029/2009WR009039.
- Pellicciotti, F., Brock, B., Strasser, U., Burlando, P., Funk, M. and Corripio, J. (2005), 'An enhanced temperature-index glacier melt model including the shortwave radiation balance: Develop-

- ment and testing for Haut Glacier d'Arolla, Switzerland', *Journal of Glaciology* **51**(175), 573–587. doi: 10.3189/172756505781829124.
- Pellicciotti, F., Burlando, P. and Vliet, K. (2007), *Recent trends in precipitation and streamflow in the Aconcagua River basin, central Chile*, number 318 in 'IAHS publication', IAHS Press, Centre for Ecology and Hydrology, pp. 17–38.
- Pipes, A. and Quick, M. (1977), 'UBC Watershed Model Users Guide. Department of Civil Engineering, University of British Columbia: Vancouver, British Columbia, Canada.'
- Quintana-Seguí, P., Le Moigne, P., Durand, Y., Martin, E., Habets, F., Baillon, M., Canellas, C., Franchisteguy, L. and Morel, S. (2008), 'Analysis of near-surface atmospheric variables: Validation of the SAFRAN analysis over France', *Journal of Applied Meteorology and Climatology* **47**(1), 92–107. doi: 10.1175/2007JAMC1636.1.
- Rabatel, A., Bermejo, A., Loarte, E., Soruco, A., Gomez, J., Leonardini, G., Vincent, C. and Sicart, J. E. (2012), 'Can the snowline be used as an indicator of the equilibrium line and mass balance for glaciers in the outer tropics?', *Journal of Glaciology* **58**(212), 1027–1036. doi: 10.3189/2012JoG12J027.
- Rabatel, A., Dedieu, J.-P. and Vincent, C. (2005), 'Using remote-sensing data to determine equilibrium-line altitude and mass-balance time series: validation on three French glaciers, 1994–2002', *Journal of Glaciology* **51**(175), 539–546. doi: 10.3189/172756505781829106.
- Rabatel, A., Dedieu, J. P. and Vincent, C. (2016), 'Spatio-temporal changes in glacier-wide mass balance quantified by optical remote sensing on 30 glaciers in the French Alps for the period 1983–2014', *Journal of Glaciology* **62**(236), 1153–1166. doi: 10.1017/jog.2016.113.
- Rabatel, A., Letréguilly, A., Dedieu, J.-P. and Eckert, N. (2013), 'Changes in glacier equilibrium-line altitude in the western Alps from 1984 to 2010: Evaluation by remote sensing and modeling of the morpho-topographic and climate controls', *Cryosphere* **7**(5), 1455–1471. doi: 10.5194/tc-7-1455-2013.
- Radić, V. and Hock, R. (2014), 'Glaciers in the Earth's Hydrological Cycle: Assessments of Glacier Mass and Runoff Changes on Global and Regional Scales', *Surveys in Geophysics* **35**(3), 813–837. doi: 10.1007/s10712-013-9262-y.
- Ragetti, S. and Pellicciotti, F. (2012), 'Calibration of a physically based, spatially distributed hydrological model in a glacierized basin: On the use of knowledge from glaciometeorological processes to constrain model parameters', *Water Resources Research* **48**(3). doi: 10.1029/2011WR010559.
- Ralph, F. M., Rauber, R. M., Jewett, B. F., Kingsmill, D. E., Pisano, P., Pugnèr, P., Rasmussen, R. M., Reynolds, D. W., Schlatter, T. W., Stewart, R. E., Tracton, S. and Waldstreicher, J. S. (2005), 'Improving Short-Term (0–48 h) Cool-Season Quantitative Precipitation Forecasting: Recommendations from a USWRP Workshop', *Bulletin of the American Meteorological Society* **86**(11), 1619–1632.
- Ranzi, R., Grossi, G., Gitti, A. and Taschner, S. (2010), 'Energy and mass balance of the mandrone glacier (Adamello, Central Alps)', *Geografia Fisica e Dinamica Quaternaria* **33**(1), 45–60.

- Rasmussen, R., Baker, B., Kochendorfer, J., Meyers, T., Landolt, S., Fischer, A. P., Black, J., Thériault, J. M., Kucera, P., Gochis, D., Smith, C., Nitu, R., Hall, M., Ikeda, K. and Gutmann, E. (2012), ‘How Well Are We Measuring Snow: The NOAA/FAA/NCAR Winter Precipitation Test Bed’, *Bulletin of the American Meteorological Society* **93**(6), 811–829. doi: 10.1175/BAMS-D-11-00052.1.
- Renard, B. (2006), *Détection et prise en compte d’éventuels impacts du changement climatique sur les extrêmes hydrologiques en France*, Ph.D Thesis Thesis, INPG/Cemagref, Lyon, France, 364 pp.
- Renard, B., Lang, M., Bois, P., Dupeyrat, A., Mestre, O., Niel, H., Sauquet, E., Prudhomme, C., Parey, S., Paquet, E., Neppel, L. and Gailhard, J. (2008), ‘Regional methods for trend detection: Assessing field significance and regional consistency’, *Water Resources Research* **44**(8). doi: 10.1029/2007WR006268.
- Réveillet, M., Six, D., Vincent, C., Rabatel, A., Dumont, M., Lafaysse, M., Morin, S., Vionnet, V. and Litt, M. (2018), ‘Relative performance of empirical and physical models in assessing the seasonal and annual glacier surface mass balance of Saint-Sorlin Glacier (French Alps)’, *The Cryosphere* **12**(4), 1367–1386. doi: 10.5194/tc-12-1367-2018.
- Réveillet, M., Vincent, C., Six, D. and Rabatel, A. (2017), ‘Which empirical model is best suited to simulate glacier mass balances?’, *Journal of Glaciology* **63**(237), 39–54. doi: 10.1017/jog.2016.110.
- Revuelto, J., Lecourt, G., Lafaysse, M., Zin, I., Charrois, L., Vionnet, V., Dumont, M., Rabatel, A., Six, D., Condom, T., Morin, S., Viani, A. and Sirguey, P. (2018), ‘Multi-Criteria Evaluation of Snowpack Simulations in Complex Alpine Terrain Using Satellite and In Situ Observations’, *Remote Sensing* **10**(8). doi: 10.3390/rs10081171.
- Reynaud, L. (1973), ‘Étude de la dynamique des séracs du Géant (Massif du Mont-Blanc). (PhD thesis, Université Scientifique et Médicale, Grenoble)’.
- Rich, P. M., Dubayah, R., Hetrick, W. A. and Saving, S. C. (1994), ‘Using Viewshed Models to Calculate Intercepted Solar Radiation: Applications in Ecology’, *American Society for Photogrammetry and Remote Sensing Technical Papers* **1**, 524–529.
- Riggs, G., Hall, D. and Salomonson, V. (2009), ‘MODIS Snow Products User Guide to Collection 5’, p. 80.
- Rohrer, M. (1989), ‘Determination of the transition air temperature from snow to rain and intensity of precipitation. In IAHS/WMO/ETH International Workshop of Precipitation Measurement, Sevruck B (ed). St. Moritz, Switzerland; 475–482.’.
- Rolland, Y., Cox, S., Boullier, A. M., Pennacchioni, G. and Mancktelow, N. (2003), ‘Rare earth and trace element mobility in mid-crustal shear zones: Insights from the Mont Blanc Massif (Western Alps)’, *Earth and Planetary Science Letters* **214**(1-2), 203–219. doi: 10.1016/S0012-821X(03)00372-8.
- Ronen, Y. (1988), ‘The Role of Uncertainties. In: Uncertainty Analysis, Y. Ronen (ed.). CRC Press’.
- Rossi, M. and Rolland, Y. (2014), ‘Stable isotope and Ar/Ar evidence of prolonged multiscale fluid flow during exhumation of orogenic crust: Example from the mont blanc and Aar Massifs (NW Alps)’,

- Tectonics* **33**(9), 1681–1709. doi: 10.1002/2013TC003438.
- Rossi, M., Rolland, Y., Vidal, O. and Cox, S. (2005), ‘Geochemical variations and element transfer during shear-zone development and related épi-syenites at middle crust depths: Insights from the Mont Blanc granite (French-Italian Alps)’, *High Strain Zones: Structure and Physical Properties* pp. 373–396.
- Röthlisberger, H. (1972), ‘Water Pressure in Intra- and Subglacial Channels’, *Journal of Glaciology* **11**(62), 177–203. doi: 10.3189/S0022143000022188.
- Ryser, C., Lüthi, M. P., Andrews, L. C., Hoffman, M. J., Catania, G. A., Hawley, R. L., Neumann, T. A. and Kristensen, S. S. (2014), ‘Sustained high basal motion of the Greenland ice sheet revealed by borehole deformation’, *Journal of Glaciology* **60**(222), 647–660. doi: 10.3189/2014JoG13J196.
- Salomonson, V. and Appel, I. (2004), ‘Estimating fractional snow cover from MODIS using the normalized difference snow index’, *Remote Sens. Environ.* **89**(3), 351–360. doi: 10.1016/j.rse.2003.10.016.
- Schaeffli, B., Hingray, B. and Musy, A. (2007), ‘Climate change and hydropower production in the Swiss Alps: quantification of potential impacts and related modelling uncertainties’, *Hydrology and Earth System Sciences* **11**(3), 1191–1205. doi: 10.5194/hess-11-1191-2007.
- Schaeffli, B., Hingray, B., Niggli, M. and Musy, A. (2005), ‘A conceptual glacio-hydrological model for high mountainous catchments’, *Hydrology and Earth System Sciences Discussions* **2**(1), 73–117. doi: 10.5194/hessd-2-73-2005.
- Schaeffli, B., Manso, P., Fischer, M., Huss, M. and Farinotti, D. (2019), ‘The role of glacier retreat for Swiss hydropower production’, *Renewable Energy* **132**, 615–627. doi: <https://doi.org/10.1016/j.renene.2018.07.104>.
- Schoof, C., Rada, C. A., Wilson, N. J., Flowers, G. E. and Haseloff, M. (2014), ‘Oscillatory subglacial drainage in the absence of surface melt’, *The Cryosphere* **8**(3), 959–976. doi: 10.5194/tc-8-959-2014.
- Seibert, J. (2000), ‘Multi-criteria calibration of a conceptual runoff model using a genetic algorithm’, *Hydrol. Earth Syst. Sci.* **4**(2), 215–224. doi: 10.5194/hess-4-215-2000.
- Seity, Y., Brousseau, P., Malardel, S., Hello, G., Bèrnard, P., Bouttier, F., Lac, C. and Masson, V. (2011), ‘The arôme-france convective-scale operational model’, *Monthly Weather Review* **139**(3), 976–991. doi: 10.1175/2010MWR3425.1.
- Sen, P. K. (1968), ‘Estimates of the Regression Coefficient Based on Kendall’s Tau’, *Journal of the American Statistical Association* **63**(324), 1379–1389. doi: 10.1080/01621459.1968.10480934.
- Sevruk, B. (1983), ‘Correction of measured precipitation in the Alps using the water equivalent of new snow’, *Nordic Hydrology* **1**, 49–58.
- Sevruk, B. (1987), ‘Point precipitation measurements: why are they not corrected’, *IAHS Publication* (164), 477–486.
- Shoemaker, E. (1986), ‘Subglacial hydrology for an ice sheet resting on a deformable aquifer’, *J. Glaciol.* **32**(110), 20–30.

- Sieck, L. C., Burges, S. J. and Steiner, M. (2007), 'Challenges in obtaining reliable measurements of point rainfall', *Water Resources Research* **43**(1). doi: 10.1029/2005WR004519.
- Six, D. and Vincent, C. (2014), 'Sensitivity of mass balance and equilibrium-line altitude to climate change in the French Alps', *Journal of Glaciology* **60**(223), 867–878. doi: 10.3189/2014JoG14J014.
- Six, D., Wagnon, P., Sicart, J. E. and Vincent, C. (2009), 'Meteorological controls on snow and ice ablation for two contrasting months on Glacier de Saint-Sorlin, France', *Annals of Glaciology* **50**(50), 66–72. doi: 10.3189/172756409787769537.
- Sobol', I. (1994), 'A Primer for the Monte Carlo Method. CRC Press'.
- Strahler, A. (1952), 'Hypsometric (area-altitude) analysis of erosional topography', *Geologic Soc. Am Bull* **63**, 1117–1141.
- Szu, H. and Hartley, R. (1987), 'Fast simulated annealing', *Physics Letters A* **122**(3), 157–162. doi: [https://doi.org/10.1016/0375-9601\(87\)90796-1](https://doi.org/10.1016/0375-9601(87)90796-1).
- Tachikawa, T., Kaku, M., Iwasaki, A., Gesch, D., Oimoen, M., Zhang, Z., Danielson, J., Krieger, T., Curtis, B., Haase, J., Abrams, M., Crippen, R. and Carabajal, C. (2011), 'ASTER Global Digital Elevation Model Version 2 — Summary of validation results. METI & NASA', p. 26.
- Teweles, S. and Wobus, H. B. (1954), 'Verification of Prognostic Charts', *Bulletin of the American Meteorological Society* **35**(10), 455–463.
- Theil, H. (1950), *A rank-invariant method of linear and polynomial regression analysis. I, II, III*, Nederl. Akad. Wetensch., Proc.53: 386–392, 521–525, 1397–1412.
- Thibert, E., Blanc, R., Vincent, C. and Eckert, N. (2008), 'Glaciological and volumetric mass-balance measurements: Error analysis over 51 years for Glacier de Sarennes, French Alps', *Journal of Glaciology* **54**(186), 522–532. doi: 10.3189/002214308785837093.
- Thirel, G., Salamon, P., Burek, P. and Kalas, M. (2013), 'Assimilation of MODIS Snow Cover Area Data in a Distributed Hydrological Model Using the Particle Filter', *Remote Sensing* **5**(11), 5825–5850. doi: 10.3390/rs5115825.
- Trenberth, K. E. (1984), 'Some Effects of Finite Sample Size and Persistence on Meteorological Statistics. Part I: Autocorrelations', *Monthly Weather Review* **112**(12), 2359–2368. doi: 10.1175/1520-0493(1984)112<2359:SEOFSS>2.0.CO;2.
- Valéry, A., Andréassian, V. and Perrin, C. (2014), 'As simple as possible but not simpler': What is useful in a temperature-based snow-accounting routine? Part 1 - Comparison of six snow accounting routines on 380 catchments', *Journal of Hydrology* **517**, 1166–1175. doi: 10.1016/j.jhydrol.2014.04.059.
- Vallot, J. (1905), 'Annales de l'Observatoire météorologique, physique et glaciaire du Mont Blanc (altitude 4,358 mètres). Tome I à VI. G Steinheil, Paris'.
- Vaughan, D. G., Comiso, J. C., Allison, I., Carrasco, J., Kaser, G., Kwok, R., Mote, P., Murray, T., Paul, F., Ren, J., Rignot, E., Solomina, O., Steffen, K. and Zhang, T. (2013), *Observations: Cryosphere*, Cambridge University Press, Cambridge, United Kingdom and New York, NY, USA,

- book section 4, pp. 317–382. doi: 10.1017/CBO9781107415324.012.
- Verbunt, M., Gurtz, J., Jasper, K., Lang, H., Warmerdam, P. and Zappa, M. (2003), ‘The hydrological role of snow and glaciers in alpine river basins and their distributed modeling’, *Journal of Hydrology* **282**(1), 36–55. doi: [https://doi.org/10.1016/S0022-1694\(03\)00251-8](https://doi.org/10.1016/S0022-1694(03)00251-8).
- Verfaillie, D., Déqué, M., Morin, S. and Lafaysse, M. (2017), ‘The method ADAMONT v1.0 for statistical adjustment of climate projections applicable to energy balance land surface models’, *Geoscientific Model Development* **10**(11), 4257–4283. doi: 10.5194/gmd-10-4257-2017.
- Viani, A., Condom, T., Vincent, C., A, R., Bacchi, B., Sicart, J. E., Revuelto, J., Six, D. and Zin, I. (2018), ‘Glacier-wide summer surface mass-balance calculation: hydrological balance applied to the Argentière and Mer de Glace drainage basins (Mont Blanc)’, *Journal of Glaciology* **64**(243), 119–131. doi: 10.1017/jog.2018.7.
- Vincent, A., Violette, S. and Aðalgeirsdóttir, G. (2018), ‘Groundwater in catchments headed by temperate glaciers: A review’, *Earth-Science Reviews* **188**, 59–76. doi: 10.1016/j.earscirev.2018.10.017.
- Vincent, C. (2002), ‘Influence of climate change over the 20th Century on four French glacier mass balances’, *Journal of Geophysical Research Atmospheres* **107**(19). doi: 10.1029/2001JD000832.
- Vincent, C., Fischer, A., Mayer, C., Bauder, A., Galos S, P., Funk, M., Thibert, E., Six, D., Braun, L. and M., H. (2017), ‘Common climatic signal from glaciers in the European Alps over the last 50 years’, *Geophysical Research Letters* **44**(3), 1376–1383. doi: 10.1002/2016GL072094.
- Vincent, C., Harter, M., Gilbert, A., Berthier, E. and Six, D. (2014), ‘Future fluctuations of Mer de Glace, French Alps, assessed using a parameterized model calibrated with past thickness changes’, *Annals of Glaciology* **55**(66), 15–24. doi: 10.3189/2014AoG66A050.
- Vincent, C., Kappenberger, G., Valla, F., Bauder, A., Funk, M. and Le Meur, E. (2004), ‘Ice ablation as evidence of climate change in the Alps over the 20th century’, *Journal of Geophysical Research: Atmospheres* **109**(D10). doi: 10.1029/2003JD003857.
- Vincent, C., Le Meur, E., Six, D. and Funk, M. (2005), ‘Solving the paradox of the end of the Little Ice Age in the Alps’, *Geophysical Research Letters* **32**(9), 1–4. doi: 10.1029/2005GL022552.
- Vincent, C. and Moreau, L. (2016), ‘Sliding velocity fluctuations and subglacial hydrology over the last two decades on Argentière glacier, Mont Blanc area’, *Journal of Glaciology* **62**(June), 1–11. doi: 10.1017/jog.2016.35.
- Vincent, C., Soruco, A., Azam, M. F., Basantes-Serrano, R., Jackson, M., Kjollmoen, B., Thibert, E., Wagnon, P., Six, D., Rabatel, A., Ramanathan, A., Berthier, E., Cusicanqui, D., Vincent, P. and Mandal, A. (2018a), ‘A Nonlinear Statistical Model for Extracting a Climatic Signal From Glacier Mass Balance Measurements’, *Journal of Geophysical Research: Earth Surface* **123**(9), 2228–2242. doi: 10.1029/2018JF004702.
- Vincent, C., Soruco, A., Six, D. and Meur, E. L. E. (2009), ‘Glacier thickening and decay analysis from 50 years of glaciological observations performed on Glacier d’Argentière, Mont Blanc area, France’, *Annals of Glaciology* **50**(50), 73–79. doi: 10.3189/172756409787769500.

- Vionnet, V., Dombrowski-Etchevers, I., Lafaysse, M., Quéno, L., Seity, Y. and Bazile, E. (2016), 'Numerical Weather Forecasts at Kilometer Scale in the French Alps: Evaluation and Application for Snowpack Modeling', *Journal of Hydrometeorology* **17**(10), 2591–2614. doi: 10.1175/JHM-D-15-0241.1.
- Vivian, R. (1975), 'Les glaciers des Alpes occidentales, étude géographique'.
- Viviroli, D., Archer, D. R., Buytaert, W., Fowler, H. J., Greenwood, G. B., Hamlet, A. F., Huang, Y., Koboltschnig, G., Litaor, M. I., Lopez-Moreno, J. I., Lorentz, S., Schodler, B., Schreier, H., Schwaiger, K., Vuille, M. and Woods, R. (2011), 'Climate change and mountain water resources: Overview and recommendations for research, management and policy', *Hydrology and Earth System Sciences* **15**(2), 471–504. doi: 10.5194/hess-15-471-2011.
- Viviroli, D., Dürr, H. H., Messerli, B., Meybeck, M. and Weingartner, R. (2007), 'Mountains of the world, water towers for humanity: Typology, mapping, and global significance', *Water Resources Research* **43**(7), 1–13. doi: 10.1029/2006WR005653.
- Viviroli, D. and Weingartner, R. (2004), 'The hydrological significance of mountains: from regional to global scale', *Hydrology and Earth System Sciences* **8**(6), 1017–1030. doi: 10.5194/hess-8-1017-2004.
- Von Storch, H. (1995), *Misuses of Statistical Analysis in Climate Research*, Springer, Berlin, Heidelberg.
- Walder, J. S. (1986), 'Hydraulics of Subglacial Cavities', *Journal of Glaciology* **32**(112), 439–445. doi: 10.3189/S0022143000012156.
- Weber, M., Braun, L., Mauser, W. and Prasch, M. (2010), 'Contribution of rain, snow- and icemelt in the Upper Danube discharge today and in the future', *Geografia Fisica e Dinamica Quaternaria* **33**(2), 221–230.
- Weertman, J. (1972), 'General theory of water flow at the base of a glacier or ice sheet', *Reviews of Geophysics* **10**(1), 287–333. doi: 10.1029/RG010i001p00287.
- Wigmosta, M. S., Vail, L. W. and Lettenmaier, D. P. (1994), 'A distributed hydrology-vegetation model for complex terrain', *Water Resources Research* **30**(6), 1665–1679. doi: 10.1029/94WR00436.
- WMO (2010), Manual on stream gauging. Vol. I: Fieldwork. WMO-No. 1044, World Meteorological Organization, Geneva, Technical report.
- World Meteorological Organisation (1986), *Intercomparison of models of snowmelt runoff*, WMO ; no. 646., Secretariat of the World Meteorological Organization, Geneva, Switzerland.
- Xiang, Y., Gubian, S., Suomela, B. and Hoeng, J. (2012), 'Generalized Simulated Annealing for Global Optimization : The GenSA Package', *The R Journal* **5**, 13–28.
- Young, G. J. (1981), 'The Mass Balance of Peyto Glacier, Alberta, Canada, 1965 To 1978', *Arctic and Alpine Research* **13**(3), 307–318. doi: 10.1080/00040851.1981.12004251.
- Yue, S., Pilon, P., Phinney, B. and Cavadias, G. (2002), 'The influence of autocorrelation on the ability to detect trend in hydrological series', *Hydrological Processes* **16**(9), 1807–1829. doi: 10.1002/hyp.1095.

- Zemp, M., Hoelzle, M. and Haeberli, W. (2009), ‘Six decades of glacier mass-balance observations: A review of the worldwide monitoring network’, *Annals of Glaciology* **50**(50), 101–111. doi: 10.3189/172756409787769591.
- Zhang, G., Kang, S., Cuo, L. and Qu, B. (2016), ‘Modeling hydrological process in a glacier basin on the central Tibetan Plateau with a distributed hydrology soil vegetation model’, *Journal of Geophysical Research: Atmospheres* **121**(16), 9521–9539. doi: 10.1002/2016JD025434.
- Zhang, X., Harvey K, D., Hogg W, D. and Yuzyk Ted, R. (2001), ‘Trends in Canadian streamflow’, *Water Resources Research* **37**(4), 987–998. doi: 10.1029/2000WR900357.
- Şorman, A. A., Şensoy, A., Tekeli, A. E., Şorman, A. Ü. and Akyürek, Z. (2009), ‘Modelling and forecasting snowmelt runoff process using the HBV model in the eastern part of Turkey’, *Hydrological Processes* **23**(7), 1031–1040. doi: 10.1002/hyp.7204.

Personal Bibliography

Under review

Viani A, Condom T, Rabatel A, Panthou G, Sicart JE, Gouttevin I and Ranzi R (September 2018). Characterization of the current and future glacier influence on the discharge seasonal cycle of five nested catchments in the French Alps, *Journal of Hydrology* (Under revision, HYDROL29345).

Published in international journals

Viani A, Condom T, Vincent C, Rabatel A, Bacchi B, Sicart JE, Revuelto J, Six D and Zin I (2018). Glacier- wide summer surface mass balance calculation: hydrological balance applied to the Argentière and Mer de Glace drainage basins (Mont Blanc). *Journal of Glaciology*, 1, 1–13 (doi: 10.1017/jog.2018.7)

Condom T, Dumont M, Mourre L, Sicart JE, Rabatel A, **Viani A** and Surco A (2018). A low-cost albedometer for snow and ice measurements – Theoretical results and application on a tropical mountain in Bolivia. *J. Geosci. Instrum. Method. Data Syst.*, 7, 169–178 (doi: 10.5194/gi-7-169- 2018)

Revuelto J, Lecourt G, Lafaysse M, Zin I, Charrois L, Vionnet V, Dumont M, Rabatel A, Six D, Condom T, Morin S, **Viani A** and Sirguey P (2018). Multi-Criteria Evaluation of Snowpack Simulations in Complex Alpine Terrain Using Satellite and In Situ Observations. *Remote Sensing*, 10 (8), 1171 (doi: 10.3390/rs10081171)

Other reports

Condom T, Coulaud C, Esteves M, Laarman O, Lafaysse M, Lebel T, Lecourt G, Rabatel A, Revuelto J, **Viani A** and Vincent C (2018). Programme de recherche sur la prévision des crues de l'Arve à Chamonix, Rapport final du projet, 57 pp.

Condom T, Coulaud C, Esteves M, Laarman O, Lafaysse M, Lebel T, Lecourt G, Rabatel A, Revuelto J, **Viani A** and Vincent C (2017). Programme de recherche sur la prévision des crues de l'Arve à Chamonix, Rapport annuel n°3, 39 pp.

Curriculum Vitae

Alessandra Viani, born on April 5, 1990, in Brescia (Italy).

Education

- 2004–2009 Scientific high school degree
- 2009–2012 Bachelor’s Degree in Civil and Environmental Engineering, University of Brescia (Italy)
- 2012–2015 Master Degree in Civil and Environmental Engineering, University of Brescia (Italy)
- 2015 – Nowadays PhD, University of Grenoble Alpes (France) and University of Brescia (Italy)

Research experience

- 2015–2014 Internship at l’Institut des Géosciences de l’Environnement (IGE), Grenoble (France) (6 months)
- 2016 Teaching assistant – Hydraulic structures course, University of Brescia (Italy)

Field Campaigns

- 2017 ; 2018 French Alps. Metereological data collection
- September 2018 French Alps. Tournée IGS Western Alps

Languages

Italian, French, English

Awards

- 2017 Winner of the research grant issued by the French embassy in Italy; 4.6 k€
- 2018 Research grant for the participation in the ‘Training School on Snow Observation and Data Assimilation’ at Bormio (IT) organised by the COST Action ES1404

International conferences

- 03.2016 SHF - Journées SHF Glaciologie Nivologie Hydrologie de Montagne, Greno-

- ble, France (Oral)
- 04.2016 EGU General Assembly, Vienna, Austria (Oral)
- 04.2017 EGU General Assembly, Vienna, Austria (Oral)
- 03.2018 AGM - 22nd Alpine Glaciology meeting, Chamonix, France (Poster)
- 04.2018 EGU General Assembly, Vienna, Austria (Poster)

DICHIARAZIONE DI CONFORMITÀ DELLE TESI PER IL CONSEGUIMENTO DEL TITOLO DI DOTTORE DI RICERCA

(DICHIARAZIONE SOSTITUTIVA DI ATTO NOTORIO E DI CERTIFICAZIONE)
(artt. 46-47 del D.P.R. 445 del 28.12.00 e relative modifiche)

La sottoscritta *Alessandra Viani* nata il *05/04/1990* a *Brescia*, Provincia/Stato *Brescia/Italia*.
Dottorato di ricerca in *Ingegneria Civile ed Ambientale*.

a conoscenza del fatto che in caso di dichiarazioni mendaci, oltre alle sanzioni previste dal Codice Penale e dalle Leggi speciali per l'ipotesi di falsità in atti ed uso di atti falsi, decade dai benefici conseguenti al provvedimento emanato sulla base di tali dichiarazioni,

DICHIARA

sotto la propria responsabilità, ai fini dell'ammissione all'esame finale per il conseguimento del titolo di Dottore di ricerca,

di essere a conoscenza che,

in conformità al Regolamento dell'Università degli Studi di Brescia per l'ammissione all'esame finale ed il rilascio del titolo per il conseguimento del titolo di Dottore di Ricerca, è tenuto a depositare all'U.O.C. Dottorati e Scuole di Specializzazione:

- n. 1 copia in formato cartaceo della propria tesi di dottorato e **l'esposizione riassuntiva (abstract) in italiano, se la redazione della tesi è stata autorizzata in lingua straniera;**
- n. 2 copie della tesi su DVD o CD-ROM per il deposito presso le Biblioteche Nazionali di Roma e di Firenze;

DICHIARA inoltre

- che il contenuto e l'organizzazione della tesi sono opera originale e non compromettono in alcun modo i diritti di terzi,
- **che sarà consultabile** immediatamente dopo il conseguimento del titolo di Dottore di ricerca, in quanto non è il risultato di attività rientranti nella normativa sulla proprietà industriale, non è stata prodotta nell'ambito di progetti finanziati da soggetti pubblici o privati con vincoli alla divulgazione dei risultati, e non è oggetto di eventuali registrazioni di tipo brevettale o di tutela,
- che l'Università è in ogni caso esente da qualsiasi responsabilità di qualsivoglia natura, civile, amministrativa o penale e sarà tenuta indenne da qualsiasi richiesta o rivendicazione da parte di terzi;

Dichiarazione di conformità

- che la tesi in formato elettronico (DVD o CD-ROM) è completa in ogni sua parte ed è del tutto identica a quella depositata in formato cartaceo all'U.O.C. Dottorati e Scuole di Specializzazione dell'Università degli Studi di Brescia e inviata ai Commissari. Di conseguenza va esclusa qualsiasi responsabilità dell'Ateneo per quanto riguarda eventuali errori, imprecisioni od omissioni nei contenuti della tesi.

Dichiara inoltre di essere consapevole che saranno effettuati dei controlli a campione. Eventuali discordanze od omissioni potranno comportare l'esclusione dal dottorato di ricerca;

Luogo e data: *Grenoble 05/02/2019*

Firma del dichiarante

